SEISMIC RESPONSE OF PARTIALLY FILLED RECTANGULAR LIQUID TANK WITH INTERNAL OBJECTS

A THESIS SUBMITTED IN FULFILLMENT OF

THE REQUIREMENT FOR THE AWARD OF THE DEGREE

OF

DOCTOR OF PHILOSOPHY

IN

CIVIL ENGINEERING

BY

SANTOSH KUMAR NAYAK

(ROLL NO. 510CE802)

NATIONAL INSTITUTE OF TECHNOLOGY
ROURKELA - 769008, INDIA

SEPTEMBER – 2013

CERTIFICATE

This to certify that the thesis entitled **"Seismic Response of Partially Filled Rectangular Liquid Tank With Internal Objects"**, submitted by **Santosh Kumar Nayak** for the award of the degree of Doctor of Philosophy in Civil Engineering, is a record of bonafide research work carried out by him under my supervision and guidance. Mr. Santosh Kumar Nayak has tirelessly worked on the above problem for more than three years at the Department of Civil Engineering, National Institute of Technology, Rourkela and this has reached the standard fulfilling the requirements and the regulation relating to the degree. The contents of this thesis, in full or part, have not been submitted to any other university or institution for the award of any degree or diploma.

Rourkela

Date:

Dr. Kishore Chandra Biswal
Associate Professor
Department of Civil Engineering
NIT, Rourkela

Dedicated

To

My Parents

Declaration

I hereby declare that I am the sole author of this thesis. This thesis contains no material that has been submitted previously, in whole or in part, for the award of any other academic degree or diploma. Except where otherwise indicated, this thesis is my own work.

Santosh Kumar Nayak
Department of Civil Engineering
National Institute of Technology, Rourkela

ACKNOWLEDGEMENT

Mobility is the quintessence of life. Stagnancy is the end of it. This work marks the culmination of three years of an arduous journey through the territories of uncertainities. It is, however, not the end of the journey. It only augurs the beginning of yet another journey. But for the inspiration, encouragement, friendship, support and guidance of so many people, this could not have been possible. To them all, at this opprtune moment, I wish to express my thanks and gratitude.

Foremost obligation demands thanks to my wife for all the support and dispensation she extended for all these years. She was virtually the only parent taking care of my daughters Sonu and Ronu. She willingly conceded her quota of time at my disposal and approved me the extra time I asked from her share. She unequivocally supported my decissions at critical junctures. Needless to say that in spite of minor hiccups, I could not have asked for a more stronger demonstration of love than that, which I promise, I will always try to pay back. A greater degree of thanks is due to my daughters for their acknowledgement of the helplessness in me. My long-hour absence often denied them the time what should genuinely have been theirs.

Next, deepest gratitudes are due to one of the most impeccable human beings I have ever come across till this point in time, my supervisor Prof. K. C. Biswal, who is not only a very good teacher with a good deal of command over his area of academic interest but also an outstanding human being. Anger being an alien element of his personality makes him the most enviable. I have never seen him demonstrating anger even in its subtlest form and even when it was a genuine necessity. His penchant appetite for learning; uncompromising stand on morale; never-say-die attitude to mathematical complexities stands him way apart. His attitude toward research, insight into the problems, and trust in me, left an indelible impression on this work. Above all, his programming prowess was of great help to me whenever I was stuck. Prof. Biswal, you are one amongst the very few, I would love to bow before.

I am also thankful to the members of Doctoral Scrutiny Committee and other professors of Civil Engineering Department, all of whom in their own way supported this endeavour. I wish to gracefully acknowledge the encouragement, affection, and moral support of Prof. S. P. Singh, Prof. Mahabir Panda and Prof. C. R. Patra. My sincere thanks reaches out to Prof. S. S. Mohapatra, Department of Mechanical

Engineering, for he lended me his valuable time to clarify things pertaining to soft computing.

Taking this opportunity, I sincerely thank Dr. Sunil Kumar Sarangi, Director, NIT, Rourkela for it is he, who transformed this institution into an acclaimed institution of academic repute and provided an ambient research environment.

I wish to thank the dexterity and intelligence of the semiliterate carpenter, Sadhu Nayak, who adroitly translated my ideas into reality through his flawless skill and helped in the preparation of experimental model tank. At instances his ideas prevailed over mine.

Special thanks are due to Samir, Lugun and Susil of Structural Engineering Laboratory for their help in conducting the experiment. A special word of thanks is addressed to Haramohan Garnayak of Transportation Engineering Laboratory for his company, especially in the moments of desperation when nobody was around to share.

I am thankful to Prabir Kumar Mohanty and Pradyot Kumar Muduli, my fellow research scholars and colleagues, not only for the lively discussion on issues concerning academic interest and beyond, but also for all those *tu-tu mein-mein* (difference of opinion), we often had on issues of conflicting interests. At times, the discussions helped to start things afresh. I am also thankful to other fellow research scholars and the two of them, Rabi and Meena need a special mention.

I am immensely grateful to my brothers and sister. It was their encouragement and inspiration that instilled in me the confidence to overcome the hurdles along the way. Having been blessed with them as my siblings, I feel fortunate and thank God.

Last but not the least, I would, however, not express my gratitude to my parents as I strongly believe that formal exposition of love and respect would demean their stature to whom I owe whatever little things I dare claim as mine. However, the sacrifice they have endured for the education of their children, not very well understood in the neighbourhood, demands a special mention. All of their children are the living proof of the discernment of their decissions. The best expression of gratitude to them is to do the same for their grand children.

Santosh Kumar Nayak

ABSTRACT

Sloshing is a phenomenon describing the disturbance in an unrestrained free surface of liquid in a container. It encompasses a wide spectrum of problems of engineering interest. The container in question may be a tea cup, a kerosene jerkin, a water or oil tank, a liquid transporting road tanker, a reservoir or even an ocean. The problem of sloshing is common to all such containers which are partially filled and thus have unrestrained free surface. This dissertation makes a small but honest attempt to study the seismic response of partially filled rigid rectangular tank, with internal objects, firmly supported to the ground. The novelty of this PhD is that it focuses on a special class of container with submerged internal objects.

This PhD investigates; numerically, experimentally, and by use of soft computing techniques, the physical aspects of sloshing in partially filled rigid rectangular tank with submerged internal objects. The numerical study is devoted towards the investigation of the linear and nonlinear seismic behaviour of tank-submerged-block system under earthquakes of various frequency contents. Finite element method in two-dimensional space is used in the study. The method is capable of considering both impulsive and convective responses of tank-liquid-submerged block system. The experimental study is undertaken in a miniature sized model rectangular tank mounted rigidly to a shake table, capable of producing sinusoidal excitation, to study the slosh damping potential of various configurations of internal objects, namely; bottom-mounted vertical baffle, surface-piercing vertical baffle, and bottom-mounted submerged block. Adaptive neuro-fuzzy inference system (ANFIS) is used to swot the potential of soft computing techniques in predicting sloshing response of liquid in tank.

The principal objectives of this PhD are:

- To understand the complex nonlinear seismic response of liquid filled tank with internal objects
- To understand the complex interrelationship of impulsive and convective response components of hydrodynamic base shear and base moment vis-à-vis frequency content of earthquakes and to document the interesting features therein

- To gain an insight into the relevant slosh damping potential of strategic internal objects of various configurations and also to provide useful data for validation of analytical and numerical results
- To explore the possible use of soft computing techniques in slosh mechanics for prediction of dynamic response

First Galerkin based finite element formulation has been developed both for linear and nonlinear sloshing. The free vibration characteristics of sloshing in a given tank dimension with varying position and dimension of the submerged internal blocks is studied next. Subsequent chapters are devoted to the linear and nonlinear seismic response of liquid filled tank with submerged internal objects followed by a chapter on experimental investigation of passive damping potential of various configurations of internal objects. The penultimate chapter deals with the effectiveness of adaptive neuro-fuzzy inference system as a soft computing tool to predict the sloshing response of liquid in tank under lateral ground motions due to two earthquakes of different frequency content. The last chapter briefly summarizes the conclusions of this dissertation with an outline of future scope of study.

TABLE OF CONTENTS

Declaration iv

Acknowledgements ..... v-vi

Abstract ..... vii-viii

Contents ..... ix-xiii

List of Tables xiv

List of Figures ..... xv-xxv

List of Symbols ..... xxvi-xxvii

1 Introduction 1

1.1 Introduction 1

1.2 Objective 2

1.3 Scope of the Present Investigation 3

1.4 Thesis Layout 3

2 Review of Literature 7

2.1 Introduction 7

2.2 Seismic Performance of Liquid Storage Tanks in Historic Earthquakes 8

2.2.1 1960, the Great Chilean Earthquake 8

2.2.2 1964, the Nigata Earthquake 8

2.2.3 1964, the Great Alaska Earthquake 8

2.2.4 1979 Imperial Valley Earthquake 9

2.2.5 1983, the Coalinga Earthquake 9

2.2.6 1989 Loma Prieta Earthquake 10

2.2.7 1992 Landers Earthquake 10

2.2.8 1994, the Northridge Earthquake 11

2.2.9 1999, the Kocaeli Earthquake 11

2.2.10 2001, Bhuj (India) Earthquake 12

2.2.11 2010, the Maule, Chile Earthquake 12

2.2.12 2010-2011 Christchurch Earthquakes 12

2.2.13 2011, the Great East Japan (Tohoku) Earthquake 12

2.3 Failure Mechanisms of Liquid Tanks 18

2.3.1 Shell Buckling 19

2.3.2 Inlet-outlet Pipe Breaks 19

2.3.3 Uplifting of Tanks 20

2.3.4 Base Sliding 20

2.3.5 Damage to Upper Tank Shell and Roof due to Sloshing 20

2.3.6 Damage to Floating Roof due to Sloshing 20

2.3.7 Soil Failure at Tank Site 20
2.3.8 Failure of Support Strucure 21
2.3.9 Failure of Tank Structure Due to Large Inertia Force 21
2.4 Ground Motion Characteristics 21
2.5 Dynamic Analysis of Liquid Containers 23
2.6 Related Analytical and Numerical Studies 37
2.7 Dynamics of Liquid Containers with Internal Components 47
2.8 Application of Soft Computing to Engineering Problems 51
2.9 Critical Observations 52
2.10 Conclusion 52
3 Mathematical Background and Finite Element Formulation 54
3.1 Introduction 54
3.2 Liquid Domain Formulation: Linear Analysis 54
3.2.1 Mathematical Formulation 54
3.2.2 Governing Equation 55
3.2.3 Boundary Conditions 56
3.2.4 Finite Element Formulation 58
3.2.4.1 Liquid Stiffness Matrix 61
3.2.4.2 Liquid Free Surface Mass Matrix 63
3.2.4.3 Liquid Load Vector 64
3.2.4.4 Base Shear and Overturning Base Moment 65
3.3 Liquid Domain Formulation: Nonlinear Analysis 68
3.3.1 Mathematical Formulation 68
3.3.1.1 Nonlinear Free Surface Boundary Conditions 68
3.3.1.2 Body Surface Boundary Condition 69
3.4 Finite Element Formulation 70
3.5 Implementation of Numerical Scheme 73
3.5.1 Mesh Generation 74
3.5.2 Time Integration 74
3.5.3 Regridding 75
4 Free Vibration Analysis of Rectangular Tank with Internal Submerged Block 77
4.1 Introduction 77
4.2 Linear Free Vibration Analysis 79
4.2.1 Effect of Submerged Block on Sloshing Frequency 79
4.2.2 Effect of Vertical Baffle on the Sloshing Frequencies 82

4.2.3 Effect of Submerged Block on the Sloshing Frequencies in Tank with different Fill-depth 83
4.2.4 Effect of Block Height and Location on the Sloshing Modes 85
4.3 Nonlinear free vibration analysis 87
4.3.1 Model Validation 87
4.3.2 Sloshing Frequencies 87
4.4 Conclusions 89
5 Linear Seismic Response of Rectangular Liquid Tank with Submerged Block 91
5.1 Introduction 91
5.2 Numerical Results and Discussion 93
5.2.1 Model Validation 95
5.2.2 Sloshing Frequencies 100
5.2.3 Sloshing Response 100
5.2.4 On Validity of Hydrostatic Base Shear 103
5.2.5 Base Moment 107
5.2.6 Impulsive and Convective Response of Base Shear and Base Moment 110
5.2.7 Free Surface Wave Profiles 121
5.2.8 Pressure Distribution on Tank Wall 122
5.2.9 Pressure Distribution on Block Wall 126
5.3 Conclusion 129
6 Nonlinear Seismic Response of Rectangular Liquid Tank 132
6.1 Introduction 132
6.2 Seismic Response and Discussion 135
6.2.1 Hydrodynamic Responses 135
6.2.2 Sloshing Response 136
6.2.3 Base Shear and Overturning Base Moment 141
6.2.4 Pressure Distribution on Tank Wall 147
6.3 Conclusion 150
7 Nonlinear Seismic Response of Rectangular Liquid Tank with Submerged Block 152
7.1 Introduction 152
7.2 Numerical Results and Discussion 154
7.2.1 Hydrodynamic Responses 155
7.2.1.1 Sloshing Response 155
7.2.1.2 Base Shear and Overturning Base Moment 159
7.2.1.3 Pressure Distribution on Tank Wall 169

7.2.1.4 Pressure Distribution on Block Wall 173
7.3 Conclusion 176

8 Fluid Damping in Rectangular Tank Fitted with Various Internal Objects – An Experimental Investigation 178
8.1 Introduction 178
8.2 Description of Laboratory Equipments 181
8.2.1 Shake Table 181
8.2.2 Power Supply 183
8.2.3 Data Acquisition and Control System 183
8.2.4 Measurement Sensors 184
8.2.5 Test tank (Partially-filled liquid tank with or without internal objects) 186
8.2.6 Internal Objects 187
8.3 Experimental Work 187
8.3.1 Experimental Test Set up 187
8.3.2 Fixing the Baffles and Submerged Blocks 188
8.4 Experimental Results and Discussion 192
8.4.1 Frequency Response Study of Sloshing by Sine Sweep Test 192
8.4.2 Effect of Baffle on Sloshing Response 197
8.4.3 Hydrodynamic Slosh Damping 198
8.4.4 Effect of the Bottom-mounted Vertical Baffles 202
8.4.5 Effect of the Surface-piercing Vertical Baffles 203
8.4.6 Comparison of the Damping Effects of Bottom-mounted and Surface-piercing Vertical Baffles 204
8.4.7 Forced Vibration Response 206
8.5 Conclusion 209

9 Prediction of Seismic Induced Sloshing Response in Baffled Rectangular Liquid Tank Using Adaptive Neuro-fuzzy Inference System 210
9.1 Introduction 210
9.2 Sloshing Data 211
9.3 ANFIS Model Description 213
9.3.1 Artificial Neural Network 216
9.3.2 Fuzzy Inference System (FIS) 217
9.3.2.1 Linguistic Variables 218
9.3.2.2 Fuzzy Sets 219
9.3.2.3 Membership Functions 219
9.3.2.4 Fuzzy If-Then Rules (Fuzzy Linguistic Rules) 220
9.4 Implementation of ANFIS 220

9.4.1 Architecture and Basic Learning Rules 222
9.4.2 Hybrid Learning Algorithm 224
9.5 Model Design 226
9.6 Results and Discussion 230
9.7 Conclusion 243
10 Summary, Conclusions and Recommendations 245
10.1 Summary 245
10.2 Conclusions 246
10.3 Recommendations for Future Studies 249
References 250
Published and Accepted Papers 267

LIST OF TABLES

Table 4.1: Non-Dimensional frequencies ($\omega_j L/g\pi$) for centrally placed block with varying *d/L* and *d/h* 80
Table 4.2: Linear and nonlinear natural frequencies for the first three sloshing modes 89
Table 5.1: Ground motion records 95
Table 5.2: Sloshing frequencies (Hz) for various submerged-block heights (*h*/*d*) 99
Table 5.3: Absolute maximum dynamic responses of various physical parameters of the tank-liquid-submerged block system[@] 114
Table 5.4: Contributions of impulsive and convective components for absolute maximum hydrodynamic responses of various physical parameters 115
Table 6.1: Linear and nonlinear peak sloshing amplitude 137
Table 6.2: Absolute maximum dynamic response of various physical parameters of the tank liquid system 139
Table 6.3: Contributions of impulsive and convective components for absolute maximum hydrodynamic response of various physical parameters 140
Table 7.1: Absolute maximum dynamic responses of various physical parameters of the tank liquid system: 157
Table 7.2: Contributions of impulsive and convective components for absolute maximum hydrodynamic response of various physical parameters: 158
Table 8.1: Effect of internal objects on first mode sloshing frequency (Hz) 195
Table 8.2: Percentage attenuation of maximum elevations 198
Table 9.1: Input and output data used for analysis. 214
Table 9.2: Two passes in the hybrid learning procedure of ANFIS 226
Table 9.3: Characteristic information of ANFIS architecture 227
Table 9.4: Statistical performance on training of ANFIS models 243
Table 9.5: Statistical performance on testing of ANFIS models 243

LIST OF FIGURES

Figure 2.1: Elephant foot buckling of broad tank 13
Figure 2.2: Diamond buckling in slender tank 14
Figure 2.3: Base sliding causing extensive damage to inlet/outlet piping 14
Figure 2.4: Failure to supporting structures: (a) Shear failure in concrete link beam, (b) Flexural cracks in supporting shafts 15
Figure 2.5: Damaged seals in tanks from sloshing of liquids 15
Figure 2.6: Implosion failure due to rapid loss of liquid contents 16
Figure 2.7: Tank pipe connections: (a) Base sliding causing extensive damage to inlet/outlet piping, (b) Flexible connections accommodate horizontal and vertical movements, and prevent pipe breaks 16
Figure 2.8: Oil tank sloshing spill over the rim (2010 Maule, Chile earthquake) 17
Figure 2.9: Typical collapsed elevated small steel water tank (2010 Maule, Chile earthquake) 17
Figure 2.10: Two damaged liquefied oxygen tanks (LOXT) and the undamaged liquefied nitrogen tank (LNT, on the right) at the Habas facility (1999 Kocaeli earthquake). 18
Figure 2.11: Classification liquid storage tanks 19
Figure 3.1: Schematic diagram of tank-liquid-submerged block system 55
Figure 3.2: Liquid free surface element in a container 63
Figure 3.3: Liquid-solid interface element in a container 64
Figure 3.4: Typical distribution of hydrodynamic pressure on tank wall and base 66
Figure 3.5: Typical distribution of hydrodynamic pressure in tank with submerged block: (a) Impulsive pressure; (b) Convective pressure 67
Figure 3.6: Typical finite element mesh 74
Figure 4.1: Sloshing frequencies (L = 30 m, d = 13 m) for: (a) variation of block height (b = 15 m, w = 10 m); (b) variation of block width (b =15 m, h = 6 m); (c) variation of block location (w = 4 m, h = 8 m) 81
Figure 4.2: Sloshing modes (L = 30 m, d = 15 m): (a) for a centrally located block (h = 0.5d, w = 0.4L) (b) for an off-centred block (h = 0.5d, w = 0.4L, b = 0.3L) 81
Figure 4.3: Sloshing and modes for various heights of a centrally placed baffle (d/L = 0.5): (a) tank with a centrally placed baffle (L = 30 m, d = 15 m); (b) sloshing frequencies; (c) mode shapes 82
Figure 4.4: Sloshing and modes for various heights of an off-center baffle (d/L = 0.5): (a) tank with an off-center baffle (L = 30 m, d = 15 m); (b) sloshing frequencies; (c) mode shapes 83

Figure 4.5: Normalized sloshing frequencies (ω_{nj}) as a function of block height (h/d) for centrally placed block ($b = 0.5L$, $w = 0.2L$): (a) First mode (b) Second mode (c) Third mode 84
Figure 4.6: Normalized sloshing frequencies (ω_{nj}) as a function of block width (w/L) for centrally placed block ($b = 0.5L$, $h = 0.6d$): (a) First mode (b) Second mode (c) Third mode 85
Figure 4.7: Normalized sloshing frequencies (ω_{nj}) as a function of block location (b/L) for off- centered block ($w = 0.2L$, $h = 0.7d$): (a) First mode (b) Second mode (c) Third mode 85
Figure 4.8: Sloshing modes for various heights of block (h/d): (a) tank with $d/L = 0.2$; (b) tank with $d/L = 0.5$. 86
Figure 4.9: Sloshing modes for various locations of block (b/L): (a) tank with $d/L = 0.2$; (b) tank with $d/L = 0.5$. 86
Figure 4.10: Time history of the sloshing elevation at right hand wall of tank in the first sloshing mode 87
Figure 4.11: Maximum wave elevation vs. excitation frequency for tank-liquid systems of varying liquid-depths: (a) $d/L = 0.20$; (b) $d/L = 0.85$ 88
Figure 4.12: Nonlinear and linear sloshing frequencies for tanks with varying fill depth (d/L) 89
Figure 5.1: Time-history of acceleration of ground motion: (a) El Centro-EW (b) Imperial Valley (c) IS Code ground motion data (d) Landers (e) San-Franscisco (f) Colianga 96
Figure 5.2: Time-history of velocity of ground motion: (a) El Centro-EW (b) Imperial Valley (c) IS Code ground motion data (d) Landers (e) San-Franscisco (f) Colianga 97
Figure 5.3: Power spectrum density function of ground acceleration: (a) El Centro-EW (b) Imperial Valley (c) IS Code ground motion data (d) Landers (e) San-Franscisco (f) Colianga 98
Figure 5.4: Time history of free surface wave amplitude at left hand wall of tank for different heights of submerged block due to El Centro-EW ground motion: (a) $h/d = 0.0$, (b) $h/d = 0.5$ 99
Figure 5.5: Temporal variation of sloshing elevation in tank with submerged block under seismic ground motions: (a) El Centro-EW (b) Imperial Valley (c) IS Code ground motion data (d) Landers (e) San-Franscisco (f) Colianga 102
Figure 5.6: Temporal variation of hydrodynamic and equivalent hydrostatic base shear for various heights of submerged block under El Centro-EW ground motion: (a) $h/d = 0.0$ (b) $h/d = 0.2$ (c) $h/d = 0.5$.....104

Figure 5.7: Temporal variation of hydrodynamic and equivalent hydrostatic base shear for various heights of submerged block under Imperial Valley ground motion: (a) *h/d* = 0.0 (b) *h/d* = 0.2 (c) *h/d* = 0.5.....104
Figure 5.8: Temporal variation of hydrodynamic and equivalent hydrostatic base shear for various heights of submerged block under IS Code ground motion data: 105
Figure 5.9: Temporal variation of hydrodynamic and equivalent hydrostatic base shear for various heights of submerged block under Landers ground motion: (a) *h/d* = 0.0 (b) *h/d* = 0.2 (c) *h/d* = 0.5 105
Figure 5.10: Temporal variation of hydrodynamic and equivalent hydrostatic base shear for various heights of submerged block under San-Franscisco ground motion: (a) *h/d* = 0.0 (b) *h/d* = 0.2 (c) *h/d* = 0.5.....106
Figure 5.11: Temporal variation of hydrodynamic and equivalent hydrostatic base shear for various heights of submerged block under Colianga ground motion: (a) *h/d* = 0.0 (b) *h/d* = 0.2 (c) *h/d* = 0.5 106
Figure 5.12: Temporal variation of base moment for various heights of submerged block under El Centro-EW ground motion: (a) *h/d* = 0.0 (b) *h/d* = 0.2 (c) *h/d* = 0.5.....107
Figure 5.13: Temporal variation of base moment for various heights of submerged block under Imperial Valley ground motion: (a) *h/d* = 0.0 (b) *h/d* = 0.2 (c) *h/d* = 0.5.....108
Figure 5.14: Time history of base moment for various heights of submerged block under IS Code ground motion: (a) *h/d* = 0.0 (b) *h/d* = 0.2 (c) *h/d* = 0.5 108
Figure 5.15: Temporal variation of base moment for various heights of submerged block under Landers ground motion data: (a) *h/d* = 0.0 (b) *h/d* = 0.2 (c) *h/d* = 0.5 109
Figure 5.16: Temporal variation of base moment for various heights of submerged block under San-Franscisco ground motion: (a) *h/d* = 0.0 (b) *h/d* = 0.2 (c) *h/d* = 0.5.....109
Figure 5.17: Temporal variation of base moment for various heights of submerged block under Colianga ground motion data: (a) *h/d* = 0.0 (b) *h/d* = 0.2 (c) *h/d* = 0.5 110
Figure 5.18: Comparison of temporal variations of impulsive and convective response components of base shear for various heights of submerged block under El Centro-EW ground motion: (a) *h/d* = 0.0 (b) *h/d* = 0.2 (c) *h/d* = 0.5 113
Figure 5.19: Comparison of temporal variations of impulsive and convective response components of base shear for various heights of submerged block under Imperial Valley ground motion: (a) *h/d* = 0.0 (b) *h/d* = 0.2 (c) *h/d* = 0.5 116

Figure 5.20: Comparison of temporal variations of impulsive and convective response components of base shear for various heights of submerged block under IS Code ground motion data: (a) *h/d* = 0.0 (b) *h/d* = 0.2 (c) *h/d* = 0.5.....116
Figure 5.21: Comparison of temporal variations of impulsive and convective response components of base shear for various heights of submerged block under Landers ground motion: (a) *h/d* = 0.0 (b) *h/d* = 0.2 (c) *h/d* = 0.5 117
Figure 5.22: Comparison of temporal variations of impulsive and convective response components of base shear for various heights of submerged block under San-Franscisco ground motion: (a) *h/d* = 0.0 (b) *h/d* = 0.2 (c) *h/d* = 0.5 117
Figure 5.23: Comparison of temporal variations of impulsive and convective response components of base shear for various heights of submerged block under Colianga ground motion: (a) *h/d* = 0.0 (b) *h/d* = 0.2 (c) *h/d* = 0.5 118
Figure 5.24: Comparison of temporal variations of impulsive and convective response components of base moment for various heights of submerged block under El Centro-EW ground motion: (a) *h/d* = 0.0 (b) *h/d* = 0.2 (c) *h/d* = 0.5.....118
Figure 5.25: Comparison of temporal variations of impulsive and convective response components of base moment for various heights of submerged block under Imperial Valley ground motion: (a) *h/d* = 0.0 (b) *h/d* = 0.2 (c) *h/d* = 0.5 119
Figure 5.26: Comparison of temporal variations of impulsive and convective response components of base moment for various heights of submerged block under IS Code ground motion data: (a) *h/d* = 0.0 (b) *h/d* = 0.2 (c) *h/d* = 0.5 119
Figure 5.27: Comparison of temporal variations of impulsive and convective response components of base moment for various heights of submerged block under Landers ground motion data: (a) *h/d* = 0.0 (b) *h/d* = 0.2 (c) *h/d* = 0.5.....120
Figure 5.28: Comparison of temporal variations of impulsive and convective response components of base moment for various heights of submerged block under San-Franscisco ground motion data: (a) *h/d* = 0.0 (b) *h/d* = 0.2 (c) *h/d* = 0.5 120
Figure 5.29: Comparison of temporal variations of impulsive and convective response components of base moment for various heights of submerged block under Colianga ground motion data: (a) *h/d* = 0.0 (b) *h/d* = 0.2 (c) *h/d* = 0.5 121
Figure 5.30: Free surface profiles at the instant of absolute maximum base shear for various heights of submerged block under various ground motions: (a) El Centro-EW (b) Imperial Valley (c) IS Code ground motion data (d) Landers (e) San-Franscisco (f) Colianga 122
Figure 5.31: Hydrodynamic pressure distribution along the left wall of the tank at the instant of maximum base shear for various heights of centrally placed submerged block under horizontal ground motion of El Centro-EW: (a) *h/d* = 0.0 (b) *h/d* = 0.2 (c) *h/d* = 0.5.....123

Figure 5.32: Hydrodynamic pressure distribution along the left wall of the tank at the instant of maximum base shear under horizontal ground motion of Imperial Valley: (a) *h/d* = 0.0 (b) *h/d* = 0.2 (c) *h/d* = 0.5 124
Figure 5.33: Hydrodynamic pressure distribution along the left wall of the tank at the instant of maximum base shear under horizontal ground motion of IS Code data: (a) *h/d* = 0.0 (b) *h/d* = 0.2 (c) *h/d* = 0.5 124
Figure 5.34: Hydrodynamic pressure distribution along the left wall of the tank at the instant of maximum base shear under horizontal ground motion of Landers: (a) *h/d* = 0.0 (b) *h/d* = 0.2 (c) *h/d* = 0.5 125
Figure 5.35: Hydrodynamic pressure distribution along the left wall of the tank at the instant of maximum base shear under horizontal San-Franscisco ground motion: (a) *h/d* = 0.0 (b) *h/d* = 0.2 (c) *h/d* = 0.5 125
Figure 5.36: Hydrodynamic pressure distribution along the left wall of the tank at the instant of maximum base shear under horizontal Colianga ground motion: (a) *h/d* = 0.0 (b) *h/d* = 0.2 (c) *h/d* = 0.5.....126
Figure 5.37: Hydrodynamic pressure distribution along the left wall of the block for various heights of centrally placed submerged block under horizontal ground motion of El Centro-EW: (a) *h/d* = 0.2 (b) *h/d* = 0.5 127
Figure 5.38: Hydrodynamic pressure distribution along the left wall of the block for various heights of centrally placed submerged block under horizontal ground motion of Imperial Valley: (a) *h/d* = 0.2 (b) *h/d* = 0.5.....127
Figure 5.39: Hydrodynamic pressure distribution along the left wall of the block for various heights of centrally placed submerged block under horizontal ground motion of IS Code data: (a) *h/d* = 0.2 (b) *h/d* = 0.5 128
Figure 5.40: Hydrodynamic pressure distribution along the left wall of the block for various heights of centrally placed submerged block under horizontal ground motion of Landers: (a) *h/d* = 0.2 (b) *h/d* = 0.5 128
Figure 5.41: Hydrodynamic pressure distribution along the left wall of the tank for various heights of centrally placed submerged block under horizontal San-Franscisco ground motion: (a) *h/d* = 0.2 (b) *h/d* = 0.5.....129
Figure 5.42: Hydrodynamic pressure distribution along the left wall of the tank for various heights of centrally placed submerged block under horizontal Coalinga ground motion: (a) *h/d* = 0.2 (b) *h/d* = 0.5 129
Figure 6.1: Temporal variation of linear and nonlinear sloshing elevation due to ground motions: (a) El Centro-EW (b) Imperial Valley (c) Landers (d) San-Franscisco 138
Figure 6.2: Time history of impulsive and convective responses of base shear: (a) El Centro-EW (b) Imperial Valley (c) Landers (d) San-Franscisco 143

Figure 6.3: Time history of impulsive and convective responses of base moment: (a) El Centro-EW (b) Imperial Va lley (c) Landers (d) San-Franscisco 143
Figure 6.4: Time history of linear and nonlinear convective base shear: (a) El Centro-EW (b) Imperial Valley.....145
Figure 6.5: Time history of linear and nonlinear convective base moment: (a) El Centro-EW (b) Imperial Valley 145
Figure 6.6: Time history of impulsive and convective responses of base shear for Imperial Valley ground motion: (a) d/L = 0.5 (b) d/L = 0.2 146
Figure 6.7: Time history of impulsive and convective responses of base moment for Imperial Valley ground motion: (a) d/L = 0.5 (b) d/L = 0.2 146
Figure 6.8: Quantitative result of absolute maximum values of impulsive, convective and total hydrodynamic responses for different ground motions: (a) Base shear (b) Base moment 146
Figure 6.9: Component-wise break up of peak hydrodynamic responses for different ground motions: (a) Base shear (b) Base moment 147
Figure 6.10: Comparison of linear and nonlinear hydrodynamic pressure distribution along the height of tank wall: (a) El Centro-EW (b) Imperial Valley (c) Landers (d) San-Franscisco 148
Figure 6.11: Distribution of impulsive and convective nonlinear hydrodynamic pressure along the height of tank wall: (a) El Centro-EW (b) Imperial Valley (c) Landers (d) San-Franscisco.....149
Figure 6.12: Hydrodynamic pressure along the height of tank wall for Imperial Valley earthquake: (a) Impulsive (b) Convective.....149
Figure 7.1: Temporal variation of sloshing elevation in tank with submerged block of varying height (h/d) under seismic ground motions: (a) Imperial Valley (b Landers (c) San-Franscisco.....156
Figure 7.2: Time history of impulsive and convective responses of base shear due to Imperial Valley with various heights of submerged block (a) h/d = 0.0 (b) h/d = 0.2 (c) h/d = 0.5.....162
Figure 7.3: Time history of impulsive and convective responses of base shear due to Landers with various heights of submerged block (a) h/d = 0.0 (b) h/d = 0.2 (c) h/d = 0.5 163
Figure 7.4: Time history of impulsive and convective responses of base shear due to San-franscisco with various heights of submerged block (a) h/d = 0.0 (b) h/d = 0.2 (c) h/d = 0.5.....163
Figure 7.5: Time history of impulsive and convective responses of base moment due to Imperial Valley with various heights of submerged block (a) h/d = 0.0 (b) h/d = 0.2 (c) h/d = 0.5.....164

Figure 7.6: Time history of impulsive and convective responses of base moment due to Landers with various heights of submerged block (a) *h/d* = 0.0 (b) *h/d* = 0.2 (c) *h/d* = 0.5 164
Figure 7.7: Time history of impulsive and convective responses of base moment due to San-Franscisco with various heights of submerged block (a) *h/d* = 0.0 (b) *h/d* = 0.2 (c) *h/d* = 0.5.....165
Figure 7.8: Time history of base shear due to ground motion of Imperial Valley with various heights of submerged block (a) *h/d* = 0.0 (b) *h/d* = 0.2 (c) *h/d* = 0.5....165
Figure 7.9: Time history of base shear due to ground motion of Landers with various heights of submerged block (a) h/d = 0.0 (b) *h/d* = 0.2 (c) *h/d* = 0.5.....166
Figure 7.10: Time history of base shear due to ground motion of San-franscisco with various heights of submerged block (a) *h/d* = 0.0 (b) *h/d* = 0.2 (c) *h/d* = 0.5 ...166
Figure 7.11: Time history of overturning base moment due to ground motion of Imperial Valley with various heights of submerged block (a) *h/d* = 0.0; (b) *h/d* = 0.2; (c) *h/d* = 0.5.....167
Figure 7.12: Time history of overturning base moment due to ground motion of Landers with various heights of submerged block (a) *h/d* = 0.0; (b) *h/d* = 0.2; (c) *h/d* = 0.5 167
Figure 7.13: Time history of overturning base moment due ground motion of San-franscisco with various heights of submerged block (a) *h/d* = 0.0 (b) *h/d* = 0.2 (c) *h/d* = 0.5 168
Figure 7.14: Component-wise break up of peak hydrodynamic responses (base shear and base moments) for different ground motions: (a) Imperial Valley (b) Landers (c) San-Franscisco.....169
Figure 7.15: Distribution of hydrodynamic pressure along the height of tank wall due to Imperial Valley earthquake with various block heights: (a) *h/d* = 0.0 (b) *h/d* = 0.2 (c) *h/d* = 0.5.....170
Figure 7.16: Distribution of impulsive and convective pressure components along the height of tank wall due to Imperial Valley earthquake with various block heights: (a) *h/d* = 0.0 (b) *h/d* = 0.2 (c) *h/d* = 0.5 171
Figure 7.17: Distribution of hydrodynamic pressure along the height of tank wall due to Landers earthquake with various block heights: (a) *h/d* = 0.0 (b) *h/d* = 0.2 (c) *h/d* = 0.5 171
Figure 7.18: Distribution of impulsive and convective pressure components along the height of tank wall due to Landers earthquake with various block heights: (a) *h/d* = 0.0 (b) *h/d* = 0.2 (c) *h/d* = 0.5.....172

Figure 7.19: Distribution of hydrodynamic pressure along the height of tank wall due to San-franscisco earthquake with various block heights: (a) h/d = 0.0 (b) h/d = 0.2 (c) h/d = 0.5 172
Figure 7.20: Distribution of impulsive and convective pressure components along the height of tank wall due to San-franscisco earthquake with various block heights: (a) h/d = 0.0 (b) h/d = 0.2 (c) h/d = 0.5 173
Figure 7.21: Pressure distribution along the left wall of the centrally placed block under horizontal ground motion of Imperial Valley: (a) h/d = 0.2 (b) h/d = 0.5 174
Figure 7.22: Pressure distribution along the left wall of the centrally placed block under horizontal ground motion of Landers: (a) h/d = 0.2 (b) h/d = 0.5 175
Figure 7.23: Pressure distribution along the left wall of the centrally placed block under horizontal ground motion of San-franscisco: (a) h/d = 0.2 (b) h/d = 0.5 . 175
Figure 8.1: Shake table 182
Figure 8.2: Components of a typical DAQ system 185
Figure 8.3: Snap shots of components of the DAQ system 186
Figure 8.4: Experimental set up and instrumentation 189
Figure 8.5: Snap shot of internal objects: (a) Bottom-mounted vertical baffles; (b) Surface-piercing vertical baffles; (c) Bottom-mounted submerged blocks 190
Figure 8.6: Baffles and associated supporting fixtures 191
Figure 8.7: Problem definition (L = 57 cm, h and d are varying) 192
Figure 8.8: Harmonic excitation with a forcing frequency, f = 0.97 cycles/sec (fundamental sloshing frequency of tank without any internal objects) and displacement amplitude x_0 = 5 mm 194
Figure 8.9: Frequency response of free surface wave elevation at left wall of tank of aspect ratio, d/L = 0.26, x_0 = 0.005m. η = sloshing elevation at different excitation frequencies; η_{f1} = sloshing elevation at excitation frequency equal to the fundamental sloshing frequency 194
Figure 8.10: Comparison of fundamental sloshing frequencies as a function of baffle height in tanks with fill depth, d/L = 0.26 and 0.52: (a) bottom-mounted vertical baffles; (b) surface-piercing wall mounted vertical baffles 196
Figure 8.11: Sloshing frequencies in tank as a function of baffle height (h/d) with: (a) bottom-mounted vertical baffles as a function of baffle height (h/d) in tanks with d/L = 0.26 and 0.52 196
Figure 8.12: Comparison of sloshing frequencies in tank with d/L = 0.26 due to bottom-mounted vertical baffles and submerged components 197
Figure 8.13: Frequency response of the free surface wave elevation at left wall of tank with d/L = 0.26 due to bottom-mounted vertical baffles of different heights; η = sloshing elevation at different excitation frequencies; η_{f0} = maximum sloshing

elevation in tank without any internal component at excitation frequency equal to its fundamental sloshing frequency 198
Figure 8.14: Time decay of sloshing amplitude in free vibration phase in tank of aspect ratio d/L = 0.26 with bottom-mounted vertical baffles of various heights 200
Figure 8.15: Time decay of sloshing amplitude in free vibration phase in tank of aspect ratio d/L = 0.52 with bottom-mounted vertical baffles of various heights 200
Figure 8.16: Time decay of sloshing amplitude in free vibration phase in tank of aspect ratio d/L = 0.26 with bottom-mounted submerged blocks of various heights (width, $w = 0.33L$) 201
Figure 8.17: Time decay of sloshing amplitude in free vibration phase in tank of aspect ratio d/L = 0.26 with surface-piercing vertical baffles of various heights 201
Figure 8.18: Time decay of sloshing amplitude in free vibration phase in tank of aspect ratio d/L = 0.52 with surface-piercing vertical baffles of various heights 202
Figure 8.19: Comparison of variation of damping ratio as a function of relative baffle height (h/d) in tanks with two different fill depths; d/L = 0.26 and 0.52 due to bottom-mounted vertical baffles 203
Figure 8.20: Comparison of variation of damping ratio as a function of relative baffle height (h/d) in tanks with two different fill depths; d/L = 0.26 and 0.52 due to surface-piercing vertical baffles 203
Figure 8.21: Comparison of damping ratios, as a function of relative baffle height(h/d), due to bottom-mounted and surface-piercing vertical baffles, in tanks with d/L = 0.26 204
Figure 8.22: Comparison of damping ratios, as a function of relative baffle height (h/d), due to bottom-mounted and surface-piercing vertical baffles, in tanks with d/L = 0.52 205
Figure 8.23: Comparison of percentage attenuation of sloshing elevation as a function of relative baffle height (h/d) in tank with fill depth, d/L = 0.26 for two different baffle configuration; bottom-mounted baffle and surface-piercing baffle.....206
Figure 8.24: Comparison of damping ratio as a function of relative baffle height (h/d) in tank with fill-depth, d/L = 0.26 for bottom-mounted vertical baffles and submerged blocks, w/L = 0.33 206
Figure 8.25: Temporal evolution of the free surface sloshing elevations at the left wall for tank with bottom-mounted baffles of varying heights (h/d) under harmonic excitation with displacement amplitude, x_0 = 5 mm and excitation frequencies, f

(cycles/sec) corresponding to their respective fundamental sloshing frequencies. 207
Figure 8.26: Temporal evolution of the free surface sloshing elevations at the left wall for tank with surface-piercing baffles of varying heights (*h/d*) under harmonic excitation with displacement amplitude, x_0 = 5 mm and excitation frequencies, *f* (cycles/sec) corresponding to their respective fundamental sloshing frequencies as presented in Table 1 208
Figure 8.27: Comparison of temporal evolution of the free surface sloshing elevations at the left wall of tank due to bottom-mounted and surface piercing baffle of equal height in tank with fill depth, *d/L* = 0.26. Excitation frequencies are equal to respective fundamental sloshing frequencies and excitation amplitude, x_0 = 5 mm 208
Figure 9.1: problem definition 212
Figure 9.2: Free surface displacement from rest level at a distance of 0.05 m from the left side of the container. 213
Figure 9.3: Schematic diagram of Fuzzy inference System 218
Figure 9.4: A typical type III Takagi-Sugeno ANFIS architecture 225
Figure 9.5: Flow chart for the ANFIS models 229
Figure 9.6: Generalized bell shaped membership function (gbellmf) plots for input variables for ANFIS model for Imperial Valley: (a) *h/d* (b) *b/L* 230
Figure 9.7: Gauss2mf membership function plots for input variables for ANFIS model for San-francisco : (a) *h/d* (b) *b/L* 231
Figure 9.8: Generalized bell shaped membership function (gbellmf) plots for input variables for combined ANFIS model: (a) *h/d* (b) *b/L*.....232
Figure 9.9: A sample set of FIS properties of adaptive neuro-fuzzy inference system for prediction of sloshing response (Combined model).....233
Figure 9.10: A sample set of ANFIS rule viewer for sloshing elevation due to ground motion of San-francisco 234
Figure 9.11: Surface plot of sloshing elevation obtained from individual and combined models: (a) Surface plot for Imperial Valley from independent model (b) Surface plot for San-Francisco from independent model (c) Surface plot for Imperial Valley from combined model (d) Surface plot for San-Francisco from combined model 235
Figure 9.12: Correlation of predicted and actual data (training) for ANFIS models: (a) Imperial Valley (b) San-Franscisco (c) Combined model 236
Figure 9.13: Correlation of predicted and actual data (testing) for ANFIS models: (a) Imperial Valley (b) San-Franscisco (c) Combined model 237

Figure 9.14: Comparison of actual and predicted sloshing (training data) for ANFIS models: (a) Imperial Valley (b) San-Franscisco (c) Combined model 238
Figure 9.15: Comparison of actual and predicted sloshing (testing data) for ANFIS models: (a) Imperial Valley (b) San-Franscisco (c) Combined model 239
Figure 9.16: Residual distribution of training data: (a) Imperial Valley (b) San-Franscisco (c) Combined model 240
Figure 9.17: Residual distribution of testing data: (a) Imperial Valley (b) San-Franscisco (c) Combined model 241

LIST OF SYMBOLS

Abbreviations

PGA	Peak ground acceleration
PGV	Peak ground velocity
PGD	Peak ground displacement
RMSE	Root mean square error
MPE	Mean percentage error
MAPE	Mean absolute percentage error

Roman symbols

b	Distance of the submerged block from the tank wall
C_f	Damping matrix
d	Depth of liquid
f	Excitation frequency in cycles/sec
F_i	Force vector
g	Acceleration
h	Height of the submerged block/ baffle
K_f	Fluid stiffness matrix
L	Length of the liquid tank
M_b	Overturning bending moment about the corner of the base of the tank
M_f	Mass matrix
n	Unit vector normal to the wetted surface of the tank
N	Shape function
p	Fluid pressure
S_b	Base shear

T_{imp}	Time instant at which impulsive response component reaches absolute maximum
T_{con}	Time instant at which impulsive response component reaches absolute maximum
w	Width of the submerged block

Greek symbols

Γ_{bt}	Domain boundary defined by block top
Γ_{bw}	Domain boundary defined by block wall
Γ_{s}	Domain boundary defined by free surface liquid
Γ_{w}	Domain boundary defined by the wetted surface of the tank as well as block wall
Γ_{tb}	Domain boundary defined by tank bottom
Γ_{tw}	Domain boundary defined by tank wall
Ω	Liquid domain
ϕ	Velocity potential
ζ	Damping ratio
η	Sloshing elevation
η_{max}	Maximum sloshing elevation
μ	Artificial damping coefficient
μ_{crit}	Critical damping coefficient
ξ	Pseudo viscous damping
ρ	Density of liquid
ω	Natural sloshing frequency in rad/sec

CHAPTER 1

1 INTRODUCTION

1.1 Introduction

Sloshing is a phenomenon describing the disturbance in an unrestrained free surface of liquid in a container. The container in question may be a tea cup, a kerosene jerkin, a water or oil tank, a liquid transporting road tanker, a reservoir or even an ocean. The problem of sloshing is common to all such containers which are partially filled and thus have unrestrained free surface. Sloshing thus encompasses a wide variety of problems of engineering interest, and one such problem is the dynamic response of lifeline liquid storage tanks under earthquake motion.

At times, sloshing induced hydrodynamic load may adversely affect the dynamic behaviour and structural safety of liquid storage tank. The liquid sloshing can generate significant localized pressure on the tank walls and roof and may inflict damage to the constituent parts and in the worst case may lead to the complete failure of the tank. The magnitude of hydrodynamic force depends on a lot of factors. Of them, tank configuration and seismic characteristics are two important parameters. The submerged internal components if any can also have considerable influence on the dynamic behaviour.

The performance of liquid storage tanks due to seismic mishap is documented in the literature (Hanson, 1973; Berg and Stratta, 1974; Rinnie, 1967). The consequences of failed liquid containers have been disastrous on many occasions resulting in more loss of life and property than the earthquake itself. Disruption in water supply leading to uncontrolled fire in wake of major earthquakes, spillage of toxic industrial chemicals and inflammable petroleum products can cause damage in a much higher scale than that due to immediate economic value of the tank and its content. The polluted

environment due to contaminated soil and water resources may have far reaching consequences than an average mind can think of.

The main purpose of the present discourse is to comprehensively investigate the time-history of dynamic response of rigid rectangular liquid storage tanks with internal submerged object under lateral earthquake ground motions. In this dissertation, linear and nonlinear finite element models have been developed in-house for two-dimensional tank geometry taking into account the liquid sloshing, fluid damping, and the earthquake characteristics in terms of their frequency content. The models are capable of dealing with the impulsive and convective components of critical hydrodynamic responses. Parametric study is conducted to assess the influence of internal objects on the dynamic responses of partially filled tank vis-à-vis frequency contents of earthquake ground motion. The effect of nonlinearity of sloshing wave on the free and force vibration dynamic responses of tank is studied against those due to linear assumption. Different analytical and numerical models proposed by earlier investigators are used for validation of the developed finite element models. The dissertation also includes experimental investigation of sloshing damping potential of internal objects of various configurations: bottom-mounted vertical baffles, surface-piercing vertical baffles, and bottom-mounted submerged blocks. In addition, a popular soft-computing technique has been tried out for the prediction of sloshing response in different situations

The objective as well as the scope of this dissertation is summarized as follows

1.2 Objective

The objectives of the study may be summarized as follows:

1. To conduct free vibration analysis of linear and nonlinear sloshing
2. To investigate the seismic response of partially filled rigid rectangular tank with submerged internal components
3. To study the effect of frequency content of the earthquake motions on the sloshing response of liquid as well as on the dynamic response of the tank in terms of base shear and overturning base moment
4. To study the effect of internal object on the sloshing response as well as on the base shear and overturning base moment of the tank vis-à-vis the frequency content of seismic motions

5. To conduct an experimental investigation on the slosh damping potential of internal objects of various configurations
6. To study the sloshing prediction capability of ANFIS as a soft computing tool

1.3 Scope of the Present Investigation

The scope of this study is summarized as follows:

1. Finite element method is used as numerical tool for developing both linear and nonlinear sloshing model. The formulaion is based on potential flow with incorporation of artificial surface damping.
2. The tank-submerged block system is assumed to be rigid, thus fluid-structure interaction is neglected.
3. Six ground motions; two from each frequency content category of ground motions are considered and the effect of frequency content on the dynamic response are studied
4. The influence of impulsive and convective response components on the overall dynamic response of tank are studied
5. The experimental study is undertaken in a miniature sized model rectangular tank mounted rigidly to a shake table, capable of producing sinusoidal excitation, to study the slosh damping potential of various configurations of internal objects, namely; bottom-mounted vertical baffle, surface-piercing vertical baffle, and bottom-mounted submerged block.
6. Adaptive neuro-fuzzy inference system (ANFIS) is used to swot the potential of soft computing techniques in predicting sloshing response of liquid in tank.

1.4 Thesis Layout

Following the objectives and scope of the research presented in the previous sections, this section presents the layout of the dissertation and serves as an outline for quick overview of the main contents. The thesis is divided into ten chapters. Each chapter bears an introduction which includes chapter specific relevant literature barring the literature cited in CHAPTER 2, dedicated specifically to the review of literature. The contents of the chapters are briefly described below.

CHAPTER 1 starts with a brief introduction to the thesis and describes the objective and scope of the research.

CHAPTER 2 of the dissertation covers an extensive literature review in the field of liquid sloshing in containers and seismic behaviour of liquid storage tanks. The discussion in this chapter has been held under several subsections relating to the objectives of the research outlined in CHAPTER 1.

In CHAPTER 3, a detail description of mathematical models and finite element formulation is described. Two separate models for linear and nonlinear sloshing in rigid rectangular liquid tanks are formed for use in the subsequennt chapters for numerical simulation.

CHAPTER 4 deals with the free vibration characteristics of sloshing in parially filled liquid tank with submerged internal components. Linear and nonlinear free vibration characteristics are compared.

Findings of this chapter have been presented in:

Nayak, S. K. and Biswal, K. C., 2012, "Dynamic characteristics of rectangular liquid tank with internal component", Fourth International Congress on Computational Mechanics and Simulation", 9-12 Dec 2012, Hyderabad, India.

Biswal, K. C. and Nayak, S. K., 2012, "Nonlinear analysis of sloshing in rigid rectangular tank under harmonic excitation", Fourth International Congress on Computational Mechanics and Simulation", 9-12 Dec 2012, Hyderabad,India.

CHAPTER 5 presents seismic response of partially filled rigid rectangular tank with centrally placed submerged internal block subjected to lateral excitations due to different frequency content earthquake motions. The dynamic responses of the tank in terms of the critical design paramters such as base shear and overturning base moment are evaluated and quantified in terms of impulsive and convective response components.

The work relevant to this chapter has been accepted/ presented for publication in:

Nayak, S.K. and Biswal, K.C., "Quantification of seismic response of partially filled rectangular liquid tank with submerged block", Journal of Earthquake Engineering, DOI: 10.1080/13632469.2013.789457.

Nayak, S. K. and Biswal, K. C., 2012, "Seismic response of partially filled rectangular liquid tank", Fourth International Congress on Computational Mechanics and Simulation", 9-12 Dec 2012,Hyderabad, India. (presented)

CHAPTER 6 describes numerical simulation of the nonlinear seismic response of parially filled rigid rectangular tank subjected to lateral ground motions due to earthquakes of different frequency content. The effects of nonlinear sloshing on the seismic response are discussed.

Findings of this chapter has been accepted for publication in:

Nayak, S.K. and Biswal, K.C., "Quantification of nonlinear seismic response of rectangular liquid tank", Journal of Structural Mechanics and Engineering, DOI: http://dx.doi.org/10.12989/sem.2013.47.5.000

CHAPTER 7 describes numerical simulation of the nonlinear seismic response of parially filled rigid rectangular tank with submerged block subjected to lateral ground motions due to earthquakes of different frequency content. Hydrodynamic response parameters in terms of hydrodanamic pressure, base shear and overturning base moments are evaluted. The effect of submerged component on the dynamic responses vis-à-vis frequency content of ground motions is discussed.

Findings related to the work incorporated in this chapter have been communicated to:

Nayak, S.K. and Biswal, K.C., "Nonlinear seismic response of partially-filled rectangular liquid tank with submerged block due to earthquakes of varying frequency content" Journal of Sound and Vibration, (revised version sent).

CHAPTER 8 is devoted to the experimental investigation of system characteristics such as natural frequency and fluid damping in a model rectangular tank fitted with various configurations of internal objects: bottom-mounted vertical baffles, surface-piercing wall-mounted vertical baffles, and bottom-mounted submerged-blocks. The

main purpose of this chapter is to study the passive damping potential of various configuration of internal objects.

The results relevant to this chapter will be communicated for publication.

Nayak, S.K. and Biswal, K.C., "Fluid damping in rectangular tank fitted with various internal objects - An experimental investigation", Ocean Engineering, (to be Communicated).

Chapter 9 deals with the effectiveness of adaptive neuro-fuzzy inference system (ANFIS) as a soft computing tool to predict the sloshing response of liquid in tank under lateral ground motions due to two earthquakes of different frequency content; one low frequency content and the other high frequency content earthquake. Three models are presented, one each for low and high frequency earthquake, and the third, combined model for both low and high frequency earthquakes.

The results relevant to this chapter will be communicated for publication.

Nayak, S.K., Biswal, K.C. and Mohapatra, S. S., "Prediction of seismic induced sloshing response in partially filled baffled rectangular liquid tank using adaptive neuro-fuzzy inference system", Expert Systems with Applications. (to be communicated)

CHAPTER 10 briefly summarizes the conclusions of this dissertation with an outline of future scope of study.

CHAPTER 2

2 REVIEW OF LITERATURE

2.1 Introduction

An extensive survey of literature pertaining to the objectives outlined in the previous chapter is presented. A historical overview of relevant research works dealing with different aspects of slosh mechanics and seismic behaviour of liquid storage tanks leading to the chapters of this disertation is discussed. Various anlytical and numerical studies used for analysis of sloshing in partially filled liquid container are discussed. Also discussed are the ground motion characteristics as a measure of severity. Discussed alongside are the reported research works on dynamics of liquid storage tanks with submerged internal components.

The survey of literature has been partitioned into several sections in order of their relevance to the present study. They are as follows:

- Seismic performance of liquid storage tanks in historic earthquakes
- Failure mechanisms of liquid tanks
- Ground motion characteristics
- Dynamic analysis of liquid containers
- Related analytical and numerical studies on liquid sloshing
- Dynamics of liquid containers with submerged internal components
- Application of soft computing to engineering problems

2.2 Seismic Performance of Liquid Storage Tanks in Historic Earthquakes

This section describes the seismic performance of liquid containing structures around the world under some of the major historical earthquakes in the last century, and also the first decade of the present century as reported by researchers. The mechanisms leading to the failure of the liquid filled tanks are also discussed. Discussed alongside are the influences of these failures on the related fields of research.

2.2.1 1960, the Great Chilean Earthquake

Measured 9.5 on moment magnitude scale, “The Great Chilean Earthquake” of 22 May 1960 is the most powerful earthquake recorded to date. The temblor caused substantial damage not only to the region close to the epicentre but also the resulting tsunami caused destruction in distant Pacific coastal area. Many elevated concrete tanks failed, or were severely damaged in the earthquake. This was particularly the case where the support system consisted of vertical columns circumferentially disposed, attached by one or more levels of circumferential beams. Failure due to plastic hinges in beams and columns in the circular frames of support structure was common (Priestley et al., 1986).

2.2.2 1964, the Nigata Earthquake

Oil tanks suffered different degrees of damage depending on whether or not the soil was stabilized. Post earthquake fire break resulting from oil tank caused extensive damage to the oil refining facilities. The Niigata earthquake brought liquefaction phenomena and their devastating effects to the attention of engineers and seismologists.

2.2.3 1964, the Great Alaska Earthquake

On March 27, 1964, the Prince William Sound region of Alaska was hit by a great earthquake of magnitude 9.2 M. This earthquake is the second largest earthquake ever recorded in the world after a 9.5 M earthquake in Chile in 1960. Damage to the tanks and other structures in surrounding cities of Anchorage, Valdez, Whittier, Seaward, etc. was extensive. The damage to tanks in all these areas was due to the combined

effect of strong shaking and ground failure; seismic sea wave, and conflagration fuelled by destroyed tank farms (Cooper, 1997). Nikisia, located 210 km from the epicentre was also substantially affected. Whittier being the closest community to the epicentre at 60 km was worst hit (Kachadoorian, 1965).

2.2.4 1979 Imperial Valley Earthquake

On October 15, 1979, the Imperial Valley earthquake occurred on the Imperial fault near the United States-Mexican border. Measured 6.5M in moment magnitude scale, the epicentre of this event was located in northern Mexico. Tragic though, this event provided an opportunity to evaluate the performance of tanks to near field strong ground motions.

About 4 km from the fault and 30 km from the epicentre, two large tanks at Imperial Irrigation District Power plant suffered roof-damage of similar kind. Both tanks were reportedly full at the time of earthquake. The separation of roof from the shell at the roof-shell weld led to the spilling of oil from the tank. Smaller tanks nearby had no significant damage while the largest tank at the site uplifted from the ground. Three tanks at another site suffered significant damage; the most significant damage to one tank was elephant foot buckling over a 90 degree arc, and opposite the buckling arc there was a 10 cm weld separation at the shell bottom plate joint. Minor damages were observed in many tanks which consisted of roof seal damage, broken anti-rotation devices, relief piping damage, grounding cable pull-off, settlement, and strain and swing line damage.

2.2.5 1983, the Coalinga Earthquake

The Coalinga M6.7 earthquake on May 2, 1983 is unique in a way that many large and medium sized tanks were at a very short distance from its epicentre; it provided an opportunity to study the performance of these tanks. Most of the large diameter floating roof oil storage tanks within 6.4 km of epicentre had seal damage with some having pontoon or roof damage. A tank farm about 6 km from epicentre had floating roof damage to two of its tanks which were nearly full. In another site, 5 km of the epicentre, two fully filled oil tanks had splashing or top spillage and some roof secondary seal damage. Designed to AWWA standard D100, one municipal water tank situated at a site approximately 3.2 km did not show any evidence of damage. Most of the affected tanks incurred damage to roof seals while some had broken cast iron valves and fitting, pulled Dresser Couplings, and a minor soil/tank settlement.

Many tanks in spite of being in close proximity to the epicentre did not have much damage as one would expect.

2.2.6 1989 Loma Prieta Earthquake

The 7.0 M Lomaprieta earthquake of October, 17, 1989 caused severe damage to tanks. Numerous reports of damage to liquid storage tanks were due to the Loma Prieta 1989 earthquake (EERI, 1990). This earthquake inflicted significant damage to tanks of different hues namely; concrete tanks, wood tanks, and steel tanks. Some of the most serious damage was at a location far from the epicentre.

Several water tanks were damaged. A 100,000 gallon capacity bolted steel tank in Los Gatos-San Jose underwent elephant foot buckling. In the Los Altos hills, a 1,100,000 gallon, prestressed concrete tank, built of precast concrete panels post-tensioned with wire, failed. A 4-inch vertical crack, created in the tank wall, released the water contents. Earthquake induced ground and water motion considerably damaged a wire-wound post-tensioned concrete tank in the Purisima Hills Water District. Built in 1964, the water tank failed due to collapse of the column supporting the roof slab and the rupture of a panel joint. The 1.1 million gal capacity tank lost its entire content. At the Moss Landing power plant, located approximately 22 km from the epicentre, a 750,000-gallon raw water storage tank suffered from rupture, occurred at the welded seam of the baseplate and shell wall that had reportedly been thinned by corrosion. The tank experienced a rapid loss of water content.

The tanks designed to American Water Works Association (AWWA) standard were found to have performed well. Many oil storage tanks at different terminals suffered heavy damages. The location with more severe damage was a terminal located at Richmond, 108 km away from the epicentre.

2.2.7 1992 Landers Earthquake

Occurred on June 28, 1992, the Landers earthquake measured 7.3 in moment magnitude scale. Centred near a small desert community of Landers, this temblor was the second largest earthquake in California since 1906. Water distribution suffered damage to storage tanks and pipelines which included two collapsed tanks. An unanchored 410, 000 gallon welded steel storage tank, installed in 1979, ruptured at

the base and suffered elephant-foot buckling around the entire perimeter. Erected in 1979 and designed by American Petroleum Institute (API) standard 12B, a 210,000 gallon bolted steel water tank failed due to a combination of elephant's foot buckling and the tearing of the shell at the clean-out door, and the pulling loose of Dresser Couplings on both the inlet and outlet piping (Cooper, 1997). The sloshing and seal damage to large floating roof oil tanks in Los Angeles area, 185 km from Landers was a cause of serious concern.

2.2.8 1994, the Northridge Earthquake

Measuring a magnitude of 6.7, an earthquake occurred in January 17, 1994 with its epicentre located in San Fernando Valley near the community of Northridge. Damage to the liquid storage tanks was extensive. Southern California Water Company had five tank failures, all of which were bolted tanks. The failures are attributed to elephant's foot buckling, resulting in loss of content. Five tanks in Santa Monica Mountains were functionally damaged. Several tanks suffered from collapse of roof. About 20 km from the epicentre, Velencia Water Company lost three tanks and one was damaged. Smaller bolted tanks experienced damage. Roof damage to the water tanks was found to be a common feature of this earthquake.

2.2.9 1999, the Kocaeli Earthquake

Occurred along the North Anatolian Fault on August 17, 1999, the Kocaeli (Izmit) earthquake with a moment magnitude of 7.4 struck north-western Turkey. This near field earthquake caused extensive damage to the liquid storage tanks in the tank farm of the Tüpras refinery and the Petkim petrochemical plant. About 80% of the tanks suffered from various types of failure such as buckling of the supports of elevated tanks, buckling of the tank walls, and elephant foot buckling of the tank wall near the base. Damage to the floating roof system as the consequence of liquid spillage caused fire break which led to significant damage to many tanks. The Habas plant lost two of its three liquefied gas storage tanks to the earthquake (Sezen et al., 2008) imposing heavy financial loss. Majority of the tanks were rendered inoperable due to buckling of tank walls, poor performance of floating roof systems and fire related damages.

2.2.10 2001, Bhuj (India) Earthquake

The Bhuj, India earthquake of January 26, 2001 measuring 7.7 on moment magnitude scale instilled damage in many elevated water tanks. Two of them with reinforced concrete (RC) frame staging collapsed while others suffered damage to their staging (support structures). Majority of these tanks, supported on cylindrical shaft staging, developed circumferential flexural cracks near the base (Dutta et al., 2009).

2.2.11 2010, the Maule, Chile Earthquake

On Saturday, February 27, 2010, at 3:34 a.m. local time, a powerful earthquake struck offshore of the Maule region in central Chile with an intense ground shaking lasting for about 120 seconds. Occurring along the boundary between the Nazca and South American tectonic plates with a moment magnitude of 8.8, this earthquake is tied for the sixth largest event in the historical record since 1900. The Cilean wine industry suffered a heavy loss due to failure of the winery tanks. Constructed of stainless steel, these tanks typically have capacities of 30,000 to 40,000 litres. The industry association of Chilean winemakers estimated that approximately 125 million of litres of wine worth up to $250 million were lost in the earthquake due to the collapse or overturning of storage tanks and the breaking of oak barrels and bottles. Of about 420 standardised type elevated water tanks installed by central Government of Chile and located in the strong earthquake-shaking areas under small rural potable water system, at least 73 tanks completely collapsed. Tank failures were due to inertial overloads.

2.2.12 2010-2011 Christchurch Earthquakes

A series of three crustal earthquakes hit Christchurch in September 2010, February 2011, and June 2011. Some of the water tanks performed well (some roof level damage still occurred), a few very small unanchored wood and steel tanks slid, and several larger pre-stressed concrete tanks had serious damage or failed completely losing all their water contents.

2.2.13 2011, the Great East Japan (Tohoku) Earthquake

On March 11, 2011, the M 9.0 earthquake hit the north-eastern part of Japan, commonly called the Tohoku region of Japan. Followed by tsunami and five

aftershocks, the 2011 Great East Japan (Tohoku) Earthquake caused devastating destruction to human lives, and to the Japanese landscape. It greatly damaged the infrastructure facilities of coastal areas as well as the Tokyo metropolitan area, and was felt across the Pacific Ocean. Liquid storage tanks were no exceptions to this. The damage of the oil storage tanks and hazmat facilities has a different aspect by area. For example, the oil storage tanks and other hazmat facilities damaged mainly by the Tsunami on the pacific coast and the strong ground motion caused the fire in LPG tank area.

Figure 2.1: Elephant foot buckling of broad tank

The tank failures presented over here speaks the volume of the problem only partially. The magnitude of the problems, however, is huge which needs a more detail discussion on the gravity of the problem relating to the failures and damage of tanks during strong earthquake motions. Figurative summary of performances of liquid storage tanks discussed as above is illustrated as follows in Figures 2.1-2.10.

In addition to the damages done to the tanks in the earthquakes described as above in some details, damages to the tanks during other earthquakes are also detailed in

Nielsen and Kiremidjian (1986). These includes: Long Beach, California, March 10, 1933; Kern County, California, July 21, 1952; San Fernando, California, February 9, 1971; Managua, Nicaragua, December 23, 1972; Miyagi-Ken-Oki, Japan, June 12, 1978; and Central Greece, February 24, 1981.

Figure 2.2: Diamond buckling in slender tank

Figure 2.3: Base sliding causing extensive damage to inlet/outlet piping

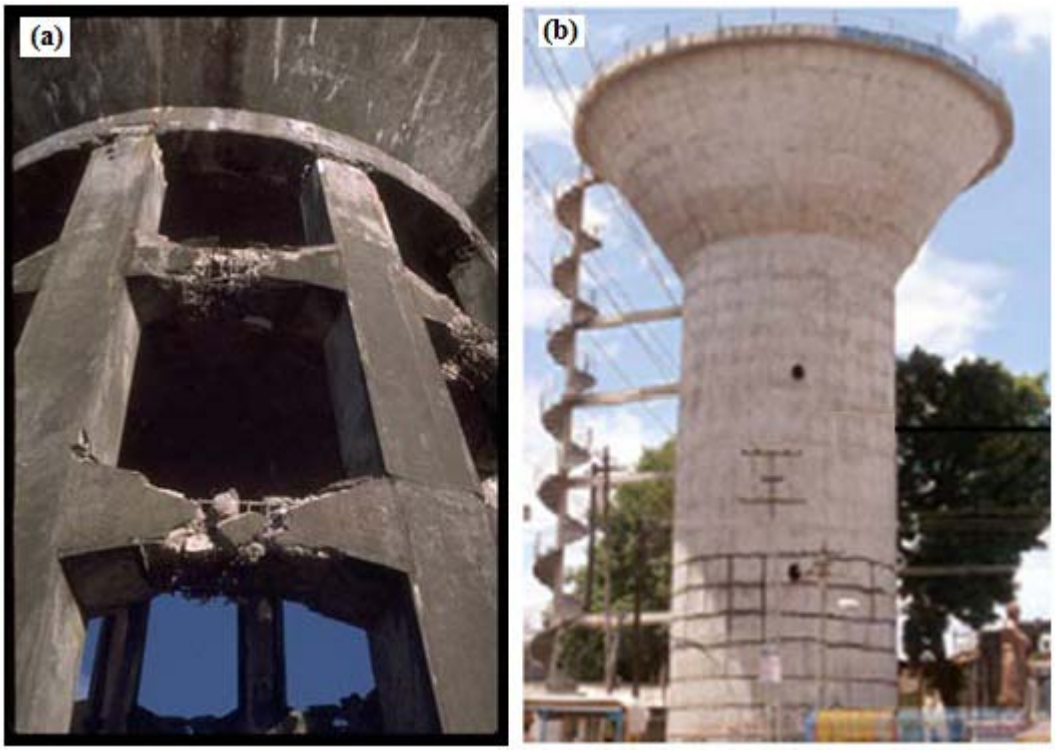

Figure 2.4: Failure to supporting structures: (a) Shear failure in concrete link beam, (b) Flexural cracks in supporting shafts

Figure 2.5: Damaged seals in tanks from sloshing of liquids

Figure 2.6: Implosion failure due to rapid loss of liquid contents

Figure 2.7: Tank pipe connections: (a) Base sliding causing extensive damage to inlet/outlet piping, (b) Flexible connections accommodate horizontal and vertical movements, and prevent pipe breaks

Figure 2.8: Oil tank sloshing spill over the rim (2010 Maule, Chile earthquake)

Figure 2.9: Typical collapsed elevated small steel water tank (2010 Maule, Chile earthquake)

Figure 2.10: Two damaged liquefied oxygen tanks (LOXT) and the undamaged liquefied nitrogen tank (LNT, on the right) at the Habas facility (1999 Kocaeli earthquake).

2.3 Failure Mechanisms of Liquid Tanks

Liquid storage tanks involve various modes of failure mechanisms. Past observations of the seismic performances of the liquid storage tanks have revealed that tank failures are manifested in a wide variety of ways. In fact a wide variety of failure mechanisms are possible, depending upon the configuration of tank geometry, possible fluid-structure-soil interaction, and a lot of other factors such as the tank material, type of support structure, etc. On the other hand, characteristics of earthquakes also significantly influence the response of liquid storage tanks. Failure modes of rectangular tank are significantly different from those of cylindrical, spherical, and conical tanks for that matter. Similarly, the failure patterns for rigid tank considerably differ from those for flexible tanks. Same is the case for on grade, below grade, and above grade or elevated tanks. Different combinations of above possible parameters make the failure mechanism all the more complex.

Liquid storage tanks may be classified into various categories based on their material, location, shape, size, support type and etc. Figure 2.11 shows the generalized classification of tanks as identified for liquid storage tanks.

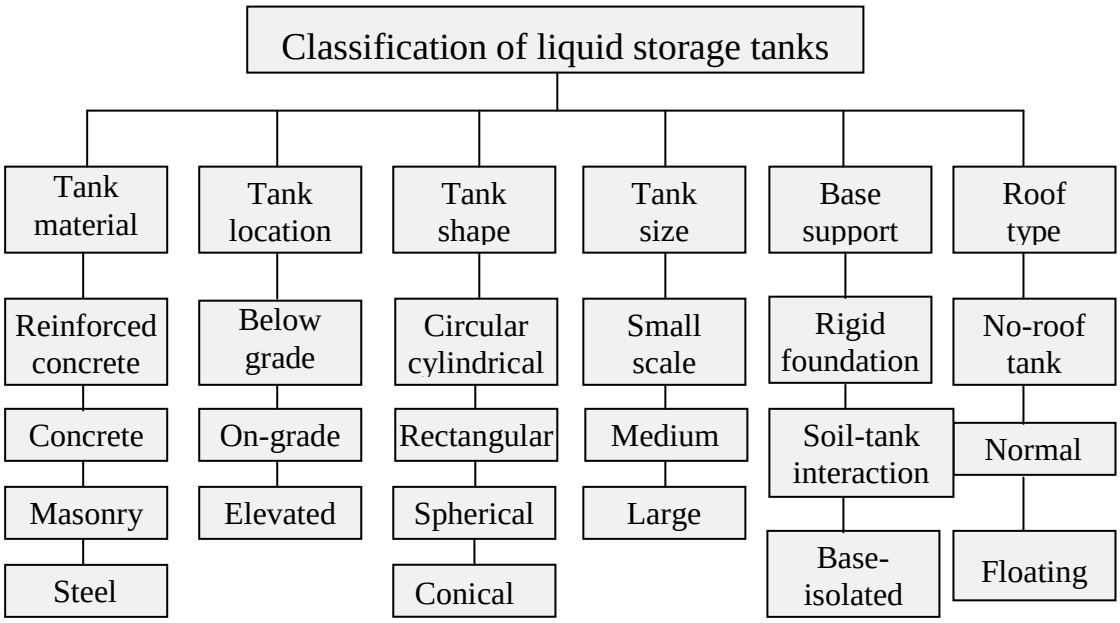

Figure 2.11: Classification liquid storage tanks

Of different types of liquid storage tanks, steel tanks and concrete tanks are very common in lifeline applications. The failure mechanisms of these two types of tanks, based on the research reports on field observations made on the seismic performances of liquid tanks in past earthquakes, are discussed in this section.

Steel tanks have undergone extensive damage during past earthquakes. Manifestation of damage or failure in steel tanks may be in one of the following ways.

2.3.1 Shell Buckling

Shell buckling, a common failure mode in cylindrical tanks, caused by combination of outward pressures generated by vertical motion and excessive axial compressive stresses generated by horizontal motion.

2.3.2 Inlet-outlet Pipe Breaks

This types of damage states are associated with unanchored or partially anchored tanks experience base uplifting. Even an anchored tank may undergo some uplift

during design ground shaking, because the anchors are designed for a fraction of the full elastic moment induced in the tank.

2.3.3 Uplifting of Tanks

Both anchored and unanchored tanks may undergo local uplift when the magnitude of the overturning moments exceeds a critical value. As a result, a strip of the base plate is also lifted from the foundation. Uplifting may cause inlet/outlet pipe break.

2.3.4 Base Sliding

Base sliding can cause extensive damage to inlet/outlet piping unless provisions are made to accommodate vertical and horizontal movements of pipe triggered by base sliding.

2.3.5 Damage to Upper Tank Shell and Roof due to Sloshing

Tanks with insufficient freeboard can be damaged by the violent sloshing of contained liquid. Impacts of sloshing liquid may cause uneven bulging of the roof.

2.3.6 Damage to Floating Roof due to Sloshing

Damages to the floating roofs are manifested mainly in three forms: sloshing induced overtopping of roof; sinking of floating roof; up and down movement of the roof may generate spark causing fire-break in case of inflammable content.

2.3.7 Soil Failure at Tank Site

Soil failure is characterized by ground settlements, lateral spreads, landslides or surface faulting. Ground failure can impose differential movements for attached pipes, leading to pipe failure.

Some of the above failures, although do not cause collapse of the tank, may hamper the functional performance of the tank.

Concrete tanks of different hues have also been reported to have undergone significant damage in previous earthquakes. Of them elevated tanks have been the

worst sufferer. Based on seismic performances study, failure modes of liquid containing concrete tanks are categorized as follows.

2.3.8 Failure of Support Strucure

A typical elevated reinforced liquid tank may have either a frame staging or shaft staging supporting structure. Shear failure in concrete link beam in frame staging type supporting structure, flexural cracks in supporting shafts or columns as the case may be due to overturning moment are the main reasons of failure of elevated concrete tanks.

2.3.9 Failure of Tank Structure Due to Large Inertia Force

Dead load of a concrete tank is considerably more than that of a steel tank of similar capacity, which may give rise to huge inertia force as a result of lateral ground motion. the colums of supporting structure may be subjected to amplified transeverse shear leading to the failure of the support structure.

Besides these, some failures are common to both steel and reinforced conrete tanks; breaking of inlet-outlet pipe due to sliding, damage to the roof structure due to sloshing impact, etc.

2.4 Ground Motion Characteristics

This section presents a brief description of the literatures relating to the importance of ground motion characterization as regard to the structural response.

The simplest way to characterize the ground motions is in terms of peak ground motion parameters or integral parameters. The peak ground motion parameters are peak ground acceleration (PGA), peak ground velocity (PGV) and peak ground displacement (PGD), and peak ground motion ratios PGV/PGA and PGD/PGV. Of these, peak ground acceleration is the parameter most often associated with severity of ground motion. However, examination of recorded seismic events has shown that earthquakes with a very large PGA may not produce appreciable structural damage. Both a short duration impulse of high frequency and long duration impulse of low frequency may have the same peak ground acceleration value, producing very

different response in the structures. This is because, more often than not, the peak acceleration corresponds to high frequencies which are out of the range of the natural frequencies of most structures. Therefore, large values of peak ground acceleration alone can seldom initiate either resonance in the elastic range or be responsible for large scale damage in the inelastic range. The integral parameters such as *Arias intensity*, Spectrum intensity, root mean square acceleration (RMSA), root mean square velocity (RMSV) and root mean square displcement (RMSD), etc. are reportedly more effective for measuring the energy content of the seismic event and hence are the better measures of earthquake destructiveness.

Therefore, different parameters are required to characterize the severity and the damage potential of the earthquake ground motion. In general, these parameters can be grouped into three categories.

- ***Peak Ground Motion***: obtained either directly or with some simple calculation from the digitized and corrected records;
- ***Spectral Values***: obtained from the parametric integration of the equation of motion of elastic and inelastic single-degree-of-freedom systems
- ***Spectral Values***: obtained considering the energy balance equation for elastic and inelastic systems

Anderson and Bertero (1987), Uang and Bertero (1988), and Bertero et al. (1991) have shown that earthquake ground motion attributes such as *frequency content, duration of strong shaking, velocity, displacement, incremental velocity,* and *incremental displacement* can have profound effects on the structural response than the peak ground acceleration, particularly in the inelastic range.

Westergaard (1933) showed that an impulsive pulse acting under a tall building causes a wave of deformations that travels through the building to the top. The wave gets reflected at the top, returns to the base, and gets reflected again. Biggs (1964) found that the pulse amplitude and pulse duration relative to the period of vibration of an SDOF system are the two important parameters controlling its peak elastic response.

Bertero et al. (1976) in his seminal study emphasized the high damage potential of earthquake motions that contained acceleration pulses, introducing the concept of “incremental ground velocity” as a measure of the impulsive character of near-field

motions. Mahin et al. (1976) and Bertero et al. (1978) attributed the structural damage sustained by the Olive View Hospital after the 1971 San Fernando, California, earthquake to the long-duration acceleration pulses rather than the high frequency acceleration spike.

Power et al. (1986) strongly emphasized the importance of frequency content of ground motion in determining the structural response. Duration was found to be significant factor influencing structural inelastic response, although secondary in comparison to the influence of frequency content. In some extreme cases, such as ground motion during 1985 Mexico City earthquake, duration may play a larger role in affecting inelastic structural response.

Anderson and Bertero (1987) studied the response of steel frames subjected to representative ground motions recorded during the 1979 Imperial Valley earthquake. Their results showed that the response of a structure is sensitive to the duration of acceleration pulses relative to the fundamental period of the structure. Rupakhety and Sigbjörnsson (2011), from their investigation of importance of higher modes in the elastic response of tall buildings subjected to near-fault ground motions, found that higher modes contribute significantly to peak interstory drifts at the upper portions of the buildings. The importance of higher modes was larger at the upper portions of the building and increased as the height of the building increased.

Bradley (2011) demonstrated that amplitude, frequency content, and duration of a ground motion are correlated and neglection of ground motion duration in ground motion selection may lead to biased seismic response analyses.

2.5 Dynamic Analysis of Liquid Containers

Extensive research on dynamic response of liquid filled tank traces its origin back to the middle of the last century. Early research pertained to the study of dynamic response of fuel tank in aerospace engineering. The fundamental difference between the dynamic response of the fuel tank in aerospace engineering and those concerning civil engineering structures subject to seismic motion is that the latter is more concerned with much larger tanks for which low frequency range becomes dominant. The dynamic behaviour of liquid storage tanks under random excitations has been the subject of numerous theoretical and experimental investigations.

This section devotes to the review of earlier studies on dynamic response of liquid storage tanks. Major contributions and research implications are briefly summarized therein.

The performance of liquid storage tanks due to seismic mishap is documented in the literature (Hanson, 1973; Berg and Stratta, 1974; Rinnie, 1967). The first solution to the problem of hydrodynamic fluid pressures in liquid filled container was by Westergaard (1933) who determined the pressures on a rectangular vertical dam subject to horizontal acceleration.

One of the earliest studies on dynamic response of liquid filled tank has been reported by Hoskins and Jacobsen (1934) on analytical and experimental investigation of hydrodynamic pressure developed in rectangular tanks under horizontal motion. Jacobsen (1949) and, Jacobsen and Ayre (1949) were among the other contemporary researchers to have worked on similar problems and developed equations for effective hydrodynamic mass and mass moment for the contents of cylindrical tanks subject to horizontal translation.

A more complete analysis of impulsive and convective pressures in rectangular container was proposed by Graham and Rodriguez (1952) in the context of a problem related to the field of aerodynamics. The bahavior of liquid content was simulated by an equivalent multi-degree-freedom mechanical spring-mass system where the different masses and spring stiffnesses represented the contributions of the different sloshing modes of vibration

The aerospace industry has also made important contributions to the research on the dynamic behavior of liquid storage vessels. Baur (1964) developed a comprehensive mathematical model for application in the design of fuel tanks in space vehicles. The study was extended further by Abramson (1966) who thoroughly investigated, both analytically and experimentally, the sloshing problem pertaining to liquid propellants in launching vehicles of satellites and rockets.

Housner (1957, 1963) in his seminal works on the subject of dynamic analysis of liquid storage tanks developed the most commonly used model by using an approximate analysis of the hydrodynamic pressures exerted on the walls of rigid tanks subject to unidirectional horizontal seismic ground motion. In a simplified

procedure, he divided the liquid into two-mass system: a part of the liquid at the bottom of the container moves in unison with the container and behaves the same way as solid material will do while the liquid above it participates in sloshing with a different dynamics having long period of vibration. Thus, the hydrodynamic pressure was divided into two parts; first, the impulsive component caused by the portion of the liquid at the bottom accelerating with the container and the convective component associated with the sloshing liquid. The liquid was assumed to be incompressible and undergo small displacement. Due to its implementational simplicity, it has been adopted in many codes and standards with certain modifications. Later, with some modification, Epstein (1976) presented simplified expressions and curves to estimate bending, overturning moments and maximum free surface displacement.

Edwards (1969) employed the finite element method to the dynamic analysis of liquid storage tanks, and was the first investigator to have considered tank flexibility to establish the hydrodynamic forces exerted on ground supported, cylindrical tanks subject to horizontal earthquake ground motions. The hydrodynamic effect is taken into account as an added mass matrix in the equation of motion of the coupled fluid-structure system. Later, Veletsos (1974) offered a simple procedure for evaluating the hydrodynamic forces induced in liquid filled flexible cylindrical tanks. He assumed single degree of freedom system for the tank such that the cross section of the tank remained circular, and the distribution of deflection along the height of the tank was of a prescribed form.

Veleteos and Yang (1977) used the Rayleigh-Ritz·methbd and presented simplified formulae to obtain the fundamental natural frequencies of both empty and completely filled cylindrical storage tanks. Yang (1976) proposed an analytical method to study the effects of wall flexibility on the pressure distribution in liquid and subsequent forces in the tank structure. The tank was assumed to be a single degree of freedom system vibrating in different modes.

In a different field of similar interest, Chwang and Housner (1978) used Von Kármán's momentum-balance method to investigate the earthquake forces on a rigid dam with an inclined upstream face of constant slope and presented explicit analytical formulae for evaluating the total horizontal, vertical and normal loads along with a useful approximate rule for practical engineers.

Wozniak and Mitchell (1978) proposed an approximate model for the seismic analysis of anchored and unanchored flat bottomed fluid storage tanks, which form the basis of the provisions in the American Petroleum Institute design standard API 650 (1979) Appendix E, and the standard of the American Water Works Association (1984) Appendix A. Later, Leon and Kausel (1986) presented a refinement on the model originally proposed by Wozniak (1978) for the seismic analysis of fluid storage tanks, and demonstrated that use of the rules incorporated in the API 650 code may, in some cases, underestimate the maximum compressive stresses that may develop in both anchored and unanchored tanks.

Ma et al. (1982) proposed an alternative approach which included both acoustic and sloshing interaction of the fluid and the structure, and studied the seismic behaviour of liquid storage tanks. The influence of tank-wall flexibility on the hydrodynamic pressure and sloshing wave height was demonstrated. They used fluid-structure interaction program FLUSTR for implementation of the model. It was observed that proper inclusion of the fluid inertia is of paramount importance in assessing the dynamic characteristics of the fluid-tank system and higher mode sloshing response are important to post-earthquake sloshing analysis.

Haroun (1983) used three full scale water storage tanks and extensively conducted a series of experiments, including free and forced vibration tests, to determine the natural frequencies and mode shapes of vibrations. Of these three tanks, two were permanently installed, equipped with instruments, to record seismic response features in case of possible future earthquakes. This study significantly improved the understanding of dynamic response of fluid storage tanks.

Using classical potential flow approach, Haroun (1984) later presented a detailed analytical method for typical loading systems in the rectangular tanks. Seismically induced hydrodynamic pressure and consequent bending moments were evaluated under the combined action of horizontal as well as vertical components of earthquake excitations. The walls were assumed to behave as elastic plates. The results were compared with those of approximate analyses. Analytical expressions for computation of both the loads and associated internal moments were also presented. Presented along were the numerical values of the ready-to-use moment coefficients for computation of design moments.

Haroun and Tayel (1985a) developed a simple and computationally effective composite theoretical model for evaluation of the axisymmetrical dynamic characteristics of ground-supported, partially-filled cylindrical liquid storage tanks under vertical earthquake excitations. The composite scheme, involving analytical treatment of liquid region and finite element modelling of the cylindrical shell, discretized into a number of ring elements, substantially brought down the number of unknowns compared to those analyses where both tank wall and liquid are subdivided into finite elements. The interaction between the shell and fluid was rigorously treated in the method. The steps in the procedure involved; analytical evaluation of hydrodynamic pressure through series solution of pressure equation derived for fluid; determination of added mass matrix due to fluid motion from the expression of the work done by the liquid-shell interface forces; and analysis of the motion of the tank wall by introducing the additional mass matrix, representing the effect of liquid dynamic pressure during vibration, in the matrix equation of shell motion. The method was analytically validated. Based on the results, a simplified formula was developed to calculate the fundamental natural frequency of the liquid shell system.

Shortly after, Haroun and Tayel (1985b) offered an analytical method for the computation of the axisymmetrical dynamic characteristics of partly filled cylindrical tanks. Two partial differential equations governing the shell motion: one of the second order governing the dynamic equilibrium in the axial direction, and the other of the fourth order governing the dynamic equilibrium in the radial direction, were solved subject to twelve boundary and compatibility conditions. The results were validated with those obtained numerically.

Veletsos and Tang (1986) proposed an approximate analysis by employing Galerkin method to study the effect of soil-structure interaction on the dynamic response of vertically excited, upright, circular cylindrical liquid storage tanks; and evaluated critical design forces for both rigidly and flexibly supported tanks. The tank-liquid system was assumed to respond as a fixed-base, single-degree-of-freedom system. It was shown that soil-structure interaction reduced the hydrodynamic effects which were attributed to the damping that stemmed exclusively from the radiational energy dissipation capacity of supporting medium as the liquid-tank system was presumed to be undamped in the solution and no material damping was considered for the

supporting medium. On the other hand, the consequence of such interaction was approximated by a change in the fundamental natural frequency of the tank-liquid system and by an increase in damping.

Soon after, Veletsos and Tang (1987) formulated exact solutions for the impulsive and convective components of the response of liquid containing, upright circular cylindrical tanks to a rocking base motion of arbitrary temporal variation. Both rigid and flexible tanks are examined. The interrelationship of the responses of a tank to rocking and lateral base motions of the same temporal variation is established. It is shown that several components of the response for the tank in rocking may be evaluated from existing data concerning its response to a lateral excitation. Additionally, they generalized the well-known mechanical model for a laterally excited tank to permit consideration of the effects of base rocking.

Park et al. (1990) conducted a time-domain study for investigation of fluid-structure interaction effect on the sloshing and hydrodynamic pressure in a flexible rectangular container by employing a coupled boundary element-finite element technique. The fluid domain, governed by Laplace equation, was modelled by boundary element method while the container structure was modelled by finite element method. On presumed small amplitude sloshing, the free surface boundary conditions were linearized. With velocities as principal unknowns, a direct integration scheme was used to facilitate coupling between the fluid and structure. It was shown that flexibility of container significantly amplified the hydrodynamic pressure and excited the higher sloshing modes, thus might require nonlinear analysis.

Haroun and Abou-Izzeddine (1992) conducted a comprehensive parametric study on the effects and relative importance of a few factors influencing the seismic response of ground-based tank supported on deformable soils under horizontal ground motion. They used analytical mechanical models for flexible cylindrical tank with a lumped-parameters idealization of foundation soil. The effect of rigid-base rocking motion and lateral translation were also accounted for in the model. The tank responses were observed to be magnified due to the tank-soil interaction, and such magnification was higher in case of soft soils as well as tall tanks.

Later, Taniguchi (2004) proposed an analytical method to adequately compute the rocking behavior of an unanchored flat-bottom cylindrical shell tank under the action of horizontal base excitation. The necessity of rock-translation interaction for evaluation of rocking response of tank is highlighted. The theory of initiation and sustenance of rocking motion is elegantly explained. The proposed method is expanded by employing an assumption of the effective moment inertia of liquid for rocking motion. The applicability of the method is corroborated through comparison of analytical results with the experimental ones. It is shown that the rocking action drastically reduces the base shear.

Following a similar procedure as in Haroun and Abou-Izzeddine (1992a), Haroun and Abou-Izzeddine (1992b) dealt with the seismic response of ground-based elastic tank supported on a rigid base (solid concrete slab) subject to a vertical excitation, taking into account shell-liquid-soil interaction. They observed that interaction of tank and foundation soil reduced critical responses of tank, and the magnitude of the reduction was a function of the soil shear-wave velocity as well as tank geometric properties, more specifically the ratio of the liquid depth to the radius of the tank and the ratio of the shell thickness to the radius of the tank. This observation is in contradiction with many of the earlier studies.

Tang (1993), in a comprehensive study of dynamic response of cylindrical tanks with two liquids under horizontal excitation, presented an exact solution for rigid tanks containing two liquids under horizontal excitation with an arbitrary temporal variation. It is shown that for tank containing two liquids, sloshing frequencies and wave heights are functions of liquid densities whereas in case of tank with one liquid it is not.

Tang (1994a) used Raleigh-Ritz procedure in combination with Lagrange's equation and presented an analytical solution for computation of natural frequencies of tank containing two liquids. It is shown that the dynamic response of tank with two liquid is controlled by six parameters instead of four for tank with single liquid. A simple approximate equation is proposed for evaluation of fundamental frequency of tank with two liquids.

Later, Tang (1994b) presented an exact solution for dynamic response of tanks containing two liquids under rocking base motion. Only rigid tanks were considered in the study. It is found that many response quantities for a tank in rocking motion may be evaluated from the corresponding response quantities for an identical tank excited laterally; in particular all the convective components of the response quantities can be evaluated.

Based on Raleigh-Ritz method, later, Kim et al. (1996) developed a 3-D approximate analytical solution procedure to evaluate dynamic response characteristics of partially filled flexible rectangular fluid containers under horizontal or vertical ground excitation. To arrive at the solution, the motion of the side wall was assumed to be a linear combination of vibration modes of the plate with suitable boundary conditions as admissible functions. 2-D methods were derived from corresponding 3- D analysis methods as particular cases. Flexibility of two walls parallel to the direction of horizontal excitation was not accounted for in the solution. Both 2-D and 3-D analysis results showed that dynamic fluid pressure could be greatly amplified due to wall flexibility.

Chen et al. (1996) presented an innovative method by way of an implicit finite difference approach to simulate large-amplitude sloshing motion in two-dimensional containers subjected to earthquake base excitations. The partial differential equation, defining the non-linear liquid sloshing problem which includes a free-moving surface, was transformed into a computational domain using a curvilinear co-ordinate system so that fixed and rectangular grids were obtained for spatial finite difference discretizations. The Crank-Nicolson time marching scheme was employed and the resulting finite difference algorithm is unconditionally stable and very lightly damped with respect to the temporal co-ordinate. A second-order numerical dissipation term was added to the system to filter out the spurious high-frequency waves caused by large convection. An upward shifting of sloshing amplitude and the the extent of period elongation was observed from numerical simulation. The linear theory was found to be generally non-conservative in the sloshing amplitude but was reasonably accurate in predicting peak hydrodynamic forces. However, the non-conservativeness of the linear theory in predicting the secondary peaks of the hydrodynamic forces ought to be taken into consideration in design in order to avoid the cumulative

structural damage caused by the repeated excursions of the hydrodynamic forces over the linear prediction.

Dogangun et al. (1996) developed finite element program for liquid domain by using a three dimensional isoparametric Lagrangian finite element which included compressibility, neglected otherwise in most of other studies, and sloshing motion; which was then incorporated into a general purpose structural analysis program SAPIV to investigate the static and seismic behaviour of rectangular liquid storage tanks. Use of Lagrangian fluid element automatically satisfied the equilibrium as well as the compatibility conditions at the finite element nodes along the fluid-structure interface because displacement was the unknown field variable common to both the elements. Hydrodynamic pressure in flexible tanks was found to be larger than that of rigid tanks.

Younan and Veletsos (1998) proposed a simple, approximate method for analysis of the dynamic responses to horizontal base shaking of vertical, rigid circular cylindrical tanks containing a uniform viscoelastic material. Approximate expressions for the critical responses were formulated for elucidation of the response of the system and the effects and relative importance of the various parameters involved. In a companion study, Veletsos and Younan (1998) extended the procedure and studied the effects of tank wall flexibility.

Malhotra (2000) presented the theoretical background of a simplified seismic design procedure, adopted in Eurocode 8, for cylindrical-ground supported tanks of two configurations: flexible steel and concrete tanks. Both impulsive and convective actions of liquid are taken into account in the procedure. By using the site response spectra and performing a few simple calculations, the seismic response parameters are calculated. This procedure is based on the works of Veletsos and Yang (1977), Veletsos (1984), and Veletsos et al. (1990).

Peek and El-Bkaily (1997) presented a refined general mechanical model by way of introducing the action of eccentric gravity loads also called p-Δ effect, from the beginning of the derivation of fully nonlinear formulation of the fluid structure-interaction problem, and then omitting only terms that are of higher order in the amplitude of motion. They questioned the introduction of p-Δ effect into the

mechanical model after derivation of the formulation, which results in wrong equation of motion. A general approach to obtain the properties of the equivalent mechanical model for a container of any shape is also described.

Hamdan (2000) presented a critical review on the behaviour and design guidelines of cylindrical steel liquid storage tanks subjected to earthquake motion. He attempted at assessing the various codes by comparing their predictions with field observations, finite element analyses and published experimental results. Based on field observations, the performance of steel versus concrete tanks is highlighted. Questions were raised on accuracy of predictions of many design parameters with suggestions of areas where future work should be oriented.

Virella (2003) investigated the influence of a fixed roof on the natural periods of vibrations of thin-walled aboveground steel tanks with clamped base. Both self supported and rafter supported roof geometries of various configurations were considered in the study. It was found that the vibration of empty tanks with a fixed roof is dictated either by cylinder modes or roof modes of vibrations. For self-supported roofs predominant roof modes resulted, whereas for tanks with roofs supported by rafters, cylinder modes dominate the dynamic behavior of the tank. Roof dominant modes had natural periods that remain constant regardless of the aspect ratio considered. Cylinder modes, on the other hand, were characterized by natural periods that showed a linear dependence with the aspect ratio of the tank.

Chen and Kianoush (2005) used the sequential method also referred to as weakly-coupled method to evaluate hydrodynamic pressure in two-dimensional rectangular tanks including wall flexibility effects. Sloshing motion of liquid, however, was ignored. In sequential method, the coupling of the fluid and the structural domain is effected by applying the hydrodynamic pressure obtained from the solution of fluid domain as force on the wall of the tank for the solution of the structural domain, the process is repeated in each time step till the analysis is complete. Comparative study for rigid tank showed that Housner's lumped mass approach significantly overestimated the base shear and base moment. In their subsequent work, Kianoush and Chen (2006), following the same procedure, investigated the response of concrete rectangular liquid storage tanks in two-dimensional space subjected to vertical ground

acceleration. It was shown that the response of the tank to vertical motion can be significant.

Kinoush et al. (2006) introduced a new method referred to as staggered method for seismic analysis of containers in three-dimensional space in time-domain. Both impulsive and convective components of hydrodynamic responses are accounted for. Behaviour of concrete rectangular container was investigated subject to scaled horizontal and vertical earthquake motion. Compared to Housner's model, these results show that in most cases the lumped mass approach overestimates the base shear and base moment significantly. Also, it is shown that although vertical excitation leads to a significant response in the container, yet the combined effect of horizontal and vertical excitations reduces the response of the structure in the considered system.

Contrary to the common assumption of cantilever beam for the cylindrical tank shell made by the researchers, Virella et al. (2006) represented roof and walls as shell elements and studied the fundamental impulsive modes of vibration of cylindrical tank-liquid systems anchored to the foundation under horizontal motion. Two different techniques were used: added mass formulation and acoustic finite element. A general purpose finite element program ANSYS was used to perform the analyses. It was concluded that the fundamental mode for the tank-liquid systems is a bending mode (n = 1), regardless of the height-to-tank diameter ratios (H/D) considered in their study. The largest natural periods are associated with cylinder modes characterized by circumferential waves n > 1 and axial half-wave m = 1. However, these modes are not the fundamental modes for predicting the response to a horizontal base motion, in the sense that they do not have the largest modal participation factors. The fundamental modes of tank models with aspect ratios (H/D) larger than 0.63 were very similar to the first mode of a cantilever beam. For the shortest tank (H/D = 0.40), the fundamental mode was a bending mode with a circumferential wave n = 1 and an axial half-wave (m) characterized by a bulge formed near the mid-height of the cylinder.

Herna´ndez-Barrios et al. (2007) proposed a numerical method based on finite difference scheme in cylindrical coordinates for the nonlinear seismic response analysis of cylindrical tanks. The equations of motion in cylindrical coordinates were

transformed from the physical domain into a computational domain by means of a change of variable. Nonlinear responses were computed by two schemes; semi-implicit and Crank-Nicholson schemes. The semi-implicit scheme was found not to be stable for most of ground motion excitations used in the study. On the other hand, the Crank-Nicholson scheme was found to be stable for all of the ground motion records used, except for the case of resonance. Of the two types of damping tried out, the pseudo-viscous damping produced better result than an explicit numerical damping. The results indicated a typical nonlinear behaviour in which the positive wave amplitudes were larger than the negative ones, besides an elongation of the oscillation period.

Chen et al. (2007) conducted a nonlinear three-dimensional numerical study on the sloshing behaviours of cylindrical and rectangular liquid tanks under the assumption that the tanks were rigid and firmly fixed to the ground. the liquid was assumed to be incompressible, inviscid, and irrotational. Boundary element method with Taylor series expansion was employed to simulate three-dimensional nonlinear sloshing behaviour for calculation of transient wave elevation. Isoparametric quadrilateral linear elements are used to mesh the boundary of the tank, and the second-order TSE with the Eulerian–Lagrangian description is adopted to trace the location of the free surface. The sloshing response was studied under harmonic as well as recorded earthquake excitation. The results were experimentlly verified by small scale model test. It was observed that linear model cannot treat the resonant excitation, if the forced frequency was equal or close to the natural frequency of the liquid.

Livaoglu (2008) adopted a simple seismic analysis procedure to evaluate the dynamic behaviour of fluid–rectangular tank–foundation system. The interaction effects were studied by Housner's two mass approximations for fluid and the cone model for soil foundation system. The results showed that the displacements and base shear forces generally decreased, with decreasing soil stiffness. However, embedment, wall flexibility, and soil–structure interaction (SSI) did not considerably affect the sloshing displacement.

Ghaemmaghami and Kianoush (2010) introduced a finite element model for the analysis of dynamic behavior of partially filled rectangular fluid container in two-dimensional space under both horizontal and vertical ground excitations of 1940 El-

Centro record. Fluid-structure interaction effects on the dynamic response of fluid containers are taken into account incorporating wall flexibility. The damping effects due to impulsive and convective components of the stored liquid are modeled using the Rayleigh method. Two different configurations including shallow and tall tank models are considered to investigate the effect of geometry on the response of the liquid-structure system. Effect of wall flexibility on the overall dynamic response of system is investigated by comparing the results between rigid and flexible models. The results showed that the impulsive components of base shear and base moment increased with due to flexibility of the tank walls. The convective response, however is almost independent of the flexibility of the wall.

Chen and Kianoush (2009) proposed a simplified method using the generalized single degree of freedom (SDOF) system for seismic analysis and design of concrete rectangular liquid storage tanks. Only impulsive hydrodynamic dynamic pressure was considered in this study. The consistent mass and the effect of flexibility of a tank wall on hydrodynamic pressures were considered. A shape functions representing the first five mode shapes for the cantilever wall boundary condition was proposed for the analysis. The appropriateness of the proposed shape functions was established through validation of results. It was concluded that the inclusion of the first two modes could provide sufficiently accurate results.

Alembagheri and Estekanchi (2011) studied the seismic response of unanchored steel liquid storage tanks investigated using the endurance time (ET) dynamic analysis procedure and compared to responses obtained for anchored tanks under actual ground motions and intensifying ET records. The reliability of ET method for estimation of the responses of unanchored tanks on rigid and flexible support at different levels of excitation was established.

Kianoush and Ghaemmaghami (2011) studied the effect of frequency content of ground motions on the dynamic response of partially filled concrete rectangular tanks considering fluid–tank–soil interaction. Finite element method in three dimensional space was used in the study and the coupled fluid-structure equations were solved using the direct integral method in time domain. Two different tank configurations were used to study the effect of tank geometry. The sloshing behavior was simulated using linear free surface boundary condition. A simple model with viscous boundary

was used to include deformable foundation effects as a linear elastic medium. This method is capable of considering both impulsive and convective responses of liquid-tank system. The results showed that convective response component is almost independent of variations of flexibility of the foundation and seemed to be related to geometric configurations of tank, earthquake characteristics and liquid properties.

Mirzabozorg et al. (2012) made use of staggered displacement method to study the seismic response of coupled liquid-tank system in three-dimensional space, subjected to an artificial as well as a three components earthquake ground motion, in time domain considering the surface sloshing effects. Appropriate damping values were applied on both convective and impulsive components. Finite element method was used to solve the tank-liquid system. The resulted responses are compared with those obtained from the ABAQUS finite element software. The highlight of the observation was that including the convective term may leads to increase or decrease of the responses due to different phases of the convective and impulsive components in the liquid domain.

Bouaanani et al. (2012) developed a new formulation referrd to as substructuring method to investigate the seismic response of symmetric and asymmetric (geometric as well as material asymmetry) rectangular liquid-containing structures. In the proposed method, the flexible liquid-containing structure is modeled using finite elements, while the impulsive effects of the fluid domain are modeled analytically through interaction forces at the fluid-structure interfaces. The technique takes account of geometrical or material asymmetry of the liquid-containing structure, fluid compressibility, and energy dissipation through reservoir-bottom absorption. The effects of geometrical and material asymmetry on the dynamic responses of liquid-containing structures was highlighted through illustrative examples.

Researches have also been directed towards the developments of effective control mechanism for seismic response of liquid storage tank. Response control through base isolation in is one such area. Kim and Lee (1995), Malhotra (1997a, 1997b), Shenton and Hampton (1999), Park et al. (2000), Wang et al. (2001), Shrimali and Jangid (2002a and 2002b), Panchal and Jangid (2008,2011,2011), Almazan et al. (2007), Shekari et al. (2009) and Ruifu et al. (2011) studied the effects of base isolation on the seismic response of liquid storage tanks.

Tung and Kiremidjian (1991), El Damatty et al. (1997a and 1997b), Shenton and Hampton (1999), Sweedan and El Damatty (2003 and 2005), Shrimali and Jangid (2003), Livaoglu and Dogangun (2006), Sezen et al. (2008), Curadelli et al. (2010) and Omidinasab and Shakib (2012) conducted studies on elevated water tanks.

Veletsos and Tang (1990), Veletsos et al. (1992), Haroun and Abou-Izzeddine (1992a and 1992b), Malhotra (1997c), Chatterjee and Basu (2001 and 2004), Cho et al. (2004), Livaoglu and Dogangun (2006), Larkin (2008) and Dutta et al. (2004, 2009) conducted studies on the effects of soil structure interaction (SSI) on the response of liquid containing tanks.

2.6 Related Analytical and Numerical Studies

Early simulations pertaining to liquid sloshing problems have mostly been performed with waves of small steepness. This allows the boundary conditions to be applied on the quiescent free surface rather than on its instantaneous location, which usually varies with time. With this simplification, the linear theory has been used widely for modeling the sloshing problems.

Although the linear theory has been used widely as a practical technique, an attention must be given to the inherent non-linear characteristics of the liquid when the amplitude of external excitation to the container is high or the frequency of such excitation is close to one of the fundamental sloshing frequencies. To accommodate this concern, later, many researchers have worked on the nonlinear sloshing problems.

This section discusses the literatures relating to both linear and nonlinear sloshing problems in various fields of applications.

Li et al. (1981) presenteded a method which was a combination of separation of variables and finite element method for computing the oscillating modes of liquid in a rigid cylindrical container. By the use of normal mode expansion, a second order differential equation was obtained for each mode. Seismic responses in terms of free surface elevation, hydrodynamic pressure, and velocity fields in the container were computed by superposition of modal responses. The study demonstrated that the container vertical acceleration was of secondary importance in determining the free

surface displacement, but had a significant effect on the pressure load on the container boundaries.

Kobayashi et al. (1989) conducted experimental and analytical studies to compute the liquid natural frequencies and the resultant slosh forces in horizontal cylindrical tanks. An effective calculation method of the small- amplitude slosh response was presented by substituting an equivalent rectangular tank for a horizontal cylindrical tank. The calculated natural frequencies, slosh wave height for longitudinal and transverse excitation were supported by experimental results. The study reported that longitudinal and transverse slosh responses were independent of each other and no effect of the vertical excitation on the slosh response was observed. The two-dimensional sloshing of a fluid in a horizontal circular cylindrical container and the three-dimensional sloshing of a fluid in a spherical container were considered by McIver (1989). The linearized theory of water waves was used to determine the frequencies of free oscillations under gravity. Two dimensional bipolar coordinates and toroidal coordinates were used respectively, for the cylindrical and spherical containers and the eigenvalue problems were formulated in terms of homogeneous integral equations which were solved numerically for the eigenvalues.

Willams and Moubayed (1990) employed boundary integral method to estimate the hydrodynamic pressure distribution on a rigid submerged cylindrical storage tank subjected to horizontal or vertical harmonic ground acceleration. The fluid was assumed to be linearly compressible and to undergo small-amplitude, irrotational motion. An axisymmetric Green's function was used to reduce the integral over the structural surface to a line integral over the generating curve of the body.

Veletsos and Shivakumar (1993) examined free vibrational characteristics and the surface sloshing action of multi-layered liquids in rigid cylindrical and long rectangular tanks. The analysis was formulated for systems with superimposed layers of different thicknesses and densities. Tokuda et al. (1995) developed a sloshing analysis method using an existing FEM structural analysis code based on the fundamental equation analogy relating elasticity equations to pressure wave equations of fluid. The effectiveness of the method was verified through the numerical examples of simple sloshing problems in a rigid cubic tank and fluid vibration in U and V-tubes under gravitational force. Shivakumar and Veletsos (1995) studied the dynamic

response of a rigid cylindrical tank containing an inviscid liquid with continuous vertical variation in density. The free vibrational sloshing characteristics of the liquid, vertical displacements at the free surface, and impulsive and convective components of the hydrodynamic wall pressures were computed assuming the liquid density to decay exponentially from the top to the bottom of the container.

Armenio and Rocca (1996) employed two mathematical models, i.e., Reynolds Averaged Navier Equations (RANSE) and Shallow Water Equation (SWE) for the analysis of sloshing of water in rectangular open tank. The RANSE were solved using a modified form of the well established MAC method (SIMAC) and able to treat both the free surface motion and viscous stresses over the rigid walls. The shallow water equations were solved by means of a simple algorithm (CE-SE) which could deal with large impacting waves over the tank walls. In their findings, RANSE provided more accurate solutions than SWE for small or moderate amplitude of excitation. A fairly good estimate of the sloshing induced wave due to large excitation was obtained using the SWE.

The sloshing phenomenon of a liquid in a rigid vertical cylindrical tank of arbitrary section was addressed by Isaacson and Ryu (1998). The tank system was subjected to both harmonic and irregular base excitation. The solution of the boundary value problem for the case of an inviscid fluid and a harmonic base motion was based on an eigenfunction expansion method. A set of boundary integral equations involving a suitable Green's function was solved for each mode. The solution was extended to the case of energy dissipation of a real fluid, that occurred at the free surface. Further extensions to a stationary random base motion, the time-domain response to a specified base acceleration record, and the estimation of the maximum forces using a modal analysis and involving earthquake response spectra were reported in their studies.

Moiseev (1958) investigated the non-linear sloshing in a container of arbitrary shape employing a perturbation method and characteristic functions. But it was difficult to use his theory for practical purposes. Dodge et al. (1965) proposed a non-linear analytical and experimental study of liquid sloshing in a longitudinally excited, rigid circular cylindrical tank. Abramson (1966) presented some experimental results for non-linear lateral sloshing in rigid containers. The container configurations were

circular cylindrical, 90-degree sector cylindrical and spherical. Theoretical prediction of non-linear sloshing responses in circular cylindrical container was presented.

Harlow and Welch (1966) analyzed large amplitude free surface motions of an incompressible and viscous fluid by solving the Navier-Stokes equations using a marker and cell method. In this method, full Navier-Stokes equations were written in finite difference form and a set of marker particles, which moved with the fluid, was introduced.

Faltinsen (1974) applied the ideas suggested by Moiseev to the sloshing in rectangular tanks subjected to horizontal or pitching excitation. The author formulated the problems as a non-linear, initial-boundary value problem with reference to the inertial co-ordinate system, and solved the problem by the use of the perturbation method, assuming the excitation amplitude to be small. The steady-state solution was compared with the experimental data in the case of the pitching excitation. The stability of the steady-state solution was also examined in the study. Longuet-Huggins and Cokelet (1976) developed a numerical technique to study the non-linear, unsteady free surface waves. At each time step an integral equation was solved for the new normal component of velocity. The free surface was represented by marked Lagrangian fluid particles, but solution technique was neither exclusively Lagrangian nor Eulerian. Assuming periodic waves, they were able to simulate propagating steep Stoke's waves, as well as realistic overturning and plunging of the wave crest when an asymmetric surface pressure was applied.

Faltinsen (1978) presented a numerical method for the study of sloshing in tanks with two-dimensional flow. The solution satisfied the non-linear free-surface conditions. The method was generalized for different tank shapes and the forced irregular oscillation of any type of motion. But the author only presented the case of rectangular tank oscillating with forced harmonic sway oscillation. Nakayama and Washizu (1980) studied the non-linear oscillation of an inviscid, incompressible fluid in a two-dimensional, rigid, open container, subjected to forced pitching oscillation. The governing equations for the liquid motion were formulated as a non-linear initial-boundary value problem with reference to the co-ordinate system fixed to the container, assuming the liquid motion to be irrotational. A pseudo-variational

principle was introduced for the problem and was discretized by finite element method. An incremental method was used for the numerical analysis.

Nakayama and Washizu (1981) applied the boundary element method to the analysis of non-linear sloshing problems in a container subjected to forced oscillations. The governing equation, (Laplace equation) and the boundary conditions, except the dynamic boundary condition on the free surface, were transformed into an integral equation by applying Green's formula. Galerkin method was used to reduce the boundary condition to a weighted residual equation. Two equations thus obtained were discretized by the use of finite element technique in the spatial domain and the finite difference method in the time domain. Collocation method was employed for the discretization of the integral equation. Komatsu (1987) proposed a numerical method based on perturbation technique to study the non-linear behaviour of liquid in rigid tanks with arbitrary geometries. The formulation employed the orthogonality of the linear mode shape and the numerical perturbation technique. The validity of the method was demonstrated through numerical examples of tanks with regular geometries.

Dommermuth and Yue (1987) developed a numerical method for non-linear three-dimensional but axisymmetric free-surface problems using a mixed Eulerian-Lagragian scheme under the assumption of potential flow. Rankine ring sources were used in a Green's theorem boundary-integral formulation to solve the field equation and the free surface was then updated in time following Lagrangian points. The need for artificial smoothing was eliminated by using regridding algorithm to remove the instabilities arising due to singularity at the intersection of body surface and free surface boundary. Later, Dommermuth et al. (1988) carried out experiments and computations to study the steep and overturning gravity waves produced by a piston wavemaker in a tank. The non-linear potential theory computations for a plunging beaker were found to be comparable with experimental results for the surface elevations, and horizontal and vertical velocities at various depths.

A non-linear, dispersive and dissipative model was developed by Lepelletier and Raichlen (1988) to describe the fluid motion in a rectangular tank, which was moved by an oscillatory and transient translational motion. The authors also conducted the experiment to validate the numerical results. Kana (1989) developed a combined

spherical and linear pendulum system to produce the same dynamic in-line and cross-axis reaction weight as liquid exhibiting rotary liquid slosh. An approximate solution of the dynamic equations for the spherical pendulum was used along with cross-axis weight measurements from slosh experiments to develop mass and damping parameters for the spherical pendulum. Similar measurements of in-line weight responses were used to develop the corresponding parameters for the linear pendulum solution. The spherical pendulum solution was verified by comparing the approximate solutions with those predicted by a time-step integration of the non-linear governing equations.

Hwang et al. (1992) presented a three-dimensional numerical simulation for the computation of sloshing loads in liquid tanks by the panel method based on the boundary integral technique. Numerical examples for the case of a partially filled spherical tank, oscillating in harmonic mode or pitch mode were solved. An arbitrary Lagrangian-Eulerian boundary element method (ALE-BEM) was used by Liu and Huang (1994) to analyze the large amplitude problems. The free surface nodes moved in an ALE manner so that element distortions were avoided. The authors introduced the concept of critical amplitude, which enabled to distinguish between the small and large amplitude sloshing. Waterhouse (1994) studied the oscillation of a liquid filled tank at a near-resonant frequency and demonstrated that the slosh response changed from a hard spring to soft spring response as the depth passed through a critical value.

Wu and Taylor (1994) addressed a two-dimensional nonlinear time domain free surface flow problem. The authors used the potential flow theory. The governing differential equations were satisfied through a variational statement. Both conventional and mixed finite element methods were employed. The former was based on the velocity potential, approximated by means of shape functions. A variational statement was used to arrive at the solution, and the velocity was obtained by the Galerkin method. In the latter, both the velocity potential and velocity itself were expressed in terms of the shape functions and both appeared in the variational statement. The advantages and disadvantages of both formulations were discussed.

Later, Wu and Taylor (1995) used two numerical methods to solve the two-dimensional non-linear free surface problem. One was based on the boundary element method in complex plane. The complex potential was assumed to vary linearly within

each element and solution was obtained by imposing the boundary conditions at the nodes of the elements. The other approach was based on the finite element formulation. The solution was obtained by the Galerkin method. Numerical results were shown for the wave elevation generated by a vertical piston-type wave maker. Romero and Ingber (1995) presented a numerical model for simulating the transient nonlinear behavior of 2-D viscous sloshing flows in rectangular containers subjected to arbitrary horizontal accelerations. Based on potential-flow theory, the formulation used Rayleigh damping to approximate the effects of viscosity. Lagrangian node movement was used to accommodate violent sloshing motions. A boundary element approach is used to efficiently handle the time-changing fluid geometry. Additionally, a corrected equation was presented for the constsaint condition relating normal and tangential derivatives of the velocity potential where the fluid free surface meets the rigid container wall. The accuracy of the model was verified with the previously published analytical and numerical results.

Celebi et al. (1998) investigated transient and steady state non-linear free surface waves and wave-body interactions in a 3-dimensional Numerical Wave Tank. Wu et al. (1998) analyzed the sloshing waves in a three dimensional tank using a finite element method based on the fully non-linear wave potential theory. Two and three-dimensional motions of the tank were considered in the analysis. Chen and Chiang (1999) studied the problem of sloshing in a simple two-dimensional rectangular tank with rigid wall, subjected to simultaneous action of horizontal and vertical ground accelerations, in order to investigate the concepts of fully nonlinear and complete dimensional analysis. The fluid is assumed to be inviscid and incompressible, and the flow is irrotational. The Euler equations as well as the nonlinear, kinematic free-surface boundary condition are used in the analysis. A time-independent finite difference method is used to evaluate the velocity fields and the surface profile of the sloshing fluid. The comparison of numerical results evaluated by the complete two-dimensional analysis and the linear superposition of results evaluated by separated ground exciting is made.

Faltinsen et al. (2000) derived the discrete infinite-dimensional modal system describing non-linear sloshing of an incompressible fluid with irrotational flow partially occupying a tank performing an arbitrary three-dimensional motion. The

derivation was based on Bateman-Luke variational principle. The free surface motion and velocity potential were expanded in generalized Fourier series. The general multidimensional structure of the equations was approximated to analyze sloshing in a rectangular tank with finite depth.

Cho and Lee (2004) introduced a finite element method for analysing the large amplitude sloshing of incompressible and inviscid liquid in two-dimensional container subjected to the forced excitation. The sloshing flow was formulated as an initial-boundary-value problem based upon the fully non-linear potential flow theory. The flow velocity field was interpolated from the velocity potential with second-order elements according to least square method, and the free surface conditions were tracked by making use of the direct time differentiation and the predictor–corrector method, together with the mass-conservative remeshing scheme. The liquid mesh were adapted such that the incompressibility condition is strictly satisfied. The accuracy and stability of the numerical method introduced were verified from the comparison with the existing reference solutions.

Bang-Fuh and Nokes (2005) used 2D Navier–Stokes equations and developed a novel time-independent finite-difference method for analyzing coupled two-dimensional and fully non-linear, viscous sloshing motion (surge, heave and pitch) in tanks. The boundary of the tank is mapped onto a fixed square domain through proper mapping functions and stretched meshes are employed near boundaries in order to more accurately evaluate the large disturbance of fluid along the boundary. The maximum transient amplitude was found to be much larger than that of the steady-state. The frequency dependence and Reynolds number effects are studied. The coupling effect was significant and simultaneous surge, heave and pitch motions should be included in the tank sloshing analysis. A simple formula was derived to approximate the horizontal force coefficient (CF), on the tank walls. The formula implies that CF was dominated by the free surface displacement when the tank is excited by small surge frequencies. Whereas CF was attributed to added mass effects when the tank is under higher surge frequency forcing. The limitations of the proposed method are also discussed.

Wang and Khoo (2005) studied nonlinear random sloshing problem in rectangular tank filled with liquid by employing finite element method based on fully nonlinear

wave velocity potential theory. The tank was subjected to specified horizontal random oscillations. The time domain second-order model is also employed to compute the nonlinear wave elevation and hydrodynamic force for comparison with the fully nonlinear model. The convergence and the accuracy of the numerical simulation and the nonlinear effects of the random waves and forces were studied; power spectra of waves and forces are obtained, and the effect of the peak frequency on spectra of wave and forces werediscussed. The later model exhibited some interesting features of nonlinear wave. It is much easier to implement and require a much smaller computational resource.

Zhang et al. (2006) employed desingularized boundary integral equation method (DBIEM) coupled with mixed Eulerian–Lagrangian (MEL) formulation to study the problem of wave propagation in a fully nonlinear numerical wave tank. The potential flow boundary value problem was solved at each time step. The fourth-order predictor–corrector Adams–Bashforth–Moulton scheme was used for the time-stepping integration of the free surface boundary conditions. The position of instantaneous free surface was tracked by applying semi-Lagrangian approach with the horizontal motion of the fluid particles on the free surface held fixed. The saw-tooth instability was overcome via a five-point Chebyshev smoothing scheme. The model was applied to several wave propagations including solitary, irregular and random incident waves.

Yuanjun et al. (2007) analytically studied nonlinear sloshing analysis of low gravity liquid in a cylindrical tank under pitching excitation. Based on variational principle, the Lagrange function of sloshing in low gravity was expressed in the form of volume integral of liquid pressure and the velocity potential function was expanded in series by wave height function at the free surface. The nonlinear equations with kinematics and dynamics free surface boundary conditions through variation were derived next. Finally, these equations are solved by multiple-scales method. The influence of Bond number on the global stable response of nonlinear liquid sloshing in circular cylinder tank is analyzed in detail.

Virella et al. (2008) used conventional finite element package ABAQUS and investigated the influence of nonlinear wave theory on the sloshing natural periods and their modal pressure distributions for rigid rectangular tanks under the assumption

of two-dimensional behaviour. Natural periods and mode shapes computed for both linear wave theory (LWT) and nonlinear wave theory (NLWT) models were compared. Linear wave theory was implemented in an acoustic model, whereas a plane strain problem with large displacements was used in NLWT. The analysis was carried out for rectangular tanks with different liquid height to tank width ratios. It was found that the nonlinearity does not have significant effects on the natural sloshing periods. The linear wave theory conservatively estimated the magnitude of the pressure distribution, whereas larger pressures resultant heights were obtained when using the nonlinear theory.

Chen et al. (2009) proposed a numerical method referred to as level set method (LSM) for simulation of dynamic sloshing load in a partially filled tank excited by a horizontal harmonic motion. A two-fluid approach based on the proposed method was used to solve the Reynolds-averaged Navier–Stokes (RANS) equations in both water and air regions and the interface was treated as a variation of the fluid properties. It required no special treatments to describe the free surface. The dependency of numerical solution on grid resolution, time step size and the interface thickness were investigated. Further, numerical tests were conducted for a rectangular tank with both 45^0 and 60^0 chamfered ceiling corners subject to a harmonic rolling motion. the results were compared with the available experimntal data.

Pal and Bhattacharyya (2010) proposed a numerical method based on meshless local Petro-Galerkin (MLPG) method for compution of the nonlinear sloshing response of liquid in a two-dimensional rigid prismatic tank subjected to external excitation. At every instant of time, velocity potential is computed at each node and the nodal positions are updated. A local symmetric weak form (LSWF) for nonlinear sloshing of liquid was developed, and a truly meshless method, based on LSWF and moving least squares (MLS) approximation, was presented for the solution of Laplace equation with the requisite boundary conditions. The numerical results were compared with those experimentally obtained by them.

2.7 Dynamics of Liquid Containers with Internal Components

Submerged components often constitute an integral part of the tank-liquid system, e.g., racks and fuel assemblies in nuclear spent fuel pool. The presence of internal components in liquid storage tanks significantly influenc the sloshing characteristics of liquid and hence the dynamic response of liquid-tank system. In a nuclear spent fuel storage pool which is a seismic Category I structure in a nuclear power plant, the hydrodynamic pressure exerted on the pool wall and the sloshing wave height of cooling water in the case with spent fuels are different from those in the case without spent fuels (Chun and Yun, 1999). Further, baffles of different configurations are extensively used as passive sloshing damping devices in liquid tanks, which are also considered as internal objects. Hence, it is of paramount importance to properly understand the influence of these submerged internal objects on the dynamic response of tank-liquid system.

Within the framework of linear as well as nonlinear sloshing, the literature related to liquid tanks with internal objects are discussed in this section. Also discussed are the experimental studies relating to liquid sloshing in tanks with baffles and/or submerged components.

Evans and McIver (1987) presented an approximate solution based on linearized water-wave theory and developed a simple formula which enables computation of the eigen-frequencies for either bottom-mounted or surface piercing vertical baffle of any length and position and for all tank dimensions. To overcome the numerical difficulties associated with the accurate approach, three different approximate methods were used and their relative merits and demerits for a range of parameters were discussed. The technique involved matching of appropriate eigenfunction expansions on either sides of the baffle across the gap in the fluid and the solution of resulting integral equation for the horizontal fluid above or below the baffle. Watson and Evans (1991) further extended the same technique and studied the resonant frequencies of oscillations of fluid in rectangular as well as circular containers having internal bodies such as surface or bottom-mounted rectangular blocks and submerged circular cylinders. They constructed appropriate eigenfunction expansions in two different fluid regions by considering symmetric and antisymmetric potentials separately, and matched them across their common boundary. The resulting integrals

were solved by using a Galerkin expansion and the resonant frequencies were expressed in the form of a simple equation involving the geometry of the problem.

Choun and Yun (1996) presented an analytical solution and investigated the effects of a bottom-mounted rectangular block on the sloshing characteristics of the fluid in rectangular tanks using the linear water wave theory. The velocity potential was decomposed into those for the wall-induced waves and the reflected, transmitted and scattered waves by the block. The reflection and transmission coefficients related to the block are determined using the continuity conditions of mass flux and energy flux on the common vertical boundaries of the fluid regions and the boundary conditions on both sides of the block. The method was verified with the available results. Analysis of the results indicated that the size and location of the block significantly influence the sloshing frequencies and mode shapes. Later, Choun and Yun (1999) conducted an analytical study to investigate the sloshing response of rectangular tanks with a submerged structure considering linear wave theory, and subjected to horizontal ground excitations. Sloshing peak wave amplitudes from time history analyses and response spectra were obtained for various models subjected to the earthquake records of El Centro NS (1940), El Centro EW (1940), Loma Prieta (1989), and Mexico City (1985). With the only exception of the Mexico City record (1985), the contribution of the first sloshing mode to the surface wave amplitude was very high, in the range between 80% and 99%. For the Mexico City earthquake, the contributions of the first mode to the surface wave amplitude were smaller (from 43% to 68%), and higher sloshing modes were necessary to accurately predict the sloshing wave amplitude, because the predominant frequency of the earthquake was closer to the second sloshing mode.

Gavrilyuk et al. (2006) proposed fundamental solutions of the linearized problem on fluid sloshing in a vertical cylindrical container having a thin rigid-ring horizontal baffle. The analytical oriented approach not only provided accurate approximations of natural frequencies and modes but also captured the singular asymptotic behaviour of the velocity potential at the sharp baffle edge. Gavrilyuk et al. (2007) used nonlinear asymptotic modal method based on the Moiseev asymptotic ordering to study the weakly nonlinear resonant sloshing in baffled cylindrical tank. They quantified the frequency domains of the steady state resonant waves versus the size and location of

the baffle. Askari and Daneshmand (2009) analytically investigated the coupled vibration of a partially filled cylindrical container with a thin-walled and open-ended cylindrical shell as an internal body. Askari and Daneshmand (2010) and Askari et al. (2011) investigated the effects of a rigid internal body on dynamic characteristics of a cylindrical container partially filled with liquid. Hasheminejad and Aghabeigi (2012) studied the effect vertical baffles on two-dimensional liquid sloshing characteristics in a half-full non-deformable horizontal cylindrical container of elliptical cross section. They employed linear potential theory in conjunction with the successive conformal transformation technique to arrive at the solution. Wang et al. (2012) proposed an improved semi-analytical scheme to study the frequencies and modes of liquid sloshing in rigid cylindrical container with multiple rigid annular baffles.

Armenio and Rocca (1996) adopted the finite difference method (FDM) to solve the two-dimensional Reynolds averaged Navier–Stokes (RANS) equations in order to account for the viscosity. They reported that the presence of a vertical baffle considerably reduced the sloshing loads in the whole range of roll frequencies. Gedikli and Ergueven (1999) developed a numerical model based on linear boundary element method to study the effect of rigid ring baffle in damping liquid oscillation in rigid cylindrical tank. Tanugula (2001) used the commercial CFD solver FLUENT and studied the slosh damping potential of four different baffle configurations (i.e., horizontal, vertical, horizontal and vertical, and diagonal) in heavy-duty trucks with circular and elliptical tanks of various fill-depths. Cho et al. (2003) employed a coupled ALE finite element method to numerically examine the damping effects of disc-type elastic baffle on the dynamic characteristics of cylindrical fuel-storage tank boosting with uniform vertical acceleration. Cho and Lee (2004) carried out a parametric investigation on the two-dimensional nonlinear liquid sloshing in baffled tank under horizontal forced excitation. A time-incremental nonlinear finite element method (FEM), based on the fully nonlinear potential flow theory in the semi-Lagrangian numerical approach, was used for numerical analysis. They showed that the liquid motion and dynamic pressure variation above the baffle are more significant than those below the baffle. In addition, they suggested that the quantities of interest in the liquid sloshing are strongly dependent on the baffle design parameters. Cho et al. (2005) conducted a frequency domain parametric investigation of sloshing damping characteristics in 2–D baffled tank subjected to forced lateral excitation.

Finite element method based on the linearized potential flow theory was used as the numerical tool for the study. An artificial damping term was employed into the kinematic free surface condition to reflect the eminent dissipation effect in resonant sloshing. Biswal et al. (2003) studied the natural frequencies and modes of liquid in a liquid-filled rigid cylindrical container with/ without baffles by using the finite element method. Biswal et al. (2006) studied 2D nonlinear sloshing response of liquid in non-deformable cylindrical and rectangular tanks with rigid baffles subjected to harmonic base excitation. Baffles close to the free surface of the fluid were found more effective in reducing the effect of sloshing.

Mitra and Sinhamohapatra (2007) proposed a pressure-based Galerkin's finite element model to study liquid sloshing on account of free lateral vibration of ground supported rectangular storage tanks with submerged internal component subjected to lateral ground motion of El Centro-EW. The parametric study was conducted to know the influence of height, width and location of the submerged structural components on the sloshing elevation and hydrodynamic pressure due to seismic ground motion. Belakroum et al (2010) developed a Galerkin Least Square (GLS) finite element model based Arbitrary Lagrangian–Eulerian (ALE) description of the Navier–Stokes equations and studied vibratory behaviours of three different configurations of tanks equipped with baffles. They found that centrally installed surface-piercing vertical baffles are the most effective passive slosh damping devices.

Strandberg (1978) carried out experimental investigation on dynamic performance and stability of horizontal circular, elliptical, and super-elliptical tank shapes of equal capacity. He also examined the overturning limit for half-full elliptical containers with various baffle configurations and established the preference of vertical baffle over horizontal one as an anti-sloshing device in elliptical container. Warnitchai (1998) used both analytical and experimental investigation to determine the damping ratios of various flow dampening devices: tank with two circular section poles, tank with a flat plate, and tank with a wire-mesh screen with a specific wire diameter and solidity ratio. Maleki and Ziyaeifar (2008) proposed a theoretical damping model to investigate the damping effect of baffles in circular cylindrical liquid storage tanks, and simultaneously carried out experiments for verification of the theoretical models. Their study concerned two kinds of baffles; horizontal ring and vertical blade baffles.

They observed that the damping ratio of the sloshing mode in the presence of these baffles depended on the tank and baffle dimensions in addition to the location of the baffle. The ring baffles were found to be more effective in reducing the sloshing oscillations. They also showed that the damping ratio depended on the sloshing wave amplitude. Panigrahy et al. (2009) used two different configurations of baffle: (1) a combination of both vertical and horizontal baffles – a set of two horizontal baffles, one at each wall perpendicular to the direction of excitation, fixed at a given vertical height irrespective of the depth of liquid in the tank together with a set of two vertical baffles with four holes each, one attached to each wall parallel to the excitation direction; (2) ring baffle. Akyildiz et al. (2013) conducted a series of experiments in cylindrical tank subjected to rolling motion and found that ring baffle arrangements are very effective in reducing the sloshing loads.

2.8 Application of Soft Computing to Engineering Problems

Soft computing is a class of computational intelligence tools and techniques shared by closely related disciplines such as genetic algorithms, belief calculus, artificial neural network, fuzzy logic and some machine learning methods like inductive reasoning. These computational tools can be used synergistically or independently; depending on the spectrum of the problem. The Core disciplines of soft computing are Fuzzy Logic, Artificial Neural Networks and Genetic Algorithms. The combination of fuzzy logic and neurocomputing has the highest degree of application. Such systems called Neuro-fuzzy systems are very important for making inferences. To this end, an effective method called Adaptive Neuro-Fuzzy Inference System (ANFIS) was proposed by Jang (1993).

In the recent years, novel soft computing techniques have been introduced in almost all fields of engineering, and application. Soft computing is one of the latest approaches for the development of systems that possess computational intelligence (Zadeh, 1994). Soft computing techniques as modelling tools have generated considerable interest among the researchers involved in diverse fields of science and engineering.

Literatures relating to application of soft computing techniques are very rare in slosh mechanics. However, soft computing techniques have widely been used in many other allied fields of engineering applications, where data prediction has been the fundamental objective of the study, to get rid of costly experimental execution. Adaptive Neural Fuzzy Inference Systems (ANFIS) is one such soft computing tool. It is increasingly becoming popular in the modern world. This is due to their ability to model or represent vagueness in day to day activities or processes.

Although soft computing techniques have made deep inroads into a wide range of scientific and research applications, their application in sloshing analysis is very limited (Kim and Lee, 2008) and can almost be treated in negation. Kim and Lee (2008) used evolutionary methods such as artificial neural network (ANN) and genetic algorithm (GA) to find the optimal design of baffle configuration. They used ANN for sloshing analysis and GA to obtain optimized baffle configuration that ensured maximum reduction of sloshing.

2.9 Critical Observations

From critical observation of the exising literature, it is found that only two works (Choun and Yun, 1999; Mitra and Sinhamahapatra, 2007) are available on the seismic response of liquid tanks with submerged internal components. No literature was found on quantification of impulsive and convective components of seismic response for tank-liquid-submerged block configuration. It was also observed that frequency content as a measure of severity of earthquake on structural response is an important parameter. Not many works on the effect of frequency content of earthquake on the dynamic response of liquid storage tank was reported.

No study is available in open literature to quantify the effect of submerged block on impulsive and convective response of dynamic behavior of liquid in a tank (Jaiswal and Jain, 2005).

2.10 Conclusion

Based on the literature survey conducted, the objectives as well as the scope of the present research as outlined in the previous chapter were set out.

The literature presented in this chapter is not exhaustive. Barring the literature cited in this chapter, specifically dedicated to survey of literature, chapter specific relevant literature are included as a part of introduction to the chapters**.** This might have led to repetitions of literatures elsewhere in the dissertation.

CHAPTER 3

3 MATHEMATICAL BACKGROUND AND FINITE ELEMENT FORMULATION

3.1 Introduction

Analytical approaches have previously been used to predict the dynamic response of liquid filled tanks of regular geometries with the assumption of small wave amplitude. The analytical techniques for the solution of large amplitude sloshing problems are still not fully developed. The numerical methods such as finite difference, boundary element and finite element are in common use. The finite element method (FEM) has been successfully applied to many problems of linear, non-linear sloshing and has been used in the present investigation. This chapter is dedicated to theoretical and finite element formulations, which are grouped under the following two categories.

(a) Liquid Domain Formulation: Linear Analysis

(b) Liquid Domain Formulation: Non-linear Analysis

3.2 Liquid Domain Formulation: Linear Analysis

3.2.1 Mathematical Formulation

The liquid filled rectangular tank with submerged internal block as shown in the Figure 3.1 defines the problem geometry. The Cartesian coordinate system O-xz for the computational domain of the liquid is defined such that the origin is at the center of the still free surface with z-axis pointing vertically upward. The bottom of the tank is assumed to be rigidly fixed to the base. Γ_s represents the free surface area of liquid

whereas $\Gamma_w (= \Gamma_{tw} \cup \Gamma_{bw})$ denotes the surface area of liquid in contact with the tank wall as well as the block wall and $\Gamma_b = (\Gamma_{tb} \cup \Gamma_{bt})$ represents the tank bottom as well as the block top. Γ_{tw} and Γ_{bw} represent the area of contact of liquid with the tank wall and the block wall respectively. Similarly, Γ_{tb} and Γ_{bt} refer to the area of contact of liquid with the tank bottom and block top respectively. Ω denotes the liquid domain and ρ_f is the density of the liquid. The liquid is assumed to be inviscid, incompressible and the flow is assumed to be irrotational.

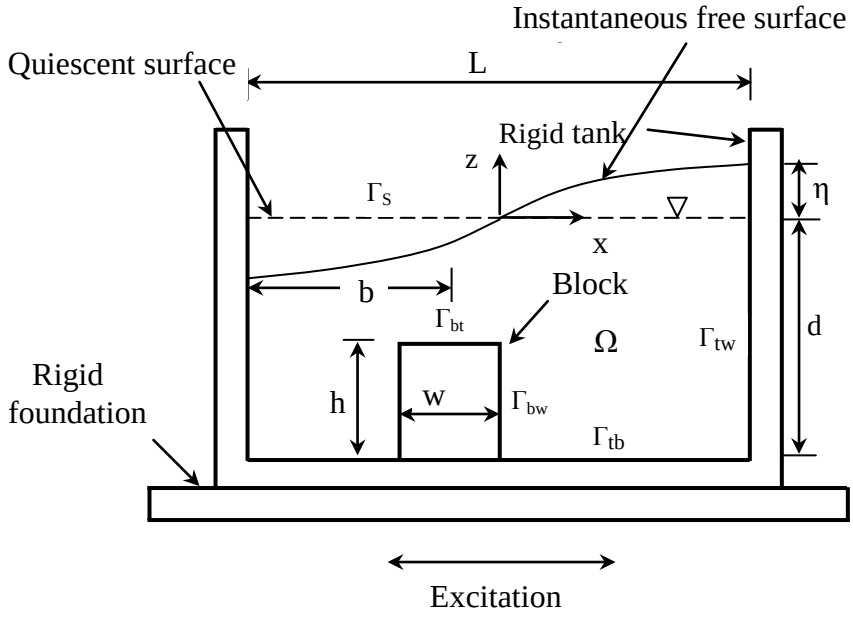

Figure 3.1: Schematic diagram of tank-liquid-submerged block system

3.2.2 Governing Equation

The governing equation for motion of liquid in terms of *velocity potential,* $\phi(x, z, t)$ is expressed by Laplace equation

$$\nabla^2 \phi = 0 \qquad \text{on } \Omega \tag{3.1}$$

where $\nabla^2 = \dfrac{\partial^2}{\partial x^2} + \dfrac{\partial^2}{\partial z^2}$ in Cartesian coordinate system.

3.2.3 Boundary Conditions

The liquid domain is bounded by the structure boundary and free liquid surface boundary. The boundary of the liquid domain, thus, can be divided into two types, namely; (1) free surface boundary condition and (2) body surface boundary condition.

Liquid free surface boundary condition

The free surface denoted by Γ_s in Figure 3.1 differs from other physical boundaries since it is a free boundary indeed; not only the potential ϕ must be determined there, but also the position of the free surface itself. Therefore, it is evident that two boundary conditions are needed for a proper mathematical description of the free surface. Thus, there exist two boundary conditions on the free surface; namely kinematic and dynamic boundary conditions. Both kinematic and dynamic boundary conditions need to be satisfied at any instant and on the exact free surface. The dynamic boundary condition derives its nomenclature from the fact that it has been deduced from a momentum equation i.e., balanced of forces whereas kinematic boundary condition owes its allegiance to the fact that it concerns the velocity field only. The kinematic boundary condition states that the liquid particle once on the free surface will always remain on the free surface. The dynamic boundary condition requires that the pressure on the free surface be uniform and equal to the external atmospheric pressure. This boundary condition can be obtained from Bernoulli's equation with the assumption of zero atmospheric pressure. By assuming the wave amplitude to be small compared to the wave length and the mean water depth, and also by dropping the nonlinear terms in the dynamic boundary condition i.e., the unsteady form of Bernoulli's equation, the linearized free surface conditions based on Eulerian description, with η as the wave elevation with respect to free surface, can be expressed as

Kinematic boundary equation,

$$\frac{\partial \eta}{\partial t} = \frac{\partial \phi}{\partial z} \quad \text{on } \Gamma_s \text{ and at } z = 0 \tag{3.2}$$

Dynamic boundary condition,

$$\frac{\partial \phi}{\partial t} = -g\eta \quad \text{on } \Gamma_s \text{ and at } z = 0 \tag{3.3}$$

Due to the assumption of inviscid nature of the liquid, potential formulation lacks the inherent damping effect arising out of fluid viscosity. The effect of viscosity is artificially introduced into dynamic free surface boundary condition in simplified manner (Faltinsen, 1978). The damping term so introduced dissipates the momentum by opposing the fluid motion with a force proportional to the local gradient of fluid velocity. The constant of proportionality or coefficient of viscosity (μ) changes with the flow regime. The damping–modified dynamic free surface condition in Equation. 3.3 becomes

$$\frac{\partial \phi}{\partial t} = -(g\eta + \mu\phi) \text{ on } \Gamma_s \text{ and at } z = 0 \tag{3.4}$$

The term $\mu\phi$ is the artificial damping term which introduces a pseudo-damping effect into the numerical model based on potential theory. The Equations 3.2 and 3.4 can be unified into a single condition to represent the free surface boundary condition as follows.

$$\frac{\partial^2 \phi}{\partial t^2} + \mu \frac{\partial \phi}{\partial t} + g \frac{\partial \phi}{\partial z} = 0 \text{ on } \Gamma_s \tag{3.5}$$

Body surface boundary condition

On the walls of the tank the velocity of liquid is equal to the wall velocity in normal direction.

$$\frac{\partial \phi}{\partial n} = V_n \text{ on } \Gamma_w = \Gamma_{tw} \bigcup \Gamma_{bw} \tag{3.6}$$

where V_n is the instantaneous velocity of the vertical wall subjected to horizontal ground acceleration and *n* is the normal to the wall surface pointing out of the liquid domain.

On the rigid bottom supported on rigid foundation, no flux condition needs to be satisfied for impermeable body surface

$$\frac{\partial \phi}{\partial n} = 0 \text{ on } \Gamma_b = \Gamma_{tb} \bigcup \Gamma_{bt} \tag{3.7}$$

3.2.4 Finite Element Formulation

The liquid domain Ω bounded by $\Gamma = \Gamma_w \bigcup \Gamma_b \bigcup \Gamma_s$ is discretized by four-noded isoparametric quadrilateral element and velocity potential is considered as the nodal degree of freedom. The velocity potential is approximated as

$$\phi \approx \phi(x,z,t) = \sum_{j=1}^{n} \phi_j(t) N_j(x,z) \tag{3.8}$$

where $\phi_j(t)$ are time dependent nodal velocity potentials, N_j are shape functions and *n* is the number of nodes.

Galerkin's weighted-residual method is applied to Laplace equation so as to set out the weighted averages of residuals to zero. Thus, the above equation gives rise to

$$\int_{\Omega} N_i \left[\frac{\partial^2 \phi}{\partial x^2} + \frac{\partial^2 \phi}{\partial z^2} \right] d\Omega = 0 \tag{3.9}$$

On application of product rule of differentiation, the derivative terms are transformed to lower order forms as follows

$$\frac{\partial}{\partial x}(N_i \frac{\partial \phi}{\partial x}) = N_i \frac{\partial^2 \phi}{\partial x^2} + \frac{\partial N_i}{\partial x}\frac{\partial \phi}{\partial x} \tag{3.10}$$

Rearrangement of terms of equation (3.10) yields

$$N_i \frac{\partial^2 \phi}{\partial x^2} = \frac{\partial}{\partial x}(N_i \frac{\partial \phi}{\partial x}) - \frac{\partial N_i}{\partial x}\frac{\partial \phi}{\partial x} \tag{3.11}$$

Similarly,

$$N_i \frac{\partial^2 \phi}{\partial z^2} = \frac{\partial}{\partial z}(N_i \frac{\partial \phi}{\partial z}) - \frac{\partial N_i}{\partial z}\frac{\partial \phi}{\partial z} \tag{3.12}$$

Substitution of Equations 3.11and 3.12 into Equation 3.9 produces

$$\int_{\Omega}\left[\frac{\partial}{\partial x}\left(N_i\sum_{j=1}^{n}\frac{\partial N_j}{\partial x}\right)\phi_j-\frac{\partial N_i}{\partial x}\sum_{j=1}^{n}\frac{\partial N_j}{\partial x}\phi_j+\frac{\partial}{\partial z}\left(N_i\sum_{j=1}^{n}\frac{\partial N_j}{\partial z}\right)\phi_j-\frac{\partial N_i}{\partial z}\sum_{j=1}^{n}\frac{\partial N_j}{\partial z}\phi_j\right]\mathrm{d}\Omega=0 \tag{3.13}$$

$$\int_{\Omega}\left(\frac{\partial N_i}{\partial x}\sum_{j=1}^{n}\frac{\partial N_j}{\partial x}+\frac{\partial N_i}{\partial z}\sum_{j=1}^{n}\frac{\partial N_j}{\partial z}\right)\phi_j\,\mathrm{d}\Omega-\int_{\Omega}\left[\frac{\partial}{\partial x}\left(N_i\frac{\partial\phi}{\partial x}\right)+\frac{\partial}{\partial z}\left(N_i\frac{\partial\phi}{\partial z}\right)\right]\mathrm{d}\Omega=0 \tag{3.14}$$

The second part of the surface integral may be transformed into line integrals expressed below.

$$\int_{\Omega}\frac{\partial}{\partial x}\left(N_i\frac{\partial\phi}{\partial x}\right)\mathrm{d}\Omega=\int_{\Gamma}N_i\frac{\partial\phi}{\partial x}l\,\mathrm{d}\Gamma \tag{3.15}$$

$$\int_{\Omega}\frac{\partial}{\partial z}\left(N_i\frac{\partial\phi}{\partial z}\right)\mathrm{d}\phi=\int_{\Gamma}N_i\frac{\partial\phi}{\partial z}k\,\mathrm{d}\Gamma \tag{3.16}$$

where l and k are the direction cosines

$$\int_{\Omega}\left(\frac{\partial N_i}{\partial x}\sum_{j=1}^{n}\frac{\partial N_j}{\partial x}+\frac{\partial N_i}{\partial z}\sum_{j=1}^{n}\frac{\partial N_j}{\partial z}\right)\phi_j\mathrm{d}\Omega=\int_{\Gamma}N_i\left(\frac{\partial\phi}{\partial x}l+\frac{\partial\phi}{\partial z}k\right)\mathrm{d}\Gamma \tag{3.17}$$

$$\int_{\Omega}\left(\frac{\partial N_i}{\partial x}\sum_{j=1}^{n}\frac{\partial N_j}{\partial x}+\frac{\partial N_i}{\partial z}\sum_{j=1}^{n}\frac{\partial N_j}{\partial z}\right)\phi_j\mathrm{d}\Omega=\int_{\Gamma}N_i\left(\frac{\partial\phi}{\partial n}\right)\mathrm{d}\Gamma \tag{3.18}$$

Substituting boundary conditions in Equations 3.5-3.7 in Equation 3.18 results in

$$\int_{\Omega}\left[\frac{\partial N_i}{\partial x}\sum_{j=1}^{n}\frac{\partial N_j}{\partial x}+\frac{\partial N_i}{\partial z}\sum_{j=1}^{n}\frac{\partial N_j}{\partial z}\right]\phi_j\mathrm{d}\Omega=\int_{\Gamma_w}N_iV_n\mathrm{d}\Gamma_w-\frac{1}{g}\int_{\Gamma_s}N_i\sum_{j=1}^{n}N_j\ddot{\phi}\,\mathrm{d}\Gamma_s$$

$$-\frac{\mu}{g}\int_{\Gamma_s}N_i\sum_{j=1}^{n}N_j\dot{\phi}\,\mathrm{d}\Gamma_s \tag{3.19}$$

On rearrangement of the terms in the above equation, we get

$$\frac{1}{g}\int_{\Gamma_s} N_i \sum_{j=1}^{n} N_j \ddot{\phi}\, d\Gamma_s + \frac{\mu}{g}\int_{\Gamma_s} N_i \sum_{j=1}^{n} N_j \dot{\phi}\, d\Gamma_s + \int_{\Omega}\left[\frac{\partial N_i}{\partial x}\sum_{j=1}^{n}\frac{\partial N_j}{\partial x} + \frac{\partial N_i}{\partial z}\sum_{j=1}^{n}\frac{\partial N_j}{\partial z}\right]\phi_j\, d\Omega$$

$$= \int_{\Gamma_w} N_i V_n\, d\Gamma_w \qquad (3.20)$$

$$[M_f]\{\ddot{\phi}\} + [C_f]\{\dot{\phi}\} + [K_f]\{\phi\} = \{F\} \qquad (3.21)$$

where $[M_f]$ is the free surface fluid matrix

$[C_f]$ is the fluid damping matrix

$[K_f]$ is the fluid coefficient matrix, and

$\{F_i\}$ is the force vector

The elements of the above matrices

$M_{ij} = \sum M^e{}_{ij}$, $C_{ij} = \sum C^e{}_{ij}$, $K_{ij} = \sum K^e{}_{ij}$ and $F_i = \sum F^e{}_i$

$$M^e{}_{ij} = \frac{1}{g}\int_{\Gamma_{se}} N_i N_j\, d\Gamma_s \qquad (3.22)$$

$$C^e{}_{ij} = \frac{\mu}{g}\int_{\Gamma_{se}} N_i N_j\, d\Gamma_s \qquad (3.23)$$

$$K^e{}_{ij} = \int_{\Omega_e}\left(\frac{\partial N_i}{\partial x}\frac{\partial N_j}{\partial x} + \frac{\partial N_i}{\partial z}\frac{\partial N_j}{\partial z}\right)d\Omega \qquad (3.24)$$

$$F^e{}_i = -\int_{\Gamma_{we}} N_i V_n\, d\Gamma_w \qquad (3.25)$$

The free slosh displacement η and hydrodynamic pressure p at any instant are obtained from the following equations.

$$\eta = -\frac{1}{g}\left(\frac{\partial \phi}{\partial t} + \mu\phi\right) \quad \text{on } \Gamma_s \text{ and } z = 0 \qquad (3.26)$$

$$p = -\rho\left(\frac{\partial \phi}{\partial t} + \mu\phi\right) \tag{3.27}$$

3.2.4.1 Liquid Stiffness Matrix

A two-dimensional finite element analysis is adopted for the sloshing analysis of liquid filled rectangular tank with submerged blocks. The liquid domain is discretized by 4-noded quadrilateral liquid elements.

The stiffness matrix of the liquid domain is computed by summation of element stiffness matrices, i.e.

$$[K_f] = \sum_{e=1}^{NK} K^e \tag{3.28}$$

where NK is the number of liquid elements and element stiffness matrix K^e is given by

$$K^e = \int_{\Omega} \left[\frac{\partial N_i}{\partial x}\frac{\partial N_j}{\partial x} + \frac{\partial N_i}{\partial z}\frac{\partial N_j}{\partial z} \right] d\Omega \tag{3.29}$$

In a two-dimensional field problem, the liquid velocity potential in a liquid element may be as approximated by the following equation.

$$\phi(x,z,t) = \sum_{j=1}^{4} N_j(x,z)\phi_j(t) \tag{3.30}$$

By taking the derivative of Equation 3.30 separately with respect to *x* and *z*, one obtains the liquid velocity potential within the *e* th liquid element as expressed below.

$$\begin{Bmatrix} \frac{\partial \phi}{\partial x} \\ \frac{\partial \phi}{\partial z} \end{Bmatrix}_e = \begin{Bmatrix} \frac{\partial N_j}{\partial x} \\ \frac{\partial N_j}{\partial z} \end{Bmatrix} \{\phi_j\}_e \tag{3.31}$$

The derivative of shape functions with respect to the natural coordinates (ξ, η) are obtained through the Jacobian transformation using the chain rule of differentiation.

$$\begin{Bmatrix} \frac{\partial N_j}{\partial \xi} \\ \frac{\partial N_j}{\partial \eta} \end{Bmatrix} = \begin{bmatrix} \frac{\partial x}{\partial \xi} & \frac{\partial z}{\partial \xi} \\ \frac{\partial x}{\partial \eta} & \frac{\partial z}{\partial \eta} \end{bmatrix} \begin{Bmatrix} \frac{\partial N_j}{\partial x} \\ \frac{\partial N_j}{\partial z} \end{Bmatrix} \tag{3.32}$$

or

$$\begin{Bmatrix} \frac{\partial N_j}{\partial \xi} \\ \frac{\partial N_j}{\partial \eta} \end{Bmatrix} = \left[J_e\right] \begin{Bmatrix} \frac{\partial N_j}{\partial x} \\ \frac{\partial N_j}{\partial z} \end{Bmatrix} \tag{3.33}$$

Where,

$$\left[J_e\right] = \begin{bmatrix} \frac{\partial x}{\partial \xi} & \frac{\partial z}{\partial \xi} \\ \frac{\partial x}{\partial \eta} & \frac{\partial z}{\partial \eta} \end{bmatrix} \text{ , is the Jacobian matrix} \tag{3.34}$$

$$\begin{Bmatrix} \frac{\partial N_j}{\partial x} \\ \frac{\partial N_j}{\partial z} \end{Bmatrix} = \left[J_e\right]^{-1} \begin{Bmatrix} \frac{\partial N_j}{\partial \xi} \\ \frac{\partial N_j}{\partial \eta} \end{Bmatrix} = \left[J_e\right]^{-1} \; T_e(\xi, \eta) \tag{3.35}$$

in which $\left[J_e\right]^{-1}$ is the inverse of the Jacobian matrix and

$T_e(\xi, \eta)$ contains the derivative of shape functions.

Let

$$\begin{Bmatrix} \frac{\partial N_j}{\partial x} \\ \frac{\partial N_j}{\partial z} \end{Bmatrix} = \left[B\right] \tag{3.36}$$

Where,

$$[\mathrm{B}] = [\mathrm{J}_e]^{-1} \ \mathrm{T}_e(\xi, \eta) \tag{3.37}$$

The liquid element stiffness matrix in Equation 3.29 may be written as

$$\mathrm{K}^e = \int_\Omega \begin{bmatrix} \dfrac{\partial N_j}{\partial x} & \dfrac{\partial N_j}{\partial z} \end{bmatrix} \begin{bmatrix} \dfrac{\partial N_j}{\partial x} \\ \dfrac{\partial N_j}{\partial z} \end{bmatrix} \mathrm{d}\Omega$$

$$= \int_\Omega [\mathrm{B}]^T \ [\mathrm{B}] \ \mathrm{d}x \ \mathrm{d}z = \int_{-1}^{+1} \int_{-1}^{+1} [\mathrm{B}]^T \ [\mathrm{B}] \, |\mathrm{J}_e| \ \mathrm{d}\xi \, \mathrm{d}\eta \tag{3.38}$$

3.2.4.2 Liquid Free Surface Mass Matrix

The liquid free surface mass matrix for the system is formed by the assembly of line elements in the liquid surface, i.e.

$$[\mathrm{M}_f] = \sum_{t=1}^{NF} \mathrm{M}^e \tag{3.39}$$

where NF is the number of liquid elements and M^e is given by

$$\mathrm{M}^e = \frac{1}{g} \int_{\Gamma_s} N_i N_j \ \mathrm{d}\Gamma_s \tag{3.40}$$

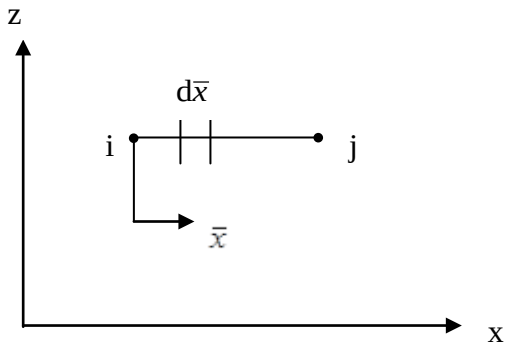

Figure 3.2: Liquid free surface element in a container

The liquid free surface element is shown in Figure 3.2, where $\bar{x}$ is the local coordinate for the free surface boundary element and L is the length of the element.

The shape functions for the line element at the free surface may be defined as

$$N_j = \left[1 - \frac{\bar{x}}{L} \qquad \frac{\bar{x}}{L}\right] \tag{3.41}$$

The liquid free surface matrix in Equation 3.40 may be written as

$$\mathrm{M}^e = \frac{1}{g}\int_0^L \begin{bmatrix} 1 - \dfrac{\bar{x}}{L} \\ \dfrac{\bar{x}}{L} \end{bmatrix} \left[1 - \frac{\bar{x}}{L} \qquad \frac{\bar{x}}{L}\right] \mathrm{d}\bar{x} \tag{3.42}$$

3.2.4.3 Liquid Load Vector

The load vector for the system is given by

$$[\mathrm{F_f}] = \sum_{e=1}^{NL} \mathrm{F}^e \tag{3.43}$$

where NL is the number of elements at the liquid-structure interface and element load vector F^e is given by

$$\mathrm{F}^e = -\int_{\Gamma_w} N_i V_n \, \mathrm{ds} \tag{3.44}$$

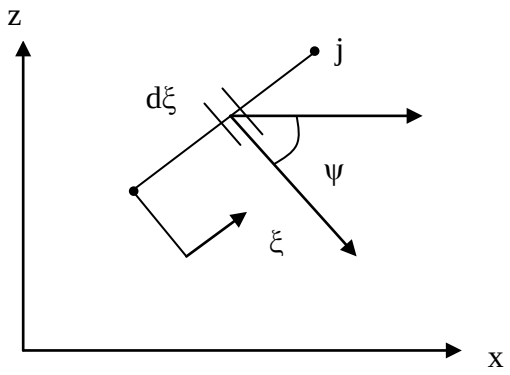

Figure 3.3: Liquid-solid interface element in a container

The liquid-solid interface element is illustrated in Figure 3.3. The shape functions for the liquid-solid interface element is expressed as

$$N_j = \left[1 - \frac{\xi}{\mathrm{L}} \qquad \frac{\xi}{\mathrm{L}}\right] \tag{3.45}$$

If V_x is the horizontal ground velocity in the x-direction then the normal velocity at the liquid solid interface may be expressed as

$$V_n = V_x \cos\psi \tag{3.46}$$

where

$\psi = \tan^{-1}(x_i - x_j)/(z_i - z_j)$.

The load vector in Equation (3.44) may be written as

$$\mathrm{F}_t = -\int_0^L \begin{Bmatrix} 1 - \dfrac{\xi}{L} \\ \dfrac{\xi}{L} \end{Bmatrix} V_x \cos\psi \; d\xi \tag{3.47}$$

3.2.4.4 Base Shear and Overturning Base Moment

Force due to hydrodynamic pressure on the wall, base shear and overturning base moment are the three fundamentally most important dynamic response parameters of special interest to the designers. The forces and moments at any given point in time during the excitation of tank are obtained once the sloshing elevation and hence the hydrodynamic pressure is determined from Equations 3.26 and 3.27. The forces and hence the base shear is determined by integrating the pressure, p over the tank wall as well as block wall area. The overturning moment acting about the bottom corner of the tank is caused due to the pressure, acting on the walls of the tank and the walls of the submerged block, normal to the direction of excitation, and also the pressure acting on the bottom of the tank and top of the submerged block.

Figures 3.4 and 3.5 depict typical qualitative distribution of hydrodynamic pressure associated with the liquid motion on account of lateral excitation of tank. The

impulsive and convective components are separately illustrated in order to have an insight into the individual contributions to the overall hydrodynamic pressure and associated base shear and base moment.

The base shear S_b and overturning base moment M_b can be calculated by the following expression

$$S_b = \int_{\Gamma_w} p\, n_x d\Gamma_w \tag{3.48}$$

$$M_b = \int_{\Gamma_w} (p\, n_x)\, x\, dx + \int_{\Gamma_b} (p\, n_z)\, z\, dz \tag{3.49}$$

where, $\vec{n} = n_x i + n_z j$ is the unit normal vector to the body surface.

The impulsive component of hydrodynamic pressure under the action of horizontal ground motion can be independently obtained from the velocity potential function by neglecting the liquid sloshing. As a consequence, the pressure at the liquid free surface vanishes, and this results in

$$\frac{\partial \phi}{\partial t}(x,0,t) = 0 \tag{3.50}$$

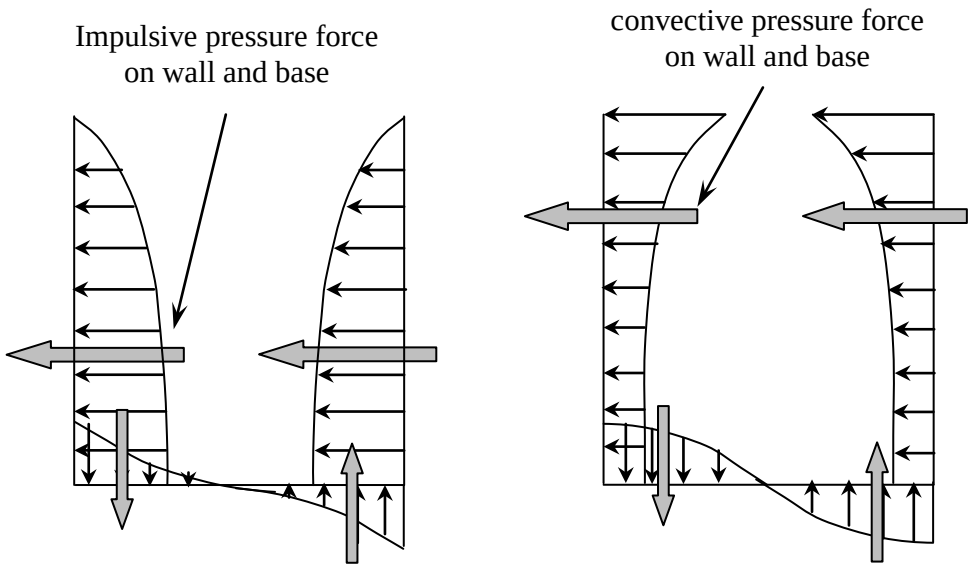

(a) Impulsive pressure (b) Convective pressure

Figure 3.4: Typical distribution of hydrodynamic pressure on tank wall and base

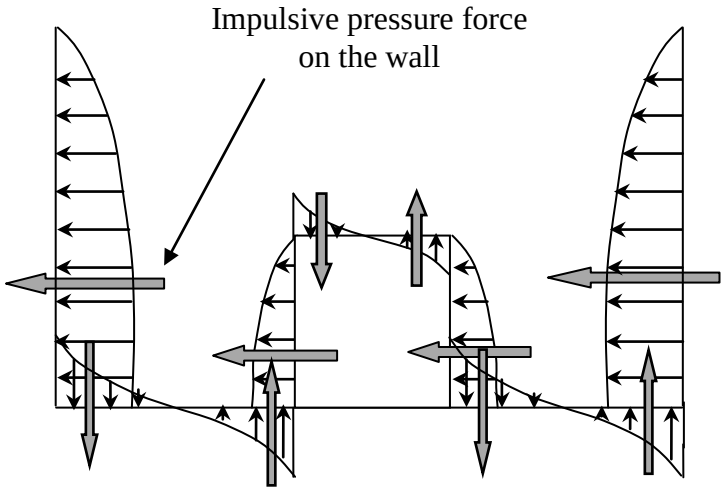

(a) Impulsive pressure

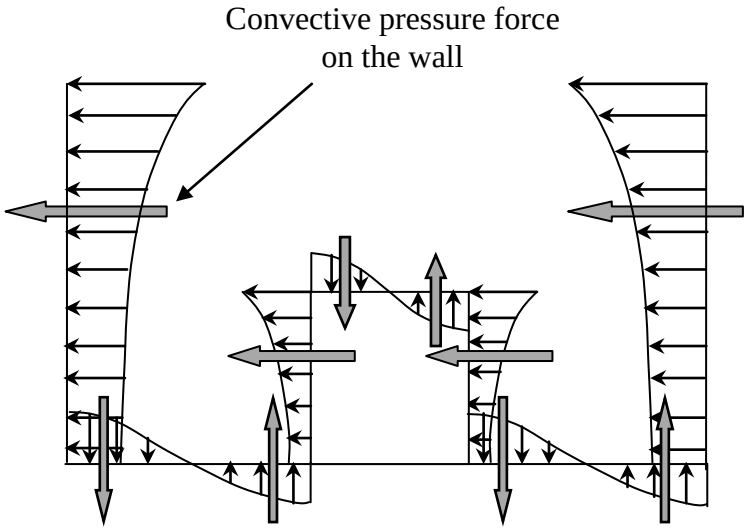

(b) Convective pressure

Figure 3.5: Typical distribution of hydrodynamic pressure in tank with submerged block: (a) Impulsive pressure; (b) Convective pressure

3.3 Liquid Domain Formulation: Nonlinear Analysis

3.3.1 Mathematical Formulation

The problem geometry for the tank-liquid system is the same as Figure 3.1. For brevity of the nonlinear formulation, the velocity potential defined governing equation is repeated in this section. However, the sloshing amplitude is assumed to be large.

$$\nabla^2\phi = 0 \tag{3.51}$$

governs the potential flow in the fluid domain Ω. Equation 3.51 is elliptic in nature and requires both free surface and body surface boundary conditions for simulation of nonlinear sloshing wave problem. The boundary conditions are described are follows.

3.3.1.1 Nonlinear Free Surface Boundary Conditions

On the time dependent free surface boundary Γ_s, both kinematic and dynamic boundary conditions need to be satisfied at any instant and on the exact free surface. The kinematic boundary condition requires that the fluid particle once on the free surface remains always on the free surface. Based on Eulerian description the free surface kinematic boundary condition is given by

$$\frac{\partial\eta}{\partial t} = \frac{\partial\phi}{\partial z} - \frac{\partial\phi}{\partial x}\frac{\partial\eta}{\partial x} \quad \text{on} \quad \Gamma_s \tag{3.52}$$

where $\eta(x,z,t)$ is the instantaneous free surface wave elevation

The dynamic boundary condition requires that the pressure on the free surface be uniform and equal to the external atmospheric pressure. This boundary condition can be obtained from Bernoulli equation with the assumption of zero atmospheric pressure. An artificial damping term may be suitably introduced into the dynamic free surface boundary condition in a simplified manner as in Faltinsen (1978), which not only accounts for the effect of viscosity in dissipating the momentum by opposing the fluid motion but also brings in numerical stability. The damping modified unsteady Bernoulli's equation may be expressed as

$$\frac{\partial\phi}{\partial t} = -g \subset \frac{1}{2}\nabla\phi.\nabla\phi - \mu\phi \quad \text{on} \quad \Gamma_s \tag{3.53}$$

where g is the gravitational acceleration.

3.3.1.2 Body Surface Boundary Condition

On the walls of the tank the velocity of liquid is equal to the wall velocity in normal direction

$$\frac{\partial \phi}{\partial n} = V_n \quad \text{on} \quad \Gamma_w \tag{3.54}$$

where V_n is the instantaneous velocity of the vertical wall subjected to horizontal ground velocity and n is the normal to the wall surface pointing out of the liquid domain.

On the rigid bottom supported on rigid foundation, no flux condition needs to satisfied for impermeable body surface

$$\frac{\partial \phi}{\partial n} = 0 \qquad \text{on } \Gamma_b \tag{3.55}$$

Thus Equations 3.51 - 3.55 define the initial and boundary value problem with nonlinear free surface boundary conditions. The nonlinearity in free surface boundary condition is attributed to: (1) *a priori* unknown free surface elevation at any given instant and (2) kinematic and dynamic boundary conditions in Equations 3.52 and 3.53 as they contain second order differential terms.

The set of Equations 3.51-3.55 are elliptic in space and parabolic in time. Mixed-Eulerian-Lagrangian method is used for numerical solution of the system of equations. In mixed-Lagrangian-Eulerian the surface nodes called ‘markers’ are allowed to move with the same velocity as the liquid. In this procedure the spatial equations are solved in Eulerian (fixed grid) frame and the integration of the free surface boundary conditions is executed in Lagrangian manner. This requires the free surface boundary conditions in Equations 3.52 and 3.53 to be written in Lagrangian form as follows.

$$\frac{d\phi}{dt} = -g\eta + \frac{1}{2}\nabla\phi.\nabla\phi - \mu\phi \quad \text{on} \quad \Gamma_w \tag{3.56}$$

$$\frac{dx}{dt} = \frac{\partial \phi}{\partial x}; \qquad \frac{dz}{dt} = \frac{\partial \phi}{\partial z} \tag{3.57}$$

After obtaining the time derivative of velocity potential, the nonlinear hydrodynamic pressure can be calculated by using the following equation:

$$p = -\rho\left(\frac{\partial\phi}{\partial t} + \frac{1}{2}|\nabla\phi|^2 + \mu\phi\right) \tag{3.58}$$

The base shear S_b and overturning base moment M_b can be calculated by the following expression

$$S_b = \int_{\Gamma_w} p \, d\Gamma_w \tag{3.59}$$

$$M_b = \int_{\Gamma_w} (p \, dz) z + \int_{\Gamma_b} (p \, dx) x \tag{3.60}$$

Impulsive pressure may be determined by assuming the whole liquid as a rigid solid block without convective mass. This assumption ignores the sloshing of the liquid and hence the convective response. As a consequence of this, the pressure at the quiescent liquid free surface vanishes at every instant during the motion.

$$\frac{\partial\phi}{\partial t}(x,0,t) = 0 \tag{3.61}$$

3.4 Finite Element Formulation

The entire liquid domain Ω, bounded by body surface Γ_w, tank bottom Γ_b and free surface Γ_s is discretized by four-noded quadrilateral elements for finite element formulation and solution of Laplace equation with appropriate boundary conditions. The velocity potential may be approximated as

$$\phi \approx \phi(x,z,t) = \sum_{j=1}^{n} \phi_j N_j(x,z) \tag{3.62}$$

where ϕ_j are time dependent nodal velocity potentials, N_j are shape functions and *n* is the number of nodes. Application of Galerkin's weighted-residual method to Laplace equation gives rise to

$$\int_{\Omega} \nabla^2\phi N_i \, d\Omega = 0 \tag{3.63}$$

Since, $\nabla(\nabla\phi N_i) = \nabla^2\phi N_i + \nabla\phi\nabla N_i$ (3.64)

Equation 3.63 may be written as

$$\int_{\Omega}\left[\nabla\left(\nabla\phi N_i\right)-\nabla\phi\nabla N_i\right]\mathrm{d}\Omega=0 \tag{3.65}$$

Application of Gauss theorm produces

$$\int_{\Gamma}N_i\frac{\partial\phi}{\partial\mathrm{n}}\mathrm{d}\Gamma-\int_{\Omega}\nabla N_i\ .\sum_{j=1}^{\mathrm{n}}\phi_j\nabla N_j\mathrm{d}\Omega \tag{3.66}$$

where $\Gamma=\Gamma_{\mathrm{w}}\bigcup\Gamma_{\mathrm{b}}\bigcup\Gamma_{\mathrm{s}}$, is the boundary of the liquid domain Ω. Substitution of the approximation function for the potential and the boundary conditions into the above equation yields

$$\int_{\Omega}\nabla N_i\sum_{i=1}^{n}\phi_j\nabla N_j\,\mathrm{d}\Omega\Big|_{j\notin\Gamma_{\mathrm{s}}}=\int_{\Gamma_{\mathrm{w}}}N_iV_{\mathrm{n}}-\int_{\Omega}\nabla N_i\sum_{i=1}^{n}\phi_j\nabla N_j\,\mathrm{d}\Omega\Big|_{j\in\Gamma_{\mathrm{s}}} \tag{3.67}$$

Where, Γ_{s} and Γ_{b} are the free surface and body (vertical wall) surface respectively on which the potential and its normal derivatives are prescribed. The potential on the free surface is known from the free surface boundary condition and the terms corresponding to the surface nodes have therefore been taken to the right hand side. This scheme suggested by Wu and Eatock Taylor (1994) was found to be effective in dealing with the singularity at the intersection point between the body surface and free surface on account of the confluence of boundary conditions.

Equation 3.67 may be expressed in matrix form as

$$[\mathrm{K}]\{\phi\}=[\mathrm{F}] \tag{3.68}$$

where,

$$\mathrm{K}_{ij}=\int\nabla N_i\,.\nabla N_j\,\mathrm{d}\Omega \tag{3.69}$$

$$\mathrm{F}_i=\int_{\Gamma_{\mathrm{w}}}N_i\mathrm{V}_n-\int_{\Omega}\nabla N_i\,.\sum_{i=1}^{n}\phi_j\nabla N_j\,\mathrm{d}\Omega\Big|_{j\in\Gamma_{\mathrm{s}}} \tag{3.70}$$

where K_{ij} is the global fluid matrix and F_i is the global right hand side vector. It must be mentioned that the matrix K_{ij} in Equation 3.69 varies with time for fully nonlinear problem.

Numerical evaluation of the dynamic and kinematic boundary conditions, Equations 3.56-3.57 require an approximation of velocity at the free surface. Although, direct differentiation of potential approximation via shape functions is a convenient option to obtain the velocity, shape functions however do not guarantee the continuity of its derivatives at the boundary of the elements and may result in lower order, discontinuous velocity with compromised accuracy. The velocity continuity can be ensured by use of higher order FE for potential approximation. In the present study, however C^0 isoparametric rectangular element is used. In order to avoid excessive accumulation of error in the time stepping procedure, the following method is used for velocity recovery.

The two dimensional velocity vector, $U = u\hat{i} + v\hat{j}$ may be approximated in terms of the same shape functions as used for velocity potential.

$$U = \sum_{j=1}^{n} U_j N_j(x, z) \tag{3.71}$$

Galerkin weighted-residual method is used to approximate the relationship $\nabla\phi = U$, in the form

$$\int_{\Omega} N_i(\nabla\phi - U)\, d\Omega = 0 \tag{3.72}$$

Substitution of Equations 3.62 and 3.71 into Equation 3.72 yields

$$\int_{\Omega} N_i \frac{\partial N_j}{\partial n}\phi_j \, d\Omega = \int_{\Omega} N_i N_j U_j \, d\Omega \tag{3.73}$$

In matrix form the above equation can be expressed as

$$[C]\{u\} = [D_1]\{\phi\} \tag{3.74}$$

$$[C]\{v\} = [D_2]\{\phi\} \tag{3.75}$$

where,

$$[\mathrm{C}] = \int_{\Omega} N_i N_j \, \mathrm{d}\Omega \tag{3.76}$$

$$[\mathrm{D}_1] = \int_{\Omega} N_i \frac{\partial N_j}{\partial x} N_j \, \mathrm{d}\Omega \tag{3.77}$$

$$[\mathrm{D}_2] = \int_{\Omega} N_i \frac{\partial N_j}{\partial z} N_j \, \mathrm{d}\Omega \tag{3.78}$$

and u and v are the components of velocity vector U_j at node j.

From the velocities thus obtained, the updated position of the free surface at the start of the next time step can be found using Equation 3.57. The updated value of the velocity potential on the free surface can also be determined from Equation 3.56. A new finite element mesh is then generated corresponding to the updated geometry which requires further solution of Laplace equation in the spatial domain, recovery of velocity and time-integration of kinematic and dynamic boundary conditions to advance the solution in time domain.

3.5 Implementation of Numerical Scheme

As stated above the implementation and accuracy of the numerical scheme involves five steps: (1) mesh generation or discretization of liquid domain, (2) the solution of FE-discretized Laplace equation in spatial domain, (3) recovery of velocity by global projection method, (4) surface tracking and location of the new position of Lagrangian free surface nodes by effective time-integration scheme, and (5) regridding at each time step or after a certain number of time steps in order to avoid inordinate concentration of Lagrangian free surface nodes in the region of higher gradients and have control over the minimum grid size for a given time step. Of the five steps mentioned above steps (2) and (3) have been discussed in earlier paragraphs and the rest of the steps are discussed in the following paragraph.

3.5.1 Mesh Generation

The liquid domain is discretized by four noded isoparametric quadrilateral elements. The entire liquid domain in the tank is divided in the x-direction by *nx*+1 uniformly placed vertical lines at as many surface nodes. The liquid depth is divided into *mz* number of meshes with *mz*+1 numbers of nodes in the vertical direction. Reduced mesh height is provided near the free surface in order that pronounced sloshing near the free surface can be better captured. The locations of free surface nodes change with time due to the Lagrangian characteristics. The total number of nodes and elements are computed as (*nx*+1) x (*nz*+1) and (*nx*)x(*nz*), respectively. A representative finite element mesh discretizing the liquid domain is shown in Figure 3.6.

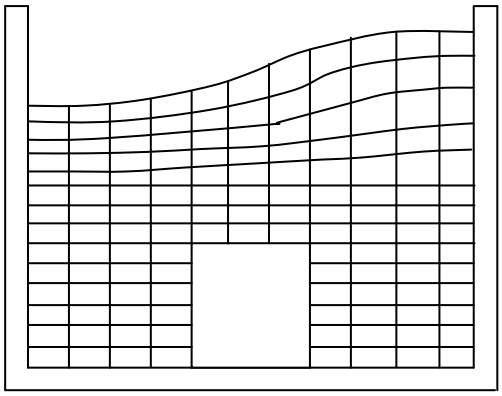

Figure 3.6: Typical finite element mesh

3.5.2 Time Integration

In material node approach $(\nabla\phi = \vec{\mathbf{v}})$ of MEL method, the surface nodes move with the fluid particles at the corresponding nodes and thus mesh distortion takes place. Fourth order explicit Runge-Kutta time-integration scheme is used to trace the moving nodes on the free surface and determine the associated velocity potential and other unknown variables of interest. The coordinates (*x*,*z*) and velocity potential at time *t* may be represented by a single variable as $Q_t(x, z, \phi)$ and expressed in matrix form as follows.

$$Q_t = (x_t,\ z_t,\ \phi_t)^T$$

$$x_t = (x_1,\ x_2,\ x_3,.....x_{nx+1})^T$$

$$z_t = (z_1,\ z_2,\ z_3,.....z_{nx+1})^T$$

$$\phi_t = (\phi_1,\ \phi_2,\ \phi_3,.....\phi_{nx+1})^T$$

Where $(x_i, z_j)_{i,j=1,2,...nx+1}$ and $(\phi_i)_{i=1,2,.....nx+1}$ respectively represent the coordinates and velocity potential of the nodes, along the free surface and nx is the number of liquid elements in the x-direction. The total derivative of Q_t with respect to time is written as

$$\frac{DQ_t}{Dt} = \left(\frac{Dx_t}{Dt}\ \ \frac{Dz_t}{Dt}\ \ \frac{D\phi_t}{Dt}\right) = F(t, Q_t)$$

The coordinates and velocity potential of the free surface nodes at the subsequent time step $t+\Delta t$ are obtained from the following relation.

$$Q_{t+\Delta t} = Q_t + \frac{Q_1}{6} + \frac{Q_2}{3} + \frac{Q_3}{3} + \frac{Q_4}{6}$$

Where,

$$Q_1 = \Delta t\ F(t, Q_t)$$

$$Q_2 = \Delta t\ F(t+\Delta t, Q_t + Q_1/2)$$

$$Q_3 = \Delta t\ F(t+\Delta t/2, Q_t + Q_2/2)$$

$$Q_4 = \Delta t\ F(t+\Delta t, Q_t + Q_3)$$

3.5.3 Regridding

At the beginning of the numerical simulation, the free surface nodes are uniformly distributed in the x-direction on the quiescent free surface with a zero surface elevation. As time elapses, the Lagrangian nodes on the liquid free surface move and

such movement leads to unequal horizontal spacing and gradual concentration of Lagrangian particles in the region of steep gradient close to the tank wall. The mesh distortion thus occurs may lead to numerical instability. To eliminate such instabilities, a mesh regridding technique is used at every time step. The numerical experiments conducted by Dommermuth and Yue (1987) showed that the regridding is extremely effective and eliminates the numerical instabilities without the use of artificial smoothing. A cubic spline is fitted through the distorted Lagragian nodes on the free surface. Subsequently, the velocity potentials and associated boundary values on the new sets of uniformly spaced Lagrangian nodes are obtained by interpolation. The liquid domain is remeshed based on the positions of newly formed Lagrangian nodes.

CHAPTER 4

4 FREE VIBRATION ANALYSIS OF RECTANGULAR TANK WITH INTERNAL SUBMERGED BLOCK

4.1 Introduction

Liquid sloshing encompasses a wide variety of practical problems of engineering interest and is a major cause of concern for safety and stability of the structures equipped with liquid filled container. Slosh-characteristics such as natural frequencies and mode shapes depend on the geometrical and material characteristics of the fluid-structure system, liquid-fill depths and the type of restraints at the container boundaries. Amplitude of slosh, in general, depends on the nature, amplitude and the frequency of external excitation, liquid-fill depth, physical properties of liquid and tank geometry. Often submerged internal components constitute an integral part of liquid-tank systems. Presence of internal components in the tank alters the sloshing characteristics of liquid in the tank in terms of its natural frequencies and modal shapes and hence the force vibration characteristics.

Numerous studies related to liquid sloshing have been carried out numerically, analytically, and experimentally in the past several decades. A limited number of studies reported on the free vibration characteristics of rectangular liquid tank with a submerged internal component.

System parameters such as natural frequencies and damping are fundamental to any system subjected to dynamic load.This chapter comprises of two sections; in the first section, the free vibration characteristics are determined by employing linear potential formulation and in the second section the free vibration characteristics are obtained employing nonlinear potential formulation. In the first section the effect of submerged block on the free vibration behaviour in terms of sloshing frequencies and mode shapes are studied. The size and location of the the submerged block is varied. The liquid fill-depth is also varied to study the effect of broad and tall tank on the free vibration characteristics. In the second section, however, liquid tanks with various fill-depth and without any submerged block is used to study the effect of nonlinearity on the sloshing frequencies is studied. The objective of this chapter is to verify as to how far the use of linear sloshing frequency in conducting force vibration is justified even when nonlinear sloshing analysis is resorted to by many researchers.

4.2 Linear Free Vibration Analysis

Free vibration analysis is conducted in a rectangular tank of length 30 m and liquid density 1,000 kg/m^3 with blocks of varying width (w), height (h) and position (b). The comparative results are presented in Table 4.1. The non dimensional sloshing frequencies $(\omega_j^2 L/g\pi)$ of present method is verified with the asymptotic solutions due to Davis (1992) and also with the analytical results due to Choun and Yun (1996) for several cases with centrally placed submerged block and the results are found to be extremely good in agreement.

4.2.1 Effect of Submerged Block on Sloshing Frequency

The natural frequencies and mode shapes are computed in a tank of width 30 m and liquid depth 13 m with varying sizes and position of the submerged block in order to study the effect of the submerged block on the free vibration characteristics of the slosh. The results are presented in Figure 4.1. Decrease in natural frequencies is observed with increase in the height of the centrally placed block of given width. However, the fundamental frequency is the most sensitive to the height of the block. The higher mode frequencies are less affected by the height of the block. Figure 4.1(b) shows a similar trend for increase in width of the centrally located block though; the effect is significantly less in such cases and the natural frequencies remain almost unaffected when the increase in width of the block is more than half the tank-width. Figure 4.1(c) shows that sloshing frequencies reduce as the block moves towards the center of the tank. The third mode sloshing frequency remains almost insensitive to the location of the block. In summary, the size and location of the block has significant influence on the sloshing frequencies of the liquid in the tank and the influence of height is more than the width for a given location. The first three sloshing mode shapes for tank with centrally located block (L = 30, d = 15 m, h = 0.5d, w = 0.4L) are presented in Figure 4.2(a,b).

Table 4.1: Non-Dimensional frequencies ($\omega_j L/g\pi$) for centrally placed block with varying *d/L* and *d/h*

			w/L = 0.25			*w/L* = 0.5			*w/L* = 0.75		
d/L	*h/d*	*j*	Davis(1992)	Choun et al. (1996)	Present FEM	Davis(1992)	Choun et al. (1996)	Present FEM	Davis(1992)	Choun et al. (1996)	Present FEM
0.25	0.5	1	0.437	0.438	0.439	0.389	0.389	0.389	0.375	0.376	0.375
		2	1.678	1.679	1.687	1.437	1.433	1.440	1.322	1.328	1.327
		3	2.834	2.834	2.848	2.694	2.693	2.712	2.508	2.513	2.524
		4	3.878	3.878	3.912	3.844	3.844	3.878	3.705	3.708	3.742
		5	4.953	4.953	5.015	4.901	4.902	4.963	4.841	4.841	4.906
	0.8	1	0.216	0.216	0.217	0.169	0.169	0.169	0.157	0.157	0.157
		2	1.251	1.252	1.256	0.769	0.768	0.775	0.624	0.629	0.626
		3	2.507	2.506	2.523	1.820	1.821	1.844	1.378	1.385	1.391
		4	3.390	3.392	3.425	3.066	3.067	3.110	2.367	2.371	1.401
		5	4.537	4.536	4.611	4.189	4.190	4.250	3.511	3.516	3.583
1.0	0.5	1	0.931	0.939	0.948	0.920	0.931	0.920	0.917	0.927	0.918
		2	1.998	1.998	2.001	1.994	1.996	1.998	1.993	1.995	1.996
		3	3.000	3.000	3.012	3.000	3.000	3.012	3.000	3.000	3.012
		4	4.000	4.000	4.028	4.000	4.000	4.028	4.000	4.000	4.028
		5	5.000	5.000	5.056	5.000	5.000	5.056	5.000	5.000	5.056
	0.8	1	0.621	0.648	0.618	0.570	0.624	0.573	0.558	0.579	0.558
		2	1.895	1.901	1.901	1.765	1.826	1.768	1.706	1.773	1.710
		3	2.972	2.974	2.984	2.926	2.931	2.940	2.872	2.892	2.886
		4	3.983	3.985	4.012	3.976	3.977	4.005	3.954	3.959	3.984
		5	4.996	4.996	5.052	4.990	4.991	5.046	4.985	4.985	5.041

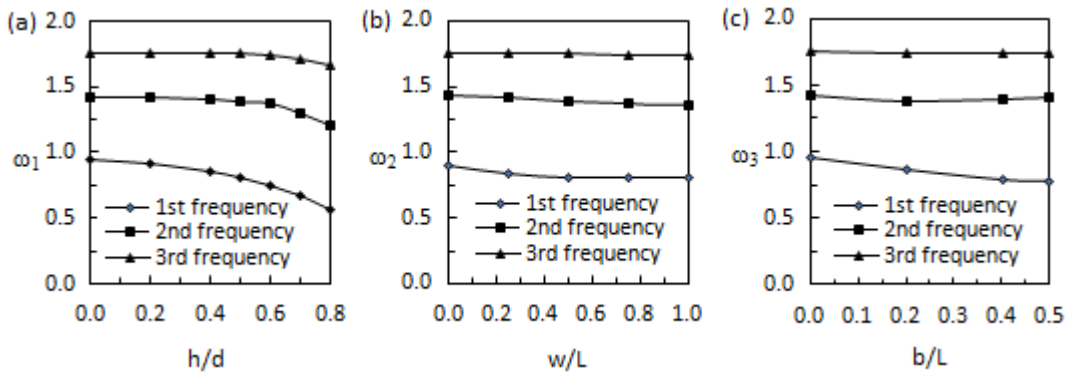

Figure 4.1: Sloshing frequencies (L = 30 m, d = 13 m) for: (a) variation of block height (b = 15 m, w = 10 m); (b) variation of block width (b =15 m, h = 6 m); (c) variation of block location (w = 4 m, h = 8 m)

It is evidently clear from the results in Figure 4.1(b) that the width of the block is not very significant in influencing the sloshing frequencies. Hence it is logical to use baffles as submerged objects for reducing the fundamental sloshing frequency or for that matter sloshing frequencies of the lower modes in order to keep the resonant frequency away from the excitation frequency.

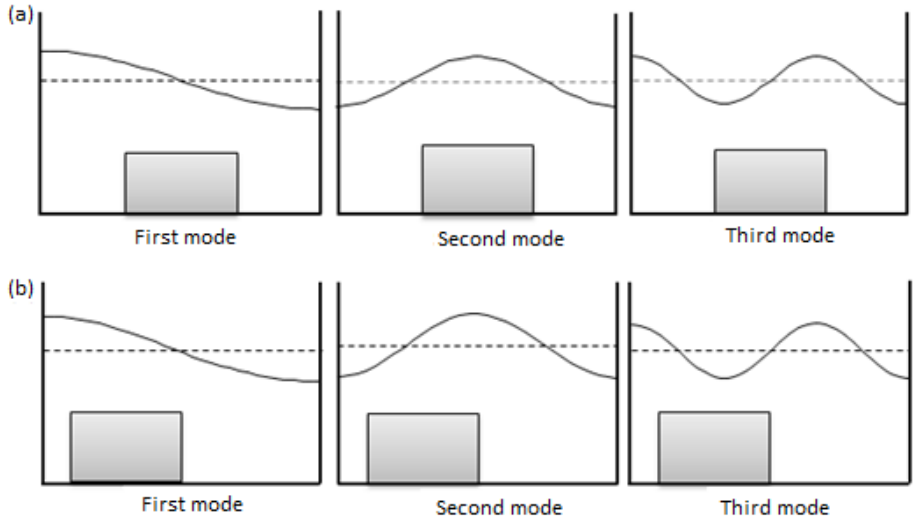

Figure 4.2: Sloshing modes (L = 30 m, d = 15 m): (a) for a centrally located block (h = 0.5d, w = 0.4L) (b) for an off-centred block (h = 0.5d, w = 0.4L, b = 0.3L)

4.2.2 Effect of Vertical Baffle on the Sloshing Frequencies

The effects of centrally placed and off-centered baffle on the sloshing frequencies and mode shapes are presented in Figure 4.3 and Figure 4.4 respectively for various baffle height to liquid depth ratio (h/d).

The natural sloshing frequencies of symmetric modes are not affected by the presence of the centrally located baffles. This is because the baffle is located under the antinode of the waves. However those of the odd modes change due to the baffle and again the variation in the fundamental mode is more prominent. . Similar results can be seen for cases with a baffle placed at $0.4L$ from the wall of the tank. The sloshing frequency of the first four modes decrease as h increases, the fifth mode does not change. It is because the baffle is located under the antinode in case of the fifth sloshing mode.

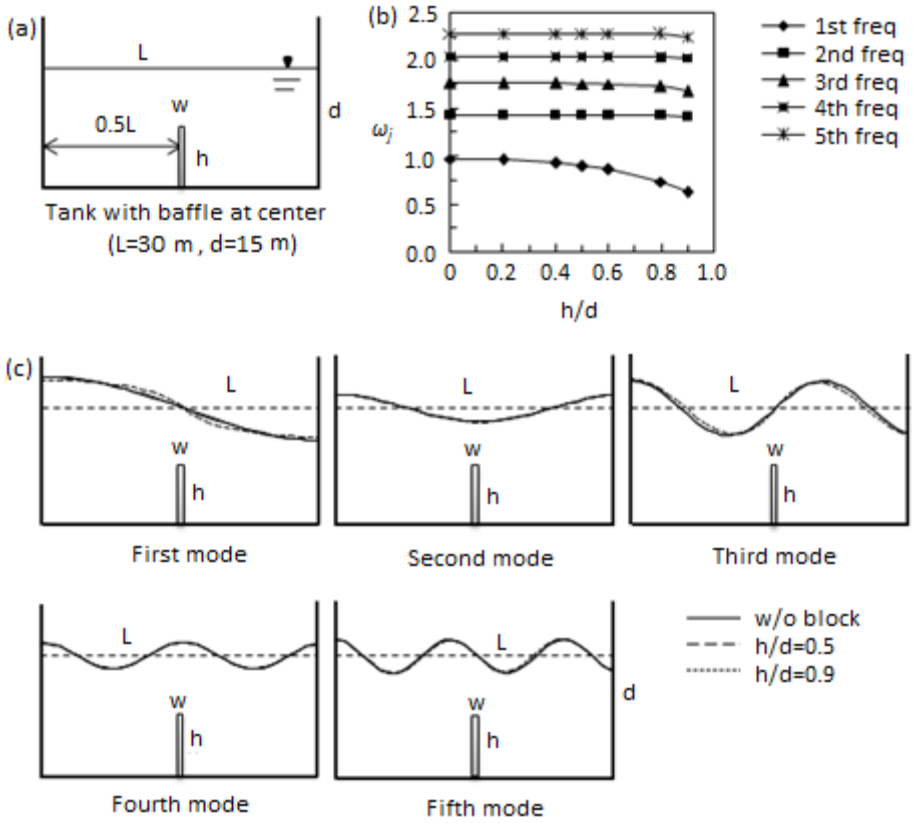

Figure 4.3: Sloshing and modes for various heights of a centrally placed baffle (d/L = 0.5): (a) tank with a centrally placed baffle (L = 30 m, d = 15 m); (b) sloshing frequencies; (c) mode shapes

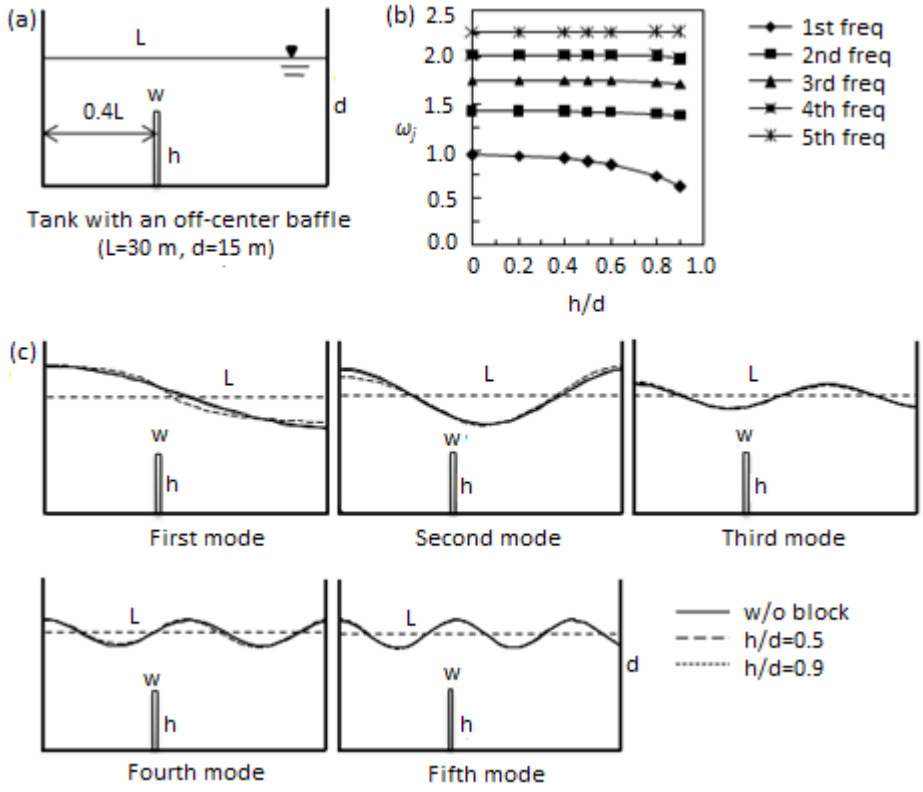

Figure 4.4: Sloshing and modes for various heights of an off-center baffle (d/L = 0.5): (a) tank with an off-center baffle (L = 30 m, d = 15 m); (b) sloshing frequencies; (c) mode shapes

4.2.3 Effect of Submerged Block on the Sloshing Frequencies in Tank with different Fill-depth

In order to investigate the effect of various fill-depths to tank width ratio (d/L) also called the aspect ratio on the sloshing frequencies in tank without and with submerged block, the sloshing frequencies of respective modes are normalized with respect to the sloshing frequency of the corresponding mode without submerged block for a given fill-depth. Normalized sloshing frequencies of first three modes vs. non-dimensional block height to fill depth (h/d), width of block to length (w/L), and location (b/L) are then plotted. Figure 4.5 shows the variation of the normalized sloshing frequencies with the height of the centrally placed block for different ratio of fill-depth to width (d/L) of the tank. The frequencies are normalized with those of the tank without block. The sloshing frequencies decrease with increase in the height of the block. The decrease is more rapid for large value of h/d. The decrease is more prominent for low sloshing modes and for broad tanks. For cases in a tall tank ($d/L \geq 2.0$) with a short

block (h/d < 0.5), very little changes in the sloshing frequencies are observed due to the submerged block.

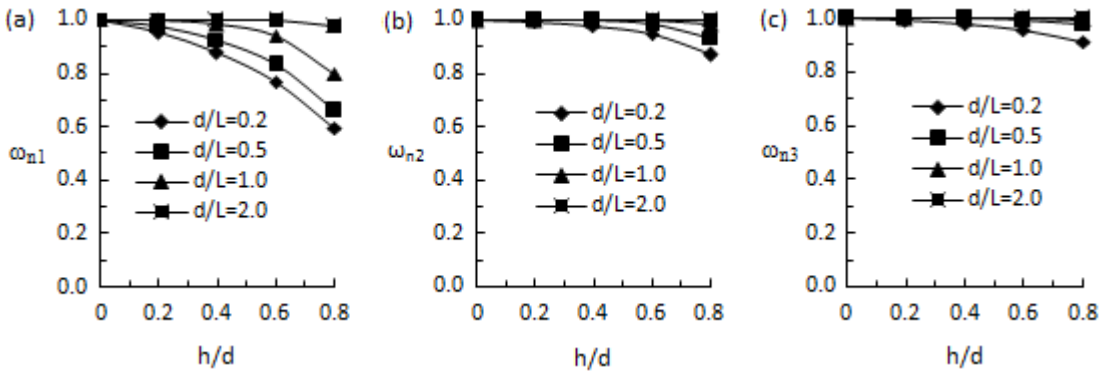

Figure 4.5: Normalized sloshing frequencies (ω_{nj}) as a function of block height (h/d) for centrally placed block (b = 0.5L, w = 0.2L): (a) First mode (b) Second mode (c) Third mode

The variation of the normalized sloshing frequencies vs. block width to tank width ratio (w/L) for centrally located block of height h=0.6d, is presented in Figure 4.6. The sloshing frequencies decrease with increase in the width of the block though; they remain almost constant for w/L > 0.7. For tall tanks with d/L > 1, the sloshing frequencies remain almost unchanged with varying width of the block. Figure 4.7 shows the variation of the normalized frequencies due to varying location b/L block of height 0.7d. Significant decrease in the first sloshing frequency can be seen as the block moves from the wall towards the center of the tank. The effect of the location of the block on the variation of second and third sloshing frequencies is very small. For tall tanks with d/L > 1.0, the variation in sloshing frequencies due to location of the block is not very significant.

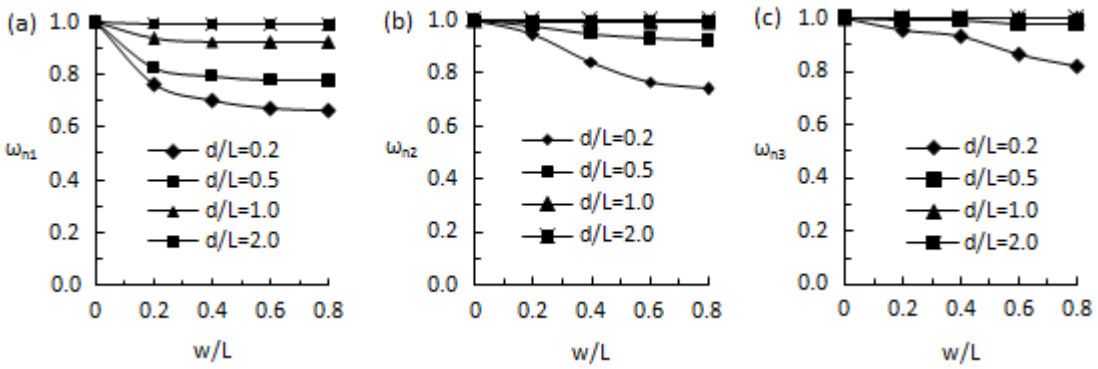

Figure 4.6: Normalized sloshing frequencies (ω_{nj}) as a function of block width (w/L) for centrally placed block (b = 0.5L, h = 0.6d): (a) First mode (b) Second mode (c) Third mode

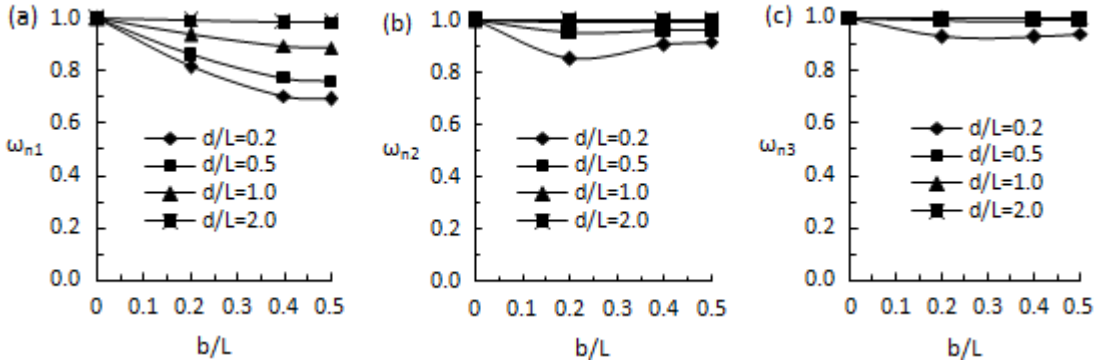

Figure 4.7: Normalized sloshing frequencies (ω_{nj}) as a function of block location (b/L) for off- centered block (w = 0.2L, h = 0.7d): (a) First mode (b) Second mode (c) Third mode

4.2.4 Effect of Block Height and Location on the Sloshing Modes

Figure 4. 8 shows the sloshing modes for different block heights in two broad tanks. It may be seen that the height of the block has significant influence on the mode shapes. The effect of the block location on sloshing modes in broad tanks is shown in Figure 4.9. The change in the shape of the sloshing modes in terms of the lateral position of nodes and antinodes are more significant due to the change in the location of the block than its height.

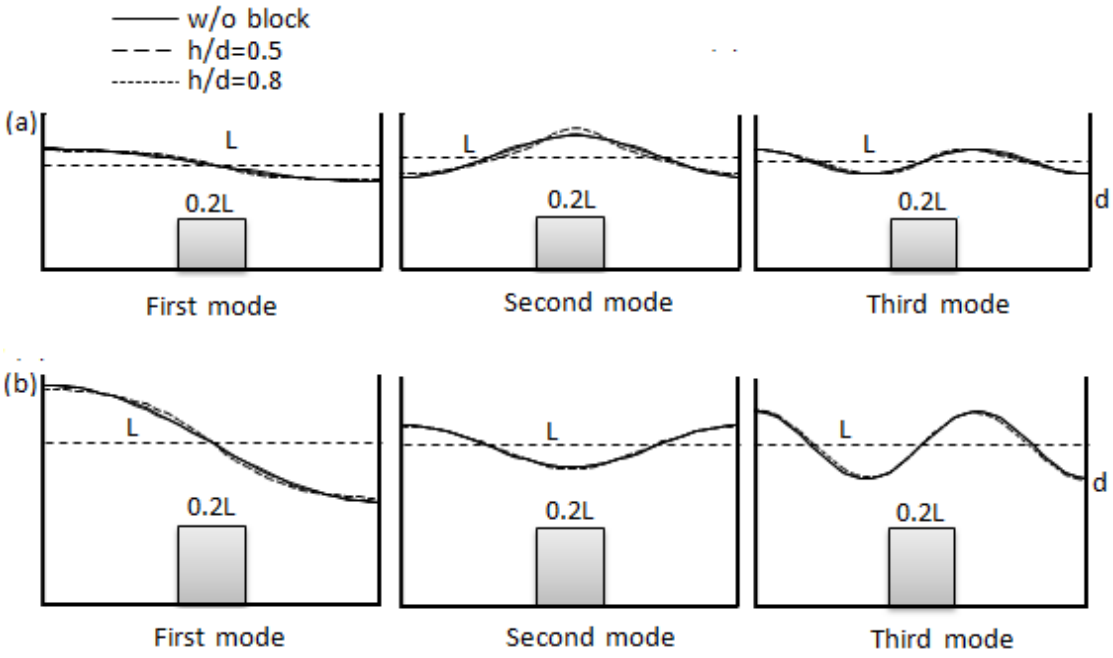

Figure 4.8: Sloshing modes for various heights of block (*h/d*): (a) tank with *d/L* = 0.2; (b) tank with *d/L* = 0.5.

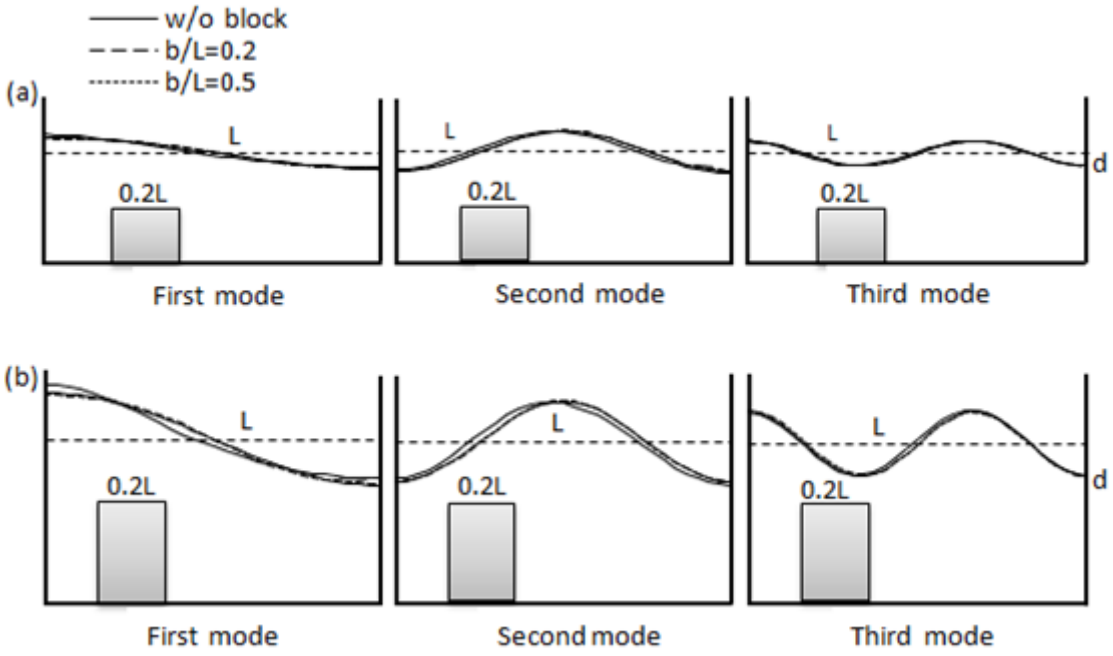

Figure 4.9: Sloshing modes for various locations of block (*b/L*): (a) tank with *d/L* = 0.2; (b) tank with *d/L* = 0.5.

4.3 Nonlinear free vibration analysis

4.3.1 Model Validation

The model validation is established by comparing the present FEM result with Virella et al. (2008). The tank of width 30.675 m and liquid depth 10.73 m with d/L ratio 0.35 is considered for the simulation. A harmonic force of $a_t = 0.01g \sin \bar{\omega} t$ is applied as base excitation, where $\bar{\omega}$ is taken as the fundamental sloshing frequency ω_1 of the liquid. The liquid considered for the study is water. Figure 4.10 shows the time variation of free surface displacement at the right hand wall of the tank. The present FEM result compares extremely well with the result of Virella et al. (2008).

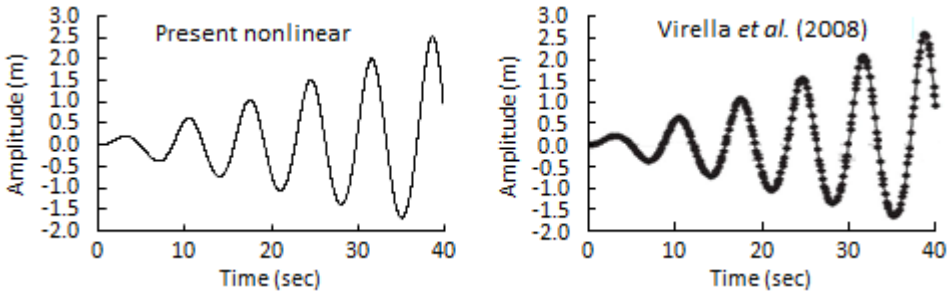

Figure 4.10: Time history of the sloshing elevation at right hand wall of tank in the first sloshing mode

4.3.2 Sloshing Frequencies

Rectangular tank of 30 m width and various fill-depths is considered to study the effect of nonlinearity on the dynamic behaviour of the tank-liquid system. Harmonic base excitation with same amplitude as in the previous section is used for the study.

The linear frequencies were obtained directly by solving the eigen-value problem from linear finite element model developed as in chapter 3. The nonlinear sloshing frequencies, however, were extracted in an indirect method from harmonic response analysis in the frequency domain. The maximum sloshing elevations, as a function of base excitation frequency, were computed for each of the tank-liquid system with varying depths of liquid. The total time of computation was taken as 40s, which produced more than four cycles of motion in the first natural frequency for any of the

selected tank-liquid systems. Figure 4.11 presents the maximum wave elevation, as a function of base excitation frequency, for systems with various d/L. It is observed that for all the cases the maximum surface wave elevations obtained for their respective first modes are significantly more than those obtained for the higher modes. The sloshing response is dominated by the first sloshing mode. The natural frequencies of first three anti-symmetric sloshing modes are recorded and presented in Table 4.2. Presented along are their respective linear sloshing modes for comparison. The fundamental frequency increases with increase in the ratio of liquid-depth to tank-width both in case of linear and nonlinear wave theories. The second and third sloshing frequencies, computed from linear theory, remain almost unchanged with increase in the ratio of fill-depth. For the nonlinear second mode, the sloshing frequency showed a marginal decreasing trend. In case of nonlinear third mode the highest reduction in sloshing frequency was observed. The results of natural frequencies for the first three antisymmetric sloshing modes, with linear and nonlinear wave theory, are presented in Figure 4.12 for easy comparison. Similar variations of natural frequencies were observed both for linear and nonlinear wave theory. Very little variations in natural frequencies are observed between linear and nonlinear theories. The fundamental frequency showed a maximum variation of less than 4.2% for broad tank of d/L = 0.2 and less than 3.2% for tall tank of d/L = 0.85. The higher mode frequencies are still less affected. Hence, one may conclude that nonlinearity has no significant effect on the natural frequencies.

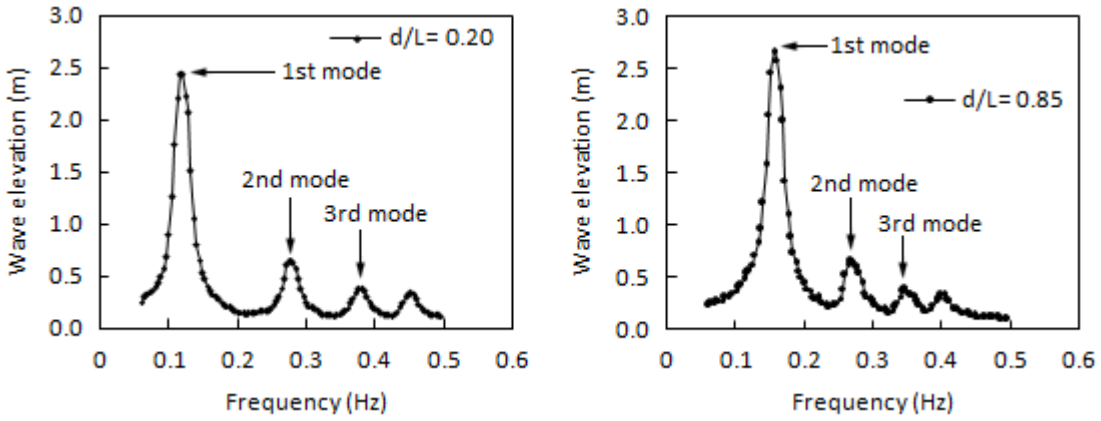

Figure 4.11: Maximum wave elevation vs. excitation frequency for tank-liquid systems of varying liquid-depths: (a) d/L= 0.20; (b) d/L= 0.85

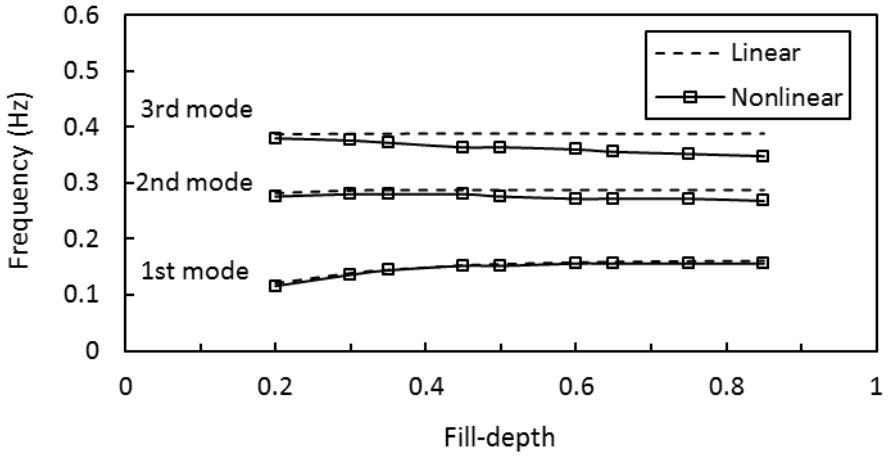

Figure 4.12: Nonlinear and linear sloshing frequencies for tanks with varying fill depth (*d/L*)

Table 4.2: Linear and nonlinear natural frequencies for the first three sloshing modes

Sl. No.	Fill-depth *(d/L)*	Sloshing modes					
		Linear			Nonlinear		
		First	Second	Third	First	Second	Third
1	0.20	0.121	0.282	0.387	0.116	0.276	0.380
2	0.30	0.139	0.286	0.387	0.136	0.280	0.376
3	0.35	0.145	0.287	0.388	0.144	0.280	0.372
4	0.45	0.152	0.287	0.388	0.152	0.280	0.364
5	0.50	0.155	0.287	0.388	0.152	0.276	0.364
6	0.60	0.158	0.287	0.388	0.156	0.272	0.360
7	0.65	0.159	0.287	0.388	0.156	0.272	0.356
8	0.75	0.160	0.287	0.388	0.156	0.272	0.352
9	0.85	0.161	0.287	0.388	0.156	0.268	0.348

4.4 Conclusions

The linear and nonlinear free vibration analysis of partially filled rigid rectangular tank resulted in the following observations.

1. The sloshing frequencies and the free surface wave elevation decrease with the increase in the height and width of the bottom-mounted submerged block. The fundamental frequency is the most sensitive to the block dimension.

2. For a given block dimension the sloshing frequencies decrease as the block move towards the center of the tank.
3. Of the three parameters, the influence of the block height is the largest on the sloshing resonant frequencies and sloshing elevation.
4. The variation of sloshing frequencies and mode shapes are more sensitive in broad tanks ($d/L < 0.5$) with a tall block ($h/d > 0.5$) than in tall tanks of similar case due to the presence of the submerged block.
5. The effect of nonlinearity on the natural sloshing frequencies of the liquid is insignificant irrespective of the fill-depths of the liquid in the tank. And nonlinearity has absolutely insignificant effect on the higher sloshing modes.
6. Nonlinearity has a major effect on the surface wave elevation and should be considered for such decisions as the free board of the tank.

The fundamental frequency mobilises more force than any other higher frequencies under resonant external excitation and the stability of the tank in question is greatly influenced when the exciting frequency matches with the fundamental frequency. It is here the bottom-mounted submerged blocks may be used to keep the fundamental resonant frequency or for that matter any other resonant frequency away from the excitation frequency. For constructional suitability bottom-mounted submerged blocks have competitive edge over wall-mounted horizontal baffles. Submerged blocks are more suitable than horizontal baffles in broad tanks because variation in liquid depth may negate the utility of horizontal baffle when the liquid level falls below the mounting height of the horizontal baffle. It can be concluded that the fundamental sloshing frequency of liquid in a tank can be kept away from the excitation frequency by adjusting the dimension and location of the submerged block.

CHAPTER 5

5 LINEAR SEISMIC RESPONSE OF RECTANGULAR LIQUID TANK WITH SUBMERGED BLOCK

5.1 Introduction

Under external excitation, the motion experienced by unrestrained liquid in a partially filled container is termed as sloshing. The free surface motion of liquid in a container represents the overall dynamics of liquid in its globality. A part of the liquid adjacent to the bottom of the container moves with the velocity equal to that of the container and behaves the same way as solid material will do while the liquid above it would participate in sloshing motion. It is the amount of this part of liquid which critically manipulates the dynamic response of the liquid-tank system in a way significantly different from the response of a similar tank containing solid material. The amount of liquid participating in the sloshing motion depends on the tank geometry and the liquid fill-depth, and internal components if any and orientation, duration, amplitude and frequency contents of earthquake. Sloshing characteristics depend on such diverse parameters of liquid-tank sy stem as tank geometry, liquid-fill depths, aspect ratio of tank, compressibility and viscosity of liquid, amplitude and frequency of external excitation, orientation and type of excitation, properties of tank material, and restraint conditions of support structure etc. This makes generalization of liquid motion impossible and its implication on the dynamics of tank-liquid system all the more difficult. Application of slosh dynamics encompasses many important fields of engineering interest exemplified as ground-supported and above ground liquid storage tanks, fuel tanks of launching vehicles, dynamics of liquid transporting vehicles and

its control, sloshing in nuclear fuel storage pool, water waves in reservoirs, cargo tanks of LNG carriers with liquid storage tank as system component. Liquid containers constitute a major chunk of critical life line structures and are extensively used in water supply facilities, oil and gas industries, and nuclear power plants for storage of a variety of liquids such as oil, liquefied natural gas, chemical fluids and industrial wastes of different forms. The prediction of sloshing behaviour is imperative for structural safety and integrity of liquid-tank system. In extreme situations when either the amplitude of external excitation is very high or the excitation frequency is very close to the fundamental sloshing frequency the liquid motion in the container becomes violent and severely damages liquid-tank system. The dynamic response of fluid-structure system is very sensitive to the characteristics of ground motion and configuration of the system.

Unlike other natural disasters, earthquakes are neither predictable nor preventable. Hence the only resort open for the engineering community is to accurately predict the dynamic behaviour and properly design of fluid-structure system to minimize the effect of earthquake so that the tank-liquid system can stand the test of nature. Although the complicated deformed configurations of liquid storage tanks and the interaction between the fluid and the structure result in a wide variety of possible failure mechanisms, reports from past earthquakes indicate that the damages to the liquid filled tanks are either by large axial compression due to beamlike bending of the container wall causing a failure characterized as “elephant-foot” buckling or by sloshing of the contained liquid with insufficient freeboard between the quiescent liquid surface and the tank roof. Markedly different failure types have been reported in cases of anchored and unanchored tanks. Previously conducted study in rectangular tanks with liquid-depth to half-width of tank ratios ranging from 0.4 to 1.65 showed that nonlinearity of the surface wave did not have major influence on the natural frequencies and on the pressure distribution on the walls.

No study is available in open literature to quantify the effect of submerged block on impulsive and convective response of dynamic behavior of liquid in a tank. To this end the present study comprehensively investigates the effect of submerged block on the impulsive and convective response of tank-liquid system under seismic motions of varying frequency content. On the basis of PGA/PGV ratio, the earthquake records

are classified into three categories: high (PGA/PGV > 1.2), intermediate (0.8< PGA/PGV< 1.2) and low (PGA/PGV < 0.8) (Heidebrecht and Lu, 1988). Six ground motions characterised on the basis of their frequency content have been used. Of them four are selected from Pacific Earthquake Engineering Research Next Generation Attenuation (PEER-NGA) strong motion database records available online at *http://peer.berkeley.edu/nga.* Ground acceleration data for El Centro-EW is obtained from *http://www.vibrationdata.com/elcentro.htm.* The sixth-one is the compatible time history of acceleration as per spectra of Indian Standard Code 1893 (Part-1): 2002 for structural design in India (Agarwal and Shrikhande, 2009). The peak ground acceleration of all the records are scaled to a fixed magnitude of 0.2g for comparison of the dynamic responses of liquid under selected seismic excitations with varying frequency contents.

A velocity potential based Galerkin finite element model is developed for the analysis. The model so developed accounts for the slosh displacement and total hydrodynamic pressure. The impulsive pressure is computed by neglecting the liquid sloshing, and as a consequence the pressure at the liquid free surface vanishes.

5.2 Numerical Results and Discussion

A finite element code developed and described in chapter 3 is executed in Matlab platform to evaluate the seismic response of partially filled rectangular liquid-tank system with centrally placed ($b = 0.5L$) bottom-mounted submerged block as internal component. The governing parameters of the tank-liquid system are as follows:

L = 10 m, d = 5 m and a block of width, $w = 0.2L$*:* density of liquid, $\rho = 1000 kg/m^3$, Artificial damping (pseudo-viscous damping), $\mu = \xi \mu_{crit}$ where ξ is the viscous type numerical damping; $\mu_{crit} = 2\omega$ and ω is the fundamental sloshing frequency of liquid.

The correct prescription of the value of ξ depends on the dimension of the tank and liquid depth and can be found from experimental validation of numerical result. In the present investigation, however, the value of ξ has been prescribed as 0.0075 by comparing the present numerical result with the analytical result (Choun and Yun, 1999) and is used for further investigation here on.

Six different ground motion data, presented in Table 5.1, are used as the excitations for the system. The PGAs of all the records are scaled to a fixed magnitude of 0.2g as shown in the Figure 5.1 for easy comparison of the dynamic responses under seismic excitations with varying frequency contents. Also presented, are the velocity time history as in Figure 5.2. On the basis of the ratios of PGA/PGV, El Centro-EW and Imperial Valley are considered as low frequency ground motions; IS Code and Landers are regarded as intermediate frequency content excitations; and San-Franscisco and Colianga are categorized as high frequency content seismic motions. All selected motions, except El Centro-EW, are about 40 seconds of duration. In addition, the power spectrum density functions (PSDF) of all ground motions are obtained which depict the frequency content as shown in the Figure 5.3

Table 5.1: Ground motion records

Records (Station)	Component	Magnitude	Epicentral Distance Km)	Duration (s)	Time step for response computation (s)	PGA (g)	PGV (m/s)	PGA/PGV
1940 El Centro-EW (Imperial Valley)	East-West	7.1	-	53.48	0.02	0.241	0.4879	0.439
1979 Imperial Valley-06 (Holtville Post office)	HVP225	6.53	19.81	37.745	0.005	0.2476	0.4765	0.519
IS Code #	-	-	-	40.0	0.01	1.0	1.0405	0.961
1992 Landers (Fort Irwin)	FTI000	7.28	120.99	40.0	0.02	0.1288	0.1244	1.035
1987 San-Franscisco (Golden Gate Park)	GGP010	5.28	11.13	39.725	0.005	0.1073	0.0377	2.846
1983 Colianga-06 (CDMG)	CHP000	4.89	9.27	40.0	0.005	0.1539	0.0640	2.405

5.2.1 Model Validation

El Centro-EW is prescribed as ground motion for computation of time history of sloshing in partially filled tank without or with block. The result obtained with a prescribed artificial viscous damping $\xi = 0.0075$ is plotted in Figure 5.4 along with the analytical result of Choun and Yun (1999) and is found to have extremely close matching in all its characteristics such as magnitude and phase etc.

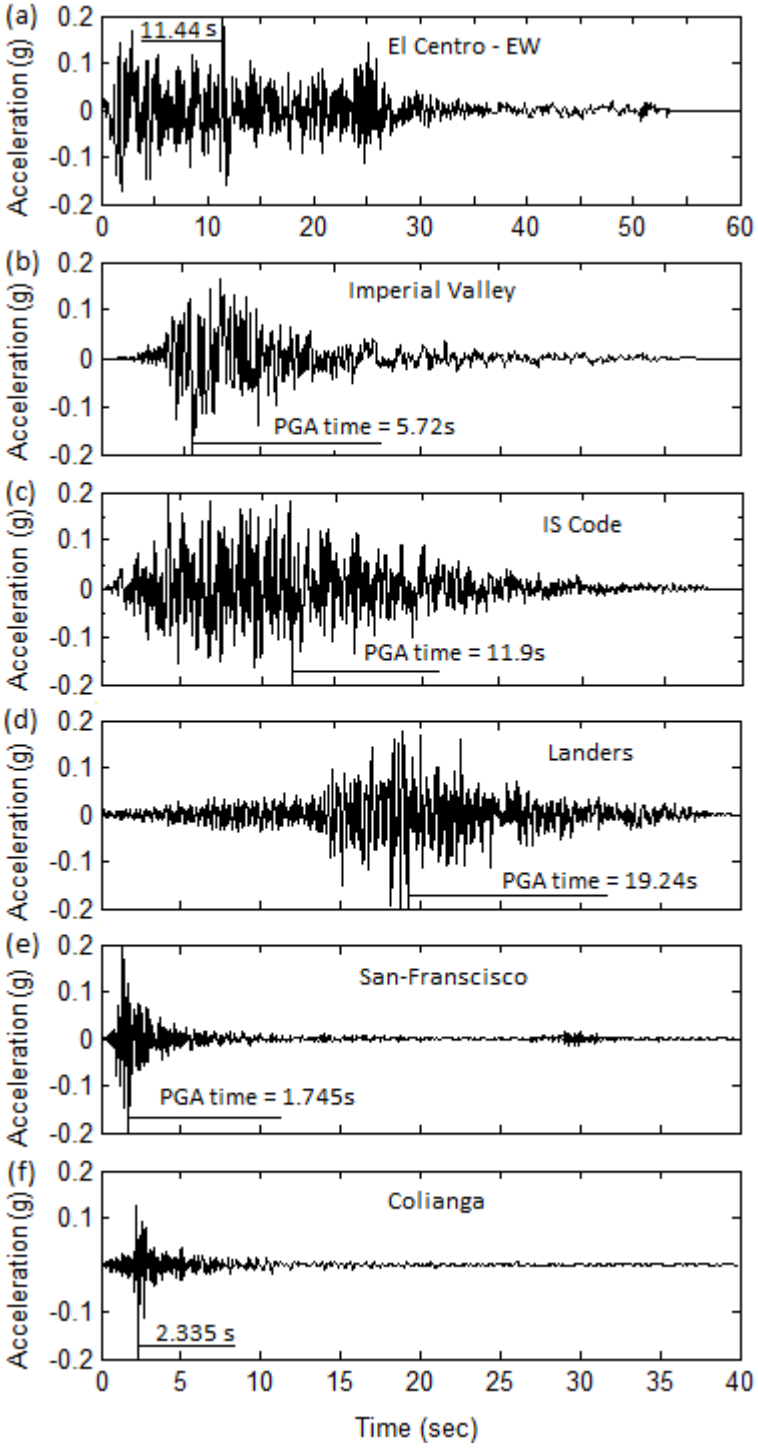

Figure 5.1: Time-history of acceleration of ground motion: (a) El Centro-EW (b) Imperial Valley (c) IS Code ground motion data (d) Landers (e) San-Franscisco (f) Colianga

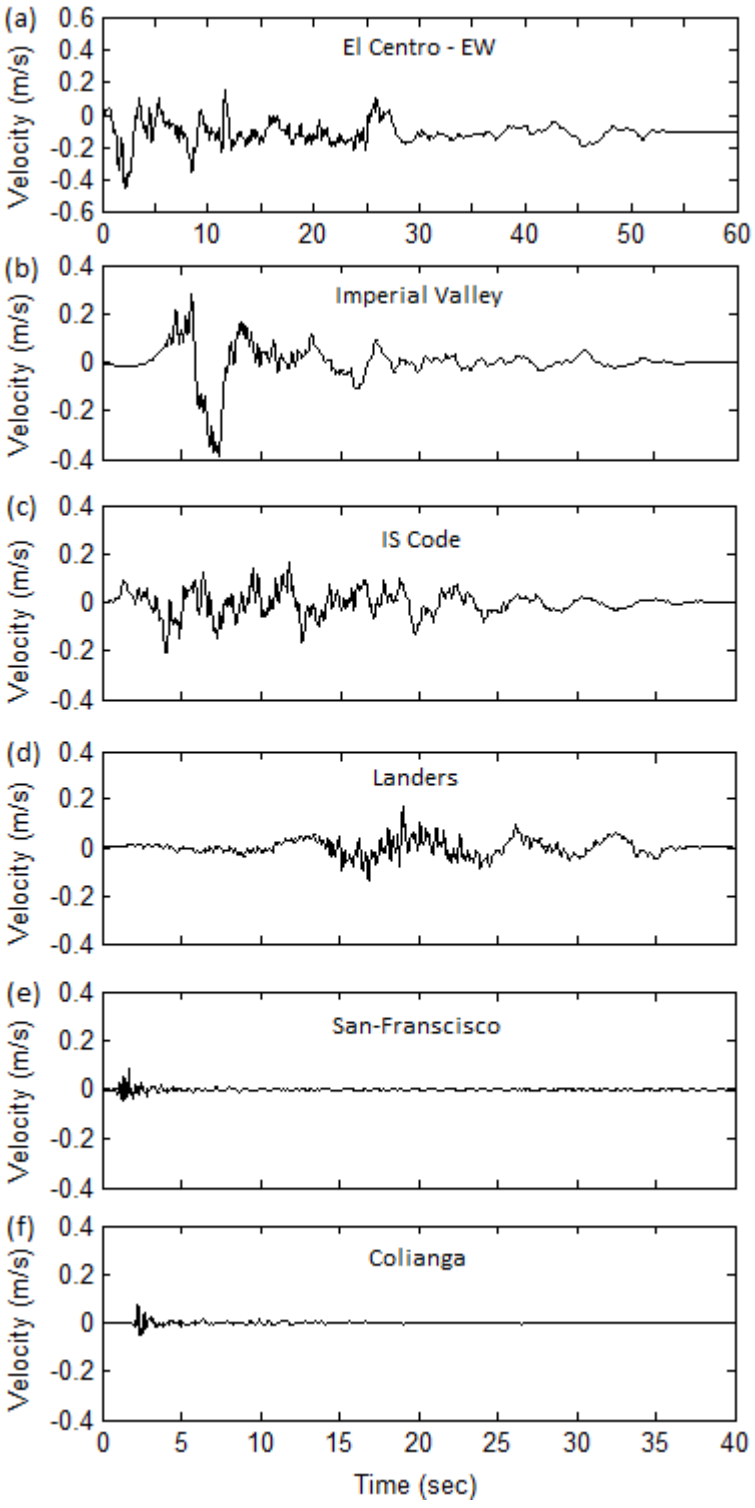

Figure 5.2: Time-history of velocity of ground motion: (a) El Centro-EW (b) Imperial Valley (c) IS Code ground motion data (d) Landers (e) San-Franscisco (f) Colianga

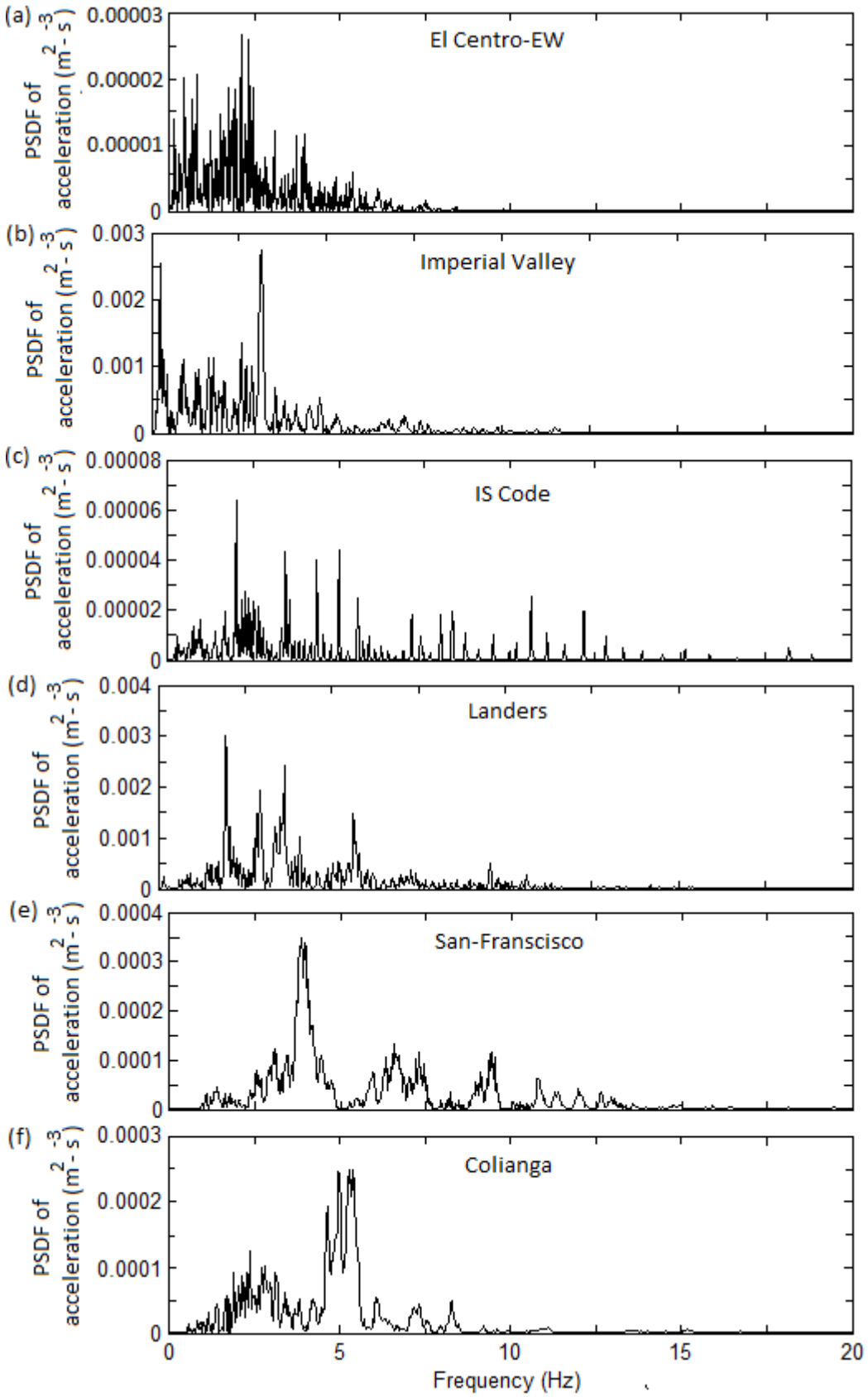

Figure 5.3: Power spectrum density function of ground acceleration: (a) El Centro-EW (b) Imperial Valley (c) IS Code ground motion data (d) Landers (e) San-Franscisco (f) Colianga

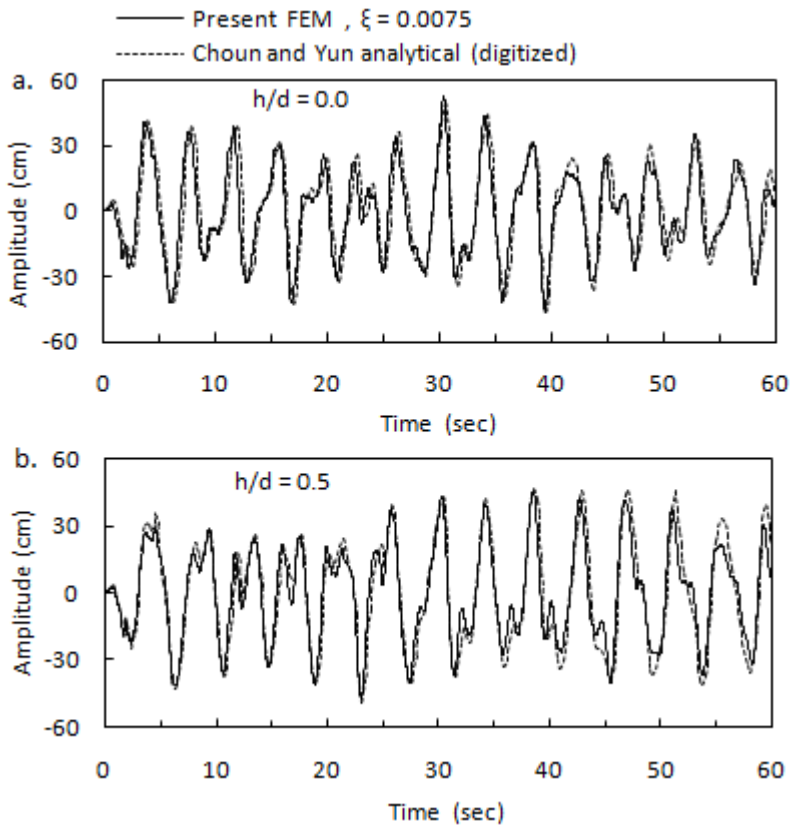

Figure 5.4: Time history of free surface wave amplitude at left hand wall of tank for different heights of submerged block due to El Centro-EW ground motion: (a) h/d = 0.0, (b) h/d = 0.5

Table 5.2: Sloshing frequencies (Hz) for various submerged-block heights (h/d)

Antisymmetric mode	Ratio of block height to liquid depth (h/d)		
	0.0	0.2	0.5
1	0.2676	0.2613	0.2368
2	0.4841	0.4840	0.4832
3	0.6254	0.6254	0.6254
4	0.7407	0.7407	0.7407
5	0.8409	0.8409	0.8409

5.2.2 Sloshing Frequencies

The sloshing frequencies for the anti-symmetric modes in the tank-liquid system as obtained from free vibration analysis are listed in Table 5.2. The sloshing frequency decreases with increase in the height of the submerged block. It may be noted that the fundamental sloshing frequency decreases considerably as the height of the submerged block increases.

5.2.3 Sloshing Response

The sloshing wave elevation itself is not only important for the seismic design of liquid containers but also gives the convective response of hydrodynamic pressure and associated base shear and base moment. Free board to be provided in a tank may be based on maximum value of sloshing wave height. Further, insufficient free board obstructs the free movement of convective mass and thus changes the amount of liquid in convective mode. If sufficient free board is not provided roof structure should be designed to resist the uplift pressure due to sloshing of liquid. Hence sensitiveness of sloshing response to the frequency content characteristics of seismic ground motions is studied. The effect of submerged block on the sloshing response of liquid, for a given ground motion, is also studied by changing the height (h/d) of the centrally placed block of width $0.2L$. Figure 5.5 presents the sloshing response at left wall of the tank in terms of sloshing elevation time history for the liquid-tank system with varying height of the block under various ground motions. The absolute maximum values of sloshing elevations are also presented in Table 5.3. It is observed that the absolute maximum value of sloshing decrease with increase in the height of the submerged block in case of low frequency ground motion of El Centro-EW, intermediate frequency motion of Landers and high frequency motions of San-Franscisco and Colianga. However low frequency content earthquake of Imperial Valley and intermediate frequency ground motion data of IS Code show a different trend in the variation of sloshing elevation. In both these cases a decrease in sloshing elevation is observed as the height of submerged block increases from $h/d = 0.0$ to $h/d = 0.2$ and the sloshing elevation increase with further increase in the height of the block from $h/d = 0.2$ to $h/d = 0.5$. Irrespective of block or no-block a significant decrease in sloshing response is observed from low frequency content to high frequency content seismic motion. Sloshing response of low frequency motions of El

Centro and Imperial Valley are the most sensitive to the presence of submerged block. And high frequency motions of San-Franscisco and Colianga are the less sensitive to the presence of submerged block in the tank.

Higher sloshing responses are observed in case of low frequency ground motions of El Centro-EW and Imperial Valley. The highest sloshing amplitude is observed for tank with h/d = 0.5 compared to h/d = 0.0 and h/d = 0.2; under Imperial Valley ground motion, which has a dominant frequency of 0.2441 Hz, which is close to the fundamental sloshing frequency (0.2368 Hz) of liquid for tank with h/d = 0.5. As one moves from low frequency ground motion to the high frequency ground motion, the dominating frequencies of ground motions deviate away from the sloshing frequencies of the tank-liquid-submerged block system which results in decrease in the sloshing response. It may be mentioned that the dominating frequencies of intermediate frequency ground motions of IS Code and Landers, and high frequency ground motions of San-Franscisco and Colianga are not within the ambit of the first five natural sloshing frequencies of the tank-liquid-submerged block systems considered in the study.

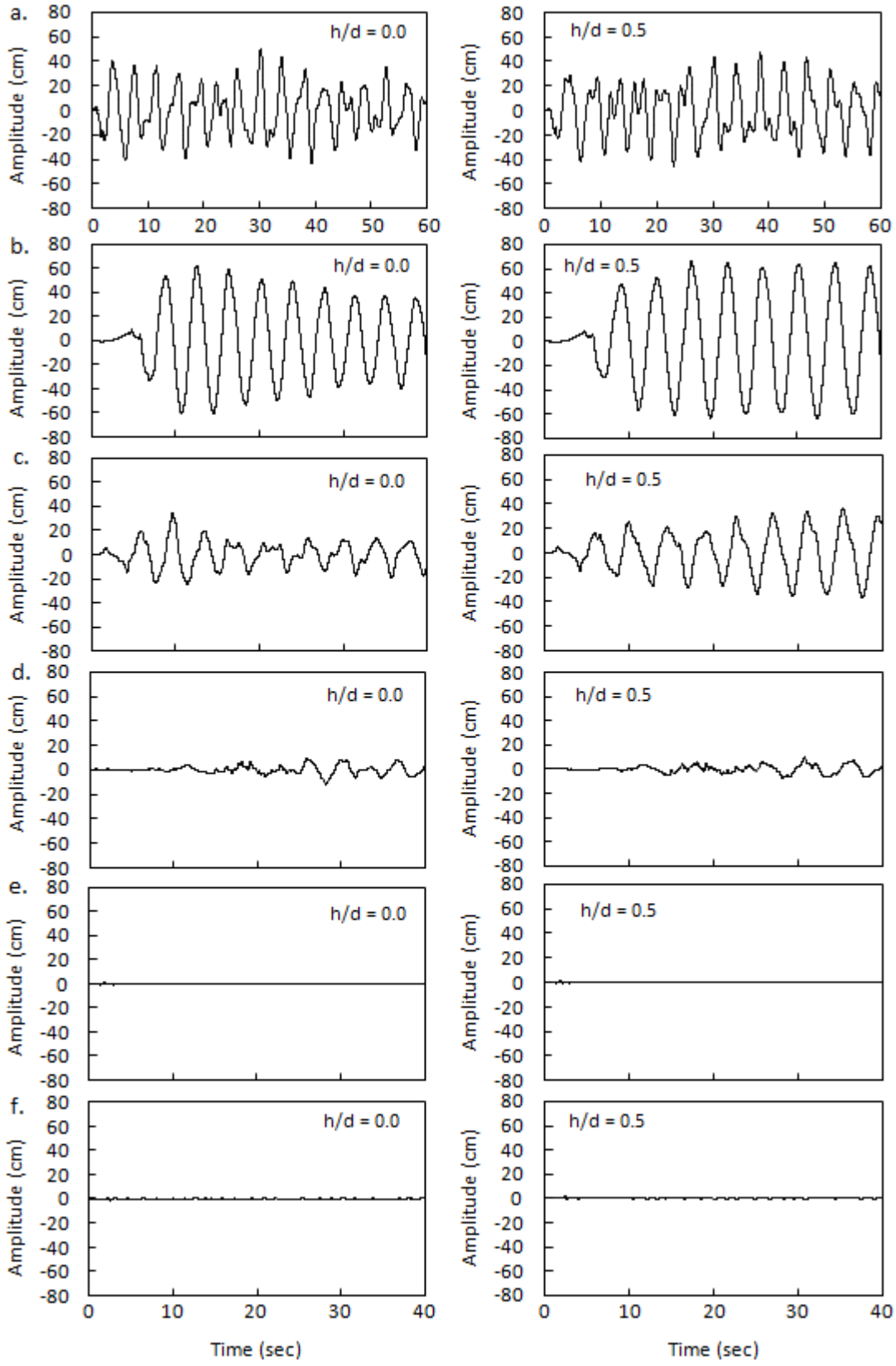

Figure 5.5: Temporal variation of sloshing elevation in tank with submerged block under seismic ground motions: (a) El Centro-EW (b) Imperial Valley (c) IS Code ground motion data (d) Landers (e) San-Franscisco (f) Colianga

5.2.4 On Validity of Hydrostatic Base Shear

In order to study the validity of the concept of equivalent hydrostatic base shear, the same is investigated alongside the hydrodynamic base shear. The so called "hydrostatic base shear" concept is based on the assumption that at a given instant during the ground motion, the liquid mass in motion is stationary with a difference in elevation of liquid at two lateral walls perpendicular to the direction of excitation. The difference between the integrated hydrostatic pressures over the two opposite walls of the container perpendicular to the direction of liquid oscillations, gives the difference of pseudo-hydrostatic force, which is called equivalent hydrostatic base shear (Banerji *et al.*, 2000). Such a force $\overline{S_b}$ is obtained as

$$\bar{S}_b = \frac{\rho g B}{2}\left(\eta_r{}^2 - \eta_l{}^2\right) \tag{5.1}$$

Where η_r and η_l are the free surface elevations at left and right tank-walls respectively measured with respect to the tank-bottom, and B is the length of the tank wall perpendicular to the direction of excitation. The hydrodynamic base shear force S_b is directly calculated from Equation (3.48). The time history of hydrodynamic base shear for all ground motions with different block heights are plotted alongside the equivalent hydrostatic base shear in Figures 5.6-5.11. It is noticed from Figure 5.7 that for low frequency content seismic motion of Imperial Valley the maximum base shears obtained from hydrostatic formula for liquid tanks with and without submerged block, closely matched with the actual hydrodynamic base shears for respective cases. However for intermediate frequency ground motion of Landers and high frequency ground motions of San-Franscisco and Colianga, the hydrostatic base shears are negligible as compared to their corresponding hydrodynamic counterparts. Further the time history of hydrostatic base shear has no close correlation with the time history of hydrodynamic base shear and the peaks in both the cases occur at significantly different instants of time. This is a clear indication that it is merely a coincidence rather than any physics behind the notion of equivalent hydrostatic base shear. The mismatch of equivalent hydrostatic base shear with the hydrodynamic base shear is also quite evident from Table 5.3.

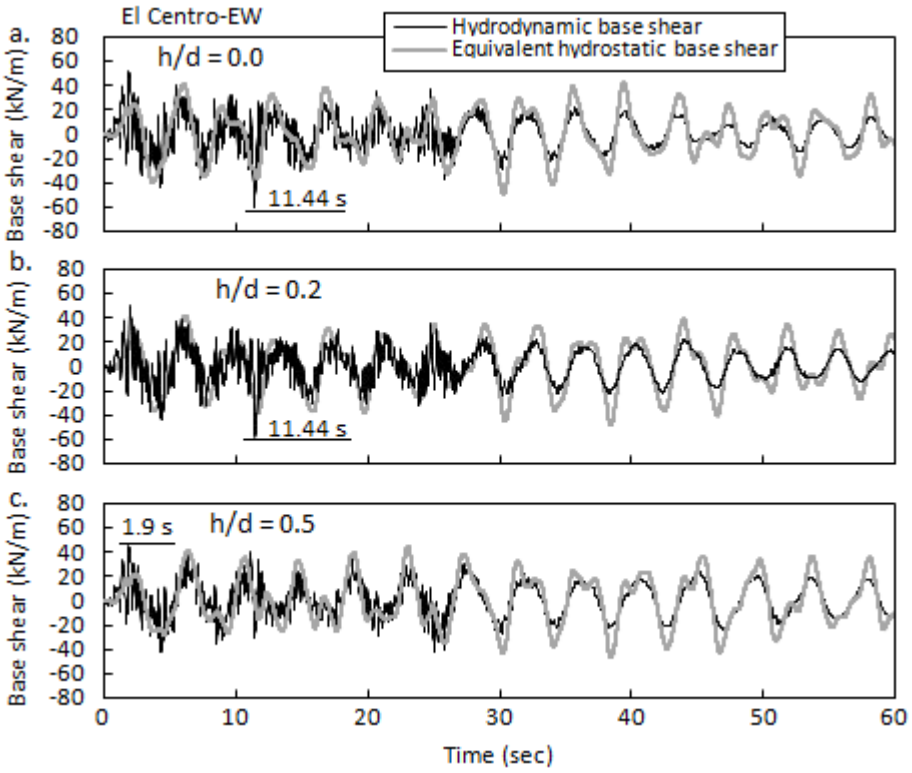

Figure 5.6: Temporal variation of hydrodynamic and equivalent hydrostatic base shear for various heights of submerged block under El Centro-EW ground motion: (a) h/d = 0.0 (b) h/d = 0.2 (c) h/d = 0.5

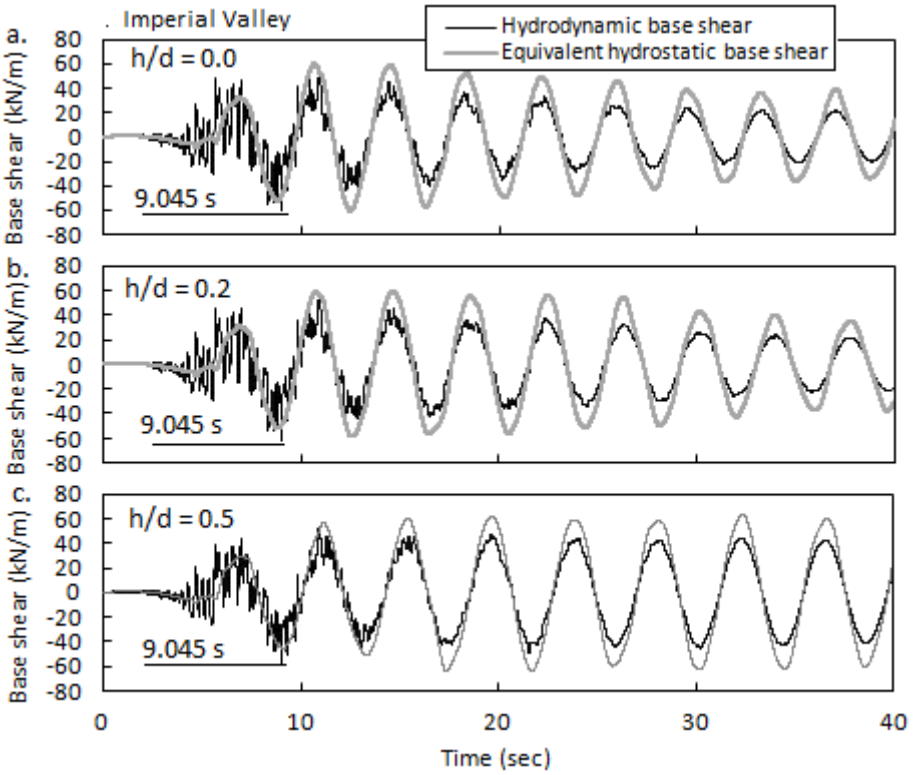

Figure 5.7: Temporal variation of hydrodynamic and equivalent hydrostatic base shear for various heights of submerged block under Imperial Valley ground motion: (a) h/d = 0.0 (b) h/d = 0.2 (c) h/d = 0.5

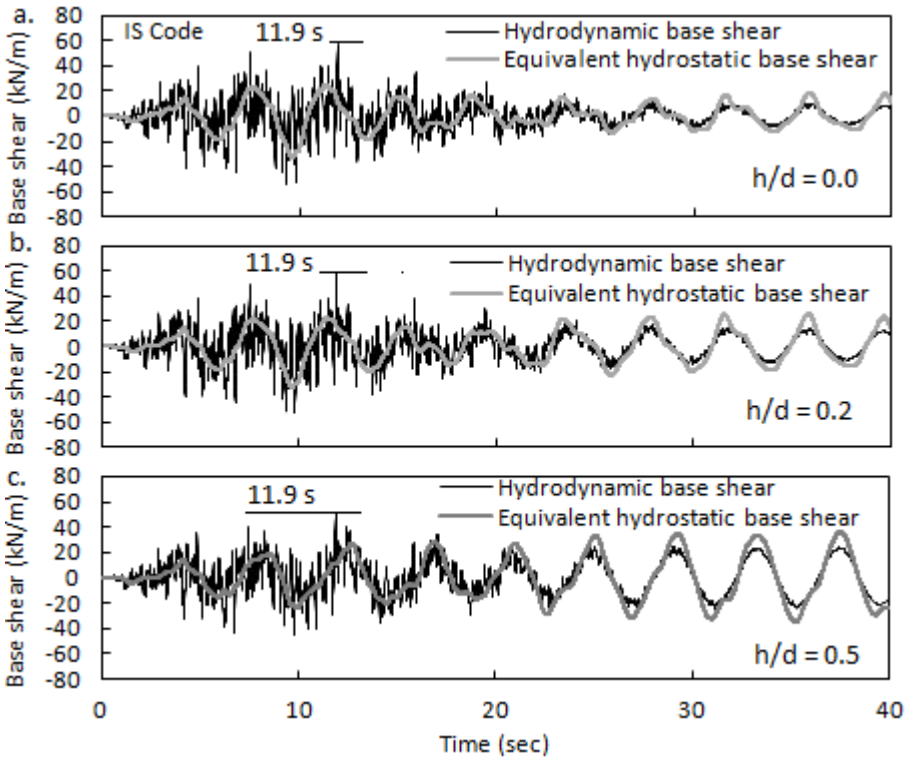

Figure 5.8: Temporal variation of hydrodynamic and equivalent hydrostatic base shear for various heights of submerged block under IS Code ground motion data: (a) *h/d* = 0.0 (b) *h/d* = 0.2 (c) *h/d* = 0.5

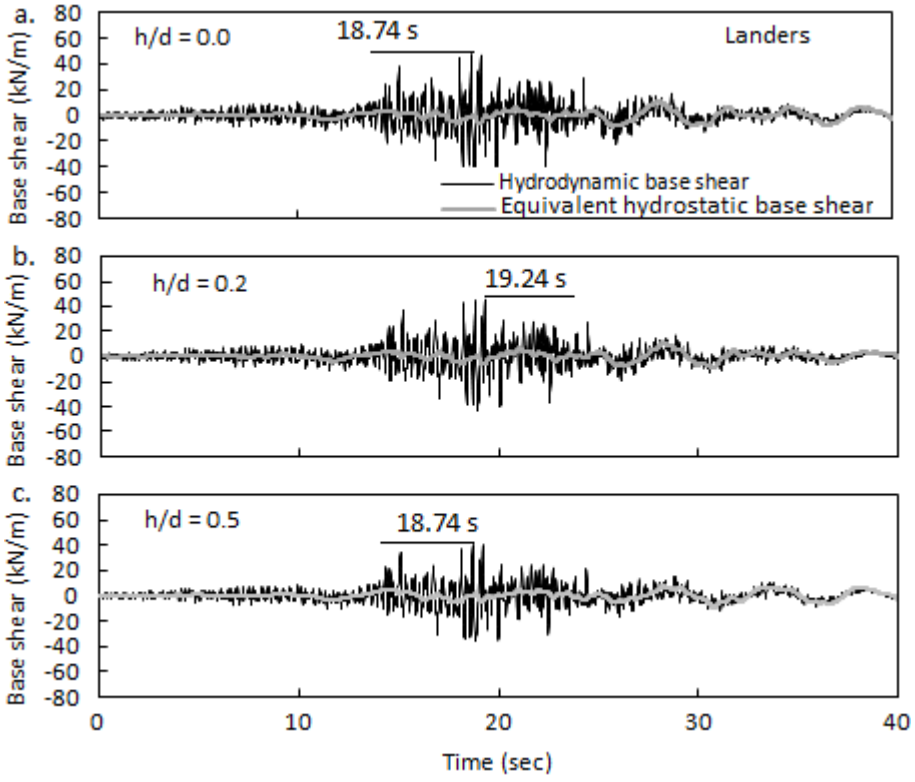

Figure 5.9: Temporal variation of hydrodynamic and equivalent hydrostatic base shear for various heights of submerged block under Landers ground motion: (a) *h/d* = 0.0 (b) *h/d* = 0.2 (c) *h/d* = 0.5

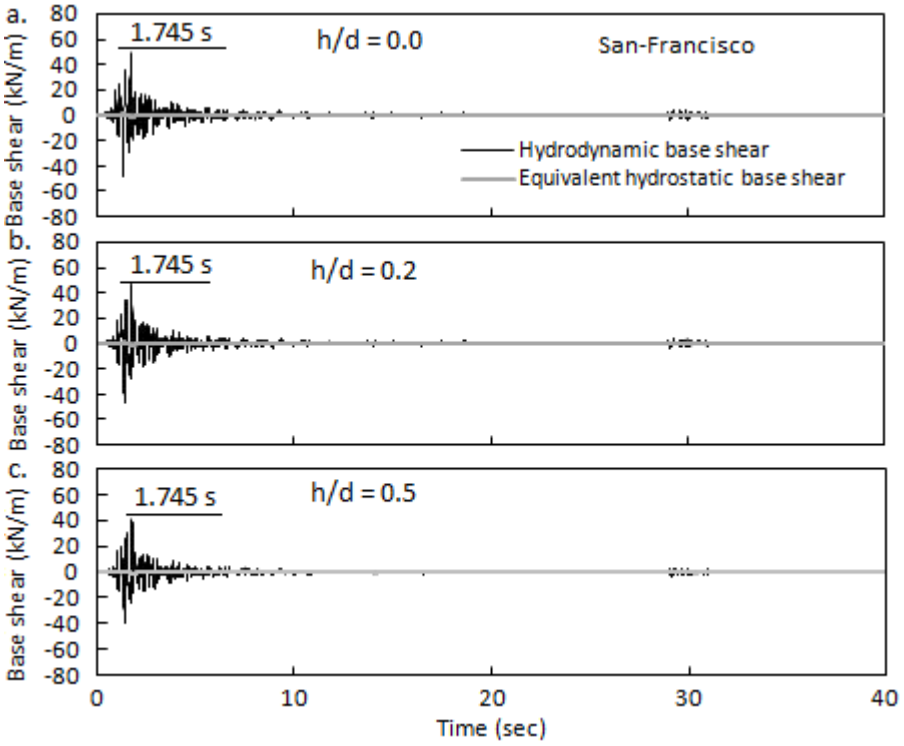

Figure 5.10: Temporal variation of hydrodynamic and equivalent hydrostatic base shear for various heights of submerged block under San-Franscisco ground motion: (a) *h/d* = 0.0 (b) *h/d* = 0.2 (c) *h/d* = 0.5

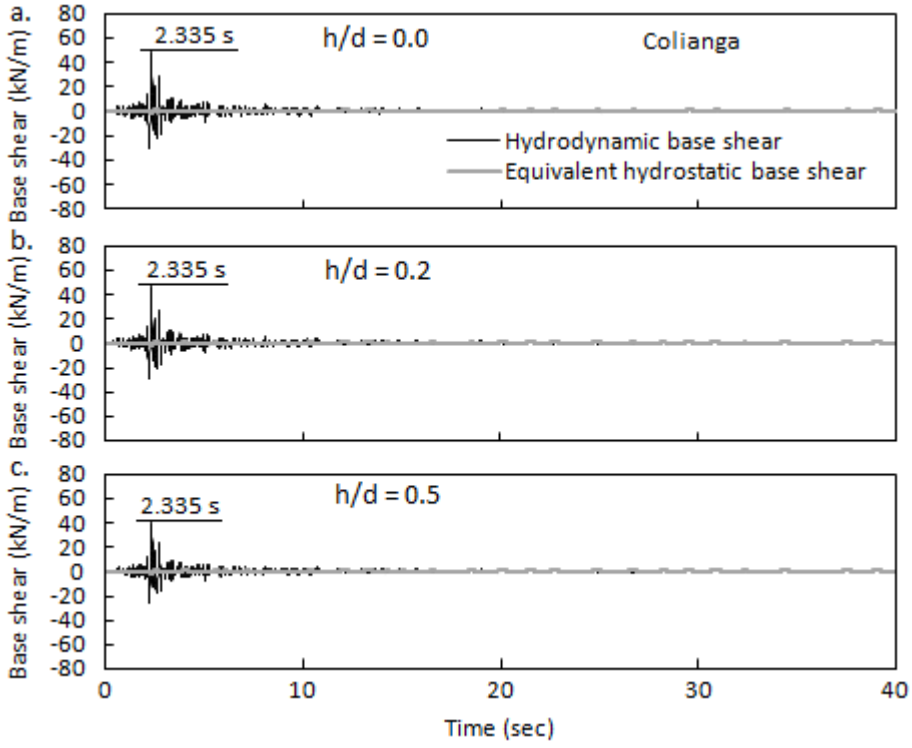

Figure 5.11: Temporal variation of hydrodynamic and equivalent hydrostatic base shear for various heights of submerged block under Colianga ground motion: (a) *h/d* = 0.0 (b) *h/d* = 0.2 (c) *h/d* = 0.5

5.2.5 Base Moment

Figures 5.12-5.17 show the time history of overturning moment about the base. The time of occurrence of absolute maximum base shear and base moment are shown in the respective figures. It may be seen that the absolute maximums occur either at the instant of PGA or at an instant close to the instant of PGA. It is observed that the absolute maximum hydrodynamic response of base shear and base moment decrease with the increase in the height of the centrally located submerged block in case of intermediate frequency and high frequency content ground motions. A deviation in this trend is marked in case of low frequency content motion of Imperial Valley, in which case the base shear and base moment initially increase with the increase in the submerged-block height and then decrease.

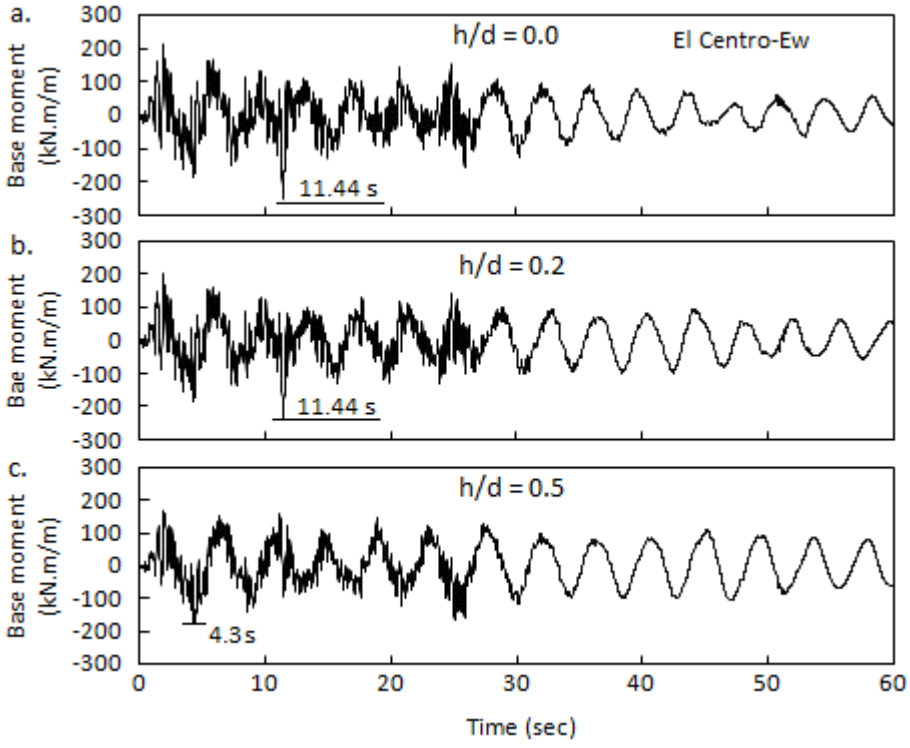

Figure 5.12: Temporal variation of base moment for various heights of submerged block under El Centro-EW ground motion: (a) *h/d* = 0.0 (b) *h/d* = 0.2 (c) *h/d* = 0.5

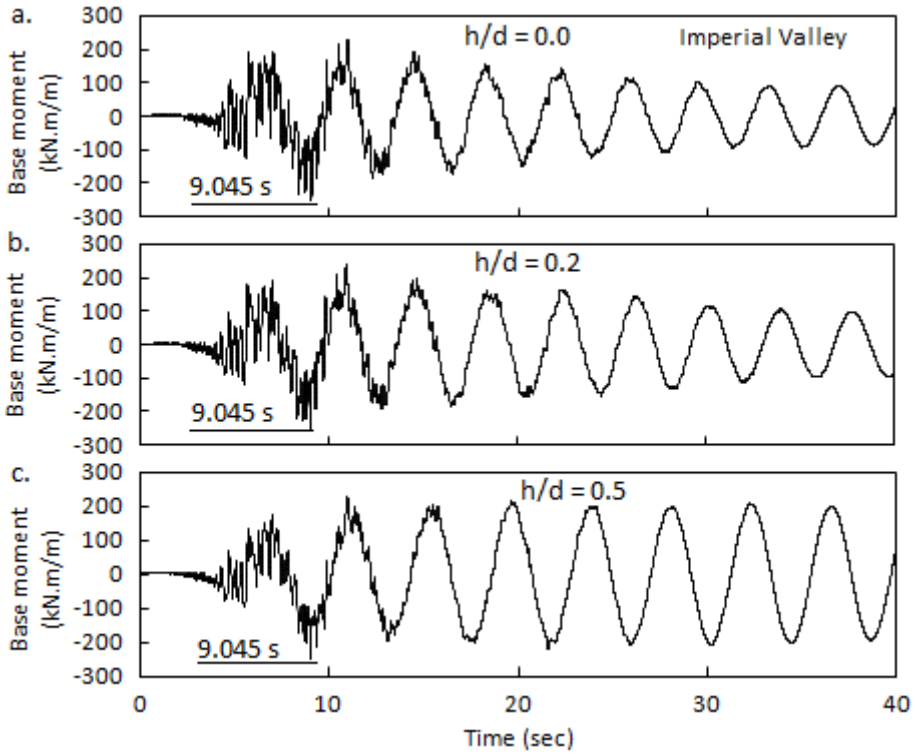

Figure 5.13: Temporal variation of base moment for various heights of submerged block under Imperial Valley ground motion: (a) *h/d* = 0.0 (b) *h/d* = 0.2 (c) *h/d* = 0.5

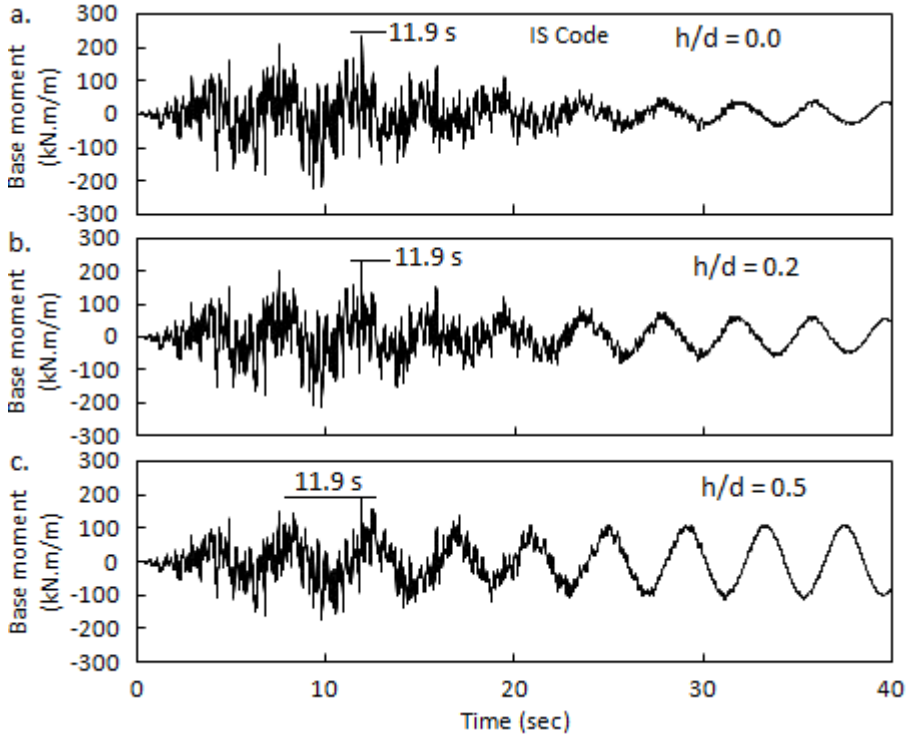

Figure 5.14: Time history of base moment for various heights of submerged block under IS Code ground motion: (a) *h/d* = 0.0 (b) *h/d* = 0.2 (c) *h/d* = 0.5

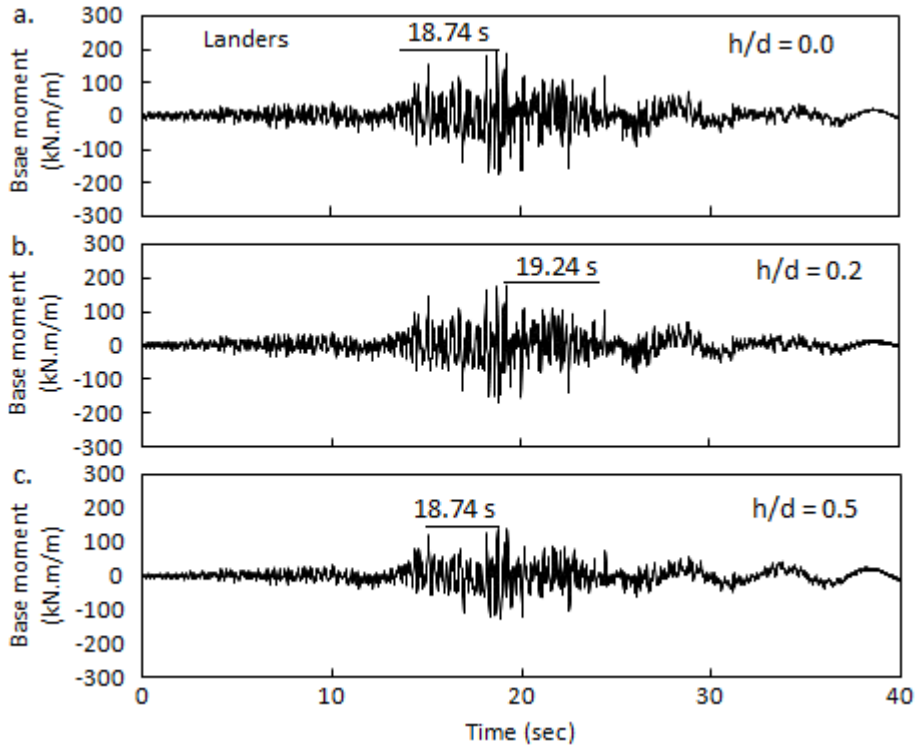

Figure 5.15: Temporal variation of base moment for various heights of submerged block under Landers ground motion data: (a) *h/d* = 0.0 (b) *h/d* = 0.2 (c) *h/d* = 0.5

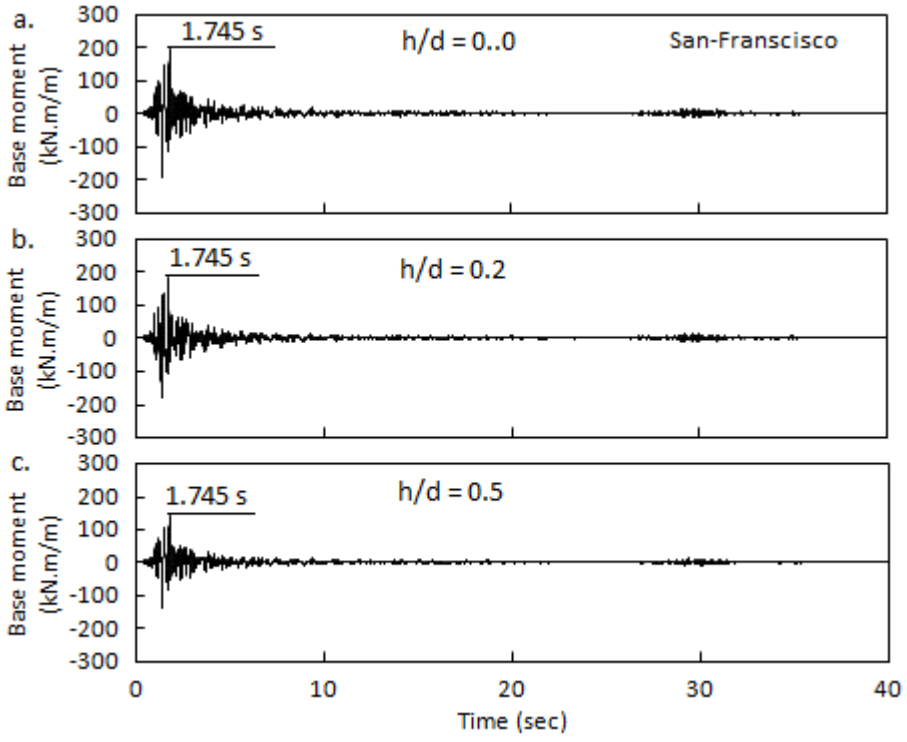

Figure 5.16: Temporal variation of base moment for various heights of submerged block under San-Franscisco ground motion: (a) *h/d* = 0.0 (b) *h/d* = 0.2 (c) *h/d* = 0.5

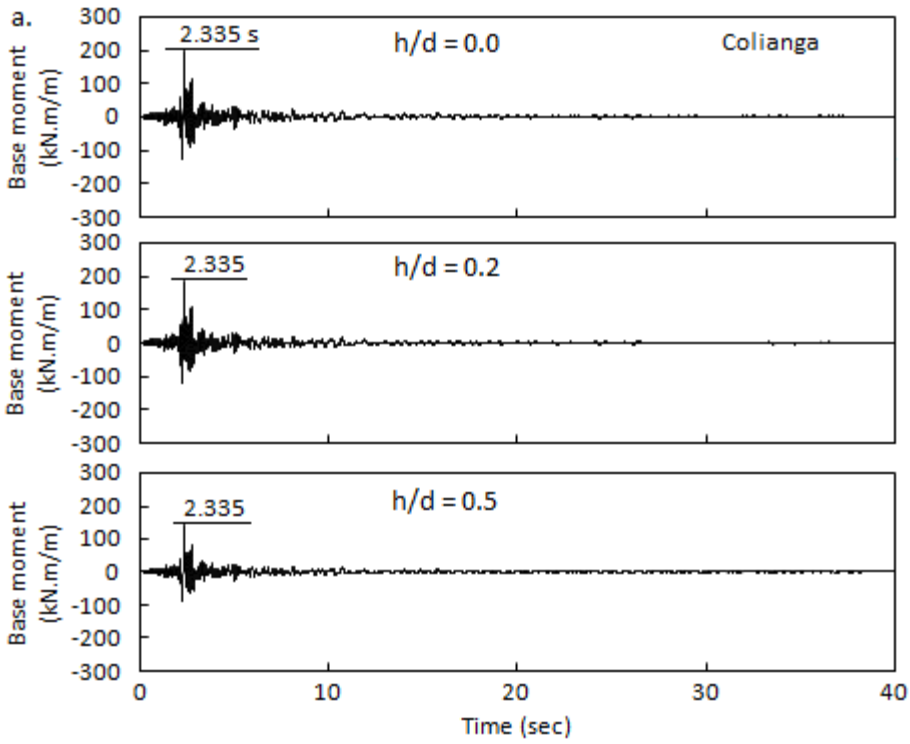

Figure 5.17: Temporal variation of base moment for various heights of submerged block under Colianga ground motion data: (a) *h/d* = 0.0 (b) *h/d* = 0.2 (c) *h/d* = 0.5

5.2.6 Impulsive and Convective Response of Base Shear and Base Moment

The time history of impulsive and convective response components of base shear and base moment are presented in Figures 5.18-5.23 and Figures 5.24-5.29 respectively which show the individual contributions of the impulsive and convective response components of base shear and base moment for a given tank-liquid-submerged block system under a given seismic motion at any instant of time during the excitation. The impulsive components of base shear and base moment decrease with the increase in the height of the centrally located submerged block irrespective of the frequency content of the ground motions used in the present numerical investigation. However the convective response components have a different trend of variation with the height of the submerged block. The convective components increase with the increase in the submerged block height under low frequency Imperial Valley ground motion and in case of intermediate frequency content as well as high frequency content ground motions they follow the same trend as the absolute maximum hydrodynamic responses of base shear and base moment do in case of low frequency ground motion. In case of intermediate frequency content of Landers and high frequency content

seismic motion of San-Franscisco, at absolute maximum responses of base shear and base moment, a phase difference between the impulsive and convective response components is seen, which helped in the reduction of the absolute maximum response of the given dynamic parameter. From Table 5.3, it is observed that for liquid tank without any submerged component inside, the hydrodynamic responses of base shear and base moment are dominated invariably by impulsive component irrespective of the frequency content of the ground motions. However, the convective component is quite appreciable in case of low frequency ground motions of El Centro-EW and Imperial Valley. For liquid tanks with submerged block inside, the convective response component dominates the hydrodynamic responses of base shear and base moment especially in case of low frequency ground motion of Imperial Valley. It should be noted that, although the maximum responses (global peaks) of base shear and base moment are critical to the design of tanks, repeated excursions of secondary peaks as compared to the global peaks in a given duration of time are equally detrimental because of cumulative damage sustained by the container structure. It is seen from Figure 5.7 (base shear) and Figure 5.13 (base moment), and from Figure 5.8 (base shear) in case of Imperial Valley and IS code ground motions respectively that the values of global peaks for various block heights are fairly close. However the secondary peaks in case of $h/d = 0.5$ exceed those in case of $h/d = 0$ and $h/d = 0.2$ by consistent wide margin.

Irrespective of the ground motions, the absolute maximum base shear and base moment occur either at the instant of peak ground acceleration or at some instant very close to the instant of PGA. It is further observed that increase in absolute maximum convective responses do not cause proportionate increase in the total hydrodynamic response. This is because there is sufficient time lag between the instant of occurrence of absolute maximums of impulsive and convective responses and these time lag further increases with increase in the height of submerged block. The occurrence time of absolute maximums of impulsive and convective response components are indicated in the figures as T(imp) and T(con) respectively. It may be noticed that the dominancy of convective response component comes into picture during the later part of the earthquakes when the impulsive responses are in the declining stage. Hence although the impulsive response is vital in computing the maximum stresses, the effect of convective response cannot be downplayed for earthquakes of long duration,

in which case sloshing dominates the overall dynamics of the tank-liquid-submerged block system.

It is observed that the magnitudes of peak impulsive response components of dynamic physical parameters are higher than the corresponding convective responses in all the ground motions, considered for the investigation, irrespective of their frequency content. For all ground motions considered, the impulsive response peaks invariably occur at the instant of PGAs of respective motions. It is further noticed that there exists a significant time lag between peak impulsive and convective response. Thus the overall seismic behaviour of the tank is governed by the impulsive response. However for low frequency content ground motions, the convective response dominates the overall dynamic behaviour during the later part of the earthquake when the impulsive response is in the declining and the convective response is at its fully developed state. Hence although the impulsive response is crucial for overall structural response, the convective response is equally important in such decisions as the correct estimation of free board between the quiescent free surface and tank cover and also in the design of roof cover which experiences convective hydrodynamic pressure in case of inadequate free board. Thus incorrect estimation of sloshing elevation may lead to under-designed free board which may result spillage of hazardous fluids or the failures in the tank roof.

The contributions of impulsive and convective response components to the absolute maximums of base shear and base moments are presented in Table 5.4. It is amply evident that for tank-liquid system without submerged block the hydrodynamic design parameters such as base shear and base moment are invariably dominated by the impulsive response irrespective of the ground motions. However the convective components are appreciable in case of Low frequency motions of El Centro and Imperial Valley. For liquid–tank system with submerged block the convective components are of comparable in magnitude with their impulsive counterparts in case of low frequency motions and play a major role in dynamic structural responses. However in case of other ground motions, although convective response increase due to the presence of submerged block, their effect is not as significant as they are in low frequency ground motions. Under intermediate frequency content seismic motion of Landers and high frequency content ground motions of San-Franscisco and Colianga, the convective responses are in opposite phase to the impulsive response at the instant

of absolute maximum response of base shear and base moment which cause the reduction in absolute maximum response.

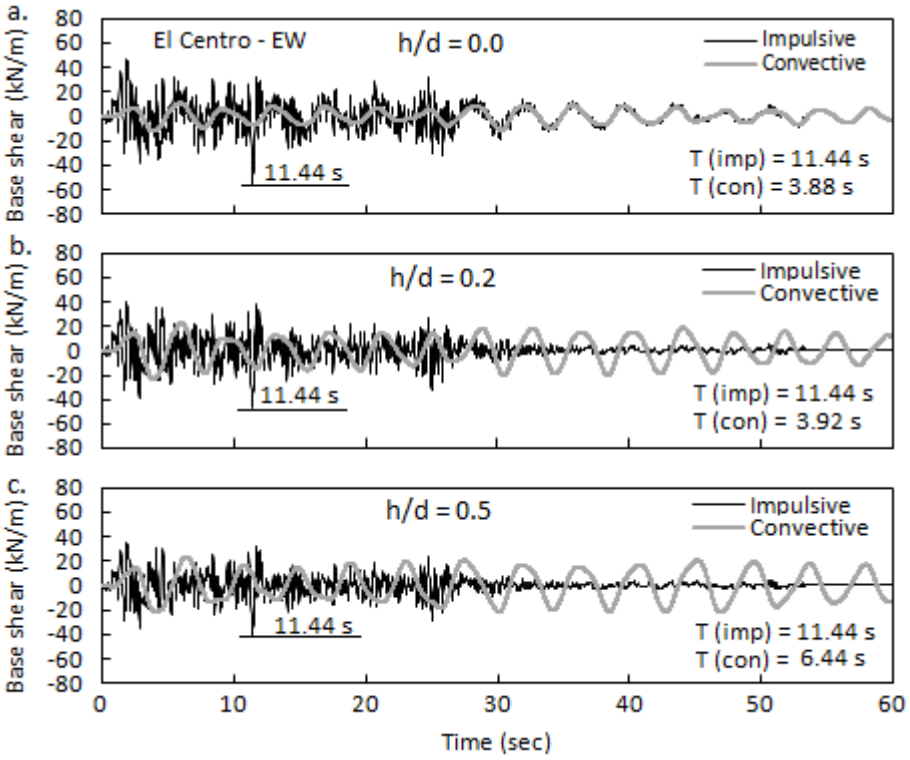

Figure 5.18: Comparison of temporal variations of impulsive and convective response components of base shear for various heights of submerged block under El Centro-EW ground motion: (a) *h/d* = 0.0 (b) *h/d* = 0.2 (c) *h/d* = 0.5

Table 5.3: Absolute maximum dynamic responses of various physical parameters of the tank-liquid-submerged block system[@]

Records	Dynamic response parameters	Hydrodynamic response components									Equivalent Hydrostatic response		
		Impulsive			Convective			Total hydrodynamic response					
		h/d = 0.0	h/d = 0.2	h/d = 0.5	h/d = 0.0	h/d = 0.2	h/d = 0.5	h/d = 0.0	h/d = 0.2	h/d = 0.5	h/d = 0.0	h/d = 0.2	h/d = 0.5
El Centro-EW	Sloshing (cm)				50.03	49.81	48.36	50.03	49.81	48.36	-	-	-
	Base shear (kN/m)	54.87	49.92	40.64	12.27	24.39	23.54	60.83	58.04	44.17	49.07	48.87	47.44
	Base moment (kN.m/m)	216.69	183.38	142.45	70.15	108.82	108.46	248.34	231.47	174.76	-	-	-
Imperial Valley	Sloshing (cm)	-	-	-	61.84	60.96	65.85	61.84	60.96	65.85	-	-	-
	Base shear (kN/m)	48.18	46.93	40.65	17.12	36.33	43.61	60.66	61.16	59.25	60.66	59.80	64.60
	Base moment (kN.m/m)	195.60	183.40	142.47	96.77	161.72	204.26	253.05	256.45	248.11	-	-	-
IS Code	Sloshing (cm)	-	-	-	34.30	33.73	36.70	34.30	33.73	36.70	-	-	-
	Base shear (kN/m)	52.70	47.58	41.21	9.59	17.63	23.02	56.46	57.84	50.20	33.65	33.09	36.0
	Base moment (kN.m/m)	208.71	185.95	144.45	48.08	78.17	107.38	230.51	231.98	187.34	-	-	-
Landers	Sloshing (cm)	-	-	-	11.83	11.09	9.49	11.83	11.09	9.49	-	-	-
	Base shear (kN/m)	47.93	47.72	41.37	3.52	5.80	4.66	47.51	45.02	39.42	11.61	10.88	9.31
	Base moment (kN.m/m)	196.34	186.51	144.88	20.75	25.88	21.79	192.40	174.48	136.39	-	-	-
San-Franscisco	Sloshing (cm)	-	-	-	1.45	1.41	1.35	1.45	1.41	1.35	-	-	-
	Base shear (kN/m)	48.82	47.02	40.72	0.18	0.37	0.39	48.64	46.66	40.38	1.43	1.41	1.32
	Base moment (kN.m/m)	197.66	183.74	142.73	0.98	1.62	1.58	196.71	182.18	141.20	-	-	-
Colianga	Sloshing (cm)	-	-	-	1.64	1.61	1.52	1.64	1.61	1.52	-	-	-
	Base shear (kN/m)	48.77	47.03	40.74	0.24	0.47	0.45	48.54	46.56	40.29	1.60	1.58	1.50
	Base moment (kN.m/m)	197.55	183.80	142.77	1.28	2.09	2.05	196.27	181.71	140.72	-	-	-

[@] The values in the table are the absolute maximum values of the respective hydrodynamic parameters. The total hydrodynamic response should not be confused as the sum of the absolute maximum impulsive response and absolute maximum convective response.

Table 5.4: Contributions of impulsive and convective components for absolute maximum hydrodynamic responses of various physical parameters

Records	Dynamic response parameters	Hydrodynamic response components								
		Impulsive			Convective			Total hydrodynamic response		
		h/d = 0.0	h/d = 0.2	h/d = 0.5	h/d = 0.0	h/d = 0.2	h/d = 0.5	h/d = 0.0	h/d = 0.2	h/d = 0.5
El Centro-EW	Base shear (kN/m)	54.87	46.92	34.77	5.96	11.11	9.40	60.83	58.04	44.17
	Base moment (kN.m/m)	216.69	183.38	73.13	31.65	48.09	100.63	248.34	231.47	174.76
Imperial Valley	Base shear (kN/m)	45.87	29.83	25.84	14.79	31.33	33.41	60.66	61.16	59.25
	Base moment (kN.m/m)	168.40	116.57	90.55	84.65	139.88	157.56	253.05	256.45	248.11
IS Code	Base shear (kN/m)	52.70	47.58	41.21	3.76	10.26	8.99	56.46	57.84	50.20
	Base moment (kN.m/m)	208.71	185.95	144.45	21.80	46.03	42.89	230.51	231.98	187.34
Landers	Base shear (kN/m)	47.85	47.72	41.33	0.34*	2.70*	1.91*	47.51	45.02	39.42
	Base moment (kN.m/m)	193.61	186.51	140.36	1.21*	12.03*	3.97*	192.40	174.48	136.39
San-Franscisco	Base shear (kN/m)	48.82	47.02	40.72	0.18*	0.36*	0.34*	48.64	46.66	40.38
	Base moment (kN.m/m)	197.66	183.74	142.73	0.95*	1.56*	1.53*	196.71	182.18	141.20
Colianga	Base shear (kN/m)	48.77	47.03	40.74	0.23*	0.47*	0.45*	48.54	46.56	40.29
	Base moment (kN.m/m)	197.55	183.80	142.77	1.28*	2.09*	2.05*	196.27	181.71	140.72

* The convective response is in opposite phase to the corresponding impulsive response

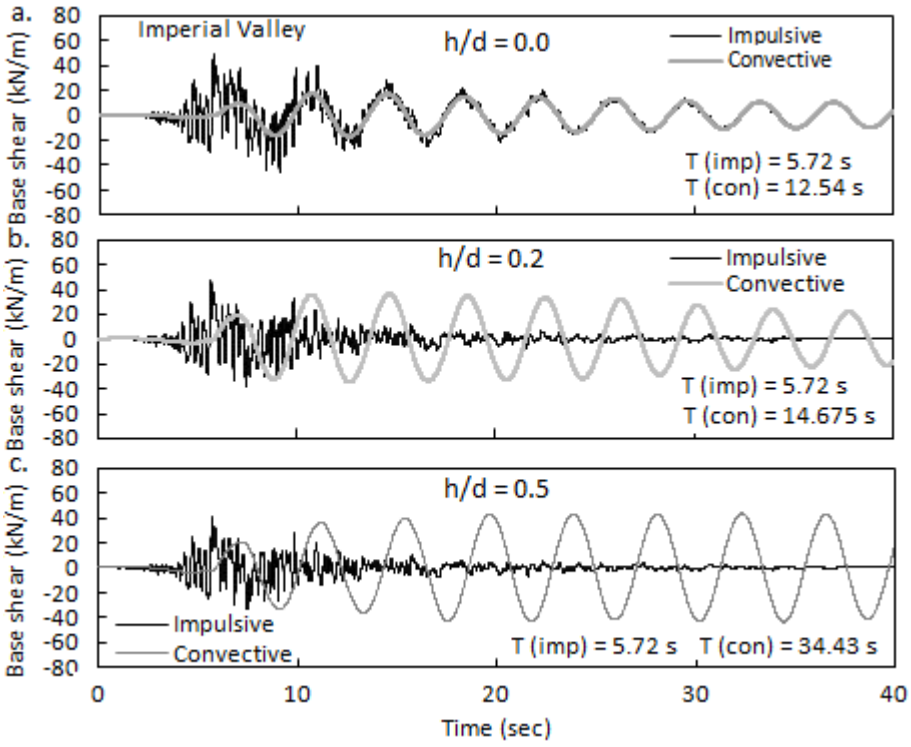

Figure 5.19: Comparison of temporal variations of impulsive and convective response components of base shear for various heights of submerged block under Imperial Valley ground motion: (a) *h/d* = 0.0 (b) *h/d* = 0.2 (c) *h/d* = 0.5

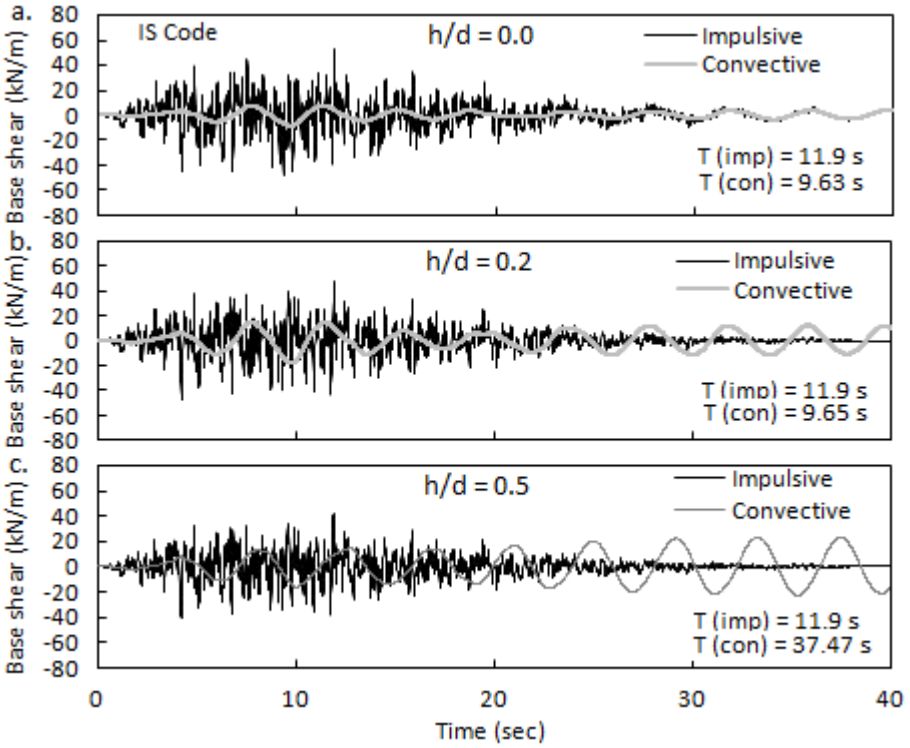

Figure 5.20: Comparison of temporal variations of impulsive and convective response components of base shear for various heights of submerged block under IS Code ground motion data: (a) *h/d* = 0.0 (b) *h/d* = 0.2 (c) *h/d* = 0.5

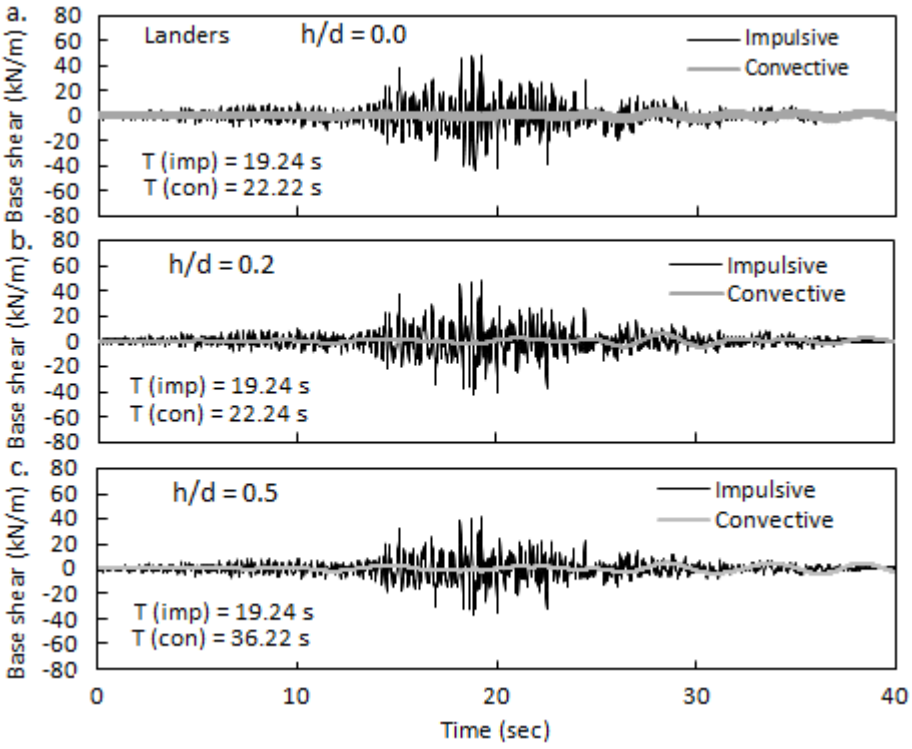

Figure 5.21: Comparison of temporal variations of impulsive and convective response components of base shear for various heights of submerged block under Landers ground motion: (a) *h/d* = 0.0 (b) *h/d* = 0.2 (c) *h/d* = 0.5

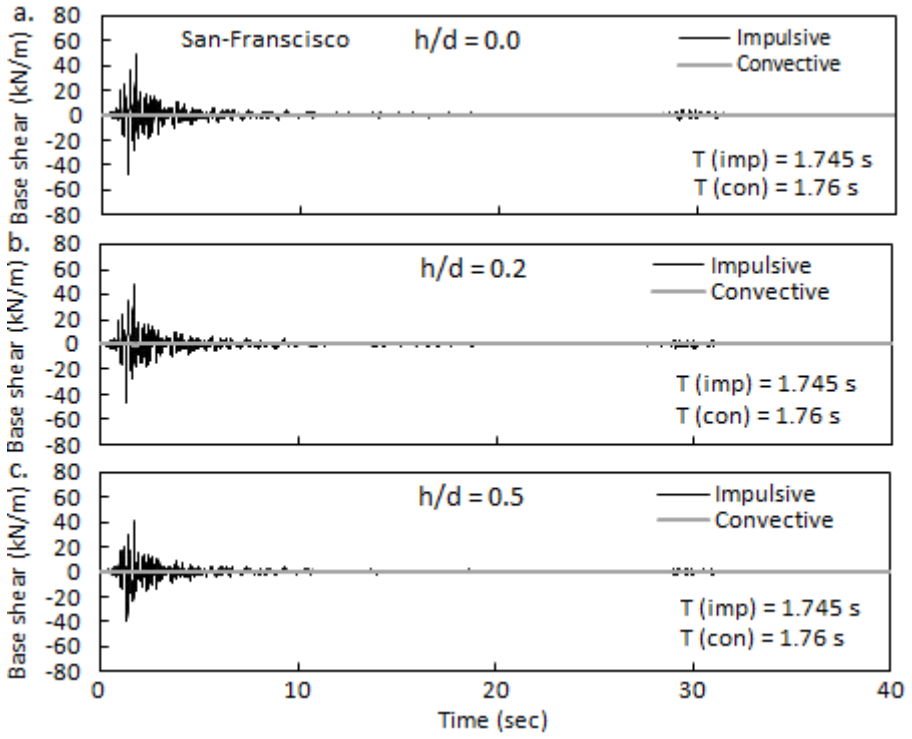

Figure 5.22: Comparison of temporal variations of impulsive and convective response components of base shear for various heights of submerged block under San-Franscisco ground motion: (a) *h/d* = 0.0 (b) *h/d* = 0.2 (c) *h/d* = 0.5

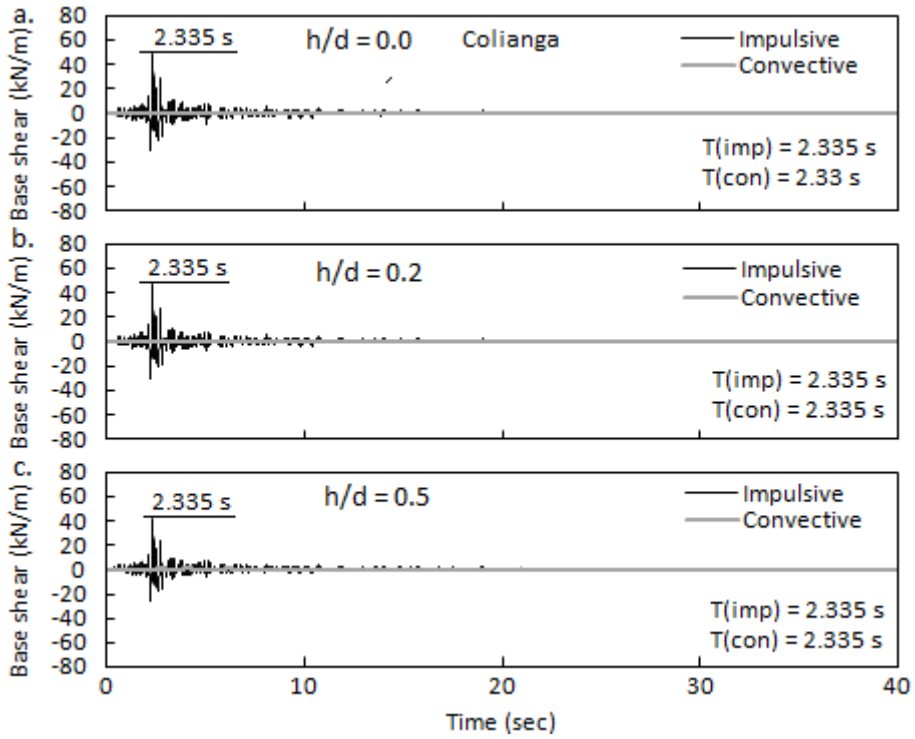

Figure 5.23: Comparison of temporal variations of impulsive and convective response components of base shear for various heights of submerged block under Colianga ground motion: (a) *h/d* = 0.0 (b) *h/d* = 0.2 (c) *h/d* = 0.5

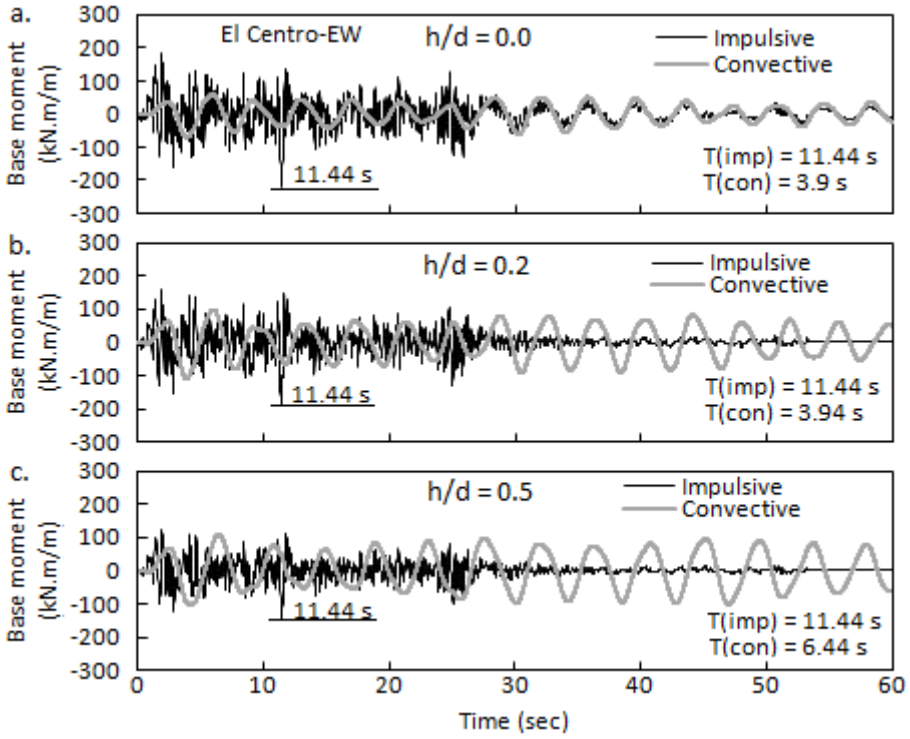

Figure 5.24: Comparison of temporal variations of impulsive and convective response components of base moment for various heights of submerged block under El Centro-EW ground motion: (a) *h/d* = 0.0 (b) *h/d* = 0.2 (c) *h/d* = 0.5

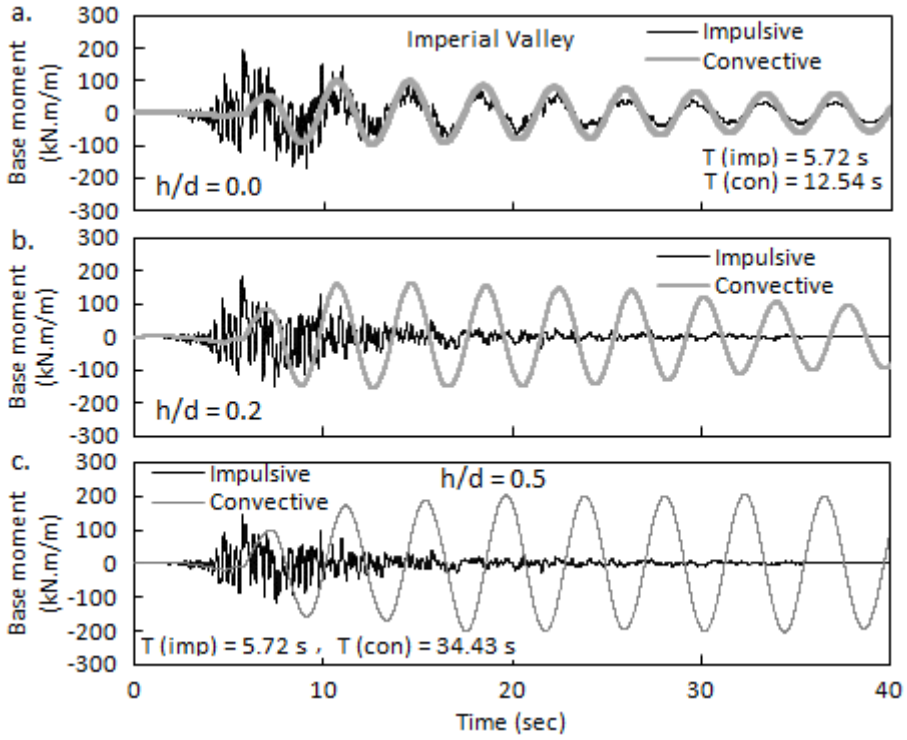

Figure 5.25: Comparison of temporal variations of impulsive and convective response components of base moment for various heights of submerged block under Imperial Valley ground motion: (a) *h/d* = 0.0 (b) *h/d* = 0.2 (c) *h/d* = 0.5

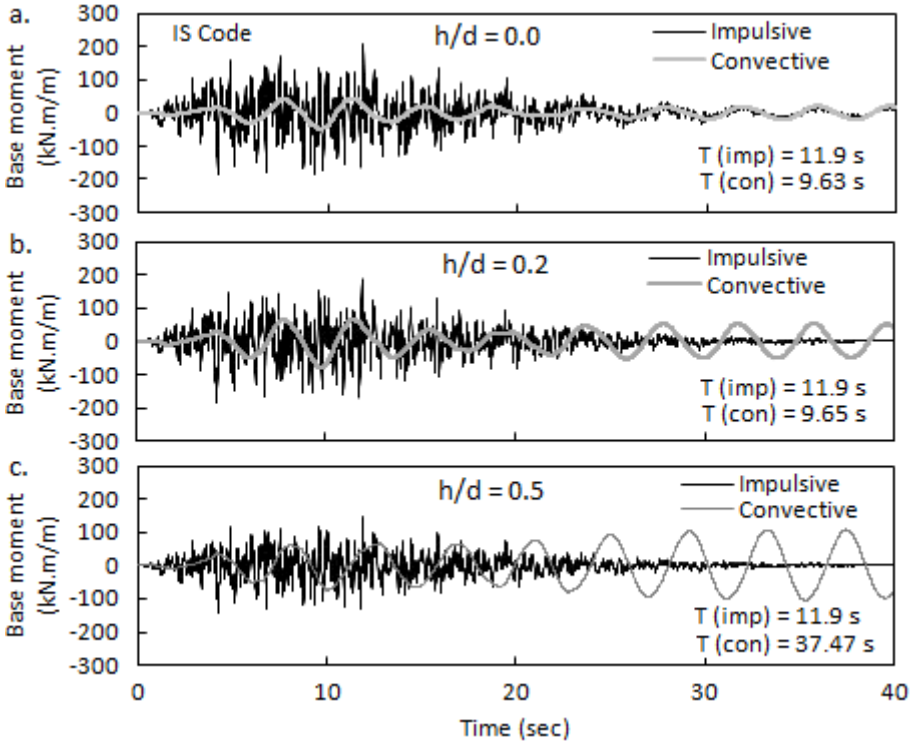

Figure 5.26: Comparison of temporal variations of impulsive and convective response components of base moment for various heights of submerged block under IS Code ground motion data: (a) *h/d* = 0.0 (b) *h/d* = 0.2 (c) *h/d* = 0.5

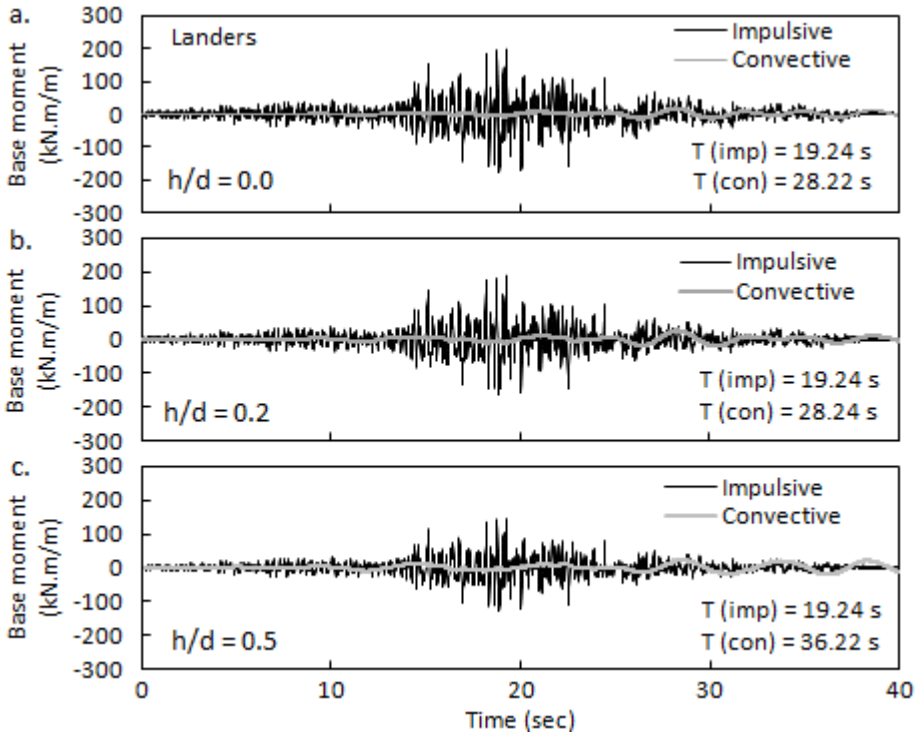

Figure 5.27: Comparison of temporal variations of impulsive and convective response components of base moment for various heights of submerged block under Landers ground motion data: (a) *h/d* = 0.0 (b) *h/d* = 0.2 (c) *h/d* = 0.5

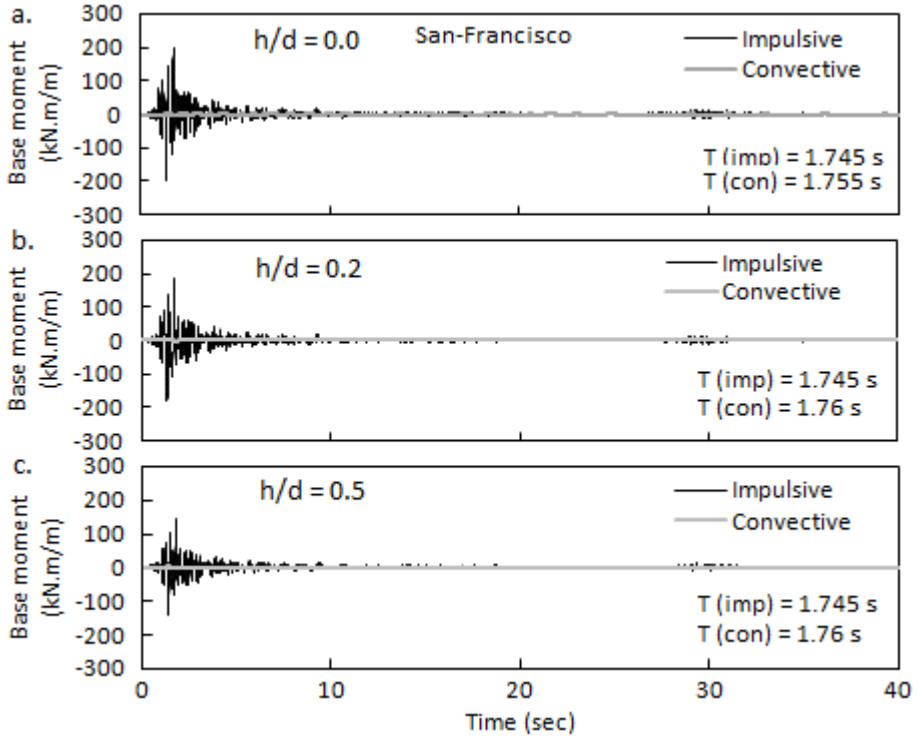

Figure 5.28: Comparison of temporal variations of impulsive and convective response components of base moment for various heights of submerged block under San-Franscisco ground motion data: (a) *h/d* = 0.0 (b) *h/d* = 0.2 (c) *h/d* = 0.5

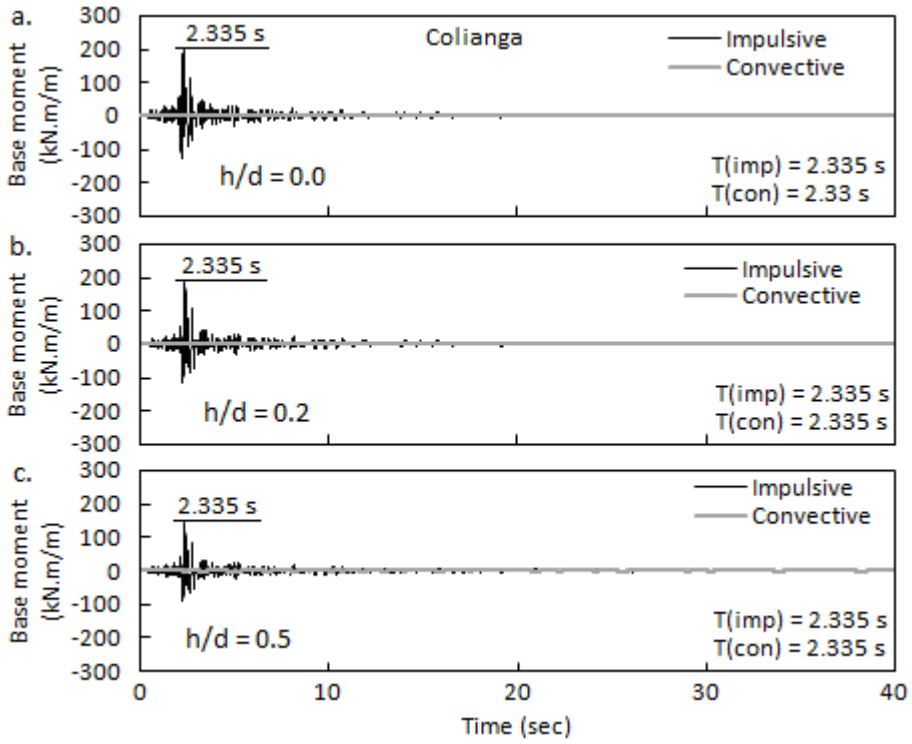

Figure 5.29: Comparison of temporal variations of impulsive and convective response components of base moment for various heights of submerged block under Colianga ground motion data: (a) *h/d* = 0.0 (b) *h/d* = 0.2 (c) *h/d* = 0.5

5.2.7 Free Surface Wave Profiles

The sloshing response of fluid-tank system is very sensitive to the characteristics of ground motion and configuration of the system and submerged internal components if any. The sloshing response reflects the overall dynamic response of the system in a sense that it indirectly gives an idea about the convective response components of design parameters such as base shear and base moment. The free surface profiles at the instant of maximum base shear for all ground motions with varying heights of submerged blocks are shown in Figure 5.30. It is evident that decrease in convective response components takes place from low frequency content to high frequency content ground motion through the intermediate frequency content ground motions. The convective responses are significantly more for low frequency earthquakes of El Centro-EW and Imperial Valley with or without submerged blocks. The surface wave profiles are found to be consistent with other structural responses presented in Tables 5.3 and 5.4 as well as the pressure distribution results of section 5.2.8. One can observe similar sloshing responses for seismic motions within a given frequency range.

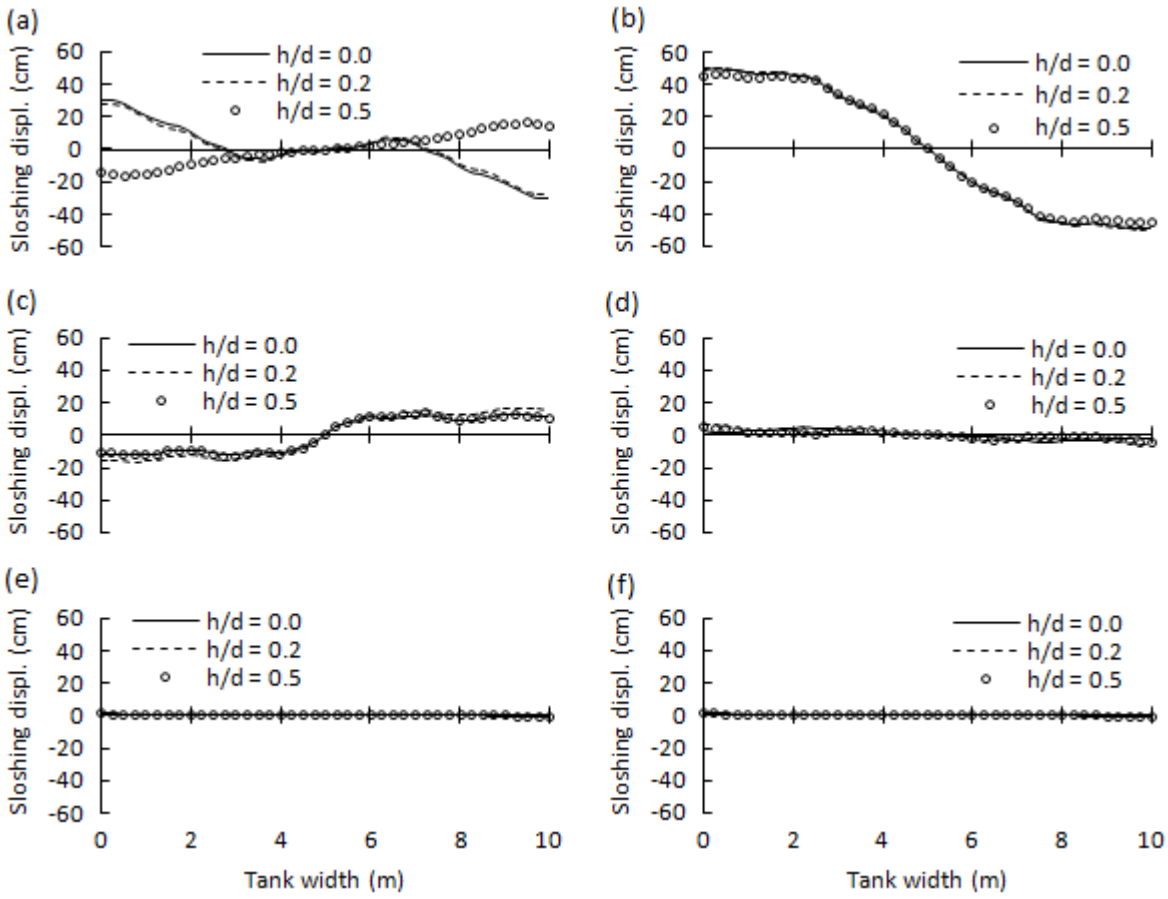

Figure 5.30: Free surface profiles at the instant of absolute maximum base shear for various heights of submerged block under various ground motions: (a) El Centro-EW (b) Imperial Valley (c) IS Code ground motion data (d) Landers (e) San-Franscisco (f) Colianga

5.2.8 Pressure Distribution on Tank Wall

The distributions of total as well as the impulsive and convective response components, at the instant of maximum base shear for respective ground motions, on the wall of the tank are presented in Figures 5.31-5.36. From the figures it can be seen that irrespective of the ground motion characteristics, the hydrodynamic pressure and its impulsive component decrease with increase in the height of the submerged block. The convective component has however a different trend of variation. It increases with the increase in the submerged block height in case of Imperial Valley and IS Code ground motions and opposite in case of Landers and San-Franscisco seismic records. It may be further emphasized that the decrease in the impulsive components in the case of Imperial Valley and IS Code are comparatively more than the

corresponding increase in the convective components which indicate that the impulsive response dominates the total dynamic response of the pressure.

In case of Landers, San-Franscisco and Colianga ground motions, the impulsive and convective responses are found to be in opposite phase. Hence decrease in the impulsive response and increase in convective response causes significant decrease in the total dynamic response of the pressure as can be marked from Table 5.4. The asterisks against the values in the table indicate that the convective responses are in opposite phase to the impulsive responses.

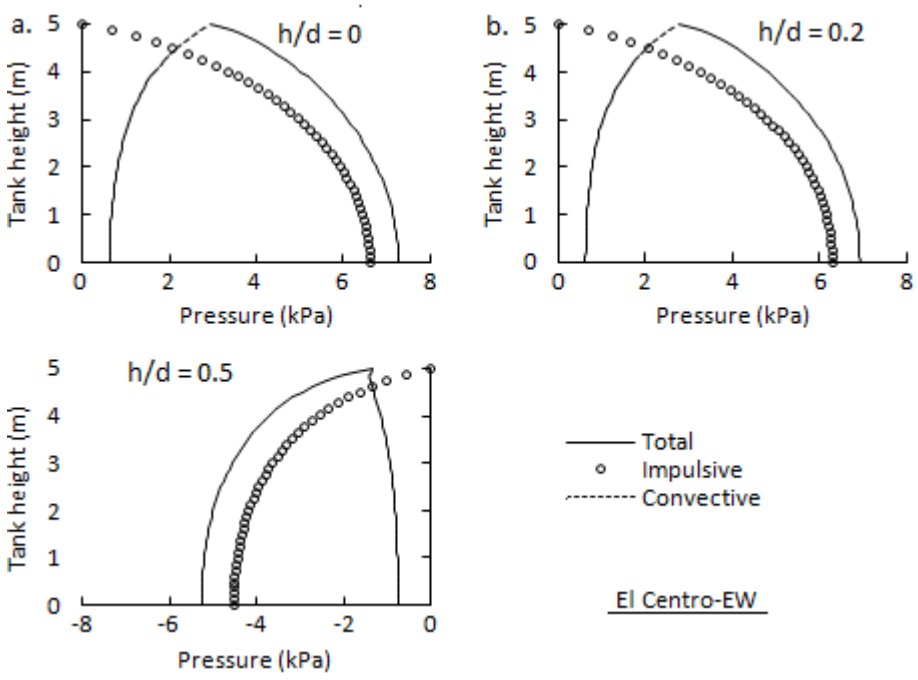

Figure 5.31: Hydrodynamic pressure distribution along the left wall of the tank at the instant of maximum base shear for various heights of centrally placed submerged block under horizontal ground motion of El Centro-EW: (a) h/d = 0.0 (b) h/d = 0.2 (c) h/d = 0.5

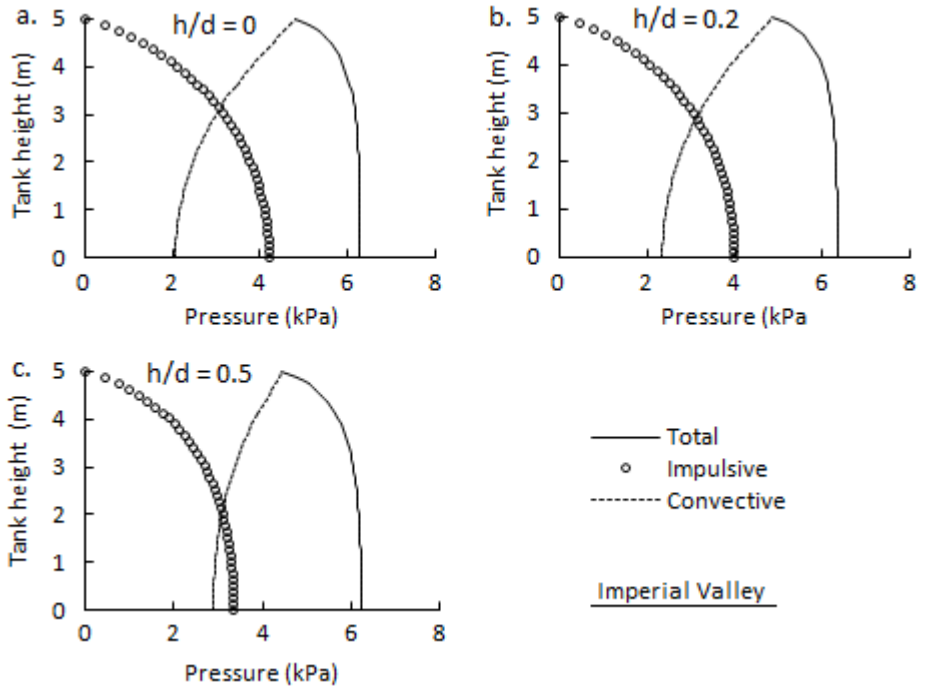

Figure 5.32: Hydrodynamic pressure distribution along the left wall of the tank at the instant of maximum base shear under horizontal ground motion of Imperial Valley: (a) *h/d* = 0.0 (b) *h/d* = 0.2 (c) *h/d* = 0.5

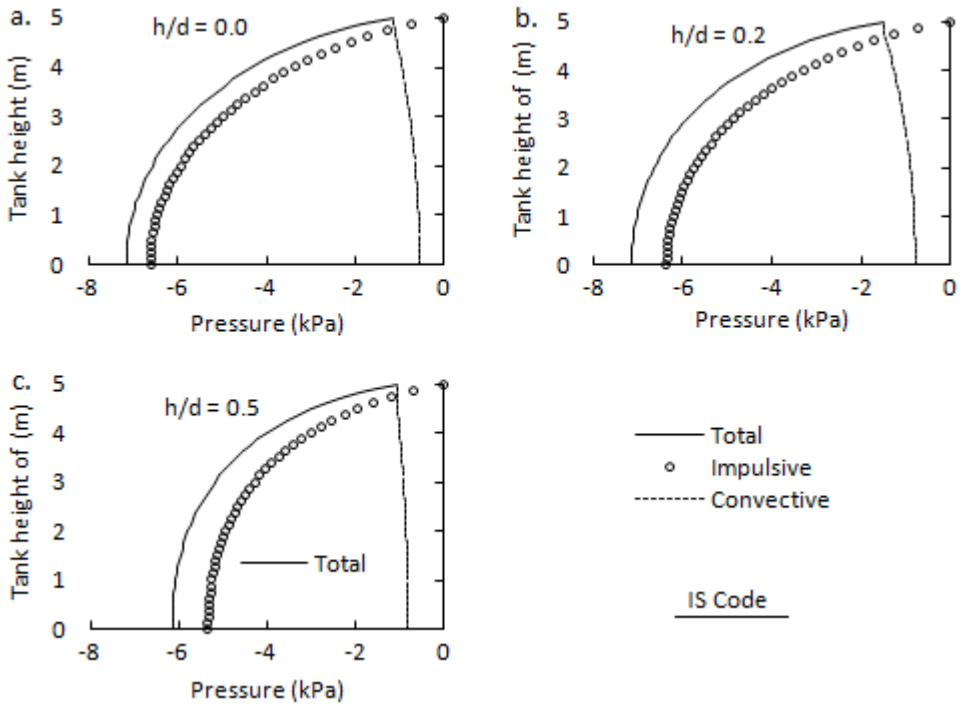

Figure 5.33: Hydrodynamic pressure distribution along the left wall of the tank at the instant of maximum base shear under horizontal ground motion of IS Code data: (a) *h/d* = 0.0 (b) *h/d* = 0.2 (c) *h/d* = 0.5

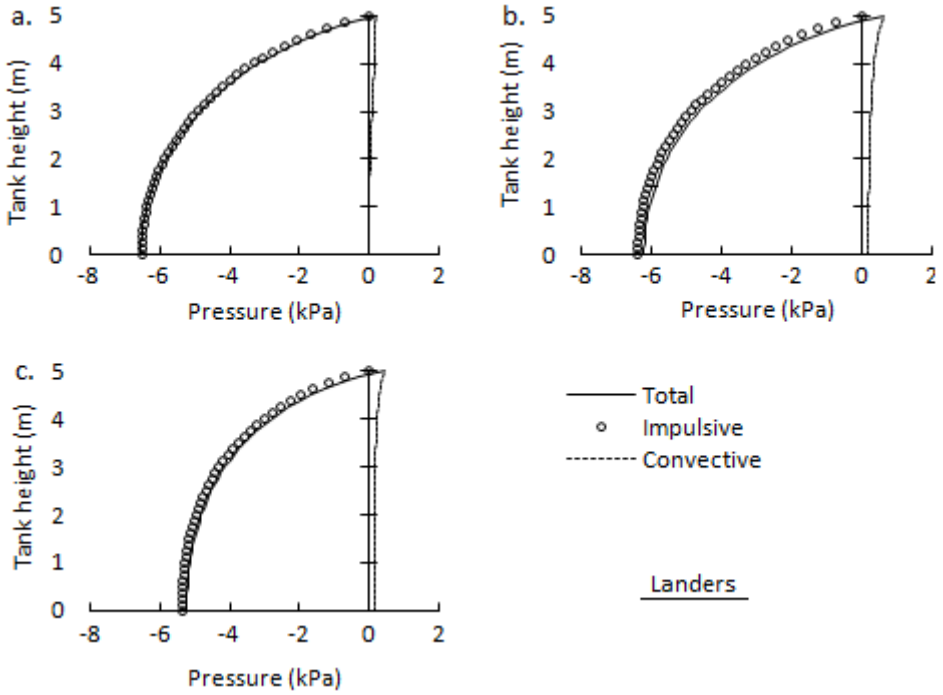

Figure 5.34: Hydrodynamic pressure distribution along the left wall of the tank at the instant of maximum base shear under horizontal ground motion of Landers: (a) *h/d* = 0.0 (b) *h/d* = 0.2 (c) *h/d* = 0.5

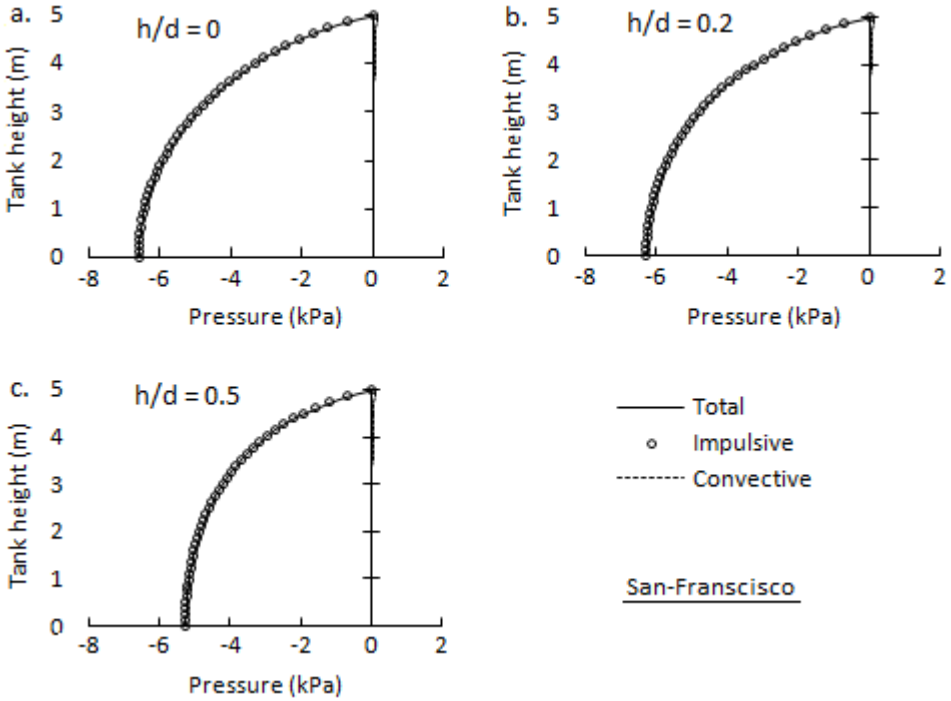

Figure 5.35: Hydrodynamic pressure distribution along the left wall of the tank at the instant of maximum base shear under horizontal San-Franscisco ground motion: (a) *h/d* = 0.0 (b) *h/d* = 0.2 (c) *h/d* = 0.5

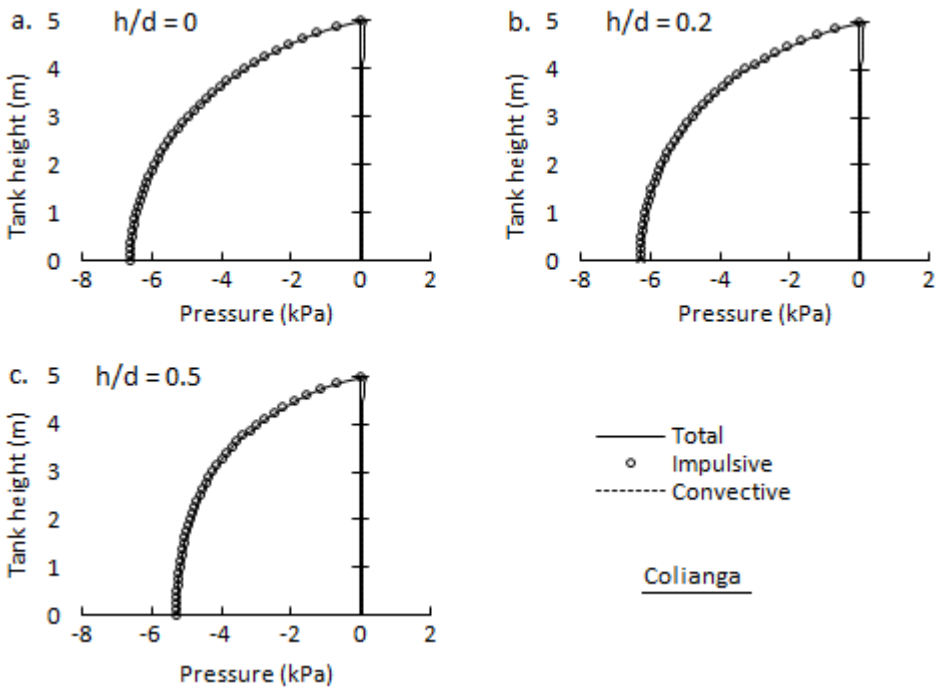

Figure 5.36: Hydrodynamic pressure distribution along the left wall of the tank at the instant of maximum base shear under horizontal Colianga ground motion: (a) *h/d* = 0.0 (b) *h/d* = 0.2 (c) *h/d* = 0.5

5.2.9 Pressure Distribution on Block Wall

The variations of hydrodynamic responses of total, impulsive and convective pressure, at the instant of maximum base shear for respective ground motions, on the wall of submerged block are presented in Figures 5.37-5.42. It is evident that the total hydrodynamic pressure on the block wall increases with increase in the height of the submerged block for all the ground motions under study and the increase is quite significant in all cases except low frequency ground motion of Imperial Valley in which case the increase is marginal in spite of significant increase in both impulsive and convective components. This is due to the fact that both components are in opposite phase and their increase is proportionate. The convective response dominates the total pressure although impulsive response is quite significant. The total pressure distribution curve is almost a vertical straight line which suggests that the pressure variation along the height of the block is negligible. The hydrodynamic pressure distribution on the block wall due to intermediate frequency content ground motion data of IS Code is dominated by convective response and impulsive response respectively for block heights of *h/d* = 0.2 and 0.5. The pressure distribution on the

wall in this case, the increase in impulsive response is substantially more than the increase in the convective response. For a given block height not much variation in the convective response along the height of the block wall is observed. In case of intermediate frequency content motion of Landers no appreciable change in convective pressure distribution is observed with the change in the height of the block. For high frequency ground motions of San-Franscisco and Colianga, it is observed from Figure 5.41 and 5.42 that the convective responses are negligibly small and the total pressure is almost equal to the impulsive response.

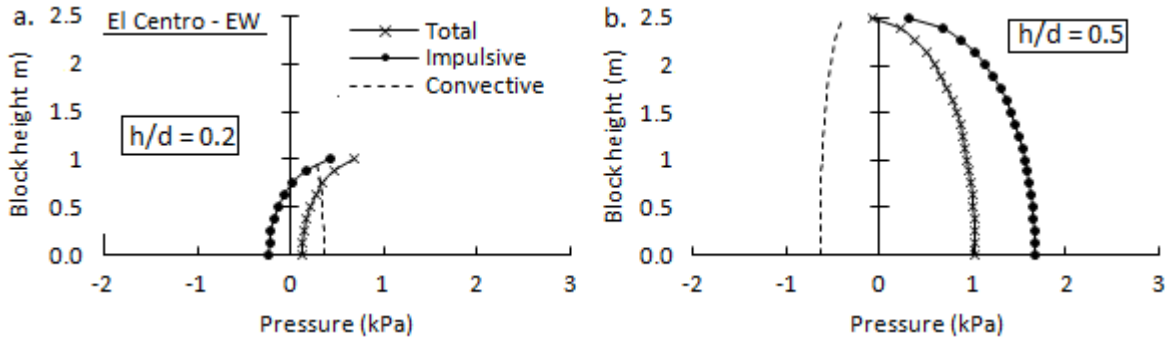

Figure 5.37: Hydrodynamic pressure distribution along the left wall of the block for various heights of centrally placed submerged block under horizontal ground motion of El Centro-EW: (a) *h/d* = 0.2 (b) *h/d* = 0.5

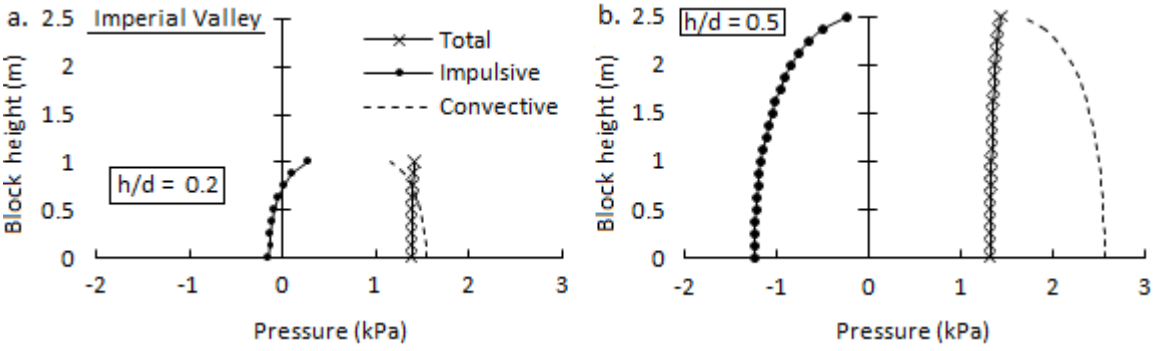

Figure 5.38: Hydrodynamic pressure distribution along the left wall of the block for various heights of centrally placed submerged block under horizontal ground motion of Imperial Valley: (a) *h/d* = 0.2 (b) *h/d* = 0.5

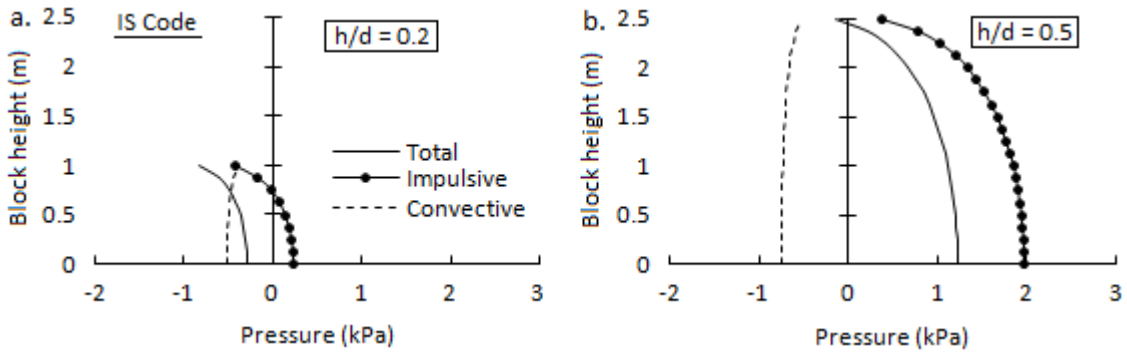

Figure 5.39: Hydrodynamic pressure distribution along the left wall of the block for various heights of centrally placed submerged block under horizontal ground motion of IS Code data: (a) h/d = 0.2 (b) h/d = 0.5

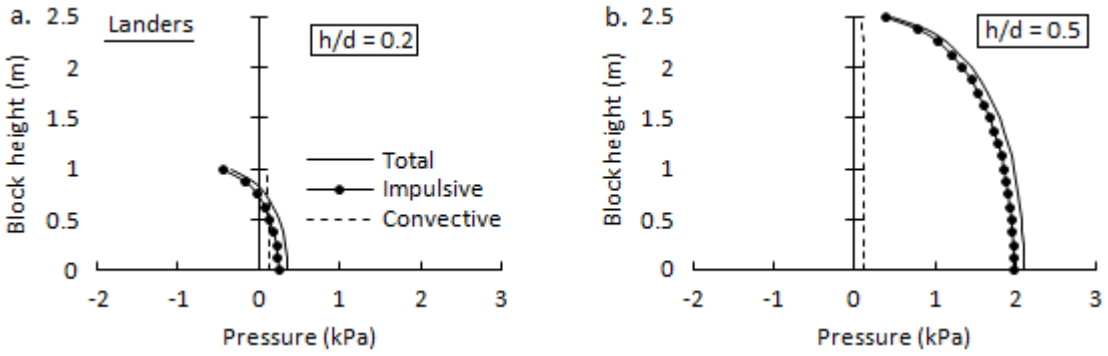

Figure 5.40: Hydrodynamic pressure distribution along the left wall of the block for various heights of centrally placed submerged block under horizontal ground motion of Landers: (a) h/d = 0.2 (b) h/d = 0.5

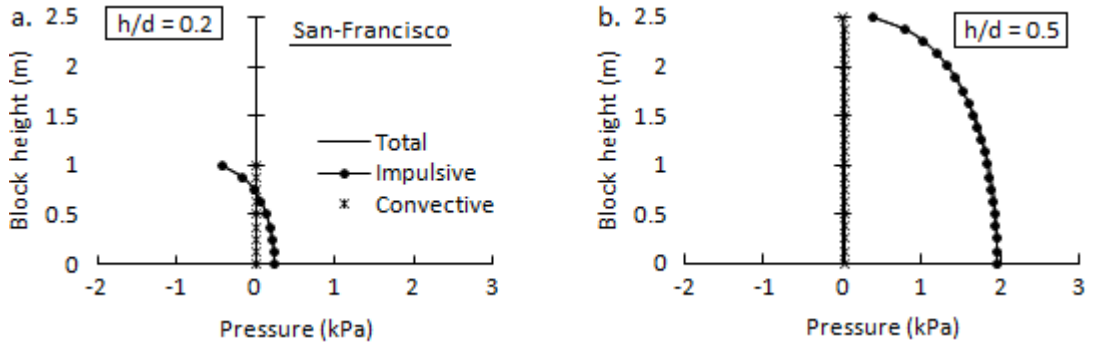

Figure 5.41: Hydrodynamic pressure distribution along the left wall of the tank for various heights of centrally placed submerged block under horizontal San-Franscisco ground motion: (a) *h/d* = 0.2 (b) *h/d* = 0.5

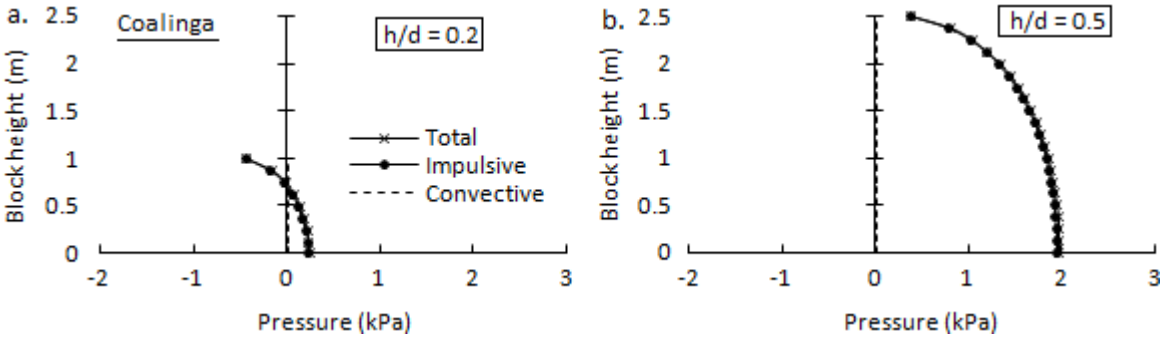

Figure 5.42: Hydrodynamic pressure distribution along the left wall of the tank for various heights of centrally placed submerged block under horizontal Coalinga ground motion: (a) *h/d* = 0.2 (b) *h/d* = 0.5

5.3 Conclusion

An efficient Galerkin based 2D finite element method has been employed for the analysis of dynamic behavior of partially filled rectangular fluid container with centrally placed bottom-mounted submerged block under horizontal ground motions. An artificial damping term μ is suitably introduced into the finite element formulation via modified surface boundary condition to mimic the surface damping on account of viscosity of liquid. It is defined as $\mu = 2\xi\omega$ where ξ is the viscous type numerical damping and ω is the fundamental sloshing frequency of liquid and a value equal to 0.0075 is used for ξ. The model is capable of finding out both convective and

impulsive response components of the dynamic physical parameters of interest. Four different horizontal ground motions with peak ground acceleration scaled to a constant value of 0.2g are applied to investigate the effect of frequency content of ground motion on the seismic behavior of tank- liquid system.

Time history analysis of dynamic physical parameters of interest for design of tank-liquid system such as sloshing elevation, structural base shear and base moment are conducted and the results in terms of their absolute maximum values are presented. Also presented are the absolute maximums of impulsive and convective responses along with the contributions of impulsive and convective response components for the total maximum values of these parameters.

It is observed that the magnitudes of peak impulsive response components of dynamic physical parameters are higher than the corresponding convective responses, in all the ground motions considered for the investigation, irrespective of their frequency content. For all ground motions considered, the impulsive response peaks invariably occur at the instant of PGAs of respective motions. It is further noticed that there exists a significant time lag between peak impulsive and convective response. Thus the overall seismic behaviour of the tank is governed by the impulsive response. However for low frequency content ground motions, the convective response dominates the overall dynamic behaviour during the later part of the earthquake when the impulsive response is in the declining and the convective response is at its fully developed state. Hence although the impulsive response is crucial for overall structural response, the convective response is equally important in such decisions as the correct estimation of free board between the quiescent free surface and tank cover and also in the design of roof cover which experiences convective hydrodynamic pressure in case of inadequate free board . Thus incorrect estimation of sloshing elevation may lead to under-designed free board which may result spillage of hazardous fluids or the failures in the tank roof.

The concept of hydrostatic base shear (Banerji *et al*, 2000) is not a valid logic for finding out the structural base shear although it gives result close to the actual hydrodynamic base shear in case of low frequency content ground motions wherein due to high amplitude sloshing convective component dominates the dynamic responses. It gives absolutely unrealistic value in case of ground motion of high

frequency content. Further the time history of hydrostatic base shear has no close correlation with the time history of hydrodynamic base shear and the peaks in both the cases occur at significantly different instants of time. This is a clear indication that it is merely a coincidence rather than any physics behind the notion of equivalent hydrostatic base shear.

In addition, the impulsive response is almost independent of the frequency content of the ground motions and is dependent on the PGA which is a measure of intensity of earthquake. However, convective response is appreciably biased by the frequency content of the ground excitation. Further, the dynamic behaviour of tank-liquid system is substantially altered due to the presence of submerged internal objects. The accumulated damage depends strongly on the duration of the earthquake. The structural degradation not only depends on the global maximum response of the structure dominated by impulsive response but also on the fatigue effect arising out of subsequent local peaks of structural responses. Once the structure incurs in the non-linear range, all the subsequent responses induce an increment in the damage, no matter how small their magnitude are. Under such situations, the contribution of amplified convective response to the local peaks of hydrodynamic forces, during the later stage of earthquake, is of paramount importance and ought to be taken into consideration in design in order to avoid accumulated structural damage caused by local peaks.

From the above investigation, it is amply clear that the effect of the bottom- mounted submerged blocks has a significant influence on the overall dynamics of the tank-liquid system and such effect differ considerably under seismic motions of different frequency content.

CHAPTER 6

6 NONLINEAR SEISMIC RESPONSE OF RECTANGULAR LIQUID TANK

6.1 Introduction

Sloshing is basically a nonlinear physical phenomenon, characterized by unrestrained free surface motion of liquid in a moving container. Understanding sloshing phenomenon is of paramount importance to the design of partially filled liquid tank subjected to seismic motion or any other motion for that matter. Liquid storage tanks are important components of many life line structures, industrial facilities and many other human infrastructures across the board. More often than not such tanks remain partially filled. Threat to the structural safety and stability of these tanks due to liquid sloshing is of great concern in a broad class of practical problems exemplified as ground-supported and elevated liquid storage tanks, fuel tanks of launching vehicles, dynamics of liquid transporting vehicles and its control, sloshing in nuclear fuel storage pool, water waves in reservoirs, cargo tanks of LNG carriers with liquid storage tank as system component. Of them the seismic response of ground supported liquid tanks deserves a special attention and is the focus of the present investigation. The prediction of sloshing behaviour is imperative for structural safety and integrity of liquid-tank system. In extreme situations when either the amplitude of external excitation is very high or the excitation frequency is very close to the fundamental frequency of free sloshing liquid or the supporting structure, the motion of liquid in the container becomes violent and creates highly localized impact pressures on the tank wall which may cause structural damage. The failure of such structures is not just critical to the huge economic value of the tank but has far reaching ramifications in

terms of environmental hazards and human health. In fact heavy damages have been reported due to strong earthquakes such as Nigaata in 1964 , Alaska in 1964 , Parkfield in 1966 , Imperial County in 1979 , Coalinga in 1979 , Loma Prieta in1989, Landers in 1992 , Northridge in 1994 , Kocaeli earthquake in 1999, and very recently 2010 Maule, 2010-11 Christchurch and 2011 Tohoku-Pacific earthquake. The seismic design standards have been revised several times to improve the performance of tanks during future earthquakes. The dynamic response of fluid-structure system is very sensitive to the characteristics of ground motion and configuration of the system.

Seismic mishap is the most likely and uncalled for threat to the structural safety and integrity of the liquid tank. Unlike other natural disasters, earthquakes are neither predictable nor preventable and their characteristics are highly nonlinear and complex. Hence the only resort open for the engineering community is to accurately predict the dynamic behaviour and properly design the fluid-structure system to minimize the effect of earthquake so that the tank-liquid system can stand the test of nature. Although the complicated deformed configurations of liquid storage tanks and the interaction between the fluid and the structure result in a wide variety of possible failure mechanisms, reports from past earthquakes indicate that the damages to the liquid filled tanks are either by large axial compression due to beamlike bending of the container wall causing a failure characterized as “elephant-foot” buckling or by sloshing of the contained liquid with insufficient freeboard. Markedly different failure types have been reported in cases of anchored and unanchored tanks.

Most of the earlier researchers have studied the effect of nonlinearity on the sloshing response with regard to harmonic excitation and many of them have studied the effect only in term of variation in free surface sloshing elevation which although a crucial sloshing behaviour and the accuracy of its calculation is a key of estimation of hydrodynamic forces, yet not the complete information in the sense of dynamic response of the tank-liquid system in so far as the safety of the tank is concerned. The excitation due to seismic motion cannot be characterized by harmonic input. Ground shaking resulting from a seismic event is stochastic in nature, and this excitation may contain a wide array of frequencies. Very few works on seismic response of liquid tank is available. Most of the earlier researchers have concentrated their study on the

simple and somewhat valid logic of overall peak hydrodynamic response. The evaluation of absolute maximum hydrodynamic response as design parameter is not only incomplete and arbitrary but also misleading. Not much effort has been put to quantify the dynamic response of liquid tank in terms of impulsive and convective response components. Hitherto, quantification of nonlinear seismic response in terms of impulsive and convective response components vis a vis frequency content of ground motion is not reported in the literature.

Damage potential of earthquake depends upon the seismic characteristics such as the duration of strong shaking, frequency content, energy content, peak ground acceleration (PGA), peak ground velocity (PGV), peak ground displacement (PGD), and the intensity at times other than the instant of PGA. Of many characteristics of ground motion, one major factor that has significant effects on the sloshing response is the frequency content of the recorded motions. The ratio of peak ground acceleration (PGA) to peak ground velocity (PGV) is a commonly accepted measure of frequency contents of earthquake records, where PGA is in g, and PGV is in m/s, (Heidebrecht and Lu, 1988). On the basis of PGA/PGV ratio, the earthquake records are classified into three categories: high (PGA/PGV > 1.2), intermediate (0.8< PGA/PGV< 1.2) and low (PGA/PGV < 0.8).

Despite long history of successful research on sloshing affiliated problems in partially filled liquid tanks and other allied fields of engineering interest, there have been unresolved issues with regard to the quantification of seismic response under earthquakes of different frequency content in terms of impulsive and convective components of hydrodynamic forces. Their individual effect on the overall dynamic response has not been studied. In the present study quantification of impulsive and convective responses of tank-liquid system under lateral earthquake motions have been comprehensively addressed and in so doing the effect of frequency content of ground motion have been considered. To this end four ground motions characterized on the basis of their frequency content have been suitably selected to evaluate and quantify the effect of frequency content on the hydrodynamic forces such as hydrodynamic pressure, base shear and overturning base moment etc. that directly affect the safety of the liquid containing structure. Each of these dynamic parameters has been quantified in terms of impulsive and convective components. The selected

ground motions include 1940 El Centro, 1970 Imperial Valley, 1992 Landers and 1987 San-Franscisco. The ground motion characteristics of interest for all the selected earthquakes are presented in Table 5.1. A velocity potential based 2D nonlinear Galerkin Finite Element Model as developed in chapter 3 is used to investigate the seismic response of the system. Mixed Eulerian-Lagrangian (MEL) method based on explicit time integration of dynamic and kinematic boundary conditions is used in the numerical scheme for surface tracking of Lagrangian nodes.

6.2 Seismic Response and Discussion

In the previous chapter, it is seen that seismic response results obtained under each frequency category are consistent and are in the similar line when the PGAs of the ground motions are scaled to a fixed magnitude. The response is more sensitive to the low frequency ground motion. Hence, in this chapter, the effect of nonlinearity on the seismic response of rigid rectangular tank is studied with only four selected ground motions; two low frequency earthquakes, and one each from intermediate and high frequency category. The selected ground motions are El Centro-EW and Imperial Valley from low frequency content earthquakes, Landers from intermediate frequency content earthquake, and San-Francisco from high frequency content earthquake. Two ground motions from low frequency category have been selected as against one each from intermediate and high frequency ground motions. This is due to the fact that low seismic response of liquid filled tank is more sensitive to low frequency earthquake. Hence by selecting two low frequency earthquakes, the objective is to focus on the dynamic response of tank to low frequency ground motion.

With the above ground motions as external excitations, the numerical experiment is conducted taking the same tank dimensions and governing parameters as in chapter 5 for the nonlinear seismic response of tank-liquid system. The PGAs of the selected records are scaled to a fixed magnitude of 0.2g as shown in the Figure 5.1 for comparison of the dynamic responses.

6.2.1 Hydrodynamic Responses

The hydrodynamic responses in terms of sloshing elevation, base shear, overturning base moment, pressure distribution on the tank wall are computed for ground motions

of different frequency content. The effect of nonlinearity of sloshing wave on each of these quantities is probed. The impulsive and convective response components are computed and their contribution to the overall hydrodynamic forces are studied and quantified.

6.2.2 Sloshing Response

The sloshing wave elevation is not only important for the seismic-safety design of liquid containers but also gives the convective response of hydrodynamic pressure and associated base shear and base moment. Free board to be provided in a tank is based on maximum value of sloshing wave height. Further, insufficient free board obstructs the free movement of convective mass and thus changes the amount of liquid in convective mode. If sufficient free board is not provided roof structure should be designed to resist the uplift pressure due to sloshing of liquid. Hence sensitiveness of sloshing response to the frequency content of seismic ground motions is studied.

The time history of surface wave elevations due to all the ground motions is presented in Figure 6.1. It is observed that both for linear and nonlinear model, the sloshing elevation is significantly more due to low frequency ground motion of Imperial Valley. Linear and nonlinear positive sloshing amplitudes at $x = -L/2$ and $x = +L/2$ and the percentage increase in nonlinear response with respect to linear response are listed in Table 6.1. Maximum positive sloshing amplitude reduces from low to high frequency ground motions. The effect of nonlinearity on free surface sloshing elevation is more pronounced in case of low frequency ground motion of Imperial Valley. The increase in sloshing elevation has a decreasing trend from low to high frequency content seismic motion.

Table 6.1: Linear and nonlinear peak sloshing amplitude

Earthquake Record	Sloshing elevation (+ ve) $x = -L/2$			Sloshing elevation (+ ve) $x = +L/2$		
	Linear (cm)	Nonlinear (cm)	% variation	Linear (cm)	Nonlinear (cm)	% variation
El-Centro EW	50.02	51.42	2.80	42.86	53.68	25.24
Imperial Valley	59.78	72.90	21.95	60.20	69.16	14.88
Landers	8.34	11.72	40.52	9.44	11.77	24.68
San-Franscisco	1.21	1.60	32.23	0.93	1.13	21.50

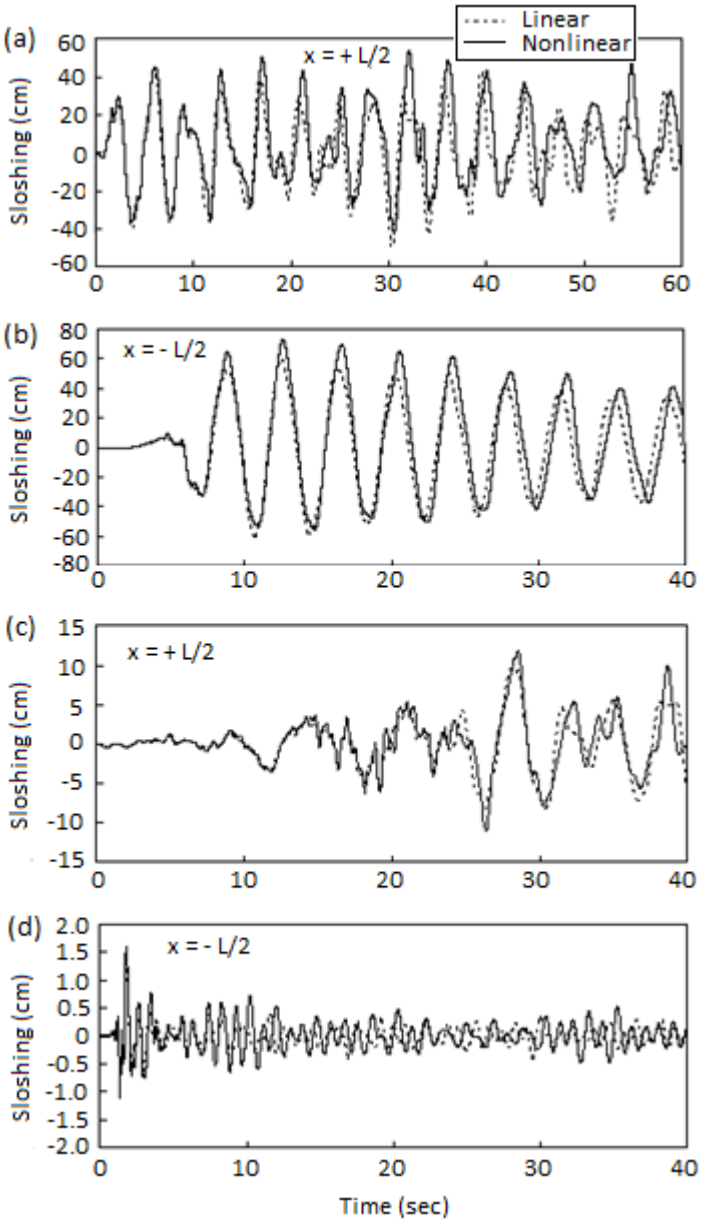

Figure 6.1: Temporal variation of linear and nonlinear sloshing elevation due to ground motions: (a) El Centro-EW (b) Imperial Valley (c) Landers (d) San-Franscisco

Table 6.2: Absolute maximum dynamic response of various physical parameters of the tank liquid system

Records	Dynamic responses	Hydrodynamic response					
		Linear			Nonlinear		
		Impulsive	Convective	Total	Impulsive	Convective	Total
El-Centro EW	Sloshing (cm)	-	50.02 (0.83)	50.02 (0.83)	-	53.68 (0.74)	53.68 (0.74)
	Base shear (kN/m)	54.87 (1.14)	12.27 (0.71)	60.83 (1.01)	54.87 (1.14)	47.50 (2.10)	59.20 (0.98)
	Base moment (kN.m/m)	216.69 (1.11)	70.14 (0.72)	248.34 (0.99)	216.69 (1.11)	216.95 (1.72)	228.30 (0.93)
Imperial Valley	Sloshing (cm)	-	60.20 (1.0)[a]	60.20 (1.0)	-	72.90 (1.0)	72.90 (1.0)
	Base shear (kN/m)	48.13 (1.0)	17.15 (1.0)	60.03 (1.0)	48.13(1.0)	22.68 (1.0)	60.50 (1.0)
	Base moment (kN.m/m)	195.40 (1.0)	97.12 (1.0)	250.19 (1.0)	195.40 (1.0)	126.11 (1.0)	245.45 (1.0)
Landers	Sloshing (cm)	-	9.44 (0.16)	9.44 (0.16)	-	11.77 (0.16)	11.77 (0.16)
	Base shear (kN/m)	48.16 (1.0)	3.15 (0.18)	46.92 (0.78)	48.16 (1.0)	29.39 (1.30)	42.71 (0.71)
	Base moment (kN.m/m)	196.64 (1.0)	19.30 (0.20)	189.70 (0.76)	196.64 (1.0)	120.45 (0.96)	170.95 (0.69)
San-Franscisco	Sloshing (cm)	-	1.21 (0.02)	1.21 (0.02)	-	1.60 (0.02)	1.60 (0.02)
	Base shear (kN/m)	48.75 (1.01)	0.18 (0.01)	48.58 (0.81)	48.75 (1.01)	10.68 (0.47)	47.63 (0.79)
	Base moment (kN.m/m)	197.40 (1.01)	0.94 (0.01)	196.49 (0.79)	197.40 (1.01)	43.17 (0.34)	192.31(0.78)

[a] The bracketed values are normalized hydrodynamic responses with respect to low frequency earthquake of Imperial Valley

Table 6.3: Contributions of impulsive and convective components for absolute maximum hydrodynamic response of various physical parameters

Records	Dynamic responses	Hydrodynamic response					
		Linear			Nonlinear		
		Impulsive	Convective	Total	Impulsive	Convective	Total
El-Centro EW	Base shear (kN/m)	54.87	5.96	60.83	52.24	6.96	59.20
	Base moment (kN.m/m)	216.69	31.65	248.34	206.07	22.23	228.30
Imperial Valley	Base shear (kN/m)	45.53	14.50	60.03	44.43	16.37	60.50
	Base moment (kN.m/m)	167.39	82.80	250.19	140.38	105.07	245.45
Landers	Base shear (kN/m)	47.52	0.60[#]	46.92	41.33	1.37	42.71
	Base moment (kN.m/m)	192.83	3.13[#]	189.70	168.80	2.15	170.95
San-Franscisco	Base shear (kN/m)	48.75	0.17[#]	48.58	45.82	1.81	47.63
	Base moment (kN.m/m)	197.40	0.91[#]	196.49	185.54	6.77	192.31

[#] The superscripted values indicate that the convective responses are in opposite phase with their impulsive counterparts.

6.2.3 Base Shear and Overturning Base Moment

The temporal history of base shear and overturning base moment due to horizontal ground motions of selected earthquakes are computed by the proposed method. The effect of frequency content on the hydrodynamic response of the tank-liquid system is probed. Both base shear and overturning base moment are quantified in terms of impulsive and convective components. It may be mentioned convective component is frequency sensitive while impulsive response is acceleration sensitive. The computed responses of base shear and base moment are presented in terms of their time history in Figures 6.2 and 6.3 respectively.

The absolute maximum peaks of base shear and base moments due to all earthquakes are presented in Table 6.2. The responses are normalized with respect to those of the low frequency Imperial Valley record and presented in brackets. The table presents both linear and nonlinear responses of each physical parameter. As nonlinearity has nothing to do with the impulsive responses, their values remain the same under linear and nonlinear columns. The results show that impulsive responses remain almost unchanged irrespective of the frequency content of ground motions. However marginally higher values are observed in case of El Centro record. Unlike impulsive response, a wide variation in maximum values is recorded for convective components. The convective responses are magnified in case of El Centro earthquake. It is observed that there exists time lag between the peaks of impulsive and convective response components. For all earthquake records considered for the study, one can notice that the magnitudes of peak impulsive response is higher than the corresponding convective response irrespective of the frequency content of ground motions. The absolute peaks of impulsive responses invariably occur at the instant of PGAs of ground motions. The total seismic response is dominated by the impulsive response and occurs at some instant close to the time of PGA.

In some sense, the reader may find the results in Table 6.2 intriguing. To clarify the confusion and for completeness of quantification, the contribution of impulsive and convective response components to the absolute total structural response are presented in Table 6.3. From Table 6.2 it can be seen that both convective and impulsive response components of base shear are significantly more in case of El Centro-EW

than their respective counterparts for Imperial Valley. However the absolute total base shear is more, although marginally, in case of low frequency Imperial Valley ground motion. An even more contrasting observation can be made in case of overturning base moment. From simultaneous observation of both the tables it is amply clear that although the maximum convective responses are more for a given ground motion they may not contribute to the absolute maximum total structural response. This is due to the time lag between the impulsive and convective peak responses. However the effect of absolute peak convective responses and/or local peaks cannot be marginalized or under estimated. This is because the amount of structural damage expected in an earthquake is proportional to the duration of the earthquake and this relationship is not linear. A longer duration of shaking causes the damage to increase. In case of long duration earthquakes amplified local peaks contribute to structural fatigue and may prove critical to the safety of the structure and hence their effect should be taken into account in design.

If sloshing of the liquid, hence the effect of convective response is ignored as is done in some simplified analysis; all the response quantities are found more than those when sloshing is considered. This observation is made in case of Landers and San-Franscisco records on the basis of linear analysis. This observation is shown with superscripted data in Table 6.3. This is due to the fact that convective responses for the said motions occur in opposite phase with respect to the impulsive responses and counter their effect.

The convective response in terms of sloshing elevation is important in such decisions as the correct estimation of free board between the quiescent free surface and tank cover and also in the design of roof cover which experiences convective hydrodynamic pressure in case of inadequate free board. Thus incorrect estimation of sloshing elevation may lead to under-designed free board which may result spillage of hazardous fluids or the failures in the tank roof.

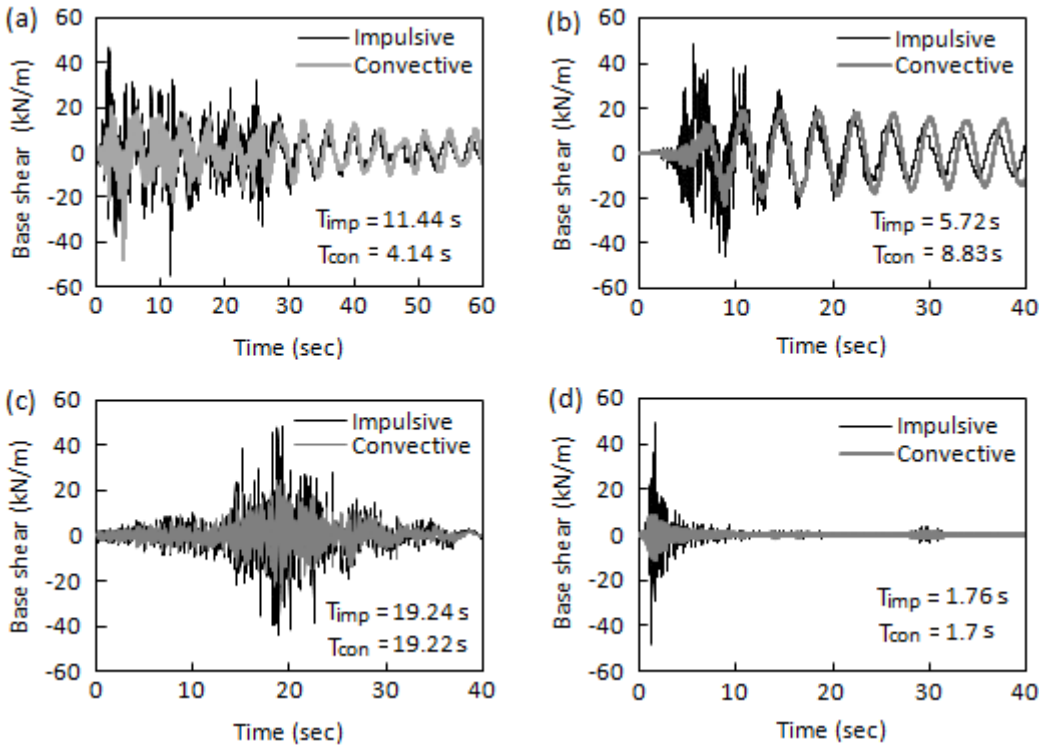

Figure 6.2: Time history of impulsive and convective responses of base shear: (a) El Centro-EW (b) Imperial Valley (c) Landers (d) San-Franscisco

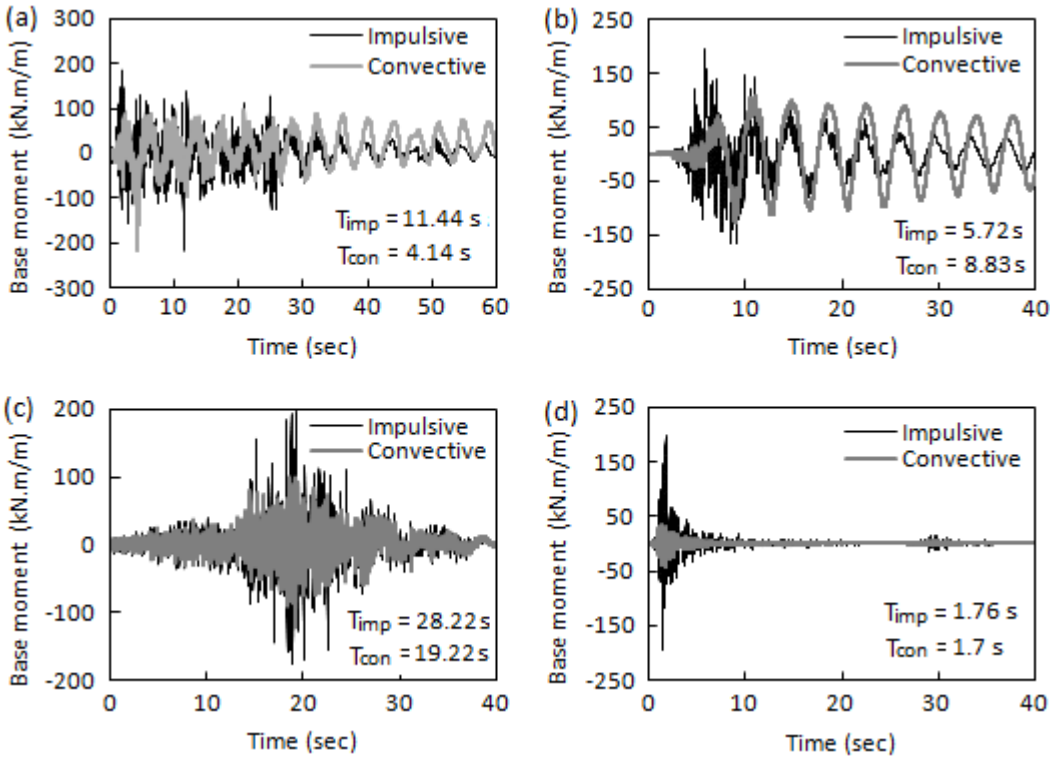

Figure 6.3: Time history of impulsive and convective responses of base moment: (a) El Centro-EW (b) Imperial Va lley (c) Landers (d) San-Franscisco

It is evident from the tables that the effect of nonlinearity of surface wave on the dynamic response is more pronounced in case of low frequency earthquake of Imperial Valley and intermediate frequency content El Centro record. Figures 6.4 and 6.5 present the comparative time history of convective responses of base shear and base moment due to Imperial Valley and El Centro records respectively. It is seen that nonlinear absolute global maximums in both the cases are significantly more than their linear counterparts. In addition, the nonlinear local peaks are consistently more, although not substantially, which may contribute to structural fatigue for long duration earthquakes and hence proof detrimental to the structural safety because of the cumulative damage sustained by the tank.

A shallow tank of $d/L = 0.2$ is considered to study the effect of nonlinearity of surface wave on the dynamic response of the tank-liquid system. The ground motion records of El Centro and Imperial Valley are used for the numerical experiment. Figures 6.6 and 6.7 present the comparative result of time history of base shear and base moment for tall tank ($d/L = 0.5$) and shallow tank ($d/L = 0.2$) respectively due to the above said ground motions. For shallow tanks, one can observe early dominance of convective response when the impulsive response is still in the dominating stage and is in the same phase with the convective response. As a result, an increase in overall total hydrodynamic response can be observed in case of shallow tank. From a comparative study of Figures 6.6(b) and 6.7(b), it can be seen that although the convective and impulsive response of base shear for shallow tanks follow the same trend both in terms of phase and magnitudes, the two significantly differ in magnitudes in their respective responses to overturning base moments. This fact is attributed to the higher convective pressure resultant height due to amplified sloshing for low frequency motion of Imperial Valley. As these forces are applied high up the tank they tend to cause overturning rather than sliding. This is in consistent with the physics that long period motions cause high surface waves in the tanks which apply large convective forces to the side of the tank. The histograms in Figures 6.8 and 6.9 show respectively the absolute peak responses and contributions of impulsive and convective components to absolute peak responses.

It is known that nonlinearity has no effect on the impulsive response since nonlinearity is associated with large amplitude sloshing.. Impulsive response being same in case of linear and nonlinear model the difference in overall dynamic behavior

is decided by the difference in temporal variation of convective responses in case of linear and nonlinear model.

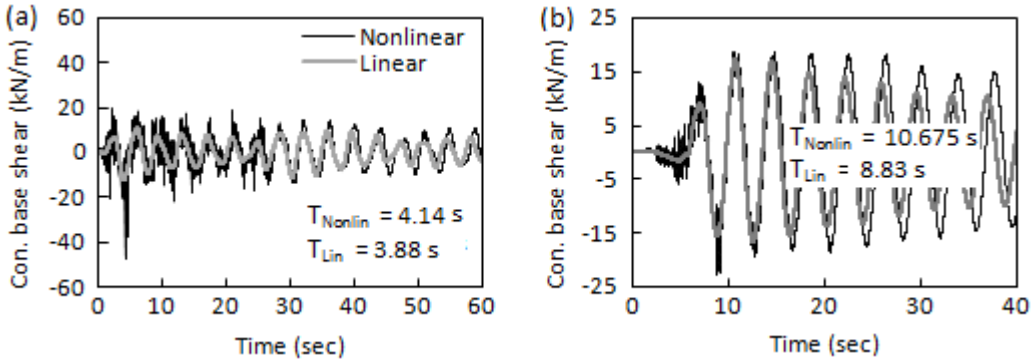

Figure 6.4: Time history of linear and nonlinear convective base shear: (a) El Centro-EW (b) Imperial Valley

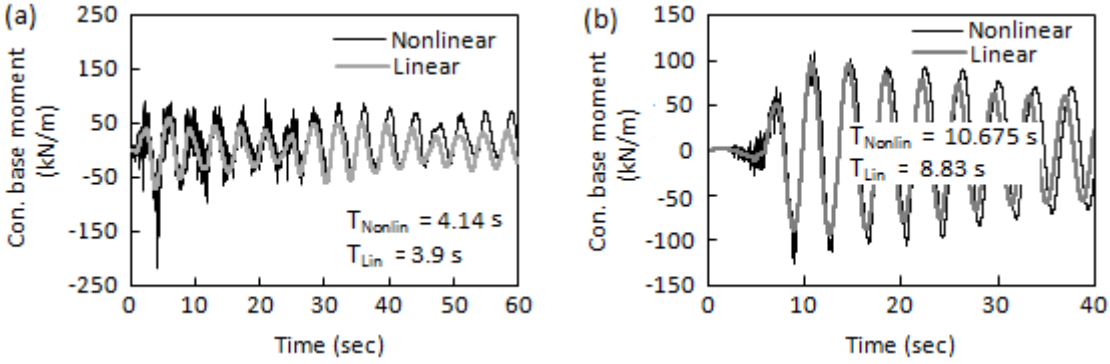

Figure 6.5: Time history of linear and nonlinear convective base moment: (a) El Centro-EW (b) Imperial Valley

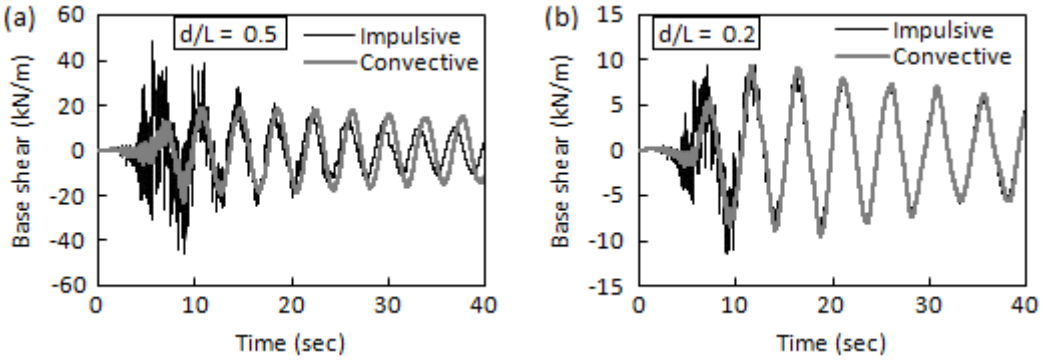

Figure 6.6: Time history of impulsive and convective responses of base shear for Imperial Valley ground motion: (a) d/L = 0.5 (b) d/L = 0.2

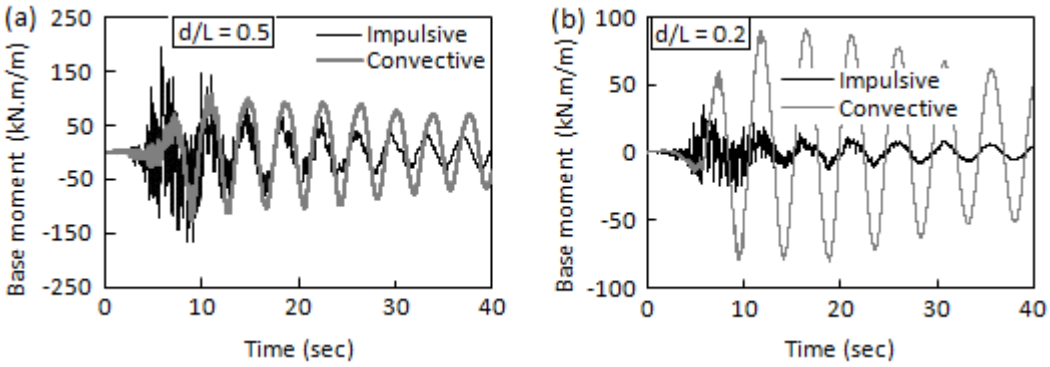

Figure 6.7: Time history of impulsive and convective responses of base moment for Imperial Valley ground motion: (a) d/L = 0.5 (b) d/L = 0.2

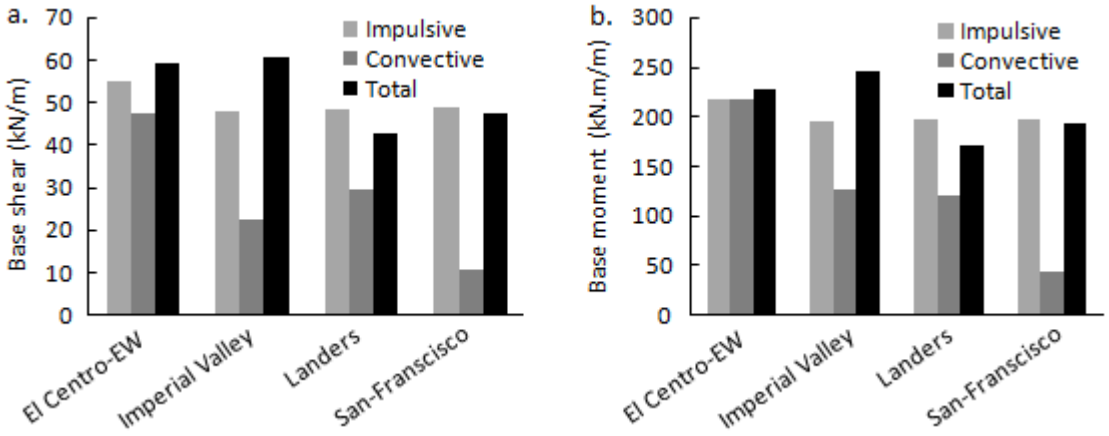

Figure 6.8: Quantitative result of absolute maximum values of impulsive, convective and total hydrodynamic responses for different ground motions: (a) Base shear (b) Base moment

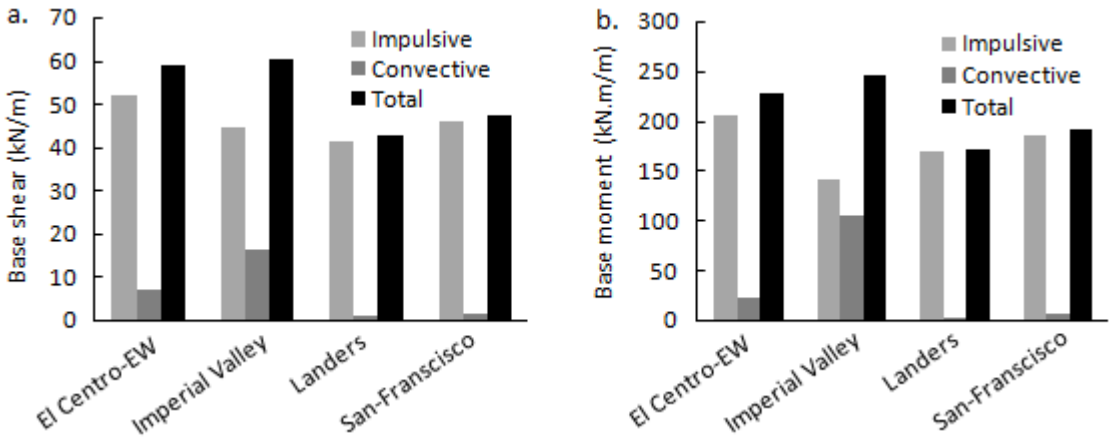

Figure 6.9: Component-wise break up of peak hydrodynamic responses for different ground motions: (a) Base shear (b) Base moment

6.2.4 Pressure Distribution on Tank Wall

The distributions of linear and nonlinear total hydrodynamic pressure on the container wall at the instant of maximum base shear are presented in Figure 6.10. In case of low frequency ground motion of Imperial Valley, the nonlinear pressure resultant is more than the linear pressure resultant and the resultant height is also more than that of linear model. However, in case of intermediate and high frequency ground motions of Landers and San-Franscisco respectively, the nonlinearity does not have major effect on the pressure distributions for the tank walls. The linear pressure resultants give conservative results for hydrodynamic force on the tank wall. However even though the pressure resultant in case of linear model is larger, the lower resultant height produces less overturning base moment than the nonlinear model and hence may give non-conservative result for overturning base moment. Hence nonlinearity of surface wave cannot be overruled by conservative result of hydrodynamic force on the wall even for high frequency motions.

Figure 6.11 shows the distributions of impulsive and convective responses of pressure at the instant of maximum base shear for all ground motions. One can observe considerably higher contribution of convective response due to Imperial Valley record as compared to other earthquakes. The convective pressure resultant height acts high up the wall. This is consistent with the other responses presented in Table 6.3 and clarifies the confusion, if any, of the reader as mentioned in paragraph 3 of 6.2.3. The convective pressure resultant due to high frequency San-Franscisco earthquake is

negligibly small and that due to Landers is not appreciable compared to the impulsive response.

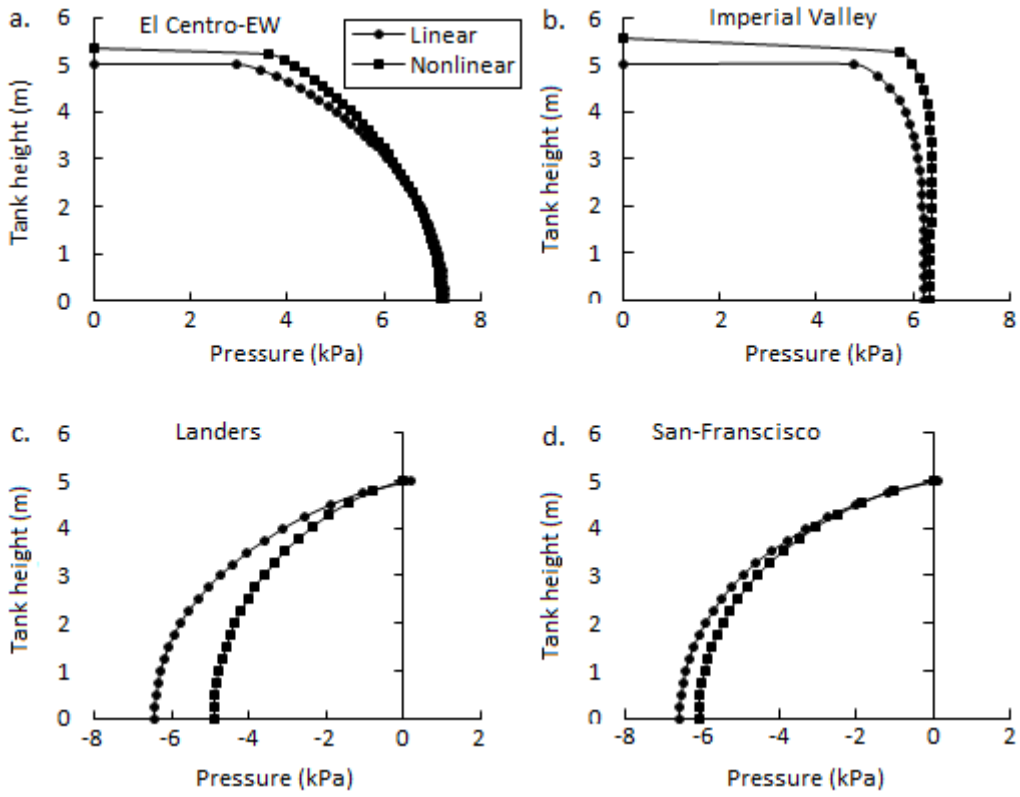

Figure 6.10: Comparison of linear and nonlinear hydrodynamic pressure distribution along the height of tank wall: (a) El Centro-EW (b) Imperial Valley (c) Landers (d) San-Franscisco

The indispensability of nonlinearity of surface wave is further buttressed in Figure 6.12. The impulsive and convective pressure distributions due to tall and shallow tank are presented in Figure 6.12. Significant increase in impulsive force is observed for tall tank of same width, which is due to the increased mass of liquid. An interesting observation with respect to the convective response is observed. The convective pressure at each point up to the depth of liquid in shallow tank is significantly more than those for the tall tank.

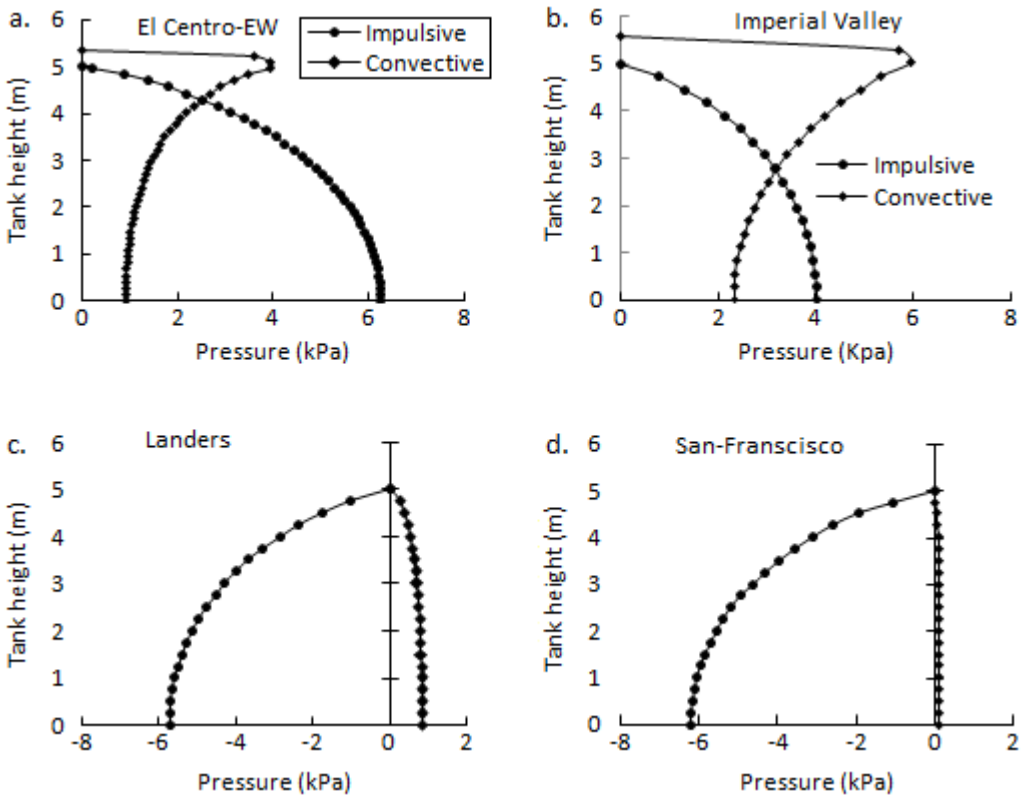

Figure 6.11: Distribution of impulsive and convective nonlinear hydrodynamic pressure along the height of tank wall: (a) El Centro-EW (b) Imperial Valley (c) Landers (d) San-Franscisco

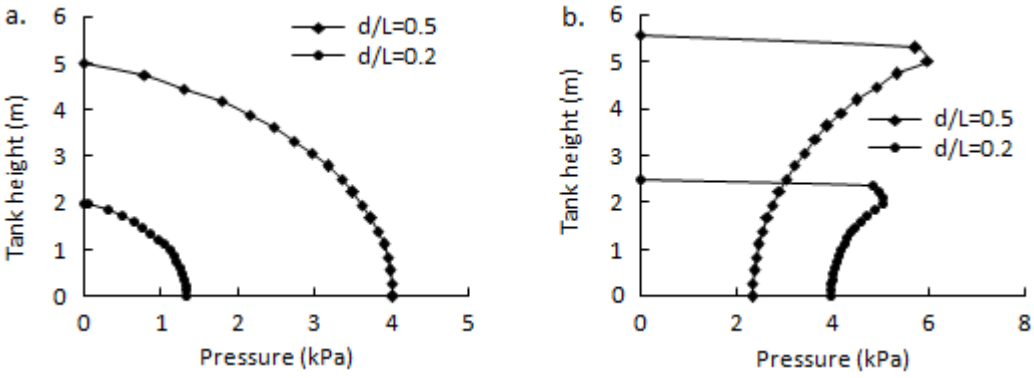

Figure 6.12: Hydrodynamic pressure along the height of tank wall for Imperial Valley earthquake: (a) Impulsive (b) Convective

6.3 Conclusion

In the present study, an efficient Galerkin based two dimensional fully nonlinear finite element model has been developed for investigation and quantification of seismic behavior of partially filled rigid rectangular liquid tank under horizontal ground motions of different frequency content. Mixed Eulerian-Lagrangian (MEL) method based fourth order explicit Runge-Kutta scheme is used for the time-stepping integration of free surface boundary conditions. An artificial damping term μ is suitably introduced into the finite element formulation via modified surface boundary condition to mimic the surface damping on account of viscosity of liquid. It is defined as $\mu = 2\xi\omega$ where ξ is the viscous type numerical damping and ω is the fundamental frequency of liquid and a value equal to 0.0075 is used for ξ. The model is capable of finding out both convective and impulsive responses of the hydrodynamic behavior. The effect of nonlinearity of surface wave on the convective response and hence on the overall hydrodynamic behaviour is investigated.

Four different horizontal ground motions with peak ground acceleration scaled to a constant value of 0.2g are applied to investigate the effect of frequency content of ground motion on the seismic behavior of tank-liquid system. Time history analysis of sloshing elevation, structural base shear, overturning base moment are carried out and the results of absolute maximum values of free surface wave elevation, structural base shear, overturning base moment are presented. In addition the absolute maximum responses of impulsive and convective components of hydrodynamic forces are presented. The hydrodynamic responses due to linear model are depicted for comparison. The hydrodynamic pressure distributions on tank wall at the instant of maximum base shear for the choosen ground motions are compared. For completeness of investigation, numerical experiment is also conducted in shallow tank to study the effect of tank geometry on the dynamic response and in so doing the only ground motion of low frequency Imperial Valley earthquake is selected as external excitation.

Important inferences drawn from the study may be summarized as follows:

1. In time domain analysis local temporal variation of nonlinear convective response and their contribution to total hydrodynamic forces is equally important if not more important than the absolute global peak of total dynamic

response and ought to be considered for the design of tank because of cumulative structural damage sustained by the tank.

2. Nonlinearity of surface wave is not only important in shallow tank design but also critical in tall tanks subjected to low frequency ground motions and thus crucial in shaping the convective responses.
3. Contrary to the generally accepted notion of dominancy of impulsive component on the hydrodynamic response, this study finds that although impulsive component dominates the hydrodynamic pressure in high frequency content earthquakes and also has a dominating share in total hydrodynamic response in all other ground motions, the convective components do also play an important role in low frequency earthquakes.
4. Design should not be biased on the basis of conservativeness of linear total hydrodynamic pressure distribution on tank wall. This is because conservativeness of hydrodynamic pressure does not necessarily guarantee other responses to be also conservative.

CHAPTER 7

7 NONLINEAR SEISMIC RESPONSE OF RECTANGULAR LIQUID TANK WITH SUBMERGED BLOCK

7.1 Introduction

Sloshing is essentially a nonlinear physical phenomenon, beyond the ambit of linear theory, characterized by low frequency free surface motion of liquid in a partially-filled moving container. Across the board, liquid containers constitute a major chunk of critical life line structures and are widely used in water supply facilities, oil and gas industries, and nuclear power plants for storage of a variety of liquids such as water, fuel, oil products, liquefied natural gas, chemical fluids and industrial wastes of different forms. Safe up-keeping and uninterrupted supplies of such products are of principal importance to the industrial houses. In this perspective, the threat to the structural safety and stability of their containers, in the event of seismic mishap, is a matter of great concern to a wide range of industrial facilities, civic bodies and environmental agencies, etc. Precise calculation of maximum sloshing force due to earthquake constitutes a fundamental issue for the structural integrity of these containers. This has been a major challenge before the scientific community, constantly thriving to understand the complex mechanism of sloshing in order to counter the threat.

Sloshing is regarded as a classic linear eigenvalue problem in terms of fluid velocity potential function, representing the small amplitude free vibrations of the surface of an ideal liquid inside a stationary container. Under a particular external excitation, sloshing represents the motion of fluid in a moving container and is treated as

transient problem. In many engineering applications, besides sloshing frequencies, sloshing induced hydrodynamic pressures and forces need to be calculated. Especially earthquake-induced sloshing has been identified as a crucial issue toward protecting the structural safety and integrity of liquid containers. Over decades, since the pioneering works of Housner (1957, 1963), sloshing has been the matter of several analytical, numerical and experimental works, and those form a vast body of available literature. Sloshing characteristics depend on such diverse parameters of liquid-tank system as tank geometry, liquid fill-depths, aspect ratio of tank, compressibility and viscosity of liquid, amplitude and frequency of external excitation, orientation and type of excitation, properties of tank material, submerged components if any, and restraint conditions of support structure etc. The dynamics of liquid storage tanks subjected to seismic loading depends on the inertia of the liquid and the interaction effects if any, depending on if the tank is rigid or flexible, between the liquid and the tank shell. Records of past earthquakes in various parts of the world bears the testimony to the extensive damages inflicted on various kinds of liquid storage tanks leading to loss of valuable contents, environmental hazards, fire-breaks and temporary loss of essential services. While the complicated deformed configurations of liquid storage tanks and the interaction between the fluid and the structure result in a wide variety of possible failure mechanisms, field reports from past earthquakes imply that the damages to the liquid-filled tanks are mainly ascribed to: (1) two nonlinear buckle mechanisms characterized as “elephant-foot buckles and diamond shape buckles” and (2) sloshing of contained liquid with inadequate freeboard between the quiescent liquid surface and the tank-roof. The dynamic response of fluid-structure system is very perceptive to the characteristics of ground motion and configuration of the system. Strikingly diverse failure patterns have been reported in cases of anchored and unanchored tanks.

The presence of submerged equipments or components like the ones in nuclear spent fuel storage pool, a structure of seismic category I, the dynamic behaviour of fluid-structure systems may be radically changed. Compared to the vast body of literature concerning liquid tanks of different geometries, only a few works on tanks with submerged internal components have been published. However, such studies are limited to linear analysis. Nevertheless, “impulsive-convective” pressure concept which lay the basis of almost all recent design codes and guide lines, e.g., API

Standard 650 (1995), Eurocode 8 (1998), and ASCE (1984), has been overlooked in the above studies.

The objective of the present paper is to methodically investigate the effect of submerged block on the nonlinear sloshing, base shear, overturning base moment and dynamic pressure distribution on the walls of the tank and block. The effect of submerged block on impulsive and convective response of dynamic behaviour of liquid in a tank is quantified. On the basis of PGA/PGV ratio, the earthquake records are classified into three categories: high (PGA/PGV > 1.2), intermediate (0.8< PGA/PGV< 1.2) and low (PGA/PGV < 0.8), (Heidebrecht and Lu, 1988). Three ground motions characterised on the basis of their frequency content have been used. The effects of frequency content of ground motions on the nonlinear dynamic response of the liquid-tank system are also investigated in the presence of submerged block.

7.2 Numerical Results and Discussion

Numerical experiment is conducted in a tank with length, L = 10 m and liquid depth, d = 5 m for the nonlinear seismic response of tank-liquid system. The width of the submerged block is kept constant as 0.2L and the height of the block is varied as h/d = 0.0, 0.2, and 0.5.

Three ground motions are selected from Pacific Earthquake Engineering Research Next Generation Attenuation (PEER-NGA) strong motion database records. The ground motion characteristics of interest for all the selected earthquakes are presented in Table 5.1. The PGAs of all the records are scaled to a fixed magnitude of 0.2g as shown in the Figure 5.1 for comparison of the dynamic responses under seismic excitations with varying frequency contents. On the basis of the ratios of PGA/PGV, Imperial Valley, Landers and San-Franscisco are considered as the low, intermediate and high frequency content seismic motions respectively. In addition, the power spectrum density functions (PSDF) of all ground motions are obtained which depict the frequency content as shown in the Figure 5.3.

7.2.1 Hydrodynamic Responses

The hydrodynamic responses in terms of sloshing elevation, base shear, overturning base moment, pressure distribution on the wall of the tank as well as the block are computed for ground motions of different frequency content. The effect of frequency content vis-a-vis the height of the submerged block on each of these dynamic parameters is comprehensively investigated. The impulsive and convective response components are computed and their contribution to the overall hydrodynamic forces are also studied and quantified.

7.2.1.1 Sloshing Response

The sloshing wave elevation is not only important for the seismic-safety design of liquid containers but also influences the convective response of hydrodynamic pressure and associated base shear and base moment. The maximum value of sloshing wave height determines the free board between the quiescent free surface and the tank-roof. Moreover, inadequate free board impedes the free movement of convective mass and thus alters the amount of liquid in convective mode which in turn modifies the convective response of hydrodynamic forces. Should the free board is insufficient; the roof structure needs to be carefully designed to resist the uplift pressure due to sloshing. Hence sensitiveness of sloshing response to the frequency content characteristics of seismic ground motions is studied.

The time history of surface wave elevations for different block heights due to all the ground motions is presented in Figure 7.1. One can see that for a given block dimension, the sloshing elevation is significantly more due to low frequency ground motion of Imperial Valley. Increase in block height increases the sloshing elevation in case of low and intermediate frequency earthquakes and such increase is significantly more for low frequency ground motion. However, for high frequency ground motion of San-Franscisco, increase in block height decreases the sloshing elevation although marginally.

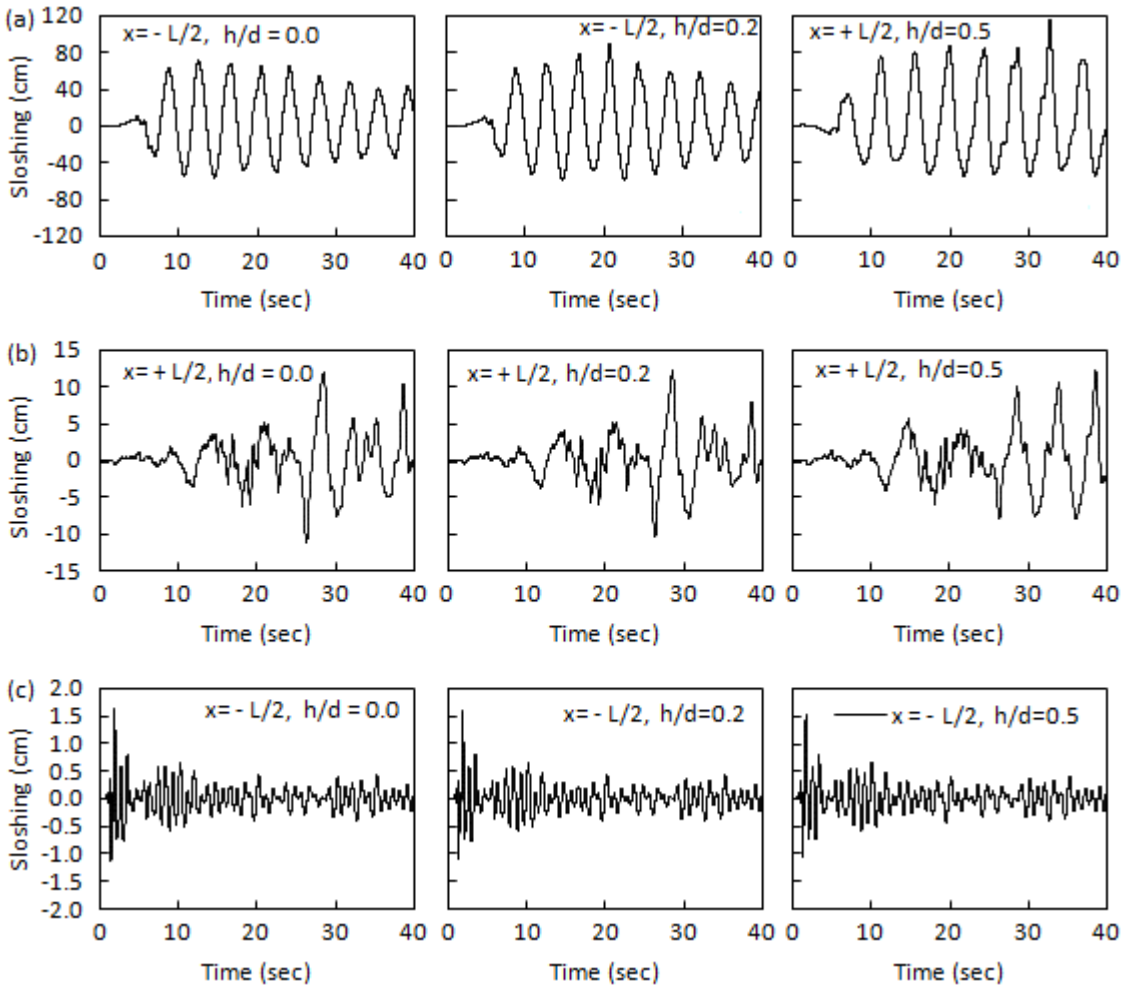

Figure 7.1: Temporal variation of sloshing elevation in tank with submerged block of varying height (*h/d*) under seismic ground motions: (a) Imperial Valley (b Landers (c) San-Franscisco

Table 7.1: Absolute maximum dynamic responses of various physical parameters of the tank liquid system:

Records	Dynamic responses parameters	Nonlinear hydrodynamic response components								
		Impulsive			Convective			Total		
		h/d=0.0	*h/d*=0.2	*h/d*=0.5	*h/d*=0.0	*h/d*=0.2	*h/d*=0.5	*h/d*=0.0	*h/d*=0.2	*h/d*=0.5
Imperial Valley	Sloshing (cm)	-	-	-	70.42 (1.0)	89.64 (1.0)	115.0 (1.0)	70.42 (1.0)	89.64 (1.0)	115.0 (1.0)
	Base shear (kN/m)	48.14 (1.0)[c]	47.0 (1.0)	40.86 (1.0)	22.51 (1.0)	38.20 (1.0)	45.35 (1.0)	60.39 (1.0)	60.52 (1.0)	56.60 (1.0)
	Base moment (kN.m/m)	195.43 (1.0)	184.59 (1.0)	143.74 (1.0)	125.23 (1.0)	237.47 (1.0)	269.70 (1.0)	245.51(1.0)	2 95.26 (1.0)	281.84 (1.0)
Landers	Sloshing (cm)	-	-	-	11.93 (0.17)	12.15 (0.14)	12.16 (0.11)	11.93 (0.17)	12.15 (0.14)	12.16 (0.11)
	Base shear (kN/m)	48.16 (1.0)	47.80 (1.02)	41.55 (1.02)	29.40 (1.31)	29.42 (0.77)	24.96 (0.55)	42.71 (0.71)	41.01 (0.68)	36.24 (0.64)
	Base moment (kN.m/m)	196.66 (1.01)	187.73 (1.02)	146.18 (1.02)	120.48 (0.96)	117.07 (0.49)	89.81 (0.33)	170.96 (0.70)	159.32 (0.54)	126.05 (0.45)
San-Franscisco	Sloshing (cm)	-	-	-	1.61 (0.02)	1.59 (0.02)	1.53 (0.01)	1.61 (0.02)	1.59 (0.02)	1.53 (0.01)
	Base shear (kN/m)	48.76 (1.01)	47.09 (1.0)	40.94 (1.0)	10.68 (0.47)	10.29 (0.27)	8.94 (0.20)	47.64 (0.79)	45.71 (0.76)	39.71 (0.70)
	Base moment (kN.m/m)	197.43 (1.01)	184.94 (1.0)	144.02 (1.0)	43.18 (0.34)	40.52 (0.17)	31.58 (0.12)	192.34 (0.78)	179.06 (0.61)	139.04 (0.49)

[c]The bracketed values are normalized hydrodynamic responses with respect to the corresponding responses due to low frequency earthquake of Imperial Valley

Table 7.2: Contributions of impulsive and convective components for absolute maximum hydrodynamic response of various physical parameters:

Records	Dynamic responses	Nonlinear hydrodynamic responses								
		Impulsive			Convective			Total		
		h/d=0.0	*h/d*=0.2	*h/d*=0.5	*h/d*=0.0	*h/d*=0.2	*h/d*=0.5	*h/d*=0.0	*h/d*=0.2	*h/d*=0.5
Imperial Valley	Base shear (kN/m)	44.14 (73.09)[d]	23.07 (38.12)	19.91 (35.18)	16.25 (26.91)	37.45 (61.88)	36.69 (64.82)	60.39	60.52	56.60
	Base moment (kN.m/m)	140.41 (57.19)	90.60 (30.68)	70.03 (24.85)	105.10 (42.81)	204.66 (69.32)	211.81 (75.15)	245.51	295.26	281.84
Landers	Base shear (kN/m)	41.33 (96.77)	40.76 (99.39)	35.43 (97.76)	1.38 (3.23)	0.25 (0.61)	0.81 (2.24)	42.71	41.01	36.24
	Base moment (kN.m/m)	168.80 (98.74)	160.06 (100.46)	124.64 (98.88)	2.16 (1.26)	0.74 (0.46)	1.41 (1.12)	170.96	159.32	126.05
San-Franscisco	Base shear (kN/m)	45.83 (96.20)	44.27 (96.85)	38.48 (96.90)	1.81 (3.80)	1.44 (3.15)	1.23 (3.10)	47.64	45.71	39.71
	Base moment (kN.m/m)	185.56 (96.47)	173.87 (97.10)	135.39 (97.37)	6.78 (3.53)	5.19 (2.90)	3.65 (2.63)	192.34	179.06	139.04

[d]The bracketed values indicate the respective response components as percentage of corresponding total hydrodynamic response.

7.2.1.2 Base Shear and Overturning Base Moment

A precise prediction of the base shear and overturning moment is crucial for judging the safety of tanks against shell buckling and uplift. The temporal history of transient base shear and overturning base moment due to horizontal ground motions of selected earthquakes are computed. The effect of frequency content on the hydrodynamic response of the tank-liquid system is probed. For a given ground motion, the effect of centrally placed submerged blocks on the hydrodynamic response is also studied. Separate contribution of impulsive and convective component of fluid motion to the total magnitude of pressure, base shear and overturning base moment are measured and reported alongside respective total response. Temporal evolution of structural base shear in terms of impulsive and convective components of base shear for all ground motions are presented in Figures 7.2 – 7.4. Similar responses for base moment are presented in Figures 7.5 – 7.7.

The absolute maximum peaks of base shear and base moments due to all earthquakes are presented in Table 7.1. The responses are normalized with respect to those of the low frequency Imperial Valley record and presented in brackets. The results show that for a given block, the impulsive response remains almost unchanged irrespective of the frequency content of ground motions. Unlike impulsive response, frequency content of ground motions is found to have considerable effect on the convective component and a wide variation in maximum values is recorded for the same. It is further observed that the absolute peak impulsive responses decrease with increase in the height of the block. Further, it is observed that although convective responses are sensitive to the block dimension, their increase or decrease is dependent on the frequency content of the ground motion. It can be seen from Table 7.1 that for low frequency ground motion of Imperial Valley, the convective responses increase with increase in the block height. However, they decrease with increase in the height of the block in case of intermediate and high frequency ground motions. The peaks of the total structural responses (combined response of impulsive and convective components) of base shear and overturning base moments, normally regarded as the design parameters, decrease with increase in the height of submerged block under the ground motions of Landers and San-Franscisco. In case of Imperial Valley, however, the total responses first increase as the height of the submerged structure increases

from *h/d* = 0.0 to *h/d* = 0.2 and then decreases as the block height increases to *h/d* = 0.5. The maximum values of base shear and overturning moment for the Imperial Valley earthquake are considerably greater than those for others for all (*h*/*d)*s. This indicates that the low-frequency contents of ground motion increase the sloshing response and hence the convective component significantly. From the observation made as above, it may be inferred that convective components are sensitive to the frequency contents of ground motion and hence structural responses are greatly influenced.

The contributions of impulsive and convective response components to the absolute maximums of base shear and base moments are presented in Table 7.2. The percentage contributions of individual responses of impulsive and convective components are presented in brackets alongside each. It is amply evident that for tank-liquid system without submerged block the response parameters such as structural base shear and base moment are invariably dominated by the impulsive response irrespective of the ground motions. However the convective components are considerable in case of low frequency motion of Imperial Valley. For liquid–tank system with submerged block the impulsive components decrease and the convective components increase with increase in the height of block. Nevertheless, the percentage increase in the convective response components is more than the corresponding decrease in their impulsive counterparts and thus convective components become dominant with increase in *h/d*. In case of other ground motions, convective responses have marginal role in the overall peak dynamic responses. The observations made as above can be clearly noticed from Figure 7.14 which shows the component-wise break up of absolute global peak of hydrodynamic responses (base shear and base moments) for different ground motions.

One can notice in Figures 7.2 – 7.7 that for all ground motions considered, the impulsive response peaks as a matter of fact occur at the instant of PGAs of respective motions. It is further noticed that there exists a significant time lag between peak impulsive and peak convective responses especially in case of low frequency Imperial Valley earthquake and the time lag further increases with increase in the height of submerged block. Thus the overall seismic behaviour of the tank is governed by the impulsive response. The time of occurrence of absolute maximums of impulsive and convective response components are indicated in Figures 7.2-7.7 as T(imp) and

T(con) respectively. It may be noticed that the dominancy of convective response component comes into picture during the later part of the earthquakes when the impulsive responses are in their waning leg. It may be stated that although the impulsive response is vital for overall structural response and computation of maximum stresses, the effect of convective response is equally imperative in such decisions as the correct estimation of free board between the quiet free surface and tank cover and also in the design of roof cover which experiences convective hydrodynamic pressure in case of insufficient free board. Thus inaccurate assessment of sloshing elevation may lead to under designed free board which may result spillage of harmful contents or the failures in the tank roof.

For all the ground motions under consideration, the structural responses of base shear in terms of their time history are presented in Figures 7.8-7.10. Also presented are the overturning base moments in Figures 7.11-7.13. The time of incidence of absolute global maximum base shear and base moment are depicted in the respective figures. One may notice that the absolute maximums occur either at the instants of PGA or at an instant close to the instants of PGA. It is observed that the absolute maximum hydrodynamic response of base shear and base moment decrease with the increase in the height of the centrally located submerged block in case of intermediate frequency and high frequency content ground motions. A deviation in this trend is marked in case of low frequency content motion of Imperial Valley, in which case the base shear and base moment initially increase with the increase in the submerged-block height and then decrease. Moreover, for Imperial Valley motion, the magnitudes of local peaks are found to be akin to the magnitude of corresponding global peaks. And these local peaks are further amplified with the increase in the height of the submerged block. Such increase in local peaks is on account of the increase in the convective response components and the fact of this matter can be easily verified from Figure 7.8 and Figure 7.11. It may be noted that the structural degradation not only depends on the global maximum response of the structure dominated by the impulsive response but also on the fatigue effect caused due to successive local peaks. Once the structure enters into the non-linear range, all the successive responses bring in an increment in the damage no matter how small are their magnitudes and more so when the magnitudes are comparable to the global peak. Under such situations, the contribution of amplified convective response to the local peaks of hydrodynamic forces, during

the later stage of earthquake, is of principal importance and ought to be taken into consideration in design in order to evade collective structural damage caused by local peaks. Nonetheless, the amount of structural damage expected in an earthquake is proportional to the duration of the earthquake and this relationship is not linear. A longer duration of shaking causes the damage to enlarge and in such cases amplified local peaks contribute to structural fatigue and may prove critical to the safety of the structure.

The histograms in Figure 7.14 show contributions of impulsive and convective components to absolute peak hydrodynamic responses due to all ground motions considered in the study. It is observed that irrespective of the frequency content of ground motion and the height of the submerged block cosidered in the study, the overal hydrodynamic responses are dominated by the impulsive response, which is acceleration dependent. However, low frequency earthquake significantly influence the dynamic responses,e.g., base shear and overturning base moments. Hence, neglecting sloshing in the dynamic analysis of liquid tanks will amount to under estimate the dynamic responses.

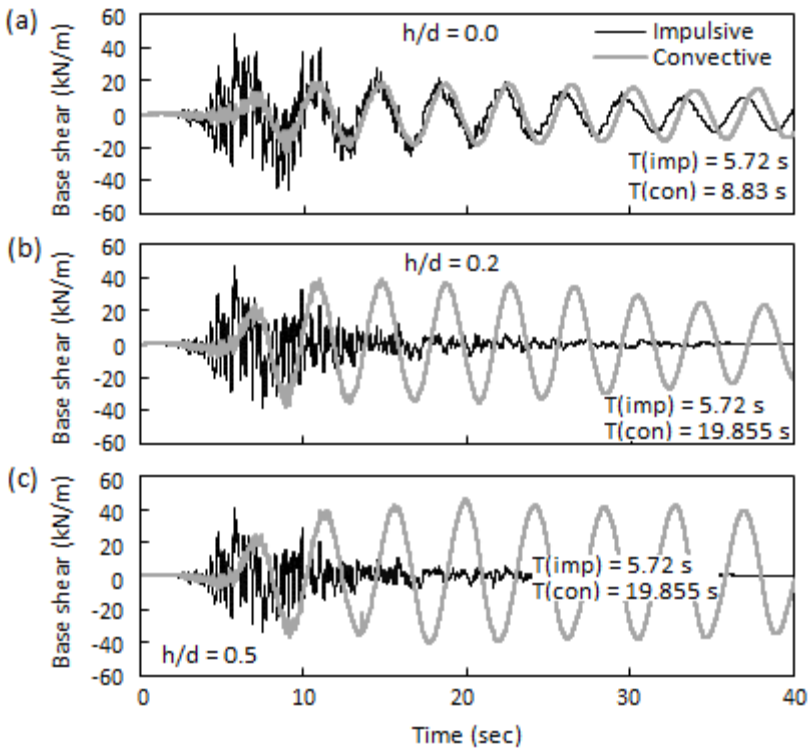

Figure 7.2: Time history of impulsive and convective responses of base shear due to Imperial Valley with various heights of submerged block (a) *h/d* = 0.0 (b) *h/d* = 0.2 (c) *h/d* = 0.5

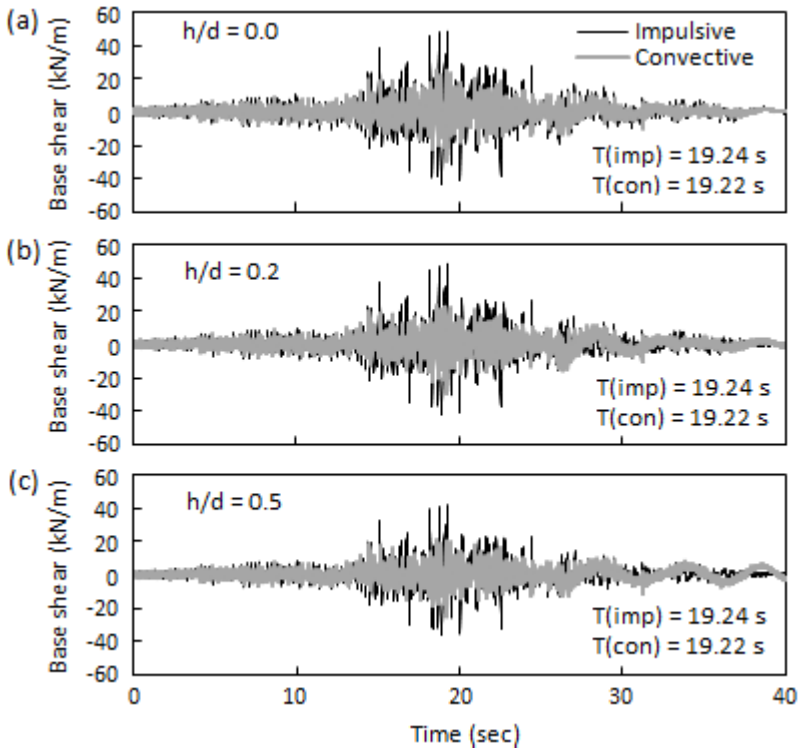

Figure 7.3: Time history of impulsive and convective responses of base shear due to Landers with various heights of submerged block (a) *h/d* = 0.0 (b) *h/d* = 0.2 (c) *h/d* = 0.5

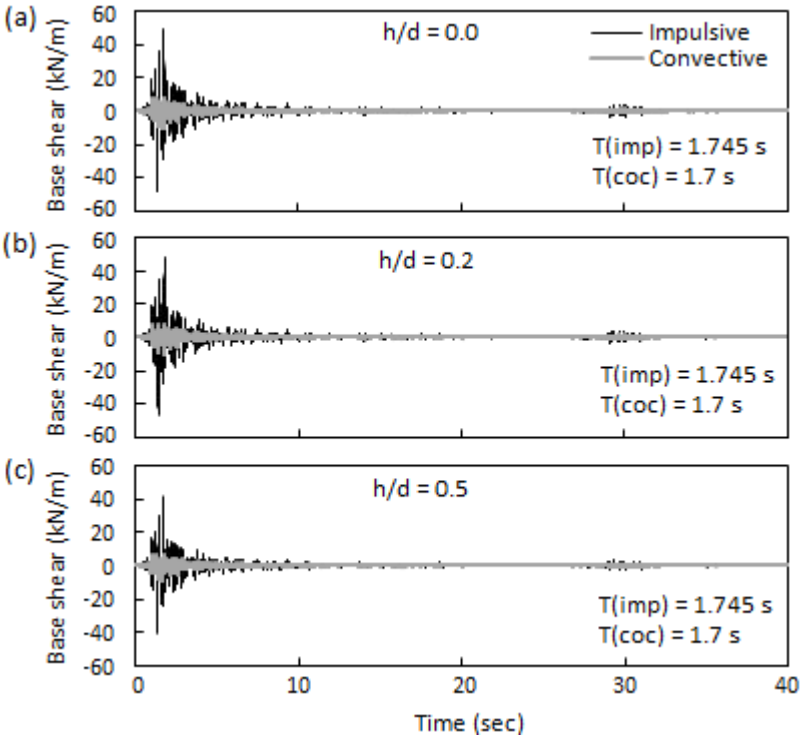

Figure 7.4: Time history of impulsive and convective responses of base shear due to San-franscisco with various heights of submerged block (a) *h/d* = 0.0 (b) *h/d* = 0.2 (c) *h/d* = 0.5

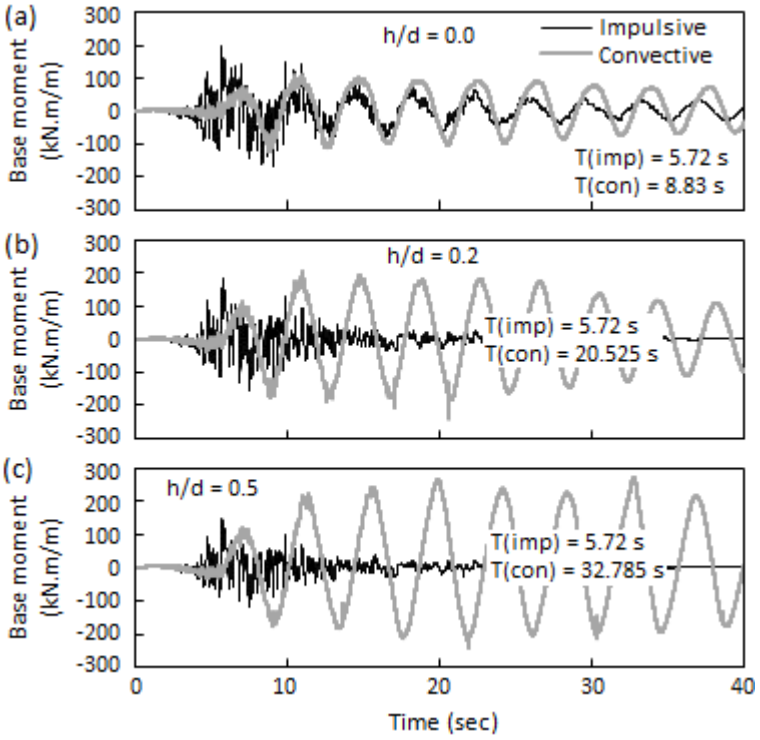

Figure 7.5: Time history of impulsive and convective responses of base moment due to Imperial Valley with various heights of submerged block (a) *h/d* = 0.0 (b) *h/d* = 0.2 (c) *h/d* = 0.5

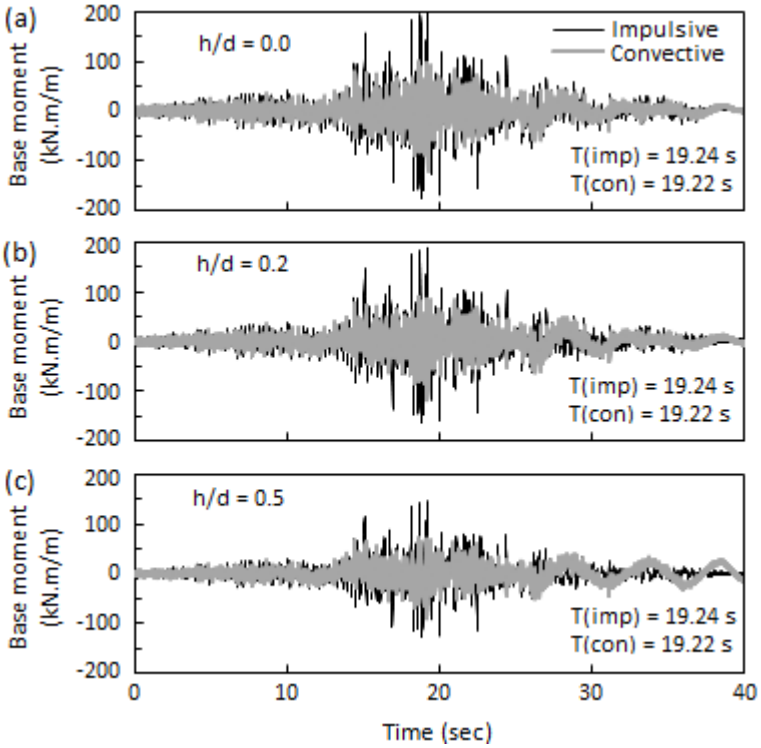

Figure 7.6: Time history of impulsive and convective responses of base moment due to Landers with various heights of submerged block (a) *h/d* = 0.0 (b) *h/d* = 0.2 (c) *h/d* = 0.5

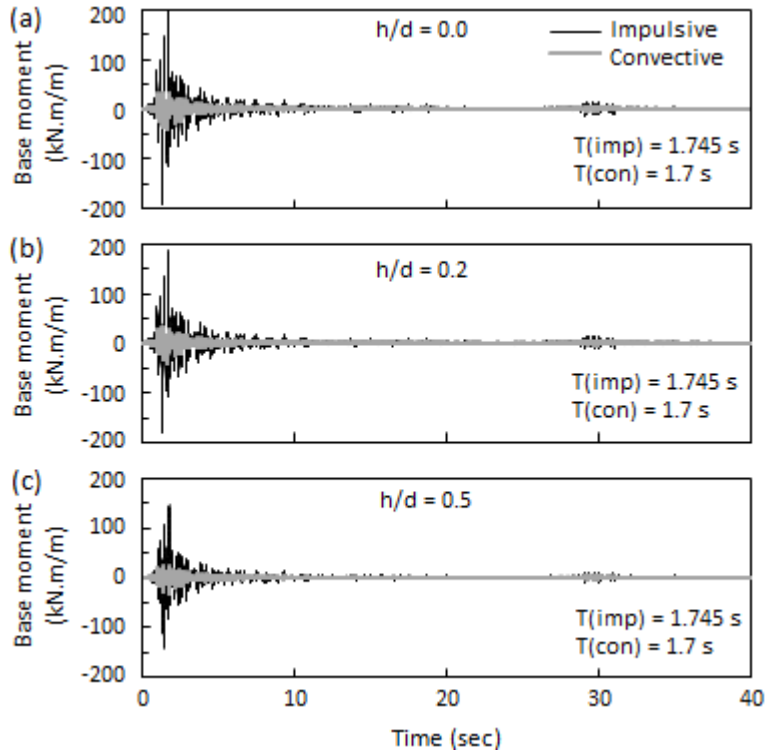

Figure 7.7: Time history of impulsive and convective responses of base moment due to San-Franscisco with various heights of submerged block (a) *h/d* = 0.0 (b) *h/d* = 0.2 (c) *h/d* = 0.5

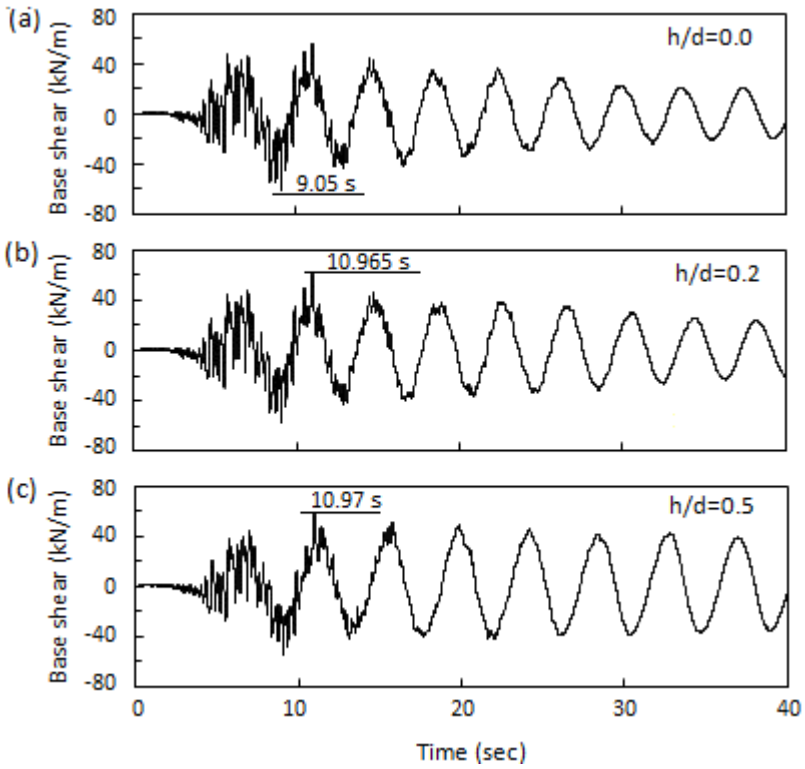

Figure 7.8: Time history of base shear due to ground motion of Imperial Valley with various heights of submerged block (a) *h/d* = 0.0 (b) *h/d* = 0.2 (c) *h/d* = 0.5

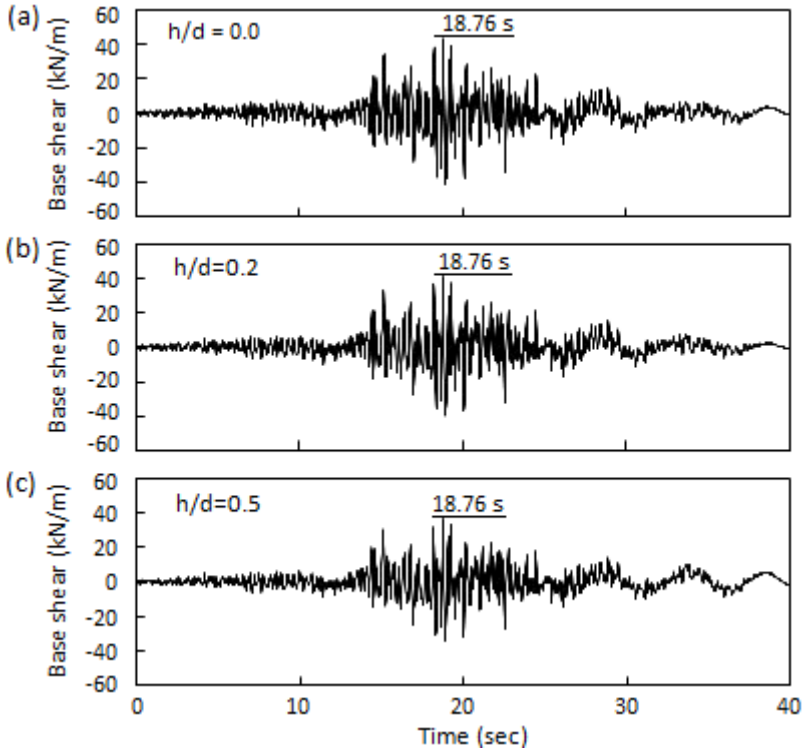

Figure 7.9: Time history of base shear due to ground motion of Landers with various heights of submerged block (a) h/d = 0.0 (b) *h/d* = 0.2 (c) *h/d* = 0.5

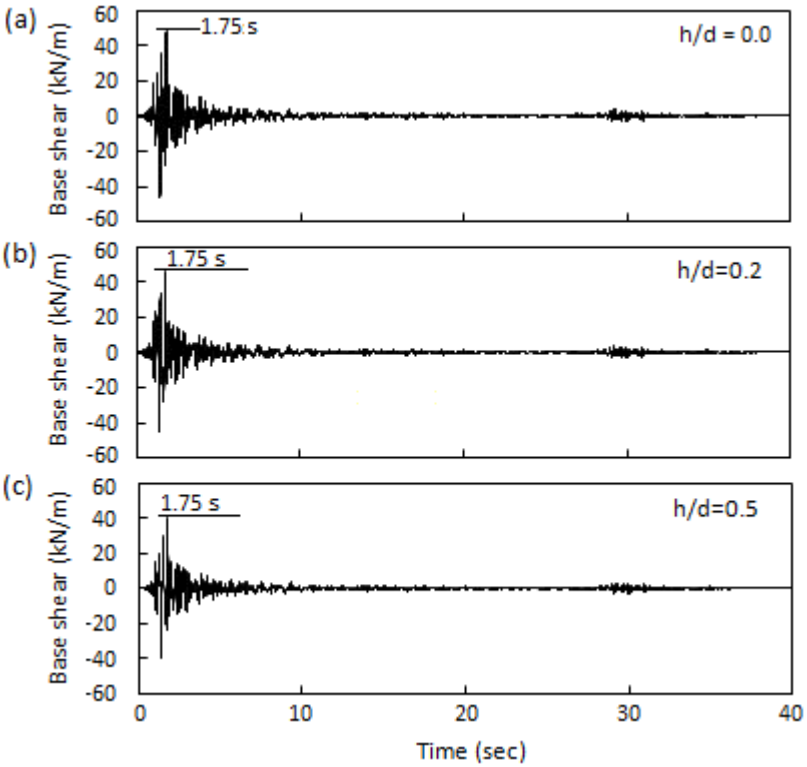

Figure 7.10: Time history of base shear due to ground motion of San-franscisco with various heights of submerged block (a) *h/d* = 0.0 (b) *h/d* = 0.2 (c) *h/d* = 0.5

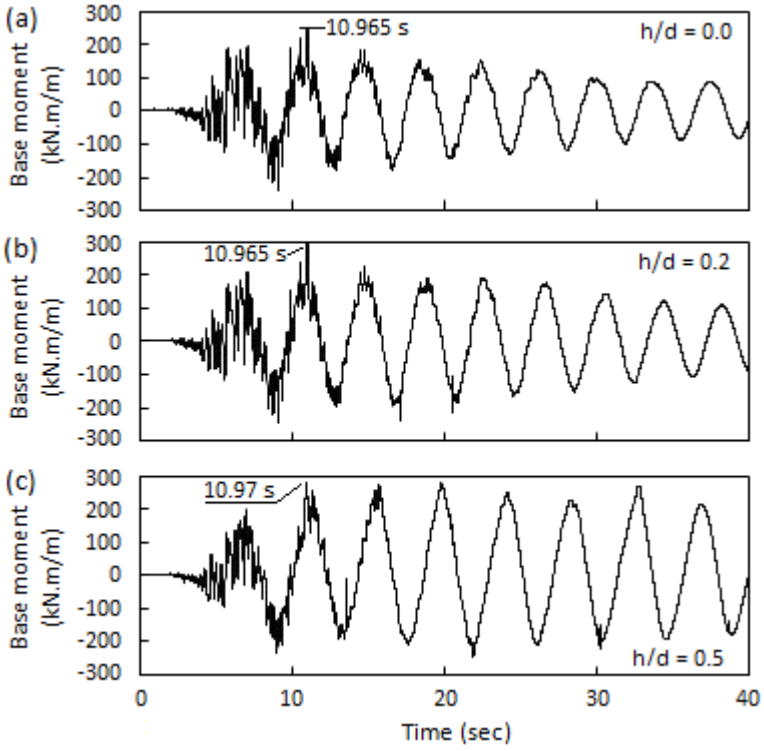

Figure 7.11: Time history of overturning base moment due to ground motion of Imperial Valley with various heights of submerged block (a) *h/d* = 0.0; (b) *h/d* = 0.2; (c) *h/d* = 0.5

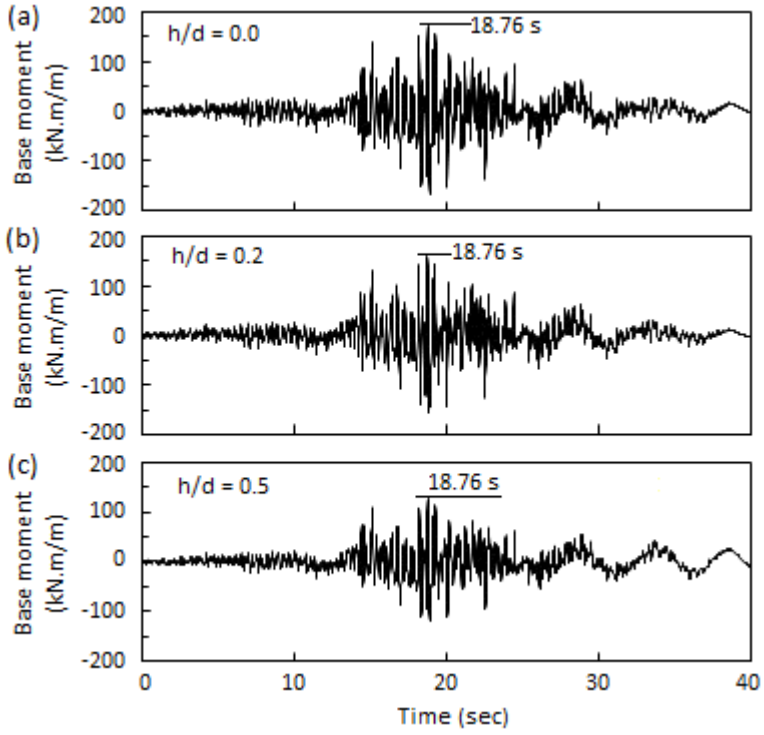

Figure 7.12: Time history of overturning base moment due to ground motion of Landers with various heights of submerged block (a) *h/d* = 0.0; (b) *h/d* = 0.2; (c) *h/d* = 0.5

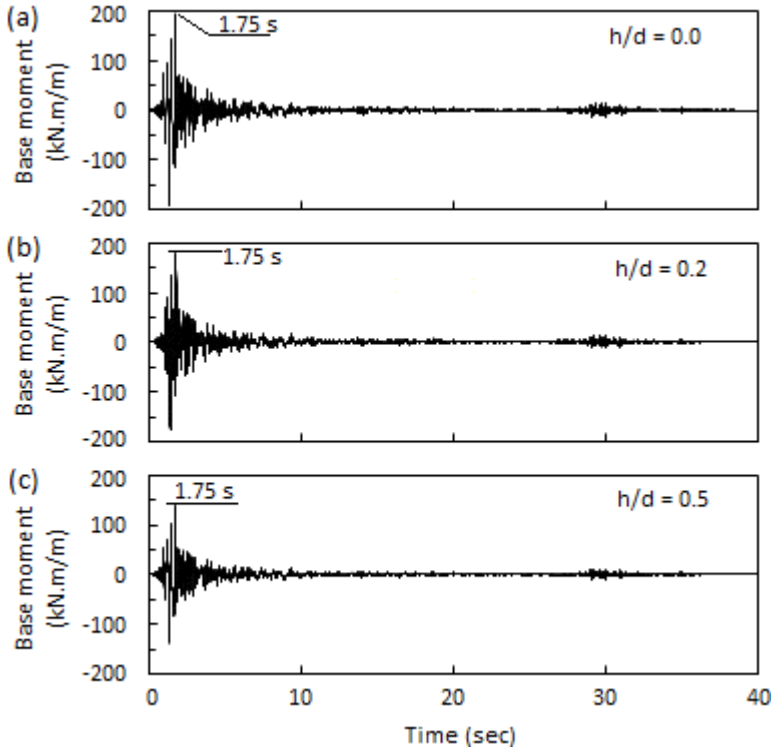

Figure 7.13: Time history of overturning base moment due ground motion of San-franscisco with various heights of submerged block (a) *h/d* = 0.0 (b) *h/d* = 0.2 (c) *h/d* = 0.5

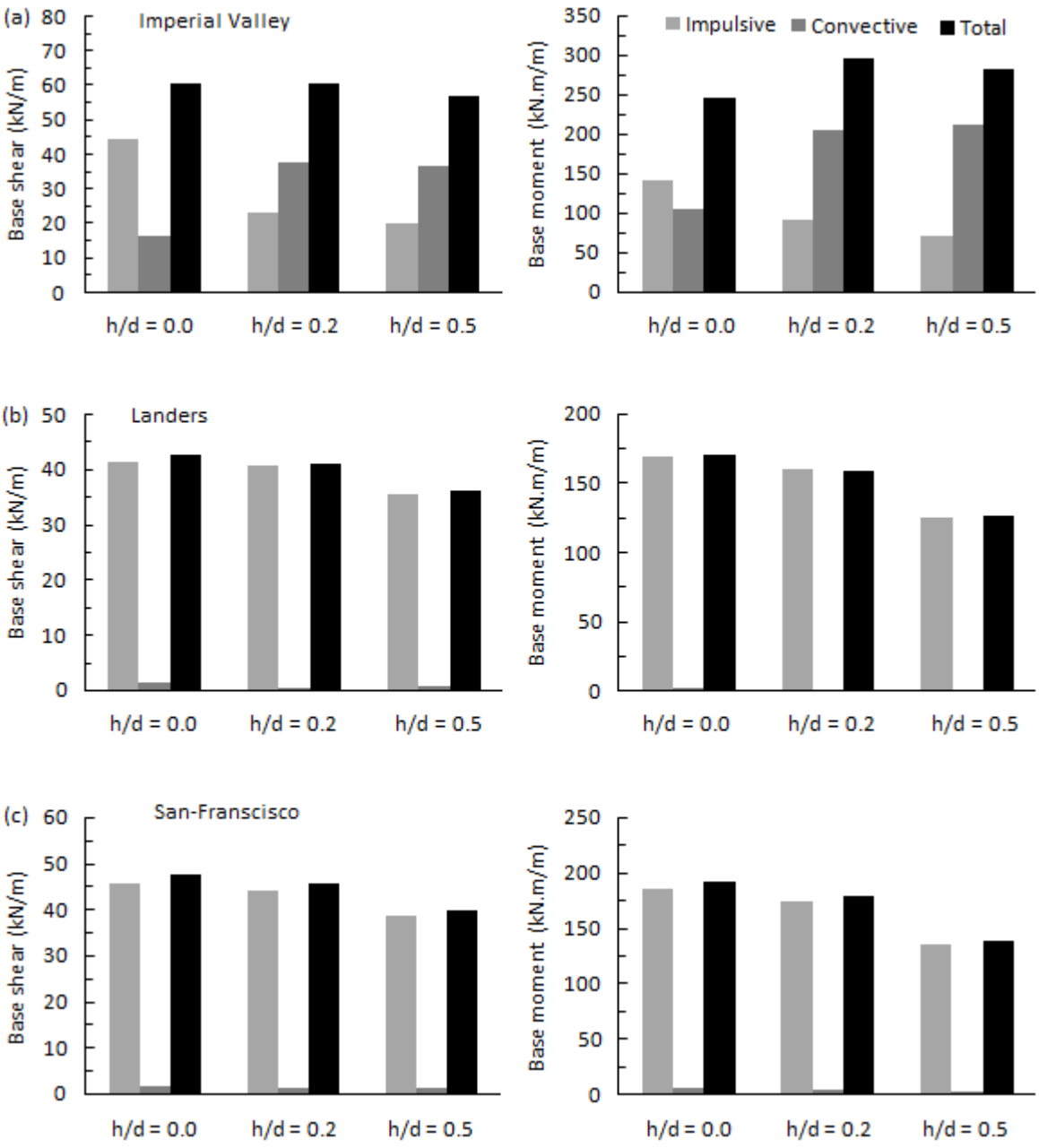

Figure 7.14: Component-wise break up of peak hydrodynamic responses (base shear and base moments) for different ground motions: (a) Imperial Valley (b) Landers (c) San-Franscisco

7.2.1.3 Pressure Distribution on Tank Wall

The distributions of nonlinear total, impulsive and convective hydrodynamic pressures on the container wall at the instant of maximum base shear are presented in Figure 7.15-7.7.20. Irrespective of the ground motions considered for the study, the hydrodynamic pressure on the tank wall decreases with the increase in the height of the submerged block. Further, for a given block dimension, the hydrodynamic

pressure is the maximum in case of low frequency ground motion of Imperial Valley and the lowest in case of ground motion of Landers. Similarly, irrespective of the ground motions, the impulsive response of pressure on the tank wall decreases with increase in the height of the block. However, for a given block dimension, the impulsive response is highest under high frequency motion of San-Franscisco and lowest for low frequency Imperial Valley ground motion. Nevertheless, one can notice a typically different trend in the response of convective component. Convective response increases with increase in the height of the block for Imperial Valley earthquake and decreases for the ground motions of Landers and San-Franscisco. Further, convective responses are in opposite phase to the impulsive responses in case of intermediate and high frequency ground motions which fact contributes to the decrease in the overall hydrodynamic force on the tank wall for the said motions.

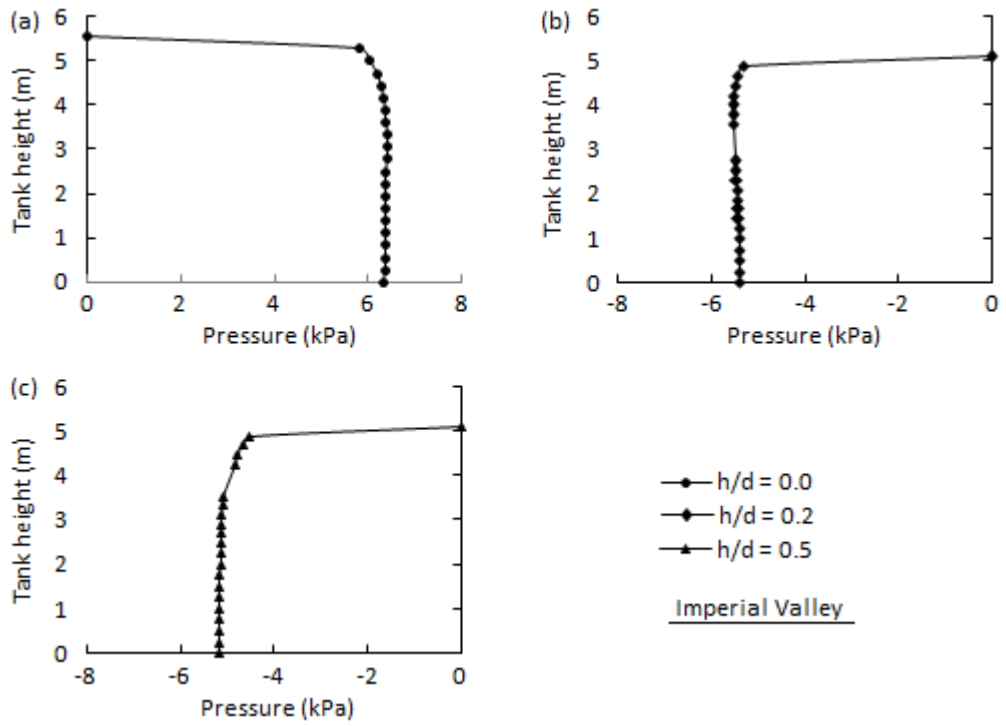

Figure 7.15: Distribution of hydrodynamic pressure along the height of tank wall due to Imperial Valley earthquake with various block heights: (a) *h/d* = 0.0 (b) *h/d* = 0.2 (c) *h/d* = 0.5

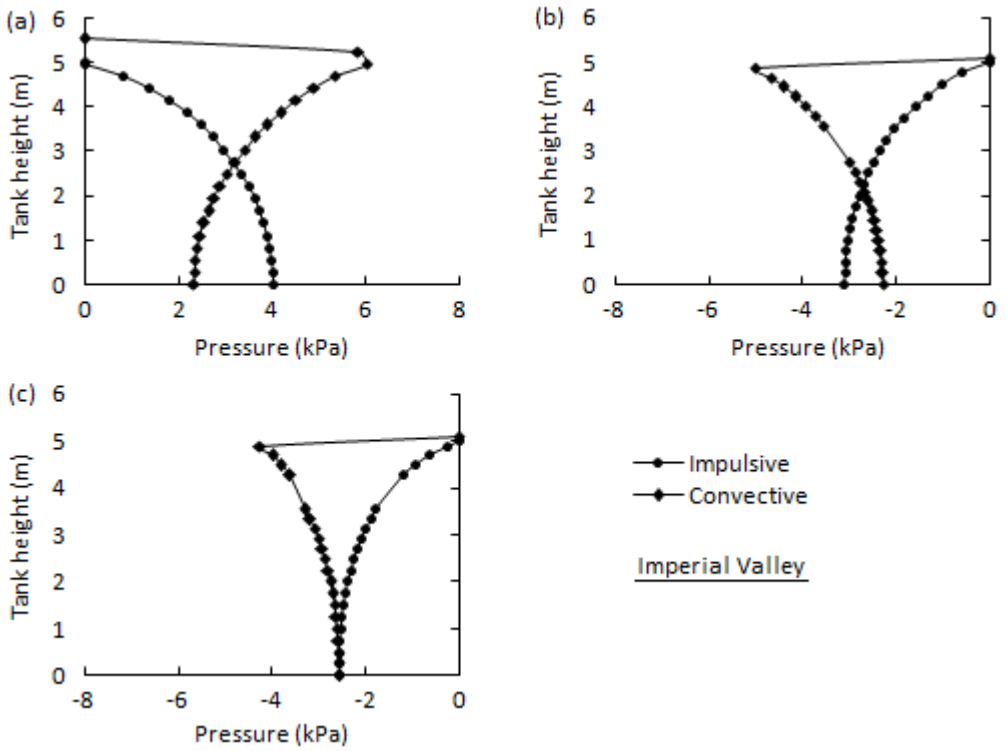

Figure 7.16: Distribution of impulsive and convective pressure components along the height of tank wall due to Imperial Valley earthquake with various block heights: (a) *h/d* = 0.0 (b) *h/d* = 0.2 (c) *h/d* = 0.5

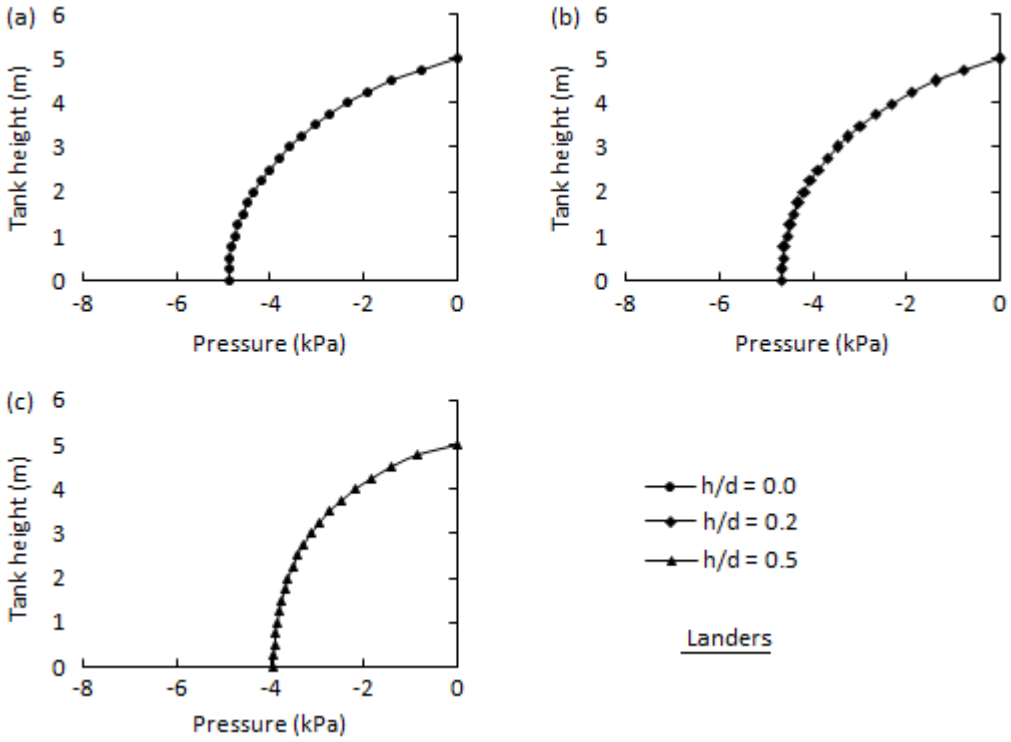

Figure 7.17: Distribution of hydrodynamic pressure along the height of tank wall due to Landers earthquake with various block heights: (a) *h/d* = 0.0 (b) *h/d* = 0.2 (c) *h/d* = 0.5

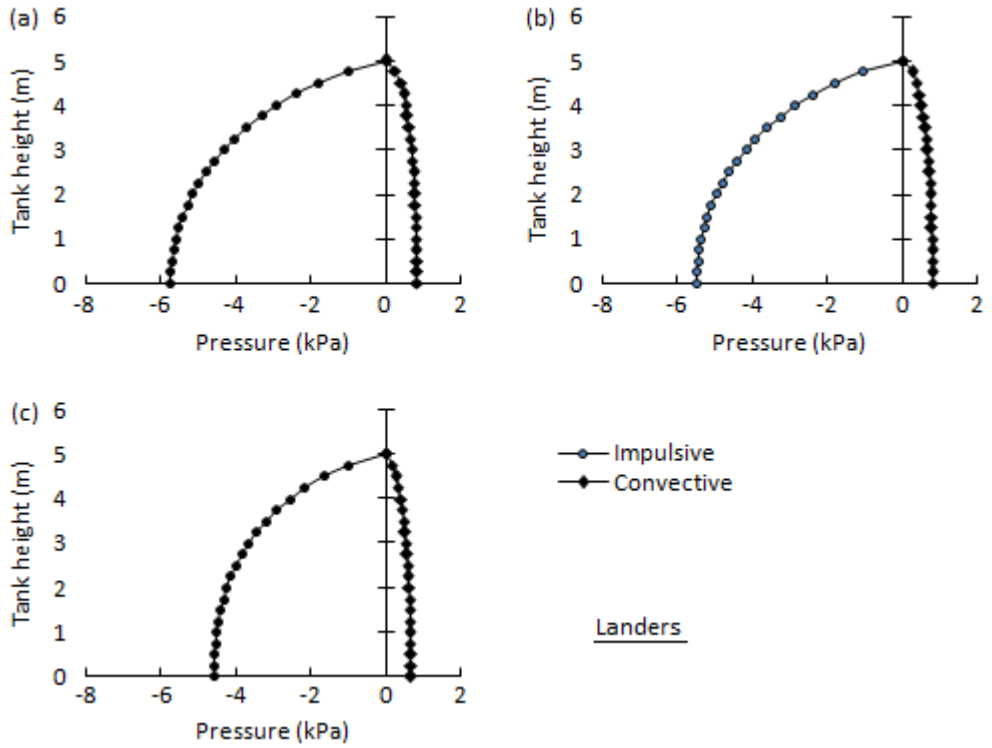

Figure 7.18: Distribution of impulsive and convective pressure components along the height of tank wall due to Landers earthquake with various block heights: (a) *h/d* = 0.0 (b) *h/d* = 0.2 (c) *h/d* = 0.5

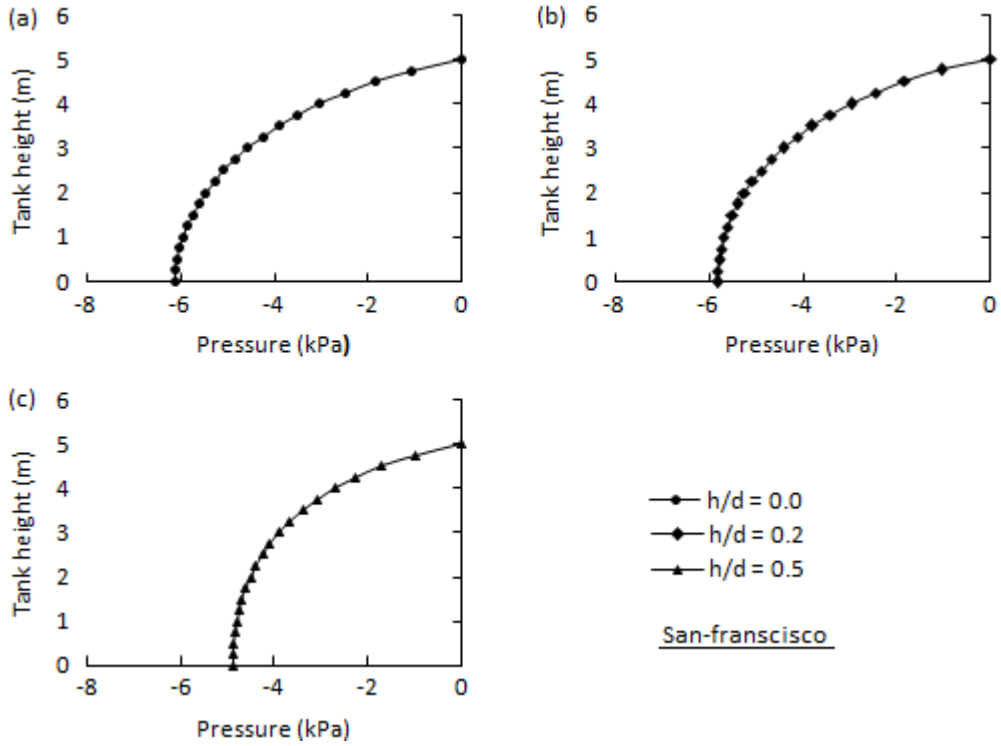

Figure 7.19: Distribution of hydrodynamic pressure along the height of tank wall due to San-franscisco earthquake with various block heights: (a) *h/d* = 0.0 (b) *h/d* = 0.2 (c) *h/d* = 0.5

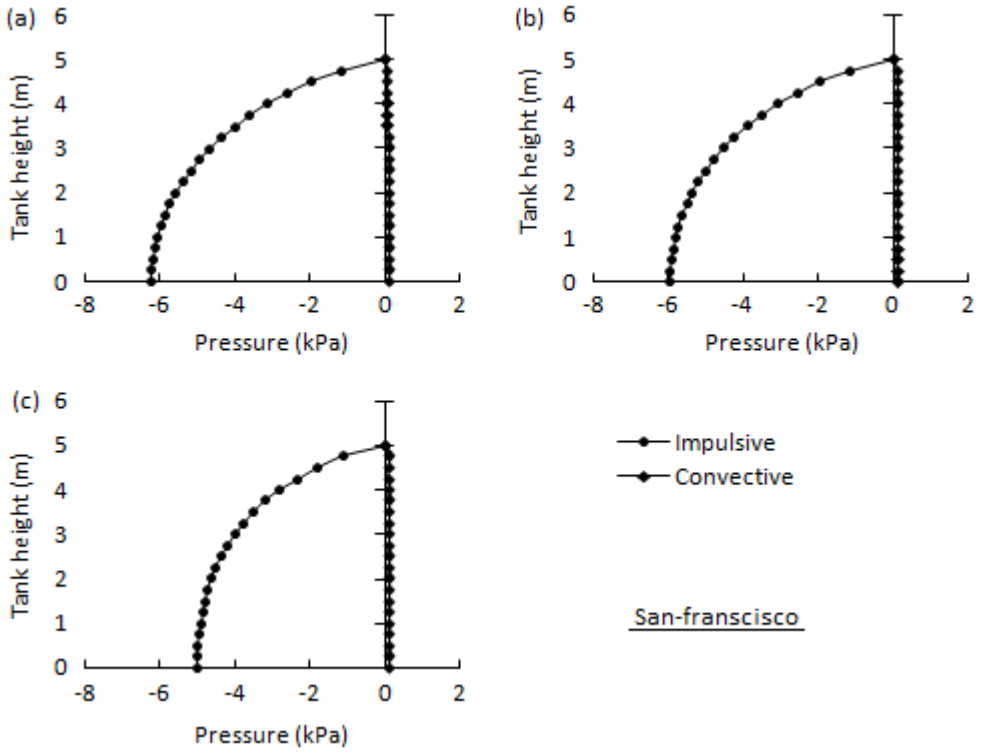

Figure 7.20: Distribution of impulsive and convective pressure components along the height of tank wall due to San-franscisco earthquake with various block heights: (a) *h/d* = 0.0 (b) *h/d* = 0.2 (c) *h/d* = 0.5

7.2.1.4 Pressure Distribution on Block Wall

The variations of hydrodynamic responses of total, impulsive and convective pressure, at the instant of maximum base shear for respective ground motions, on the wall of submerged block are presented in Figures 7.21-7.23. For all the ground motions under study, it is apparent that the total hydrodynamic pressure on the block-wall increases with increase in the height of the submerged block and the increase is quite significant in cases of intermediate and high frequency earthquakes. However, in spite of considerable increase in both impulsive and convective pressure components, the increase in total hydrodynamic pressure is marginal in case of Imperial Valley earthquake. This is due to the fact that both components are in opposite phase and their increase is proportionate. The total pressure distribution curve is almost a vertical straight line which suggests that the pressure variation along the height of the block is negligible. In case of intermediate frequency content motion of Landers no appreciable change in convective pressure distribution is observed with the change in the height of the block. For high frequency ground motions of San-Franscisco, it is observed from Figure 7.23 that the convective response is negligibly

small and the total pressure is almost equal to the impulsive response. The pressure distribution on the wall in this case, the increase in impulsive response is substantially more than the increase in the convective response. For a given block height not much variation in the convective response along the height of the block wall is observed.

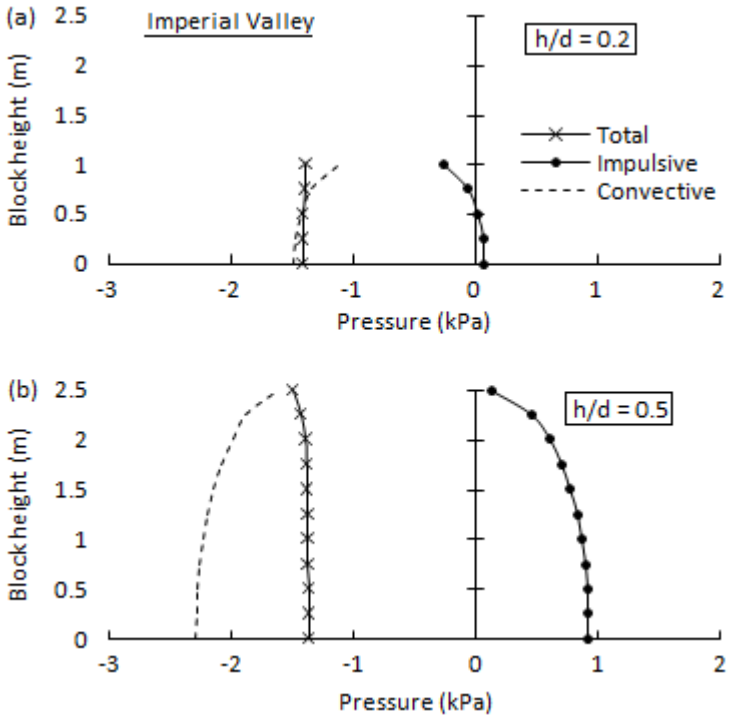

Figure 7.21: Pressure distribution along the left wall of the centrally placed block under horizontal ground motion of Imperial Valley: (a) *h/d* = 0.2 (b) *h/d* = 0.5

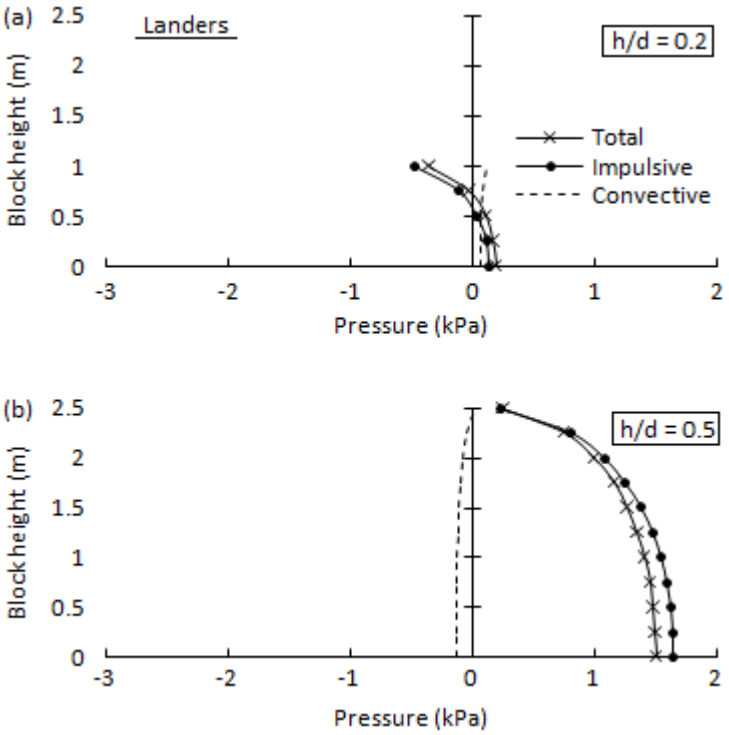

Figure 7.22: Pressure distribution along the left wall of the centrally placed block under horizontal ground motion of Landers: (a) *h/d* = 0.2 (b) *h/d* = 0.5

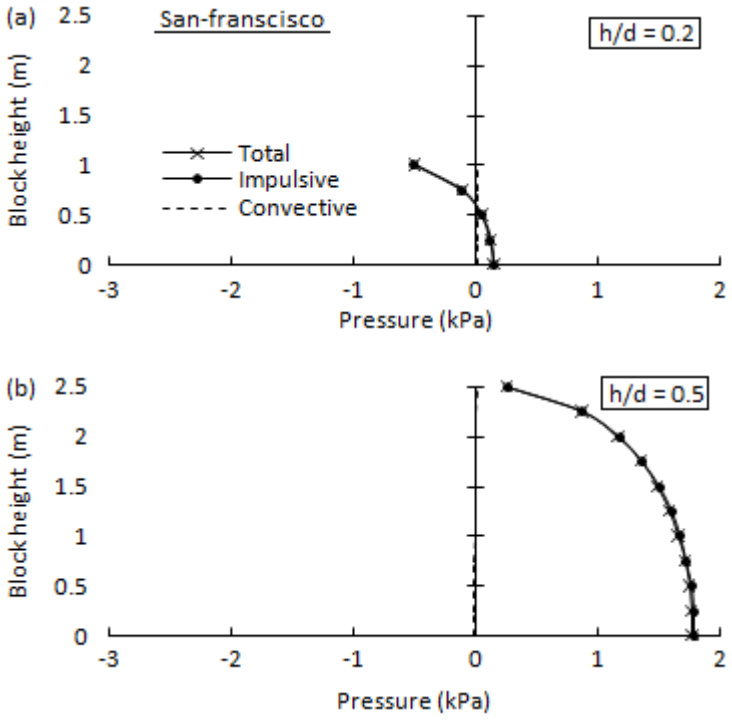

Figure 7.23: Pressure distribution along the left wall of the centrally placed block under horizontal ground motion of San-franscisco: (a) *h/d* = 0.2 (b) *h/d* = 0.5

7.3 Conclusion

In the present study, an efficient Galerkin based two dimensional fully nonlinear finite element model has been used for investigation of seismic behavior of partially filled rigid rectangular liquid tank with submerged internal components under horizontal ground motions of different frequency content. Mixed Eulerian-Lagrangian (MEL) method based fourth order explicit Runge-Kutta scheme is used for the time-stepping integration of free surface boundary conditions. An artificial damping term μ is suitably introduced into the finite element formulation via modified surface boundary condition to mimic the surface damping on account of viscosity of liquid. It is defined as $\mu = 2\xi\omega$ where ξ is the viscous type numerical damping and ω is the fundamental frequency of liquid and a value equal to 0.0075 is used for ξ. The model is capable of finding out both convective and impulsive responses of the hydrodynamic behaviour. It may be mentioned that "impulsive-convective" pressure concept laid the basis of almost all recent design codes and guide lines.

Three different horizontal ground motions with peak ground acceleration scaled to a constant value of 0.2g are applied to investigate the effect of frequency content of ground motion on the seismic behaviour of tank-liquid-submerged block system. Time domain analysis of sloshing elevation, structural base shear, overturning base moment are carried out and the results of absolute maximum values of free surface wave elevation, structural base shear, overturning base moment are presented. In addition the absolute maximum responses of impulsive and convective components of hydrodynamic forces are presented. The hydrodynamic pressure distributions on tank as well as block wall at the instant of maximum base shear during the recommended ground motions are presented.

The enumerated result of the investigation confirmed that the presence of submerged block radically influenced the dynamics of the tank-liquid system. Further, the frequency contents of earthquakes do also have significant effect on the non-linear dynamic behaviour. The maximums of total hydrodynamic forces may not occur either at the instant of maximum impulsive response or at the instant of maximum convective response. This is because of the time lag between the global peaks of the two components. The dominancy of convective response components comes into picture during the later part of the earthquakes when the impulsive responses are in

their waning legs. For all ground motions considered, the impulsive response peaks invariably occur at the instant of PGAs of respective motions. The frequency contents of ground motions have negligible effect on the impulsive responses. However, frequency contents of ground motions do have significant effect on the convective responses and such effect is considerably more in case of low frequency motion. Nonetheless, a submerged block considerably changes the convective response. Moreover, in case of low frequency ground motion of Imperial Valley, increase in the height of submerged block greatly increases the convective response so much so that the total dynamic response is dominated by the convective component which is an antithesis to the result obtained for tank without any submerged block. In addition, submerged blocks decrease the impulsive responses equally irrespective of the frequency content of the ground motion.

It is amply clear that the effect of the bottom-mounted submerged blocks has a significant influence on the overall dynamics of the tank-liquid system and the effect differs considerably under seismic motions of different frequency content. The present approach is not only capable of predicting the non-linear dynamic responses of tank-liquid–submerged block systems but also equally adept in quantifying the impulsive and convective responses of the system.

CHAPTER 8

8 FLUID DAMPING IN RECTANGULAR TANK FITTED WITH VARIOUS INTERNAL OBJECTS – AN EXPERIMENTAL INVESTIGATION

8.1 Introduction

Low frequency fluctuation of free surface liquid in a partially filled liquid container is regarded as sloshing, which becomes violent under favourable condition. Sloshing is an important physical phenomenon in many fields of engineering interest wherein partially filled liquid container is an important structural component of the system. The problem of liquid sloshing in containers of various shapes has received considerable attention in transportation engineering since the middle of last century. To begin with, the requirement for a precise assessment of the sloshing induced hydrodynamic forces was felt in aerospace applications, due to the vicious motion of the liquid fuel inside the tanks of aerospace vehicles. In offshore applications, the effect of free surface liquids on board can create problems which may lead to loss of stability of the ocean going vessel and to structural damages.

Liquid carrying road tankers constitute an important problem, and have dragged the attention of many researchers involved in the field of slosh mechanics. Sloshing has often been a potential source of danger for road tankers resulting in accidents due to poor manoeuvrability during turning on account of the unexpected hydrodynamic force coming into action leading to the instability, often amounting to rollover accidents. Precise estimation of sloshing related hydrodynamic loads is one of the major design issues of liquid transporting containers. Sloshing and its associated

forces depend on wide varieties of variables as geometrical, physical and material parameters: shape and dimension of the container; liquid fill-depth; type and direction of external excitation; magnitude of acceleration; frequency of excitation, flexibility of the container, etc. The slosh so generated, on account of possible critical combination of above parameters, should not exceed a certain prescribed maximum value; and if so does, it needs to be suppressed by some means in order to avoid undue hydrodynamic forces, thus produced. The inherent damping due to liquid viscosity is very useful in small size containers. In relatively large containers, natural damping on account of the viscous boundary layers has often been found inadequate to counter violent sloshing and hence several artificial means have been tried to undermine this threat. Although, various means have been adopted for this, yet suppression of excessive sloshing by use of passive anti-slosh devices such as baffles of various configurations, floating cans, floating lids and mats, and flexible baffles are the most sought after means for slosh suppression. Baffles and other such flow obstructing internal objects are found to have given promising results in controlling and preventing the vehicle instability during manoeuvring. This has inspired many researchers to conduct analytical, numerical and experimental methods of investigation to corroborate the reliability of these damping devices.

The damping of bare wall containers owes its origin to three sources: (i) viscous dissipation at the free surface of liquid, (ii) viscous dissipation at the side walls and bottom of the tank, and (iii) viscous dissipation in the interior of the tank which is negligible in relatively large liquid containers. In case of baffled tank, an additional source due to relative motion between the liquid and the baffle wall comes into the damping domain. It is often not feasible analytically to accommodate damping contribution from so many sources or computationally costly to determine the damping ratio. Hence, the effect of different types of baffles on fluid damping is usually determined experimentally.

From an extensive survey of literature made as in the chapter of literature review, the following summary of observations is deduced.

1. The liquid viscosity in tanks without baffles does not have much effect in reducing the sloshing amplitudes in tanks of practical dimensions.

2. The effects of baffle configuration on dynamic system characteristics, namely fundamental sloshing frequency and damping of liquid in the tank are significantly different from those in tank without baffle.
3. The analytical means for damping estimation are not easy due to the complications involved in the boundary conditions and the inclusion of baffles makes it even more difficult.
4. Experimental investigations are the most reliable for estimating damping characteristics of the liquid sloshing.
5. The comparison among different baffle configurations is seldom reported.
6. On the other hand, although, the computational methods provide powerful means in the solution of mathematical models for analyzing the real world problems, yet developing the precise numerical models considering baffle damping effects may be a challenging task.

Furthermore, most of the studies on damping on account of baffles involve cylindrical tanks with single or multiple ring baffles. In this respect, rectangular tanks with surface-mounted baffles and bottom-mounted submerged blocks have received very little attention. The major objectives of the present experimental investigation are to examine the relative effectiveness of various configurations of internal objects in slosh damping in order to enrich test data bank for the verification of the numerical models proposed by various investigators and also to recommend the most effective arrangement of internal objects for sloshing attenuation. For these purposes, a series of experiments are performed for partially-filled rectangular tanks with three different configurations of internal objects namely; bottom-mounted vertical baffles, surface-piercing vertical baffles, and bottom-mounted submerged blocks in tanks with two different aspect ratios (fill-depths). The parameters are systematically changed to conduct free vibration analysis, determine damping ratio, and measure the sloshing wave height for specific aspect ratio and internal object parameters. During the experiments, the tank is subjected to lateral harmonic excitation defined by the expression: $x = x_0 \sin 2\pi ft$ where, x_0 and f are the amplitude and frequency of excitation respectively.

With the above objectives in view, the experimental domain is fixed up. The experimental program includes:

- Frequency response study of sloshing in rectangular tank fitted with three different configurations of centrally placed internal objects (bottom-mounted baffles, surface-piercing wall-mounted baffles, bottom-mounted submerged block) by means of *sine sweep test*
- Free vibration study for identification of important dynamic property of liquid-damping in term of hydrodynamic damping ratio.
- Dynamic response analysis of tank-liquid system with centrally placed internal objects subjected to sinusoidal horizontal excitation at resonant frequencies.
- Comparative study on the relative effectiveness of various internal objects on sloshing damping

8.2 Description of Laboratory Equipments

- Shake Table
- Power Supply to shake table and sensors
- Data Acquisition and Control System
- Measurement Sensors
- Test Structure (Partially-filled liquid tank with or without internal objects)

8.2.1 Shake Table

The horizontal, unidirectional shake table consists of 1000 mm x 1000 mm sliding platform which is driven by a 3-hp three-phase electric motor (Figure 8.1). The sliding platform slides on low friction linear ball bearings which are mounted on two ground-hardened shafts. The platform surface has 81 tie-down points located on a 100 mm x 100 mm grid. The operational frequencies of the shake table range from 0 to 20 Hz. The maximum displacement of the table is 100 mm $(\pm 50\,\text{mm})$ with amplitude resolution of 5 mm. The maximum payload is 100 kg. The table is capable of reproducing simple waveforms e.g., sine waves. The frequency of the table is controlled by a control panel run by input voltage of 440 volts.

Figure 8.1: Shake table

8.2.2 Power Supply

The power supply includes a three phase 440 volt power supply for driving the 3-hp three-phase motor of the shake table (see Figure 8.1). In addition, it includes an independent ± 24 volt DC power supply as shown in Figure 8.3 to provide power to sensors.

8.2.3 Data Acquisition and Control System

NI PCI 6255 multi-function data acquisition (DAQ) system manufactured by National Instruments is used to obtain measurements of physical quantities using sensors and transducers. These measurements may be temperature, pressure, wind, distance, acceleration, etc. In civil engineering applications the most common types of sensors measure displacement, acceleration, force and strain. In this experiment, we are going to use two vertical entry liquid level sensors to obtain records of sloshing wave heights over time in tanks partially filled with liquid. Also used will be a dynamic LVDT to measure the displacement of the shake table. The computer system used to perform the tests described herein consisted of a Intel(R) Core(TM) i5 processor with 4GB RAM, 32-bit operating system and running Windows 7 professional. In addition to plug-in data acquisition DAQ devices, most computer-based measurement systems include some form of signal conditioning. This is because the signals from various sensors and transducers need to be amplified or filtered to prepare them for digitizing. The manipulation of signals to prepare them for digitizing is called signal conditioning. Signal conditioning is required for sensor measurements or voltage inputs greater than 10 V. The present DAQ system has a front-end signal conditioning and switching system, NI SCXI. It is a versatile, high-performance signal conditioning platform optimized for high-channel-count applications. The softwares used for data acquisition are NI-DAQmx driver software and NI LabVIEW SignalExpress LE interactive data-logging software. Figure 8.2 shows a typical DAQ system, which includes sensors, transducers, signal conditioning devices, cables that connect the various devices to the accessories, programming software, and PC. The components of data acquisition system are are photographically shown in Figure 8.3.

8.2.4 Measurement Sensors

Two vertical entry liquid level sensors (Honeywell Model-LL-V) with a pressure range 0 to 508 mm, accuracy $\pm 0.1\%$, screen flush diaphragm pressure port, and output voltage 0 to 5 Vdc are used to measure the height of sloshing wave at specified distances from the two end walls of the tank along the direction of excitation. A photograph of one vertical entry liquid level sensor is shown in Figure 8.3 (b) One dynamic LVDT (Endevco Model-SX20MER300) with a stroke range of 150 mm (± 75), input voltage 24 Vdc, and output voltage 0/10 Vdc is used for measuring the excitation amplitude of the shake table. A photograph of the LVDT is shown in the Figure 8.3(b).

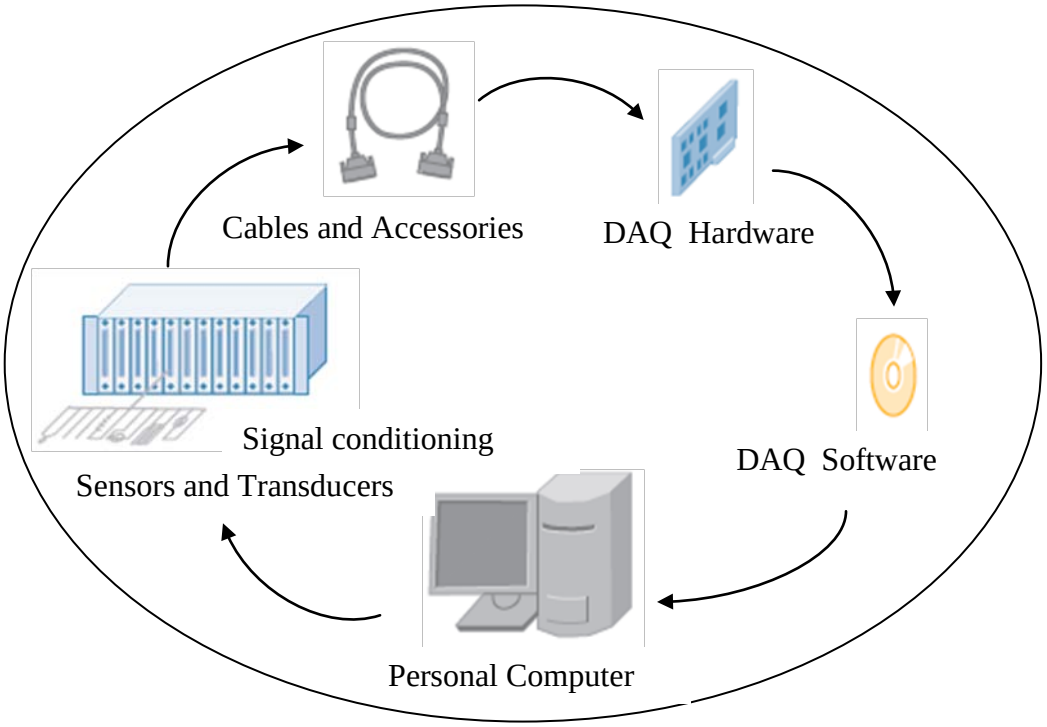

Figure 8.2: Components of a typical DAQ system

8.2.5 Test tank (Partially-filled liquid tank with or without internal objects)

A rectangular test tank of 570 mm x 310 mm x 450 mm (length x width x height) is manufactured from Perspex sheet of 11.7 mm thickness for the experiment. In the fixed base configuration, the projected base plate of the tank is rigidly attached to the shake table.

(a) Power supply

(b) Sensors: 1. Vertical entry level sensor
2. LVDT

(c) PC loaded with LabView SignalExpress software

(d) Signal conditioner

(e) NI PCI 6255 DAQ

Figure 8.3: Snap shots of components of the DAQ system

8.2.6 Internal Objects

Internal objects of three different configurations are manufactured from 11.7 mm thick Perspex sheet in order to ensure that the objects are rigid: (1) bottom-mounted vertical baffles, (2) surface-mounted vertical baffles, and (3) bottom-mounted submerged blocks. The fixtures for fixing the internal objects to their desired locations in the tank are also designed in-house and are described in the subsequent sections.

8.3 Experimental Work

The prediction of hydrodynamic loads on fluid-filled tankers moving on road is often an important requirement in design. The extent of sloshing and thus the magnitude of sloshing loads are modified due to energy dissipation. Particularly, significant energy dissipation may occur on account of flow separation effects as the fluid oscillates past baffles or other obstacles in the tank. When a rectangular container partially filled with liquid (such as water in a road tanker) fitted with internal objects say baffles, is moved, it rapidly dissipates its kinetic energy, and as a result the sloshing is attenuated. Baffles of various configurations have significant potential for energy dissipation. The objective of the experiments discussed in this paper is to investigate the effects of three different configurations of internal objects and their important parameters on energy dissipation and sloshing attenuation. In the following sections, the experimental procedure is explained in detail. The summary of the observations from an extensive investigation is presented. The experimental study involves: (i) bottom-mounted vertical baffles, (ii) surface-mounted vertical baffles, and (iii) bottom-mounted submerged blocks as internal objects for energy dissipation.

8.3.1 Experimental Test Set up

Experimental tests were carried out using a harmonically excited shake-table in the Structural Engineering Laboratory of the Department of Civil Engineering at National Institute of Technology, Rourkela, India.

The experimental test set up as illustrated in Figure 8.4 consists of:

i. a Millennium make, 1 m x 1 m shake table of 100 kg pay load and capable of giving horizontal harmonic motion and minimum amplitude capacity of 5 mm;
ii. shake table control unit to vary the frequency of motion with an increment of 0.01 Hz;
iii. a model rectangular tank of 57 cm length, 31 cm width, and 45 cm height constructed of 11.7 mm thick Perspex sheet to prevent deformation of tank due to hydrodynamic impact of water and thus to ensure the assumption of rigid tank;
iv. two vertical entry liquid level sensors of Honeywell make fitted at both ends of the tank and kept at a distance of 0.03 m from the walls perpendicular to the direction of excitation, to measure the sloshing elevations;
v. a dynamic LVDT (Honeywell make) fitted to the shake table for accurate measurement the displacement amplitude of the shake table;
vi. Multichannel data acquisition system PCI 6255 from National Instruments;
vii. a PC loaded with LabView SignalExpress software from National Instruments for data acquisition and post processing;
viii. two sets of baffles for two different configurations with varying dimensions, *h/d* (bottom-mounted and surface-piercing wall-mounted), made of Perspex sheet, with all fixtures for installing them with the tank; (snap shots of baffles are demonstrated in Figure 8.5) and one set of submerged-blocks also made of Perspex sheet
ix. accessories and fittings for fixing the baffles in the tank

Two liquid depths are considered, coincident with d/L = 0.26 (15 cm water depth) and 0.53 (30 cm water depth). '*d*' is the height of still water in the tank and '*h*' is the height of the internal object used for damping potential.

8.3.2 Fixing the Baffles and Submerged Blocks

The baffles of two different configurations and their supporting setup are demonstrated in Figure 8.6. The bottom-mounted vertical baffles are supported firmly to the base of the tank at the middle since this position is expected to correspond to the maximum relative horizontal velocity. The firmness of the baffle is ensured by the compressive force given by the two vertical stainless steel rods screwed to the two clamps fixed at two ends of the baffle. The stainless steel rods are in turn clamped to

two horizontal rods provided at the top of the tank. Adequate compressive force is applied by pushing the rods down while tightening them with the horizontal rods, pulled upward. For larger baffles an additional provision of bolts, two each at both ends of the baffle, is made. By tightening these bolts, the friction between the ends of the bolts and the wall of the tank provides the baffle with the additional strength required to resist the drag force of water on the baffle and prevent its lateral movement. The surface-piercing wall-mounted vertical baffle with its top flushed with the quiescent free surface of the liquid is fixed to the wall of the tank by four sets of bolts; two each at both ends, equally distanced from the centre. Again by tightening these bolts, the friction between the end of the bolts and the wall of the tank provided the baffle with the required strength to resist the drag force on baffle and prevent it from moving. The bottom-mounted submerged blocks are fixed to the bottom of the tank in the same manner as is done in case of bottom-mounted vertical baffles. The clamp configuration is slightly different as can be marked from the Figure 8.5.

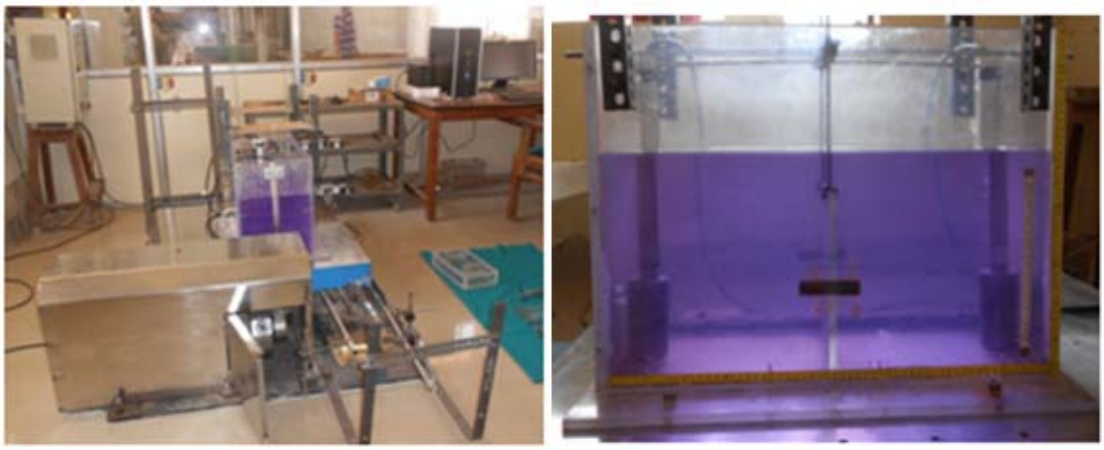

Figure 8.4: Experimental set up and instrumentation

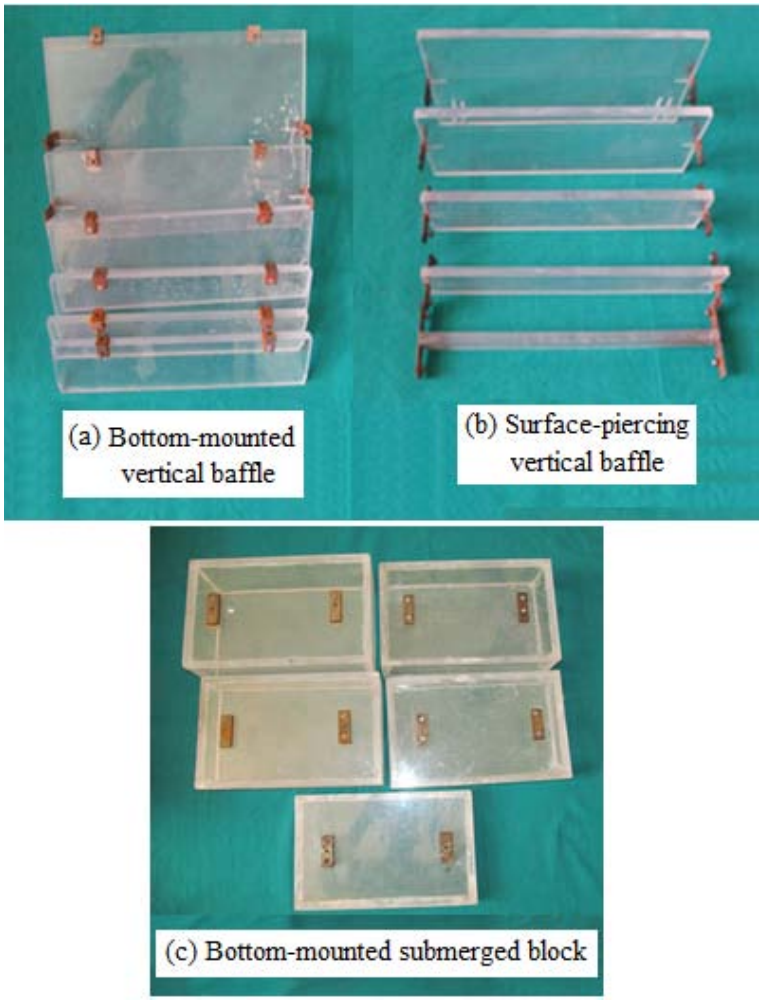

Figure 8.5: Snap shot of internal objects: (a) Bottom-mounted vertical baffles; (b) Surface-piercing vertical baffles; (c) Bottom-mounted submerged blocks

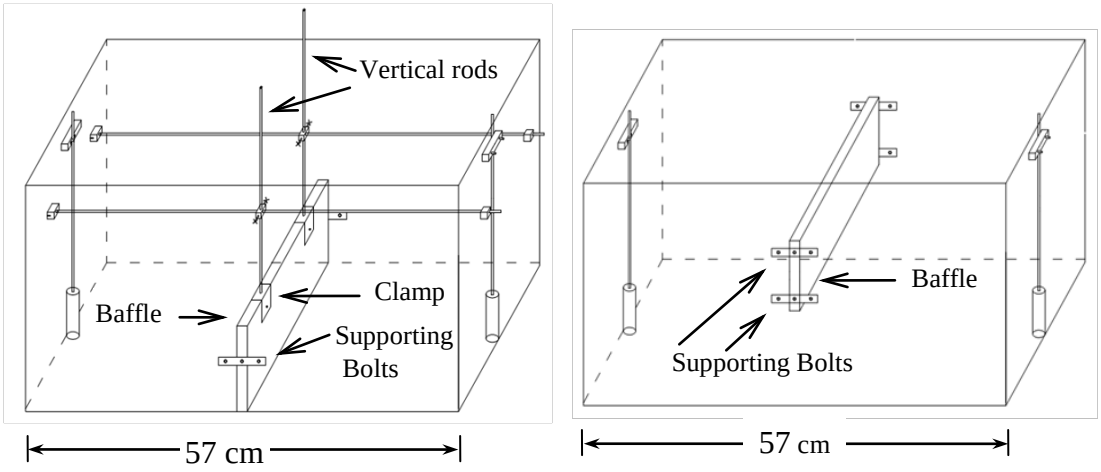

(a) Bottom-mounted baffle (b) Surface-piercing baffle

Figure 8.6: Baffles and associated supporting fixtures

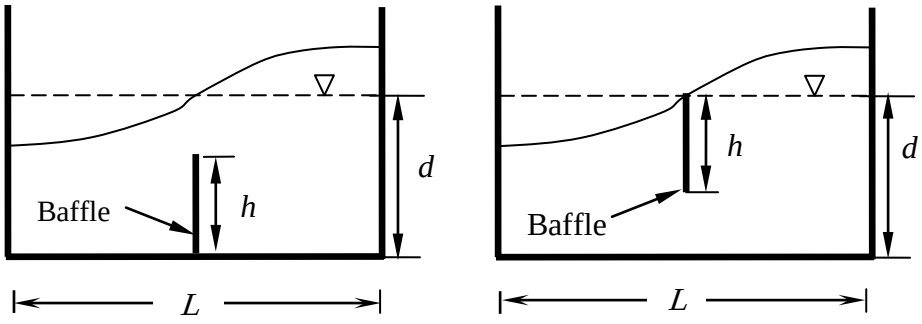

(a) Tank with bottom-mounted baffle (b) Tank with surface-piercing baffle

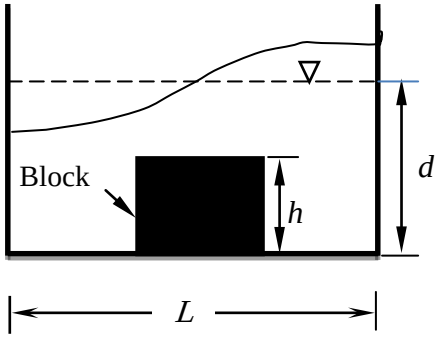

(c) Tank with bottom-mounted Suberged block

Figure 8.7: Problem definition (L = 57 cm, h and d are varying)

Experiments are carried out in tanks of two aspect ratios (d/L) of 0.26 and 0.52 corresponding to fill-depths of 15 cm and 30 cm respectively with two different baffle configurations (bottom-mounted and surface-piercing) and bottom-mounted submerged block. The relative height of baffles *(h/d)* as well as that of the submerged blocks is varied as 0.2, 0.4, 0.5, 0.6 and 0.8.

Figurative representation of problem definition is illustrated in Figure 8.7.

8.4 Experimental Results and Discussion

8.4.1 Frequency Response Study of Sloshing by Sine Sweep Test

For a certain liquid-tank system, with fixed system parameters, excitation frequency has a significant effect on the amplitude of sloshing elevations and thus on the whole lot of associated dynamic characteristics. In this regard, frequency response study of sloshing is carried out in tanks with two aspect ratios (fill-depths); d/L = 0.26 and 0.52. Three different configurations of centrally placed internal objects are used as

passive slosh damping devices to assess their slosh damping potential. The relative baffle heights (*h/d*) for each case of fill depth were varied as 0.2, 0.4, 0.5, 0.6, and 0.8. The effect of height submerged block (width, $w = 0.33L$) was investigated only for the tank with low fill depth, $d/L = 0.26$.

Lateral sine sweep tests were conducted in tanks without and with various configurations of internal objects as mentioned earlier to identify the natural frequencies of the systems. Each of the liquid-tank systems were excited with sinusoidal harmonic loading defined by expression $x = x_0 \sin 2\pi ft$ (where x_0 is the amplitude of excitation and *f* is the excitation frequency in cycles/sec) over a range of excitation frequencies which included the natural sloshing frequencies of the system. A typical harmonic force given to the shake table at an excitation frequency of 0.97 Hz as recorded by the dynamic LVDT is depicted in Figure 8.8. The displacement amplitude of the excitation was kept constant as 5 mm. The shaking was allowed over a significantly long period so as to allow the sloshing to reach steady state. The time domain sloshing elevation data for each excitation frequency was recorded with the help of vertical entry liquid level sensor, fixed near the two end walls perpendicular to the direction of excitation, via NI 6225 data acquisition system (DAQ) and LabView SignalExpress software. The peak amplitude of sloshing was then recorded and all the sloshing peaks were plotted against their respective excitation frequencies to obtain the frequency response curve of a particular liquid-tank system. The excitation frequencies corresponding to the sloshing peaks of frequency response plots gave the respective natural frequencies of sloshing. One such frequency response plot for tank with fill depth $d/L = 0.26$ and without any internal element is demonstrated in Figure 8.9. The first two natural mode of sloshing frequencies obtained for the above tank are 0.97 Hz and 2.02 Hz respectively. The fundamental modes of sloshing frequencies for other cases of tanks, similarly obtained, are presented in Table 8.1.

It can be seen that presence of internal objects reduced the fundamental frequency of the liquid. For a certain baffle height, the decrease in sloshing frequency was more in case of surface-piercing baffle. Of three different configurations, a maximum reduction in fundamental frequency was observed in case of submerged block.

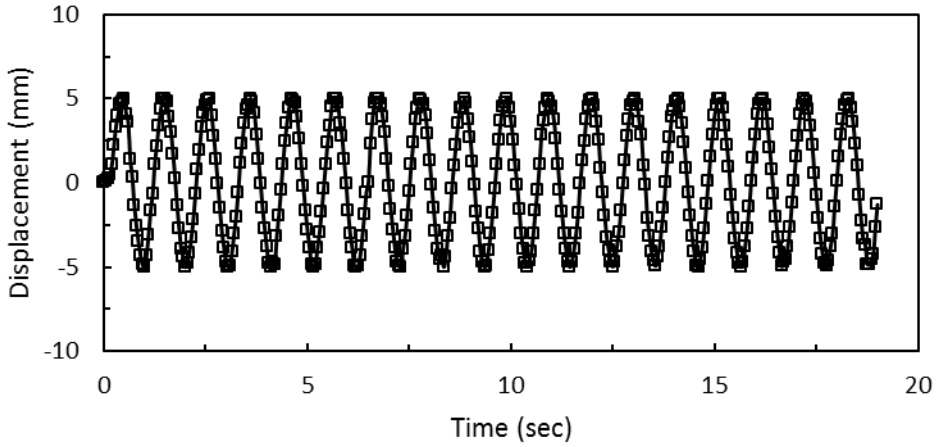

Figure 8.8: Harmonic excitation with a forcing frequency, f = 0.97 cycles/sec (fundamental sloshing frequency of tank without any internal objects) and displacement amplitude x_0 = 5 mm

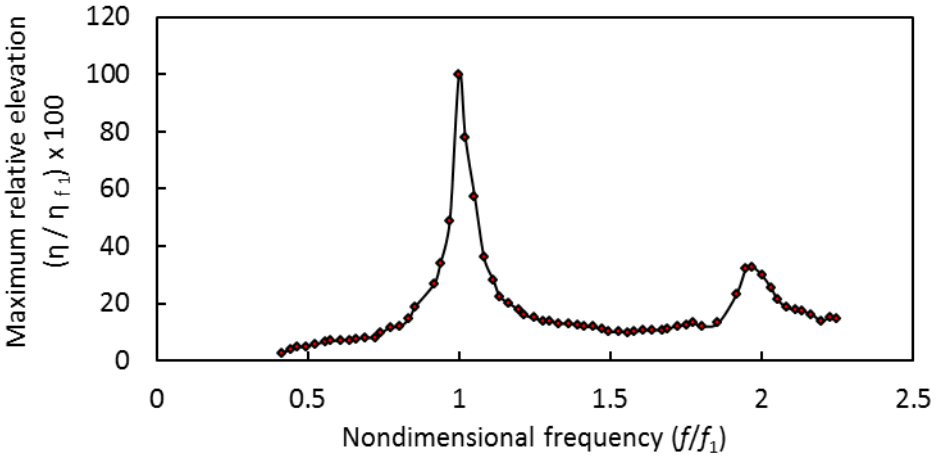

Figure 8.9: Frequency response of free surface wave elevation at left wall of tank of aspect ratio, d/L = 0.26, x_0 = 0.005m. η = sloshing elevation at different excitation frequencies; η_{f1} = sloshing elevation at excitation frequency equal to the fundamental sloshing frequency

Table 8.1: Effect of internal objects on first mode sloshing frequency (Hz)

h/d	Bottom-mounted baffle		Surface-piercing wall-mounted baffle		Bottom-mounted submerged block
	d/L = 0.26	*d/L* = 0.52	*d/L* = 0.26	*d/L* = 0.52	*d/L* = 0.26, *w* = *L*/3
0.0	0.96	1.13	0.96	1.13	0.96
0.2	0.95	1.12	0.95	1.07	0.91
0.4	0.91	1.08	0.89	0.94	0.82
0.5	0.88	1.05	0.86	0.88	0.77
0.6	0.85	1.01	0.80	0.82	0.71
0.8	0.74	0.87	0.69	0.70	0.53

For a certain baffle configuration, the effects of baffle height on the fundamental sloshing frequencies in tanks with different fill depths are compared on Figure 8.10. The fundamental frequency decreases with increase in the height of the baffle. For a given relative baffle height, the sloshing frequency of liquid in tank with high fill depth and bottom-mounted baffles is always more than that for low fill depth. In case of surface-piercing baffle, the sloshing frequencies in both the fill depth cases considered for study come closer as the relative height of the baffles increase. As can be seen from Figure 8.10(b), for baffle height h/d > 0.5, the fundamental natural frequency is not much affected.

Figure 8.11 shows the comparative results of the effects of bottom-mounted and surface-piercing baffles on the fundamental frequency of the baffled rectangular liquid tank. One can find from Figure 8.11(b) that the reduction in the fundamental frequency due to the surface-piercing baffle of same height is significantly more than that due to the bottom-mounted baffle.

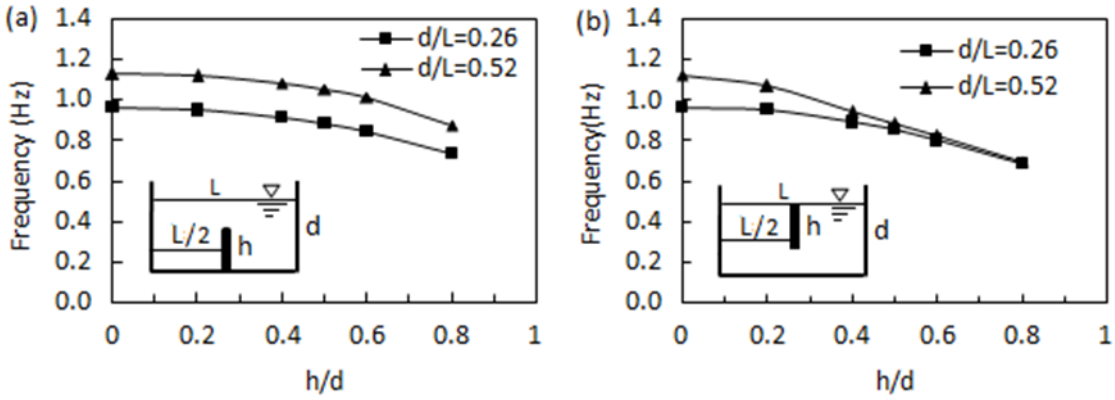

Figure 8.10: Comparison of fundamental sloshing frequencies as a function of baffle height in tanks with fill depth, d/L = 0.26 and 0.52: (a) bottom-mounted vertical baffles; (b) surface-piercing wall mounted vertical baffles

Figure 8.12 illustrates the effect of submerged block on the fundamental frequency of liquid in the tank with fill depth 0.26. The results are compared with those obtained for bottom-mounted baffles of equal heights. It may be noted that submerged blocks are nothing but baffles with comparatively larger width. One can see that a submerged block of similar height causes considerably greater decrease in frequency than bottom-mounted vertical baffle.

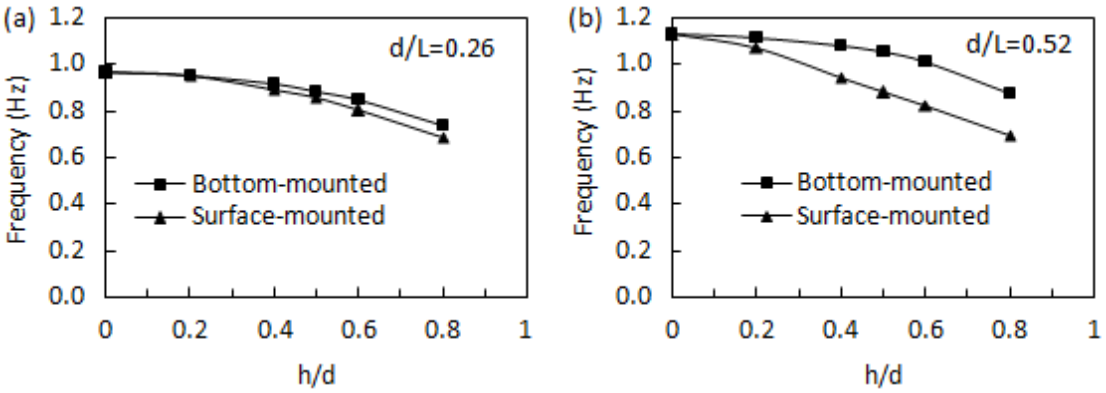

Figure 8.11: Sloshing frequencies in tank as a function of baffle height (*h/d*) with: (a) bottom-mounted vertical baffles as a function of baffle height (*h/d*) in tanks with *d/L* = 0.26 and 0.52

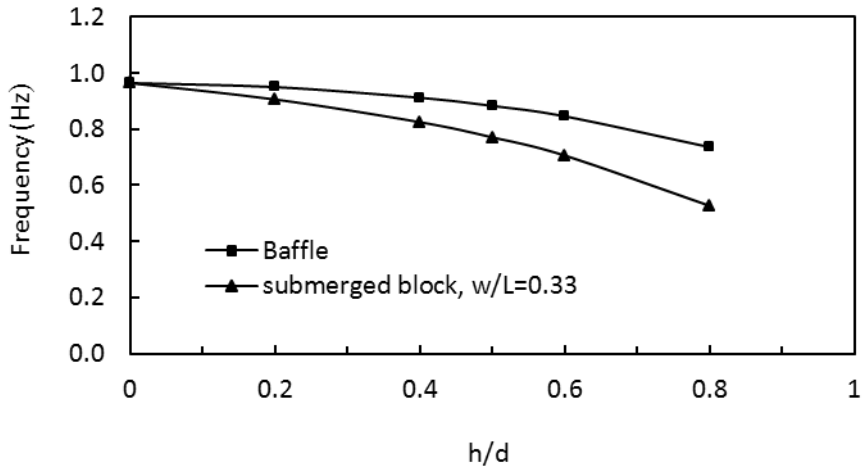

Figure 8.12: Comparison of sloshing frequencies in tank with *d/L* = 0.26 due to bottom-mounted vertical baffles and submerged components

8.4.2 Effect of Baffle on Sloshing Response

The basic concept behind the passive damping techniques of sloshing in tanks is manipulation of tank geometry so as to break the flow field into several sub-fields which helps in dissipation of kinetic energy of the liquid in motion. With an aim to judge the effectiveness of bottom-mounted baffles studied in this work for sloshing damping, the frequency response of free surface sloshing elevation at the left wall was studied. The free surface elevation for unbaffled and baffled (bottom-mounted) tanks with two different baffle heights are shown in Figure 8.13.

The damping effect is reflected by the reductions observed in maximum relative elevations especially close to the fundamental frequency. Dramatic reduction in sloshing wave height was noticed over a wide range of lateral excitation frequencies in presence baffle height, *h/d* = 0.8. In particular, under resonant condition, more than 80% reduction in wave height was noted. The percentages of attenuations of maximum elevations for three different configurations of internal objects compared to the reference case of a tank without internal objects are summarized in Table 8.2.

The percentage attenuations of maximum sloshing elevations due to presence of internal objects in tank with *d/L* = 0.52 could not be presented because it was not possible to find the maximum sloshing elevation in tank without any internal objects as the water sloshed out of the tank due to lack of sufficient free board.

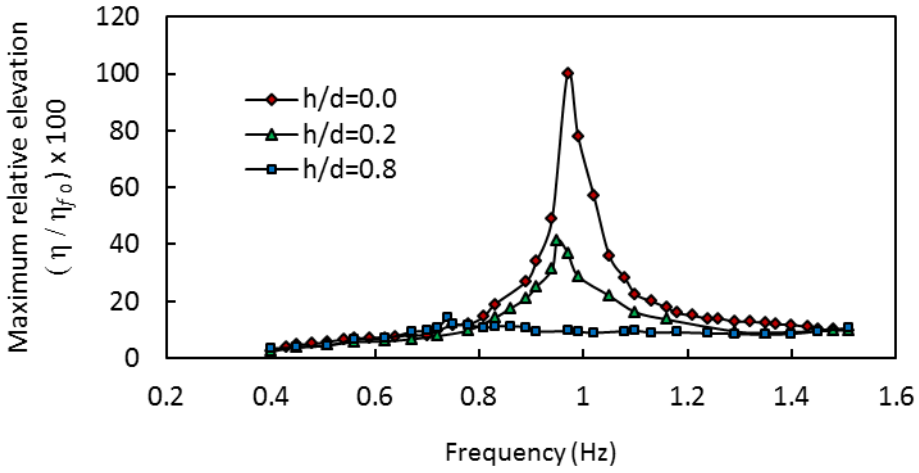

Figure 8.13: Frequency response of the free surface wave elevation at left wall of tank with *d/L* = 0.26 due to bottom-mounted vertical baffles of different heights; η = sloshing elevation at different excitation frequencies; η_{f0} = maximum sloshing elevation in tank without any internal component at excitation frequency equal to its fundamental sloshing frequency

Table 8.2: Percentage attenuation of maximum elevations

h/d	Bottom-mounted baffle *d/L* = 0.26	Surface-piercing wall-mounted baffle *d/L* = 0.26	Bottom-mounted submerged block *d/L* = 0.26, *w* = *L*/3
0.2	58.46	68.56	40.44
0.5	79.31	82.61	73.64
0.8	85.83	92.07	91.89

8.4.3 Hydrodynamic Slosh Damping

In order to investigate the hydrodynamic slosh damping effect of baffles on the first mode sloshing, the method of logarithmic decay of wave amplitude of free vibrating liquid is employed. In this method, the tank was harmonically excited at frequency close enough to the first mode frequency so as to induce first mode sloshing. The displacement amplitude of excitation was kept small as 5 mm. Sufficient time was allowed for the sloshing to attend steady state and then the oscillation was swiftly stopped to initiate free vibration. The time history of free surface wave elevation η (0,t) during the free vibration phase was recorded. The rate of decay (δ) of wave

amplitude was then computed, from which the damping ratio (ζ) was calculated as follows.

$$\delta = \frac{1}{j} ln \frac{\eta_i}{\eta_{i+j}}$$

$$\delta = \frac{2\pi\zeta}{\sqrt{1-\zeta^2}}, \quad \zeta \text{ is the damping ratio}$$

Where η_i and η_{i+j} are the sloshing amplitudes in *i* and *i+j* cycles of oscillations.

Experiments were conducted for each baffle with water height equal to 15 and 30 cm, with equivalent aspect ratios (*d/L*) of 0.26 and 0.52 respectively. In each case, two sets of baffle of two different configurations as mentioned earlier were used. For both configurations, the baffles are centrally placed. For a given aspect ratio and baffle configuration, the relative baffle height was varied as *h/d* = 0.2, 0.4, 0.5, 0.6, and 0.8. As explained in the previous paragraph, the time history of sloshing elevations during free vibration phase was recorded by vertical entry liquid level sensors, located near the two walls perpendicular to the direction of excitation. Similar experiments were also conducted for bottom-mounted submerged blocks.

Time history of sloshing wave heights during the free vibration phases for different cases of fill depths and internal object arrangements are shown in Figure 8.14 to Figure 8.18. According to the figures, the systems which show lower settling time responses have higher damping ratios and vice versa.

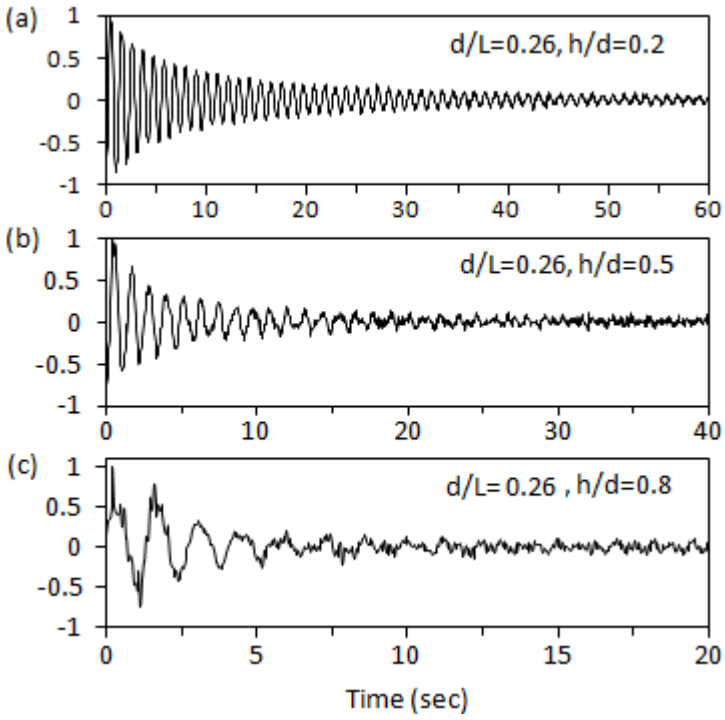

Figure 8.14: Time decay of sloshing amplitude in free vibration phase in tank of aspect ratio *d/L* = 0.26 with bottom-mounted vertical baffles of various heights

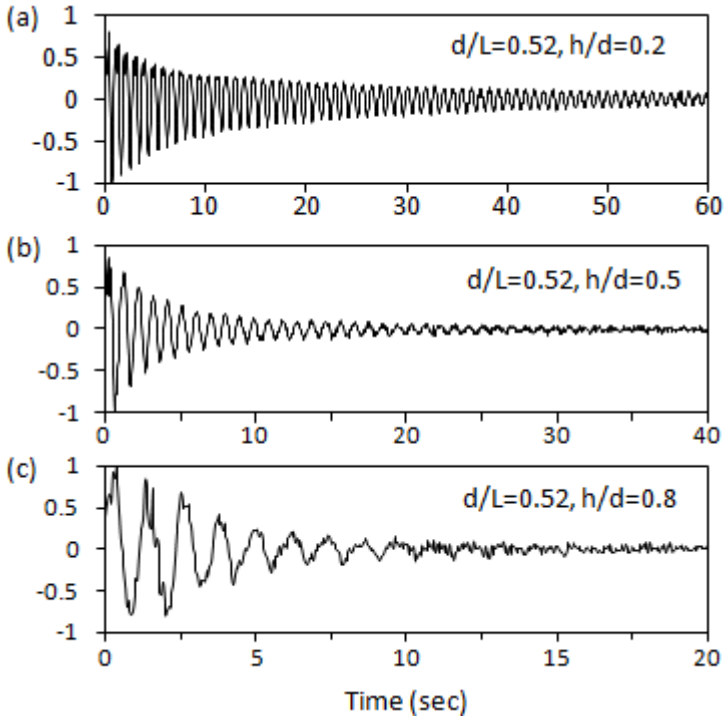

Figure 8.15: Time decay of sloshing amplitude in free vibration phase in tank of aspect ratio *d/L* = 0.52 with bottom-mounted vertical baffles of various heights

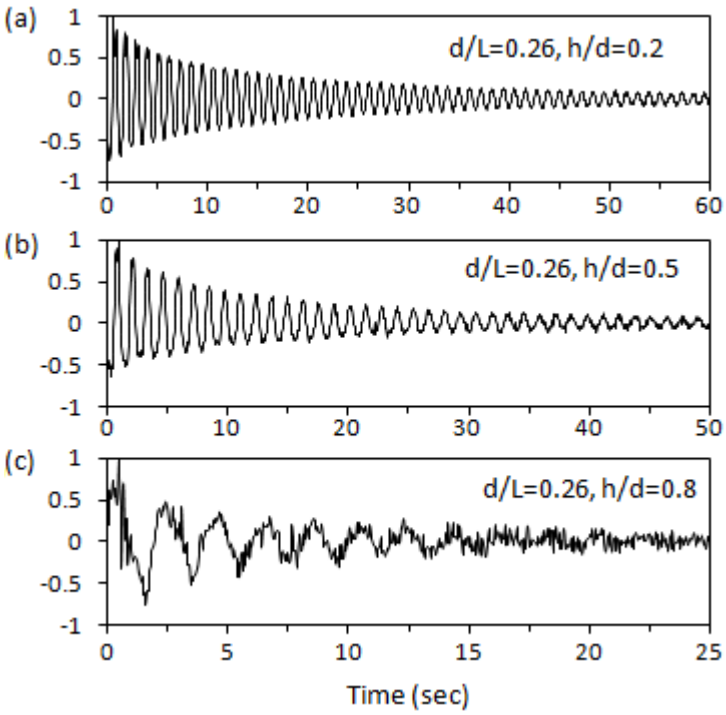

Figure 8.16: Time decay of sloshing amplitude in free vibration phase in tank of aspect ratio d/L = 0.26 with bottom-mounted submerged blocks of various heights (width, $w = 0.33L$)

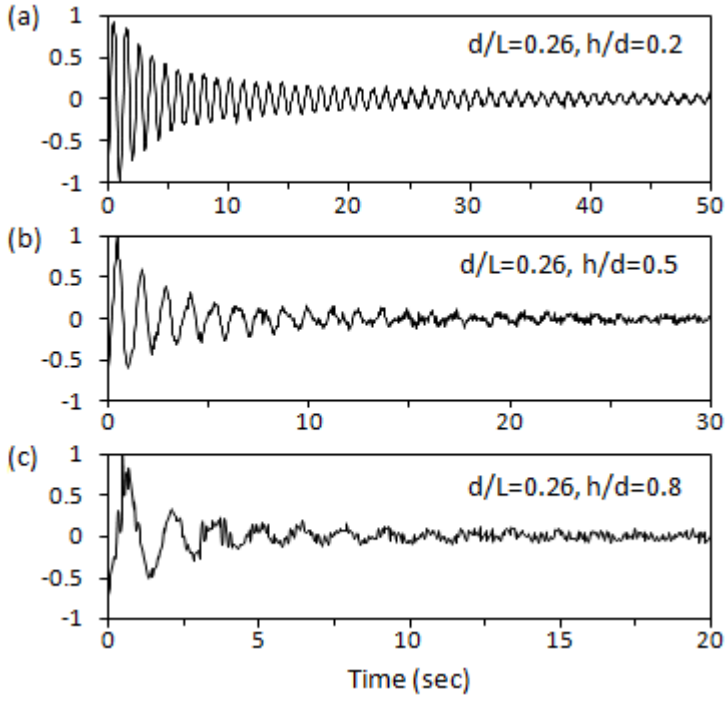

Figure 8.17: Time decay of sloshing amplitude in free vibration phase in tank of aspect ratio d/L = 0.26 with surface-piercing vertical baffles of various heights

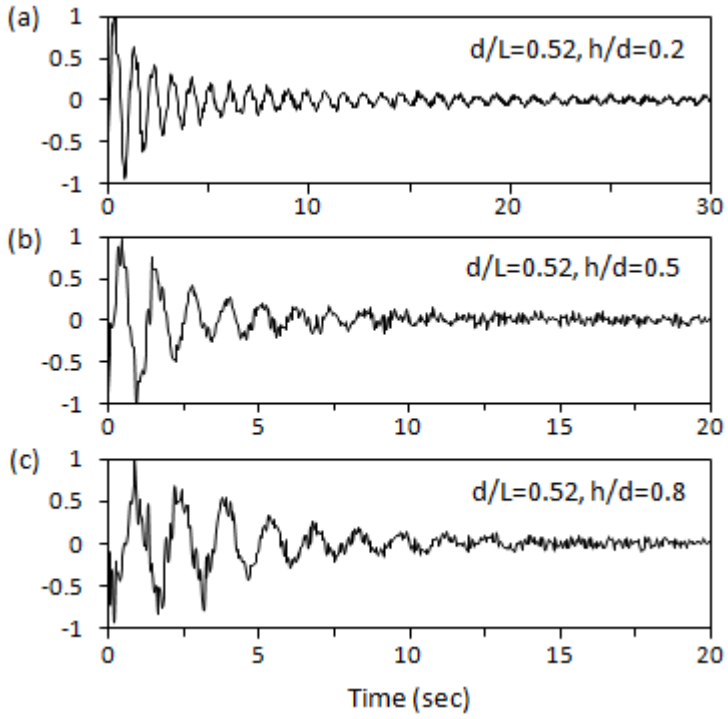

Figure 8.18: Time decay of sloshing amplitude in free vibration phase in tank of aspect ratio d/L = 0.52 with surface-piercing vertical baffles of various heights

8.4.4 Effect of the Bottom-mounted Vertical Baffles

The effect of baffle heights (h/d) and the fill depth on the damping ratio ζ is illustrated in Figure 8.19 for two fill depths of water; d/L =0.26, and 0.52. It is observed that for a certain relative height of baffle (h/d), the damping ratio decreases with increase in the liquid fill depth. The fact of the matter may be attributed to the increase in the convective mass of liquid for higher fill depth. Irrespective of the fill depth, the damping ratio increases with increase in the relative height (h/d) of the baffle. With the top of the baffle approaching closer to the quiescent free surface, the damping ratio significantly increases. This fact is consistent with the flow dynamics as there is higher concentration of convective mass near the free surface of fluid block. The relative motion between the convective fluid block and the baffle helps in dissipating the sloshing energy and thus the increase in damping ratio.

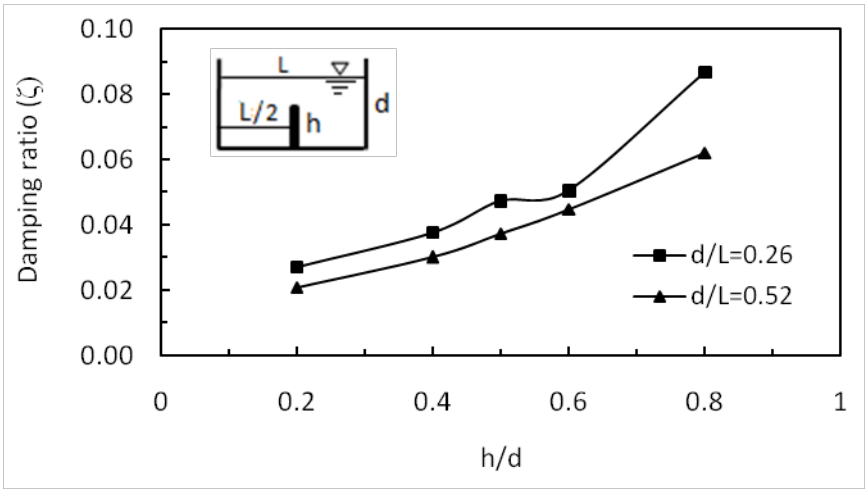

Figure 8.19: Comparison of variation of damping ratio as a function of relative baffle height (*h/d*) in tanks with two different fill depths; *d/L* = 0.26 and 0.52 due to bottom-mounted vertical baffles

8.4.5 Effect of the Surface-piercing Vertical Baffles

Figure 8.20 presents the variation of damping ratio ζ as a function of relative baffle height for two different liquid fill depths. A typical trend in the variation of damping ratio is marked in case of surface-piercing wall-mounted baffles. Up to a certain ratio of baffle height to liquid depth (*h/d*), the damping ratios obtained for tank with higher fill depth was found to be more than those for the low fill-depth and there after a reverse trend was marked. The exact reason for this fact could not be ascribed in the present study and needs to be further investigated.

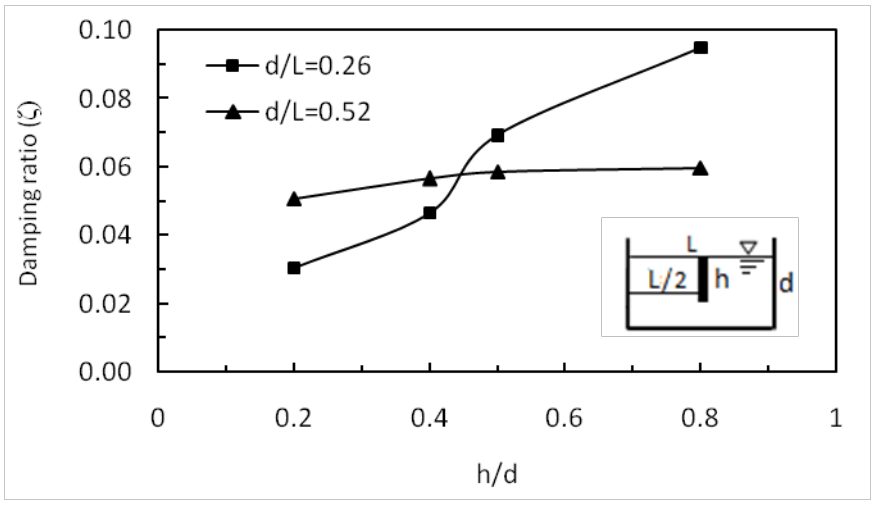

Figure 8.20: Comparison of variation of damping ratio as a function of relative baffle height (*h/d*) in tanks with two different fill depths; *d/L* = 0.26 and 0.52 due to surface-piercing vertical baffles

8.4.6 Comparison of the Damping Effects of Bottom-mounted and Surface-piercing Vertical Baffles

Figures 8.21 and 8.22 depict a comparative study of the damping effects of bottom-mounted and surface-piercing vertical baffles. Irrespective of the fill depths considered in the present study, for a certain baffle height (*h/d*) the damping ratio is always more due to surface-piercing baffle. However, in case of high fill depth, the slosh damping effect of surface-piercing baffle is significantly more than that due to bottom-mounted baffle of similar height. Furthermore, the damping effect of both baffle configurations become equal as the baffle heights approach the height of liquid in the tank. It can be seen that for baffle height equal to 80% the height of water in the tank, the damping ratios for both baffle configurations approach each other. The fact of the matter is understandable, as in both the cases the tank is almost divided into two separate tanks.

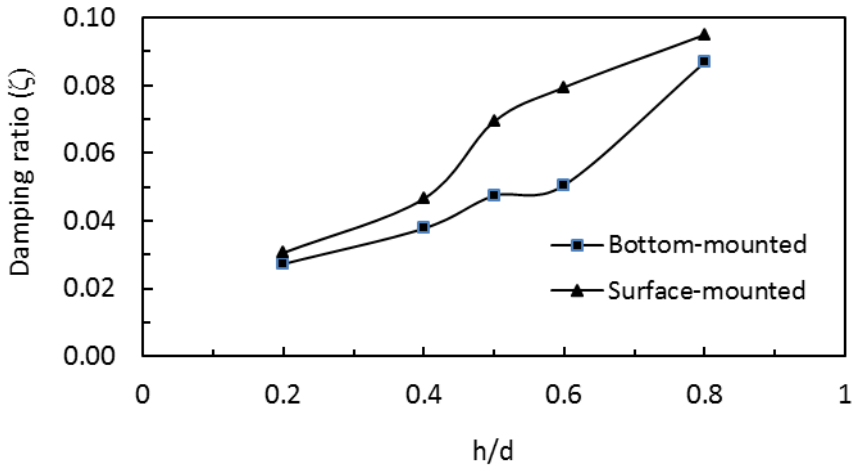

Figure 8.21: Comparison of damping ratios, as a function of relative baffle height(*h/d*), due to bottom-mounted and surface-piercing vertical baffles, in tanks with $d/L = 0.26$

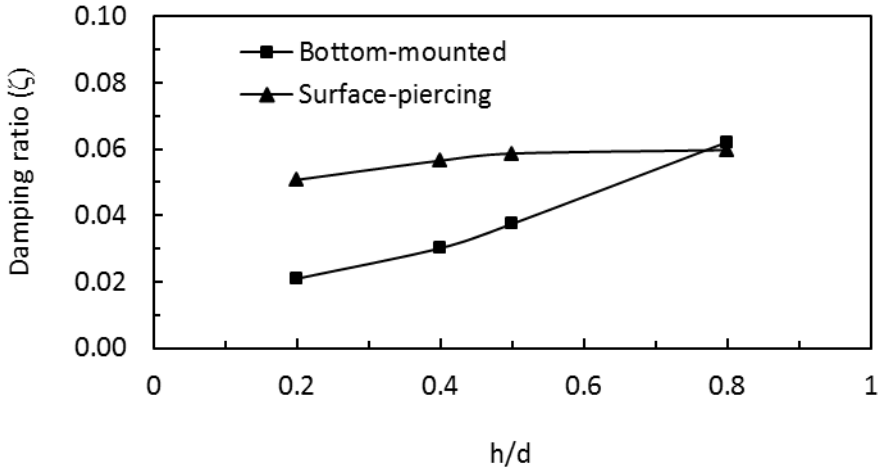

Figure 8.22: Comparison of damping ratios, as a function of relative baffle height (*h/d*), due to bottom-mounted and surface-piercing vertical baffles, in tanks with *d/L* = 0.52

In addition, percentage attenuation of free surface sloshing elevation, as a function of relative baffle height, for two baffle arrangements in tank with fill-depth 0.26 is depicted in Figure 8.23. One can see that the performance of surface-piercing baffle as passive slosh damper is better than bottom-mounted baffle. The same could not be presented for tank with fill depth 0.52 as the sloshing height in unbaffled tank could not be recorded because oscillating water splashed out of the tank due to lack of sufficient free board.

As observed from Table 8.1, submerged blocks are found to reduce the fundamental sloshing frequencies more as compared to the bottom-mounted vertical baffles of similar heights. However, such reductions do not translate into increase in damping ratio. The fact of the matter can be observed from Figure 8.24, wherein it is seen that compared to the bottom-mounted vertical baffles, submerged blocks of equal height with comparatively more width (*w/L* = 0.33) have less damping potential. The reason may be ascribed to the fact that due to greater width of the submerged block the sharp-edge effect gets diminished.

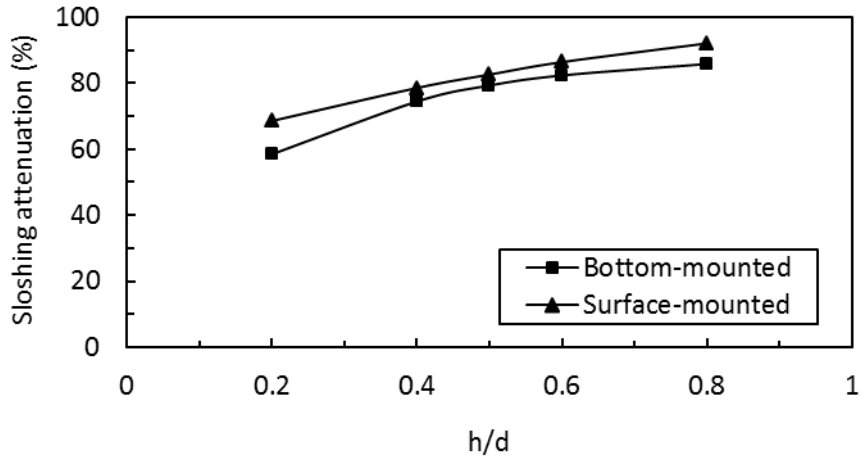

Figure 8.23: Comparison of percentage attenuation of sloshing elevation as a function of relative baffle height (*h/d*) in tank with fill depth, *d/L* = 0.26 for two different baffle configuration; bottom-mounted baffle and surface-piercing baffle

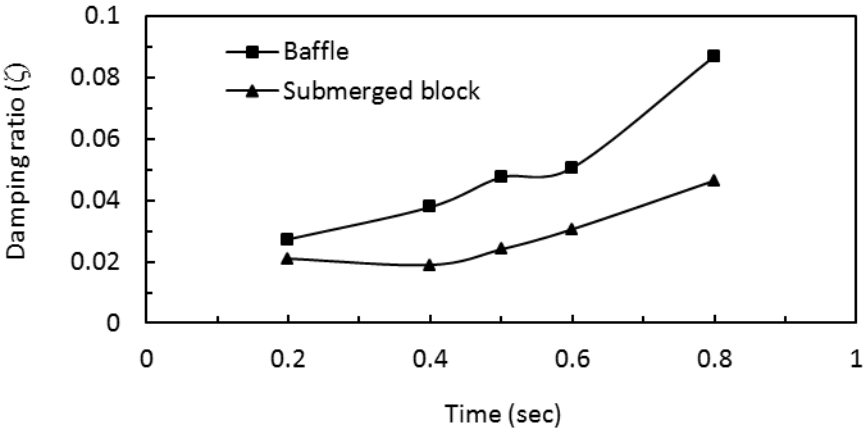

Figure 8.24: Comparison of damping ratio as a function of relative baffle height (*h/d*) in tank with fill-depth, *d/L* = 0.26 for bottom-mounted vertical baffles and submerged blocks, *w/L* = 0.33

8.4.7 Forced Vibration Response

The tank with different heights of bottom-mounted vertical baffles was subjected to forced harmonic vibrations with excitation frequencies equal to the fundamental sloshing frequencies of water of respective tank-liquid-baffle configurations. The excitation amplitude was kept constant as 5 mm for all the cases. The baffle height relative to the water depth was varied as *h/d* = 0.0, 0.2, 0.5, and 0.8. The temporal evolutions of free surface sloshing elevation measured from the bottom of the tank for

tank with fill depth, d/L = 0.26 with bottom-mounted baffle as the internal object is illustrated in Figure 8.25. The plots of temporal evolution of free surface sloshing elevation for different baffle heights clearly underlined the damping effect of respective baffles. It was observed that baffle of height equal to eighty percent the height of water in the tank dramatically reduced the sloshing.

A plot on the similar line as above for surface-piercing vertical baffles of various heights in tank with same fill depth of 0.26 is also depicted in Figure 8.26. From a close comparison of Figure 8. 25 and 8.26, one can notice that for a certain height of baffle, surface-piercing vertical baffle is potentially more effective in slosh damping than bottom-mounted vertical baffle. To make the above observation further clear, a comparison of temporal evolutions of sloshing for two configurations of baffles of equal height, h/d = 0.2 was made on Figure 8.27. It clearly shows that surface-piercing baffle is more effective in slosh damping.

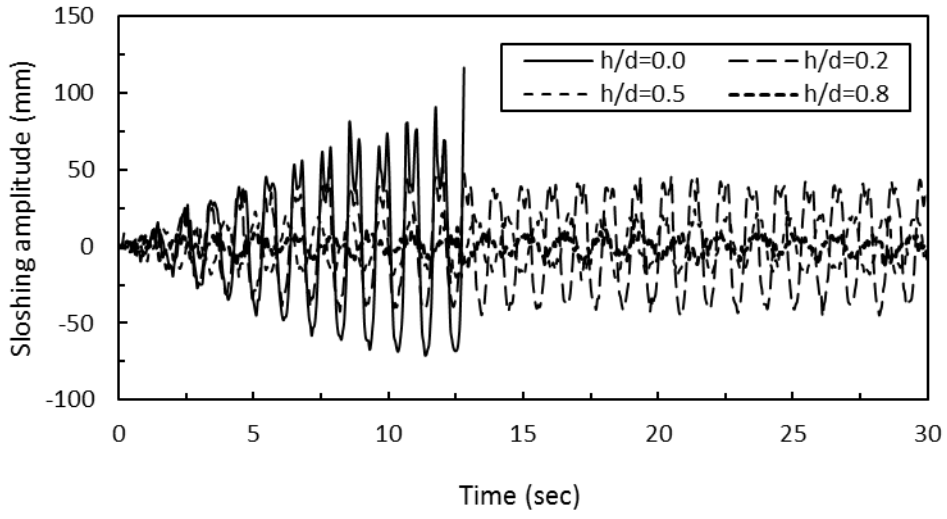

Figure 8.25: Temporal evolution of the free surface sloshing elevations at the left wall for tank with bottom-mounted baffles of varying heights (h/d) under harmonic excitation with displacement amplitude, x_0 = 5 mm and excitation frequencies, f (cycles/sec) corresponding to their respective fundamental sloshing frequencies.

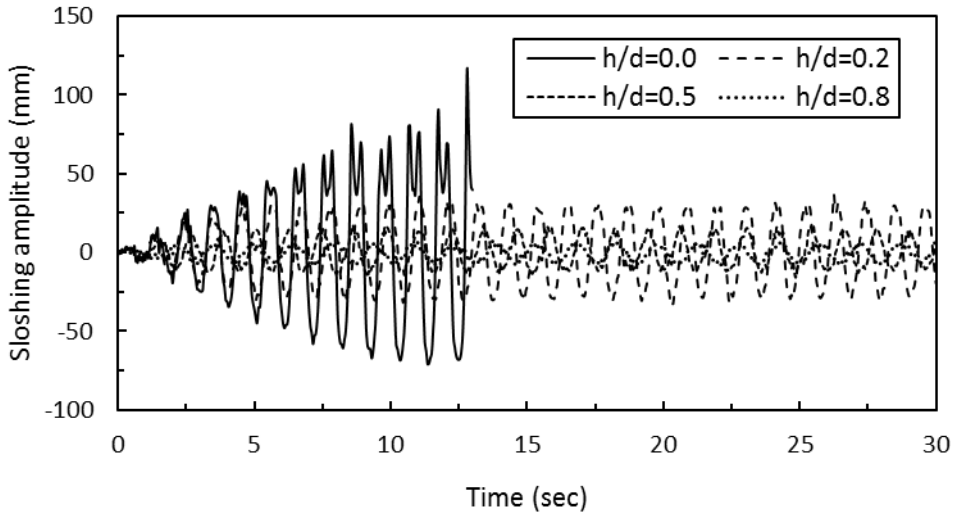

Figure 8.26: Temporal evolution of the free surface sloshing elevations at the left wall for tank with surface-piercing baffles of varying heights (*h/d*) under harmonic excitation with displacement amplitude, x_0 = 5 mm and excitation frequencies, *f* (cycles/sec) corresponding to their respective fundamental sloshing frequencies as presented in Table 1

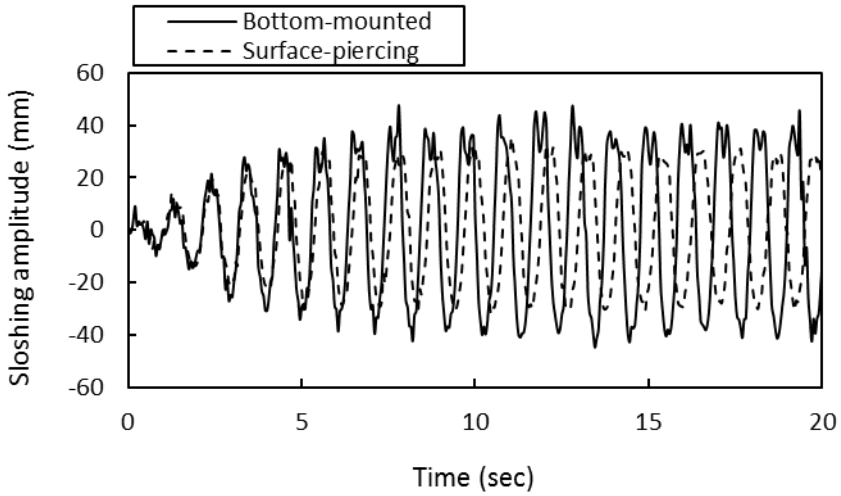

Figure 8.27: Comparison of temporal evolution of the free surface sloshing elevations at the left wall of tank due to bottom-mounted and surface piercing baffle of equal height in tank with fill depth, *d/L* = 0.26. Excitation frequencies are equal to respective fundamental sloshing frequencies and excitation amplitude, x_0 = 5 mm

8.5 Conclusion

The main endeavour of this chapter was to investigate the hydrodynamic damping potential of three different configurations of centrally installed internal objects perpendicular to the direction of lateral excitation in a rectangular tank partially filled with water. The objects used are bottom mounted vertical baffles, surface-piercing vertical baffles, and bottom mounted submerged blocks ($w = 0.33\ L$) in tank with two different fill depths (ratio of liquid height to tank width in the direction of excitation), $d/L = 0.26$ and 0.52. The height of the internal objects (h) were selected relative to the stationary water height (d) as a ratio of the height of internal object to the stationary water height and for each configuration the object height was varied as $h/d = 0.2$, 0.4, 0.5, 0.6, and 0.8.

The following observations are highlighted:

1. Presence of centrally installed internal object decreases the fundamental frequency of liquid and such decrease is monotonic with the increase in height of the internal object regardless of the configurations: bottom-mounted vertical baffle, surface-piercing baffles, and bottom-mounted submerged blocks.
2. Flow over a vertical baffle produces a shear layer and energy is dissipated by viscous effect of the water.
3. Submerged blocks were found to reduce the fundamental sloshing frequencies more as compared to the bottom-mounted vertical baffles of similar heights. However, such reductions did not translate into increase in damping ratio. The reason may be ascribed to the fact that due to greater width of the submerged block the sharp edge effect gets diminished.
4. With the top of the baffle approaching closer to the quiescent free surface, the damping ratio significantly increases. This fact is consistent with the flow dynamics as there is higher concentration of convective mass near the free surface of fluid block. The relative motion between the convective fluid block and the baffle helps in dissipating the sloshing energy and thus the increase in damping ratio.
5. For certain baffle height, surface-mounted baffle is more effective in sloshing damping.

CHAPTER 9

9 PREDICTION OF SEISMIC INDUCED SLOSHING RESPONSE IN BAFFLED RECTANGULAR LIQUID TANK USING ADAPTIVE NEURO-FUZZY INFERENCE SYSTEM

9.1 Introduction

In the recent years, novel soft computing techniques have been introduced in almost all fields of engineering for prediction purpose due to accurate mapping of nonlinear behaviour of inputs with outputs. Soft computing techniques as modelling tools have generated considerable interest among the researchers involved in diverse fields of science and engineering due to their ability in tackling the imprecision and uncertainty involved in complex nonlinear systems (Zadeh, 1994). The evolution of soft computing techniques not only helps in predicting the desired output parameters of the problem at hand but also helps in understanding various aspects of nonlinear systems. Artificial Neural Networks (ANNs), Fuzzy Inference Systems (FIS), Decision Trees (DTs), Support Vector Machines (SVMs) and Bayesian Networks (BNs) are the most popular soft computing techniques for regression and/or data classification. Over a decade or so, it has been widely established that soft computing can be effectively used for modelling large scale complex phenomena. Soft computing methodologies such as artificial neural networks (ANNs), genetic programming (GP), fuzzy inference system (FIS) etc. have proven their competencies in pattern recognition, signal processing, data clustering and many other scientific applications. Based on a set of sample data and fuzzy "if-then rules", fuzzy logic methods have been used to model various highly complex and nonlinear systems. A

fuzzy inference system can model the qualitative aspects of human knowledge without employing any quantitative analyses. These methodologies were initially used as tools for optimizing the design methods. Later, these were used in more subtle engineering applications. Of late, soft computing techniques have pervaded into almost all fields of engineering application. Attempts to integrate various computing paradigms together to form hybrid techniques, which could capture the predicting potential of both, have resulted in more soft computing tools. Competencies of computing tools such as artificial neural network (ANN) and fuzzy logic method, when applied individually to a variety of problems, have been established. Later on, the rising interests in combining both these approaches have resulted in evolution of neuro-fuzzy computing techniques.

Although soft computing techniques have made deep inroads into a wide range of scientific and research applications, their application in sloshing analysis is very limited and can almost be treated in negation. In the present study, adaptive neuro-fuzzy inference system is used for prediction of sloshing elevation. The potential of ANFIS in predicting the sloshing response has not been tried out by any researcher so far. To this end, an attempt has been made to assess the predictive potential of ANFIS in computing the sloshing response of liquid which by itself is very complex and nonlinear dynamic phenomenon.

9.2 Sloshing Data

A data set is created by conducting numerical experiment employing Galerkin finite element method as developed in chapter 3. A two-dimensional tank model of 1 m length (L) and 0.5 m still liquid depth (d) is used. Figure 9.1 illustrates the problem definition. Two different earthquakes viz; Imperial Valley and San-Franscisco with low and high frequency content respectively are used as ground motions for generation of sloshing response data. The ratio of peak ground acceleration (PGA) to peak ground velocity (PGV) is a commonly accepted measure of frequency content of earthquake records, where PGA is in g and PGV is in m/s (Heidebrecht and Lu,1988). On the basis of the ratio of peak ground acceleration (PGA) to peak ground velocity (PGV), the earthquakes are classified into three categories: high (PGA/PGV > 1.2), intermediate (0.8<PGA/PGV<1.2) and low (PGA/PGV<0.8). A rigid baffle is used as

a passive slosh damping device in the tank in the numerical simulation. The position and the height of the baffle are varied to find out their effects on the sloshing response of the liquid. The tank is assumed to be rigid to negate the effect of flexibility of the tank walls and hence fluid-structure interaction as the same is not accounted in the numerical modelling. The miniature size of the tank has been conceived keeping in view the future prospects of conducting experimental tests. Further, the tank in question has the same dimension as the one used by Faltinsen (1978) and Romero and Ingber (1995). The details about the numerical model are presented in chapter 3. However, the validation of the numerical model used for the generation of data set is presented in this chapter to avoid any ambiguity regarding the numerical model. For validation of the numerical model a sinusoidal motion given by $x = a \sin \omega t$ is prescribed as lateral external excitation along the length of the tank. The amplitude and angular frequency of the excitation are a = 0.025 m and ω = 3.1416 rad/s. The sloshing elevation is measured by deviation in surface height from the mean liquid level. The free surface displacement also called sloshing elevation is measured at a location of 0.05m from the left wall of the tank. The time history of sloshing elevation depicted in Figure 9.2 shows a very good agreement with that due to Faltinsen (1978).

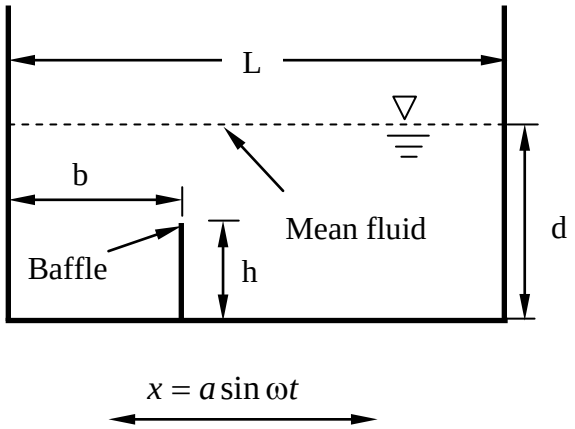

Figure 9.1: problem definition

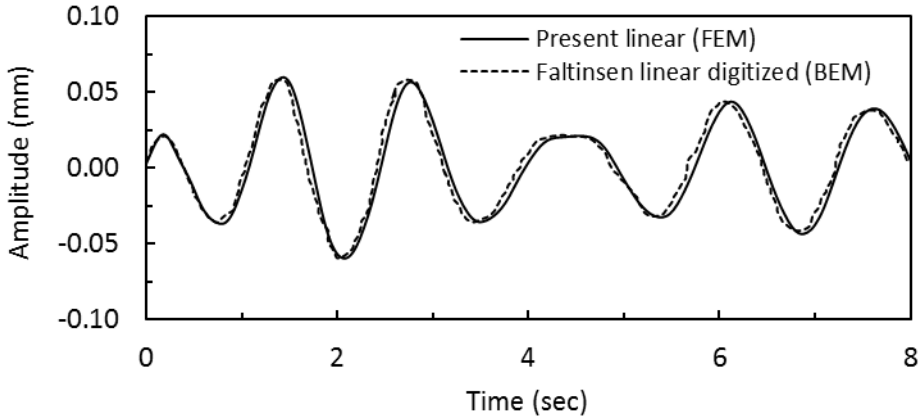

Figure 9.2: Free surface displacement from rest level at a distance of 0.05 m from the left side of the container.

Hereafter, the seismic motion of Imperial Valley (low frequency content earthquake) and San-Francisco (high frequency content earthquake) with their peak accelerations scaled to a constant amplitude of 0.2g are prescribed as external excitations. The position (*b/L*) and the height of the baffle (*h/d*) are changed for generation of sloshing response data in terms of sloshing elevation for further use in the ANFIS model. The data set as obtained from the numerical simulation is presented in the Table 9.1.

9.3 ANFIS Model Description

Adaptive neuro-fuzzy inference system also known as adaptive network-based fuzzy inference system is a mixed blend of artificial neural networks (ANN) and fuzzy systems (FS). It imbibes the best features and offsets the limitations of both the systems. ANFIS integrates neural network learning capabilities with the qualitative approach of fuzzy inference system in the form of fuzzy *if-then* rules for decision making. The imbibed features complement each other in a completely new computing environment. In short, adaptive neuro-fuzzy inference system is a fuzzy inference system implemented in the framework of an adaptive neural network.

Table 9.1: Input and output data used for analysis.

Serial No.	Ground motion data	*h*/*d*	*b*/*L*	Sloshing elevation (mm)
1	Imperial Valley-06	0.2	0.5	96.52
2	Imperial Valley-06	0.3	0.5	87.75
3	Imperial Valley-06	0.4	0.5	74.91
4	Imperial Valley-06 #	0.5	0.5	68.47
5	Imperial Valley-06	0.6	0.5	60.03
6	Imperial Valley-06 #	0.7	0.5	50.26
7	Imperial Valley-06	0.8	0.5	58.0
8	Imperial Valley-06 #	0.9	0.5	78.79
9	Imperial Valley-06	1.0	0.5	60.10
10	Imperial Valley-06	0.2	0.2	101.80
11	Imperial Valley-06 #	0.3	0.2	98.75
12	Imperial Valley-06	0.4	0.2	93.75
13	Imperial Valley-06	0.5	0.2	85.98
14	Imperial Valley-06	0.6	0.2	75.85
15	Imperial Valley-06 #	0.7	0.2	82.67
16	Imperial Valley-06	0.8	0.2	91.64
17	Imperial Valley-06	0.9	0.2	89.15
18	Imperial Valley-06 #	1.0	0.2	34.24
19	Imperial Valley-06 #	0.2	0.3	99.50
20	Imperial Valley-06	0.3	0.3	93.70
21	Imperial Valley-06	0.4	0.3	84.46
22	Imperial Valley-06 #	0.5	0.3	73.87
23	Imperial Valley-06	0.6	0.3	70.44
24	Imperial Valley-06	0.7	0.3	73.87
25	Imperial Valley-06 #	0.8	0.3	74.79
26	Imperial Valley-06	0.9	0.3	72.53
27	Imperial Valley-06	1.0	0.3	42.29
28	Imperial Valley-06	0.2	0.4	97.44
29	Imperial Valley-06	0.3	0.4	89.42
30	Imperial Valley-06 #	0.4	0.4	76.07

Contd.

31	Imperial Valley-06	0.5	0.4	69.82
32	Imperial Valley-06	0.6	0.4	64.27
33	Imperial Valley-06 #	0.7	0.4	58.58
34	Imperial Valley-06	0.8	0.4	55.86
35	Imperial Valley-06	0.9	0.4	79.18
36	San-franscisco	0.2	0.5	13.41
37	San-franscisco	0.3	0.5	13.14
38	San-franscisco #	0.4	0.5	12.75
39	San-franscisco	0.5	0.5	12.27
40	San-franscisco	0.6	0.5	11.70
41	San-franscisco #	0.7	0.5	11.10
42	San-franscisco	0.8	0.5	10.60
43	San-franscisco #	0.9	0.5	12.08
44	San-franscisco	1.0	0.5	17.03
45	San-franscisco	0.2	0.2	13.58
46	San-franscisco	0.3	0.2	13.51
47	San-franscisco #	0.4	0.2	13.42
48	San-franscisco	0.5	0.2	13.30
49	San-franscisco #	0.6	0.2	13.14
50	San-franscisco	0.7	0.2	13.0
51	San-franscisco	0.8	0.2	12.88
52	San-franscisco	0.9	0.2	12.93
53	San-franscisco #	1.0	0.2	13.43
54	San-franscisco #	0.2	0.3	13.53
55	San-franscisco	0.3	0.3	13.40
56	San-franscisco #	0.4	0.3	13.22
57	San-franscisco	0.5	0.3	13.0
58	San-franscisco	0.6	0.3	12.75
59	San-franscisco #	0.7	0.3	12.51
60	San-franscisco	0.8	0.3	12.35
61	San-franscisco	0.9	0.3	12.43
62	San-franscisco	1.0	0.3	13.12

Contd.

63	San-franscisco	0.2	0.4	13.47
64	San-franscisco [#]	0.3	0.4	13.26
65	San-franscisco	0.4	0.4	12.98
66	San-franscisco [#]	0.5	0.4	12.64
67	San-franscisco	0.6	0.4	12.25
68	San-franscisco	0.7	0.4	11.87
69	San-franscisco [#]	0.8	0.4	11.60
70	San-franscisco	0.9	0.4	13.43
71	San-franscisco	1.0	0.4	14.13

[#] Superscripted data are used as testing data set for validation of *ANFIS* model and rest of the data are used as training data set

9.3.1 Artificial Neural Network

Artificial neural network (ANN) represents a powerful information processing tool for identification of relevant parameters and their interactions in a complex and highly nonlinear platform involving a number of parameters. ANNs are very efficient in adaptation and learning which is why they are popular as modelling tools in a wide spectrum of engineering application. A three layer neural network comprises of an input layer for accepting the input variables, a hidden layer, and a output layer. All layers are in general composed of a number of neurons. These neurons perform specific data processing tasks using nonlinear function such as a sigmoid. The neurons of successive layers are connected with each other through interconnection weights between them. Each neuron of the hidden and output layers is offset by a threshold value. The back propagation learning algorithm is commonly used to train the network by adjusting the interconnection weights and neuron thresholds between the layers so as to minimize the cost function. The process is repeated until either the mean-square error (MSE) between the measured data points and the predicted ANN values for elements in the training set has achieved a pre-defined limiting value or after the completion of previously selected number of iterative learning processes, called epoch. The model thus obtained is subsequently used to classify or predict from previously unseen data output. By optimizing neural network (NN) architecture and suitable selection of input parameters, the number of training data required can be

reduced. However, requirement of number of data increases with increase in the complexity of the nonlinear relationship between the input and the output of the system.

9.3.2 Fuzzy Inference System (FIS)

Fuzzy logic methods referred to as fuzzy inference system are widely used to model highly nonlinear and complex systems in various fields of engineering application and otherwise. Fuzzy logic is a mathematical tool for dealing with uncertainty. It provides a technique to deal with imprecision and information obliquity. To soft computing, it offers an important paradigm of "computing with words". Fuzzy inference systems (FISs) are based on a set of sample data and fuzzy "*if-then rules*". The concepts and reasoning modes underlining fuzzy logic makes it a suitable candidate for solving problems that require human instinct due to the absence of precise or correct answer. In general, fuzzy inference systems are capable of modelling qualitative aspects of human knowledge without employing any quantitative analysis. Basically, a fuzzy inference system is composed of five functional blocks as shown in Figure 9.3

- a *rule base* containing a number of fuzzy if-then rules;
- a *database* which defines the membership functions of the fuzzy sets used in fuzzy rules;
- a *decision-making unit* which performs the inference operation on the rules;
- a *fuzzification interface* which transforms the crisp inputs into degrees of match with linguistic values;
- a *defuzzification interface* which transform the fuzzy results of inference into crisp output.

Usually, the rule base and the data base are together referred to as the *knowledge base.* The steps of inference operations upon fuzzy *if-then* rules also known as *fuzzy reasoning* performed by fuzzy inference systems are:

1. Compare the input variables with the membership functions on the premise part to obtain the membership values (or compatibility measures) of each linguistic label. This step is often referred to as *fuzzification*.

2. Combine (through a specific T-norm operator, usually multiplication or min.) the membership values on the premise part to get *firing strength (weight)* of each rule.
3. Generate the qualified consequent (either fuzzy or crisp) of each rule depending on the firing strength.
4. Aggregate the qualified consequents to produce a crisp output. This step is called *defuzzification.*

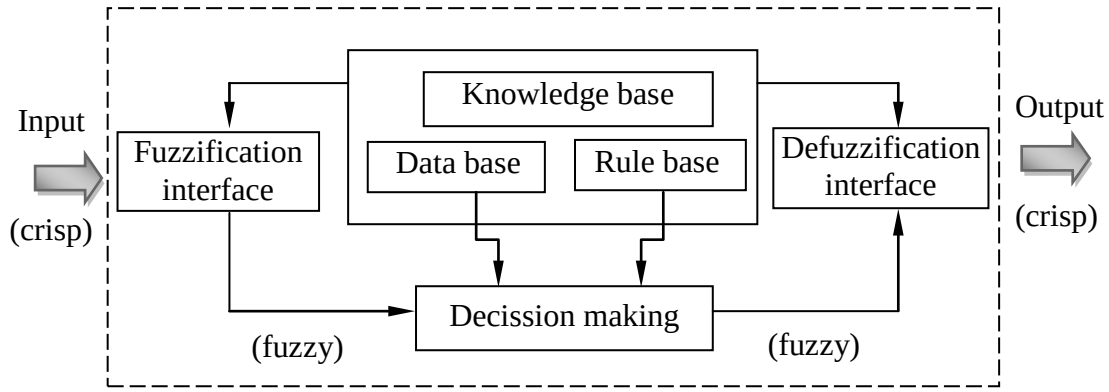

Figure 9.3: Schematic diagram of Fuzzy inference System

Some of the notations commonly used in fuzzy logic are explained in brief as follows.

9.3.2.1 Linguistic Variables

Linguistic variables are central to fuzzy logic manipulations. Linguistic variables represent crisp information in a form and precision appropriate for the problem. In the lexicon of fuzzy logic, by a linguistic variable one means a variable whose values are words or sentences in a natural or artificial/machine language. For example, for the problem herein in this chapter, ***baffle-height* (*h/d*)** is a linguistic variable if its values are linguistic rather than numerical, i.e., height is zero, height is close to zero, height is very less, height is less, height is medium, height is more etc. rather than 0, 0.05, 0.2, 0.5, 0.8 etc. Linguistic variables have been found to be particularly useful in complex non-linear applications. The use of linguistic variables in many real world applications reduces the overall computation complexity of the application. The main function of linguistic variables is to provide a systematic means for an approximate characterization of complex or ill-defined phenomena. Linguistic descriptions of

variables enable to deal with systems which are much too complex to be susceptible to analysis in the conventional mathematical terms. Details on the concept of a linguistic variable and its applications can be found in Zadeh (1975).

9.3.2.2 Fuzzy Sets

A fuzzy set is a set of elements with an imprecise (vague) boundary. As opposed to classical set, a *fuzzy set* is a set without a crisp (rigid) boundary, i.e. the changeover from "belong to a set" to "not belong to a set" is gradual and this smooth changeover is characterized by membership (characteristic) function that gives fuzzy set the flexibility in modelling the commonly used linguistic expressions. For the problem modelled herein, a linguistic expression could be "submerged block is very high" or "submerged block is close to the centre of the tank" etc. Fuzzy sets theory aims at defining sets where belongingness or membership is a matter of degree. In other words, a fuzzy set is a class of objects with a continuum of grades of membership and such a set is characterized by a membership function which assigns to each object a grade of membership ranging between zero and one. Detail explanation to fuzzy sets can be found in Zadeh (1965)

Mathematically, if X is a collection of objects generically denoted by x, then a fuzzy set A in X is defined as a set of order pairs:

$$A = \left\{ \left(x, \mu_A(x) \right) \middle| x \in X \right\}, \tag{9.1}$$

where $\mu_A(x)$ is called the *membership value* (degree of belongingness) for the fuzzy set A. The membership function maps each element of X to the membership grade between 0 and 1. X is referred to as 'universe of discourse', or simply the universe. It may consist of discrete objects or continuous space.

9.3.2.3 Membership Functions

The membership function of a fuzzy set is a generalization of the indicator function (characteristic function) in classical sets. In fuzzy logic, it represents the degree of truth as an extension of valuation. Degrees of truth are often confused with probabilities, although they are conceptually different. Fuzzy truth represents membership in vaguely defined sets whereas probability represents likelihood of some

event or condition. Membership function decides the degree of belongingness of an element to a fuzzy set. Membership function specifies the degree to which an element or input satisfies the linguistic label or quantifier.

9.3.2.4 Fuzzy If-Then Rules (Fuzzy Linguistic Rules)

Linguistic *if-then* rules also known as fuzzy conditional statements characterize simple relations between fuzzy variables or linguistic variables in the similar manner as is done for characterization of the dependence between two numerically valued variables in case of quantitative system analysis. A single fuzzy "if-then" rule takes the form "if x is A then y is B" where A and B are linguistic labels of fuzzy sets characterized by appropriate membership functions. In case of more complex relation, fuzzy algorithm may be required for the characterization of dependence of x on y. The if-part of the rule is called the antecedent or premise while the then-part of the rule is called the consequent or resultant. Due to their succinct form, fuzzy if-then rules are often employed to capture the vague modes of reasoning that play an essential role in the human ability to make decisions in an environment of ambiguity and imprecision. Fuzzy *if-then* rules form a mainstay of the fuzzy inference system.

9.4 Implementation of ANFIS

An adaptive network-based fuzzy inference system is a synergy of artificial neural networks (ANN) and fuzzy inference systems (FIS), which judiciously takes on the strengths and eliminates the limitations of both the systems. The features thus acquired complement each other and improve the modelling efficiency of the new system called ANFIS. A neural network has the ability to learn from data, however, understanding the knowledge or the pattern learned by it has been difficult and hence not easy to implement, particularly, in the situation of uncertainty or imprecision. Fuzzy inference system (FIS), on the other hand, although easy to implement due to linguistic *if-then* rules, faces difficulties in system modeling due to lack of definite criteria for selection of shape of membership functions, their degree of overlapping and above all optimization of system parameters. An integration of ANN and FIS can build a versatile intelligence system where neural network with their learning capabilities is made to learn fuzzy decision rules; thus creating a hybrid intelligent system.

In the present work, an adaptive network based fuzzy inference system (ANFIS) described as follows is implemented by using MATLAB with Fuzzy Logic Toolbox to determine the maximum sloshing wave elevation in rigidly fixed ground supported partially filled rigid rectangular tank with submerged internal components of varying dimensions and positions.

Two sets of data base for sloshing elevation, due to an equal number of earthquake motions, created by numerical experiment using linear FEM model developed as in chapter 3 and described as in 9.2, are used for ANFIS modelling. The data sets correspond to two earthquakes of two different frequency content - low frequency content and high frequency content. It is observed from the numerical result that the sloshing elevation is governed by the height (h/d) and position (b/L) of the baffle inside the tank for a given tank dimension and liquid fill depth. It is to be further noted that frequency content of ground motion has considerable influence on the sloshing response of the liquid. Although, earthquakes can be categorised into three distinct classes depending upon the frequency content (PGA/PGV ratio), yet within one category of earthquake, there can be a whole lot of earthquakes with distinct PGA/PGV values, whose characteristics as regard to the sloshing may be significantly different from other earthquakes in the same category. It is pertinent to mention that earthquakes can be characterized in many different ways based on their peak ground acceleration, peak ground velocity, peak ground displacement, duration of earthquake, significant duration, etc. In the present study, however, we have selected two earthquakes - one from low frequency category and the other from high frequency category to study as to how the sloshing response of liquid in the tank due to earthquake of one category differs from that due to the other. Further, the main objective of the present study is to assess the potential of ANFIS for prediction of sloshing elevation.

Hence, it is decided to go for three different ANFIS models for an equal number of earthquakes, each with a distinct value of PGA/PGV ratio. Thus, relative height ($h/d = h_r$) and position ($b/L = b_r$) of the baffle are considered as two input variables whereas maximum sloshing elevation (η) is considered as the only output variable.

In the present investigation, type-3 ANFIS (Jang, 1993) topology based on first-order Takagi–Sugeno (TSK) (Takagi & Sugeno, 1985) if-then rules has been used.

9.4.1 Architecture and Basic Learning Rules

A typical first-order TSK fuzzy inference system with two inputs and one output can be expressed in the following form. Suppose that the rule base contain *N* number of fuzzy if-then rules of Takagi-Sugeno type, the *i*th rule may be written as follows:

Rule *i*:

If h_r is A_j and b_r is B_k, then $f_i = p_i h_r + q_i b_r + r_i$

Where $j = 1 \ldots, N_1$;

$k = 1 \ldots, N_2$;

and $i = 1, \ldots\ldots., N_1 \times N_2$

A and *B* are the fuzzy sets defined on input variables h_r and b_r respectively. N_1 and N_2 indicate the number of membership functions covering the universe of discourse defined by the indicated fuzzy input variables; f_i is a linear consequent function of *i*th node defined in terms of the input variables and *p*, *q* and *r* are linear coefficients referred to as consequent parameters of the first order Takagi–Sugeno fuzzy model (1985). In this model, node functions in the same layer belong to the same function family as described below. The output of the *i*th node of *j*th layer is denoted as O^j_i.

A schematic diagram of fuzzy inference system composed of five layers with three inputs and one output is illustrated in Figure 9.3. The inference system involves several nodes in each layer. The output signals from the nodes of one layer are accepted as the input signals in the subsequent layers which on manipulation by the respective node functions in the current layer are served as the input signals for the next layer.

Layer 1:

The first layer of ANFIS architecture represents a fuzzy layer. Represented by a square, each node of this layer generates membership grade of a linguistic label (***low, high*** etc.). The nodes in this layer are adaptive nodes. By adaptive nodes, it is meant that the outputs of the nodes depend on the parameter(s) relating to these nodes and the learning rule stipulates the changes in the parameters so as to minimize a prescribed error measure. The relationship between the input to and output from a node in this layer may be expressed as

$$O_j^1 = \mu_{A_j}(h_r), \qquad j = 1, ..., N_1 \tag{9.2}$$

$$O_k^1 = \mu_{B_k}(b_r), \qquad k = 1, ..., N_2 \tag{9.3}$$

where h_r and b_r are the crisp inputs to nodes j and k respectively; A_j, and B_k, are the linguistic labels associated with corresponding node functions. In other words, O_j^1 and O_k^1 are the membership functions of A_j and B_k, and they specify the respective degrees to which the inputs h_r and b_r satisfy the quantifiers A_j and B_k . Any appropriately parametrized continuous and piecewise differentiable functions, such as commonly used triangular-shaped, trapezoidal, Gaussian, generalized bell-shaped, and sigmoid etc are qualified candidates for membership functions (MFs) in this layer. One such membership function, the Gaussian function is given as

$$Gaussian(x, c, \sigma, m) = \exp\left\{-\frac{1}{2}\left(\frac{x-c}{\sigma}\right)^m\right\} \tag{9.4}$$

where $\{c, \sigma, m\}$ is the parameter set of the membership function, where c represents the centre of membership function, σ represents the width of MF, and m is the fuzzification factor (e.g., m = 2). As the values of these parameters change, the Gaussian functions vary accordingly, thus displaying various forms of membership functions on the associated linguistic labels. Parameters in this layer are referred to as "premise parameters" or "antecedents".

Layer 2:

Nodes in this layer are represented by circles labelled as Π. Each node in this layer multiplies the incoming signals from the previous layer and sends out the product as firing strength that serves as the input for the next layer. The operation carried out in this layer is referred to as T-norm operation. For example,

$$O_i^2 = \mu_{A_j}(h_r)\mu_{B_k}(b_r) = \omega_i \tag{9.5}$$

where ω_i is the firing strength of ith rule, also called the "degree of fulfilment or degree of satisfaction" of the fuzzy rule. It represents the degree to which the antecedent part of the rule is satisfied.

Layer 3:

Labelled as *N*, each node in this layer is a circular node. The nodes in this layer are fixed nodes. Nodes of this layer normalize the firing strength of each rule i.e., *i*th node computes the ratio of the firing strength of *i*th rule to the sum of the firing strengths of all rules. For instance,

$$O_i^3 = \overline{\omega}_i = \frac{\omega_i}{\sum_{i=1}^{N_1 N_2} \omega_i} \tag{9.6}$$

Layer 4:

Nodes in this layer are square nodes and are adaptive. The node function of each node in this layer computes the contribution of each rule toward the total output and the *i*th node function may be expressed as:

$$O_i^4 = \overline{\omega}_i f_i = \overline{\omega}_i \left(p_i h_r + q_i b_r + r_i \right) \tag{9.7}$$

where ω_i is the output of layer 3 and $\left(p_i, q_i, r_i \right)$ is the parameter set. Parameters in this layer are referred to as "consequent parameters".

Layer 5:

This layer has a single fixed node represented by a circle and labelled as $\sum$. This node computes the overall output as the summation of contributions from each rule. Mathematically,

$$O_i^5 = \sum_{i=1}^{n} \overline{\omega}_i f_i \tag{9.8}$$

where *n* is the total number of rules and is equal to N_1 x N_2.

The network thus explained is an adaptive network known as adaptive neuro-fuzzy inference system and is functionally equivalent to a type 3 fuzzy inference system illustrated in Figure 9.3. Figure 9.4 depicts a typical architecture of two inputs and one output, type 3 adaptive neuro-fuzzy inference system (ANFIS) with *n* rules.

9.4.2 Hybrid Learning Algorithm

Hybrid learning rule proposed in the present ANFIS model combines gradient method and the least squares estimate (LSE) to identify and update the parameters in an

adaptive network. Each epoch of this hybrid learning procedure is composed of a forward pass and a backward pass. This type of hybrid learning is known as *batch learning* or *off-line learning*. In this paradigm of learning, the update action takes place only after the whole training data set has been presented, i.e., only after each *epoch* or *sweep***.** In the forward pass of the hybrid learning algorithm, functional signals go forward till layer 4 and the consequent parameters (p_i, q_i, r_i) are identified by the least squares estimate and error measure (sum of squared error) is calculated. In the backward pass, the error rates (derivative of error measure with respect to each node output) so calculated propagate backward and the premise parameters (c, σ) are updated by the gradient descent. Table 2 summarizes the activities in each pass. The consequent parameters thus identified are optimal under the condition that the premise parameters are fixed. The hybrid learning rule not only decreases the dimension of the search space in the gradient descent method (also called back-propagation method), but, in general, also substantially reduces the convergence time (Jang 1993, Jang et al., 1997). Thus, the hybrid learning rule substantially speeds up the learning process.

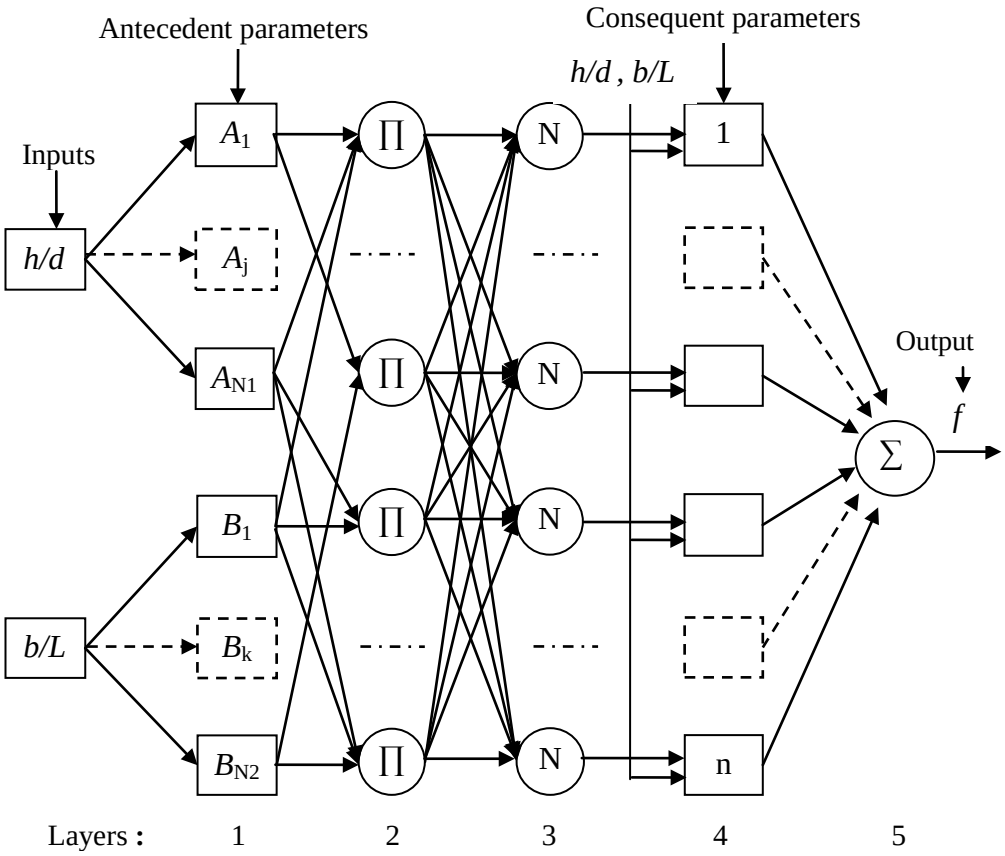

Figure 9.4: A typical type III Takagi-Sugeno ANFIS architecture

Table 9.2: Two passes in the hybrid learning procedure of ANFIS

	Forward pass	Backward pass
Premise parameters	Fixed	Gradient descent
Consequent parameters	Least-square estimate	Fixed
Signals	Node outputs	Error rates

9.5 Model Design

Herein, modelling of the sloshing response of the liquid in a baffled tank due to two ground motions, each of different frequency content with their peak accelerations scaled to a constant amplitude of 0.2g, is realized using ANFIS. The data used in the modelling did not require normalization as there was parity in the values in the data set and the differences between the maximum and minimum values of the input variables are not very high in which case the data may require normalization. In the present data set, however, the input variables, relative baffle height (*h/d*) and relative baffle position (*b/L*) as well as the output variable, maximum sloshing elevation (η), are within narrow ranges. The resulting data set obtained from numerical simulation is divided into training and testing data. Out of 71 data, two-third of the data is selected as training data set and one-third is used as testing data set.

It is decided to go for independent models for earthquakes of distinct frequency content as it is not possible to incorporate frequency content of earthquake as an input variable in which case this may require a large number of earthquakes, at least four to five earthquakes from each frequency content category. However, the objective of the present study is to investigate the potential of ANFIS in prediction of sloshing response. It is to be worth mentioned that the frequency content of earthquake is based on the ratio of peak ground acceleration (PGA) to the peak ground velocity (PGV) which is an accepted parameter for defining the frequency content of earthquakes. On the basis of PGA/PGV ratio, the earthquake records are classified into three frequency content categories: high (PGA/PGV > 1.2), intermediate (0.8< PGA/PGV< 1.2) and low (PGA/PGV < 0.8) (Heidebrecht and Lu, 1988). In this study two earthquakes, one each from low and high frequency category, are selected. Two different ANFIS models, one for low frequency content earthquake of Imperial Valley and the other for high frequency earthquake of San-francisco are constructed

in the present study to predict the sloshing response of liquid in the tank. Finally, a different approach is tried out to accommodate both earthquakes in one model wherein frequency content has been considered as an additional independent input variable. Although earthquakes do have A/V values to define their frequency content, frequency content can not be exclusively used as an input variable as only two earthquakes are considered in this study. Therefore two earthquakes under considerations have been arbitrarily assigned two distinct values of 0 and 1 as input variables. Low frequency earthquake of Imperial Valley has been assigned a distinct value of 0 whereas high frequency earthquake of San-francisco has been assigned 1. Had there been sloshing response data for a number of earthquakes over wide range of frequency content, A/V ratio could have been assigned as the input variable defining the frequency content of respective earthquakes.

Table 9.3: Characteristic information of ANFIS architecture

ANFIS characteristics	Imperial Valley	San-francisco	Combined model
Number of input variables (*n*)	2	2	3
Number of output variables	1	1	1
Number of fuzzy partitions or number of membership functions	3-3	3-3	2-3-3
Number of input membership functions	6	6	8
Number of rules	9	9	18
Input membership function parameters	18	24	24
Output membership function parameters	27	27	72
ANFIS model type	Sugeno	Sugeno	Sugeno
Input MF type	gbellmf	Gauss2mf	gbellmf
Output MF type	linear	linear	linear
ANFIS training method	hybrid	hybrid	hybrid
Defuzzification method	wtaver	wtaver	wtaver

The data for training is suitably selected so as to train the model possibly within a wide range of the input variables in order to enable the model to capture the details of the features of the input-output mapping. During training, five layered ANFIS models are constructed. The flow chart for the complete approach including the ANFIS algorithm is presented in Figure 9.5. The network was run on MATLAB platform using Pentium IV PC. The numbers of membership functions are chosen to be 3-3 corresponding to the inputs, *h/d* and *b/L* for the two individual models for Imperial Valley and San-francisco. The number of membership functions for the combined model is chosen to be 2-3-3 corresponding to the inputs; earthquake type (EQ), relative baffle height (*h/d*) and relative baffle position (*b/L*). The selection of the types of membership functions for different models are based on the training–testing result and the one producing the best result has been finally accounted in the developed model. A summary of the characteristics of the ANFIS networks is presented in Table 9.3

In order to assess the effectiveness of models and their ability to make precise predictions, their performances are evaluated by using three statistical performance criteria namely; root mean square error (RMSE), coefficient of determination (R^2), mean percentage error (MPE), and mean absolute percentage error (MAPE) as follows:

$$\text{RSME} = \left((1/n) \sum_{i=1}^{n} |t_i - o_i|^2 \right)^{1/2} \tag{9.9}$$

$$\text{R}^2 = \left(\frac{\sum_{i=1}^{n} (t_i - o_i)^2}{\sum_{i=1}^{p} o_i^2} \right) \tag{9.10}$$

$$\text{MPE} = \frac{1}{n} \sum_{i=1}^{n} \left(\frac{t_i - o_i}{t_i} \right) \times 100 \tag{9.11}$$

$$\text{MAPE} = \frac{1}{n} \sum_{i=1}^{n} \left(\left| \frac{t_i - o_i}{t_i} \right| \right) \times 100 \tag{9.12}$$

where ‘*t* ‘ is the target value or observed value and ‘*o*’ is the predicted or output value and ‘*n*’ is the number of data items.

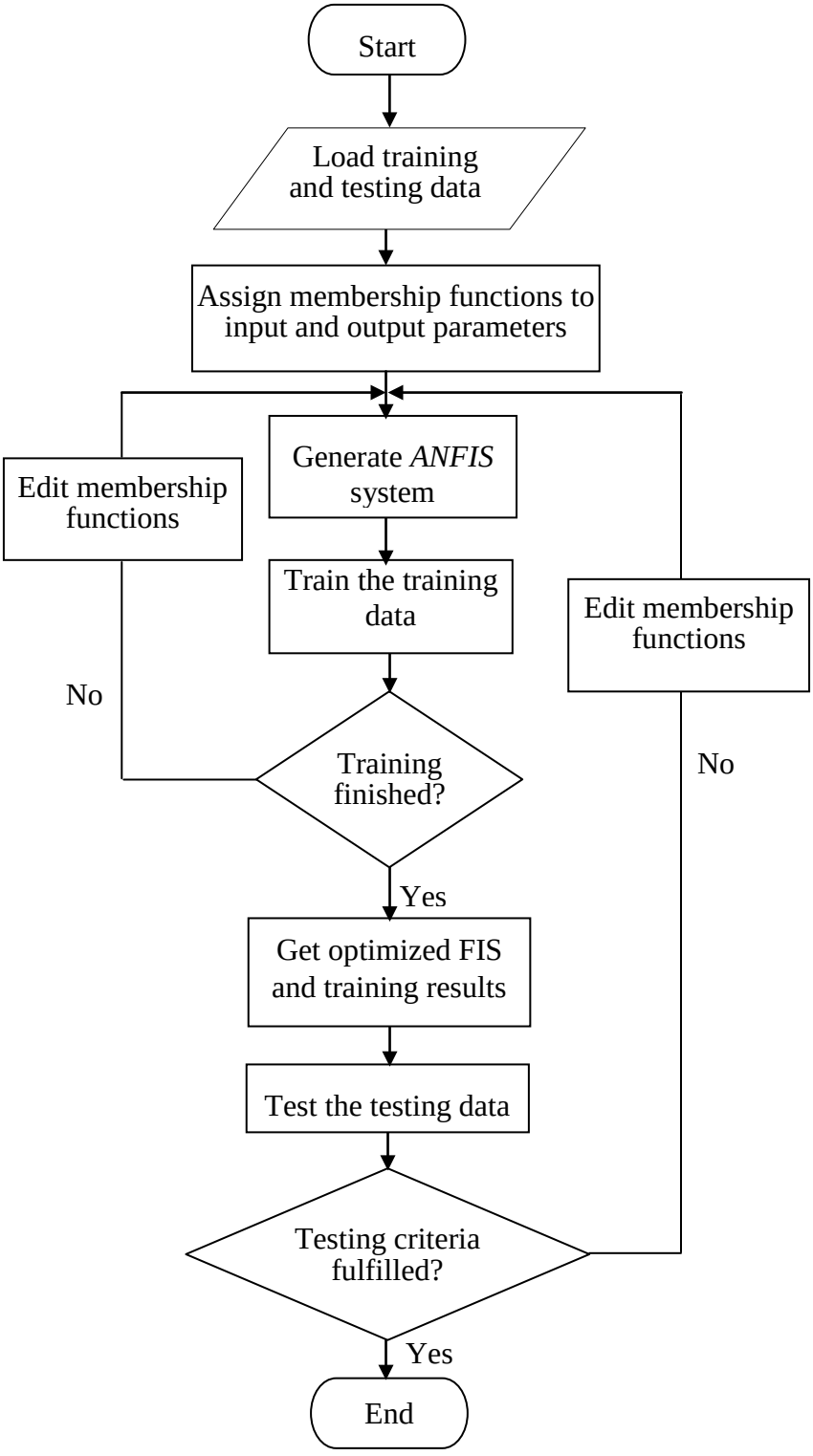

Figure 9.5: Flow chart for the ANFIS models

9.6 Results and Discussion

As has been said in the previous section, three different models have been developed. Figure 9.6 - 9.8 demonstrates the post-trained membership functions of the input variables for the three developed models - one each for Imperial Valley and San-francisco earthquake data and one for the combined data of both the earthquakes. On training, the membership parameters are automatically adjusted based on the input-output data in the entire decision space. The membership parameters so adjusted as to capture to the maximum extent all the features of both the input variables, *h/d* and *b/L*, within the range of their variation, vis-à-vis the output variable. A sample set of FIS properties, for the one for the combined ANFIS model, is presented in Figure 9.9

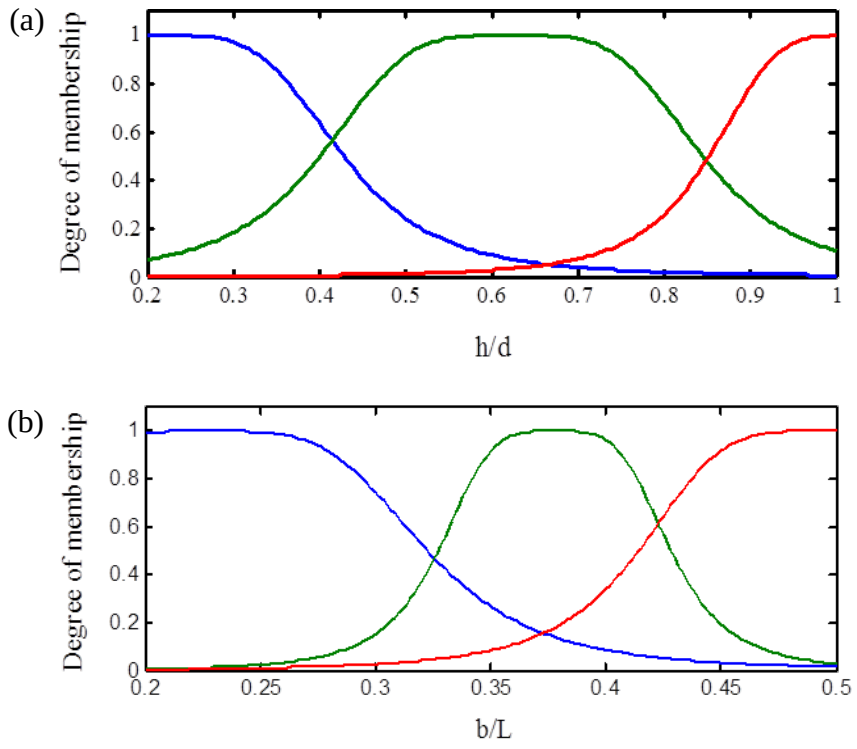

Figure 9.6: Generalized bell shaped membership function (gbellmf) plots for input variables for ANFIS model for Imperial Valley: (a) *h/d* (b) *b/L*

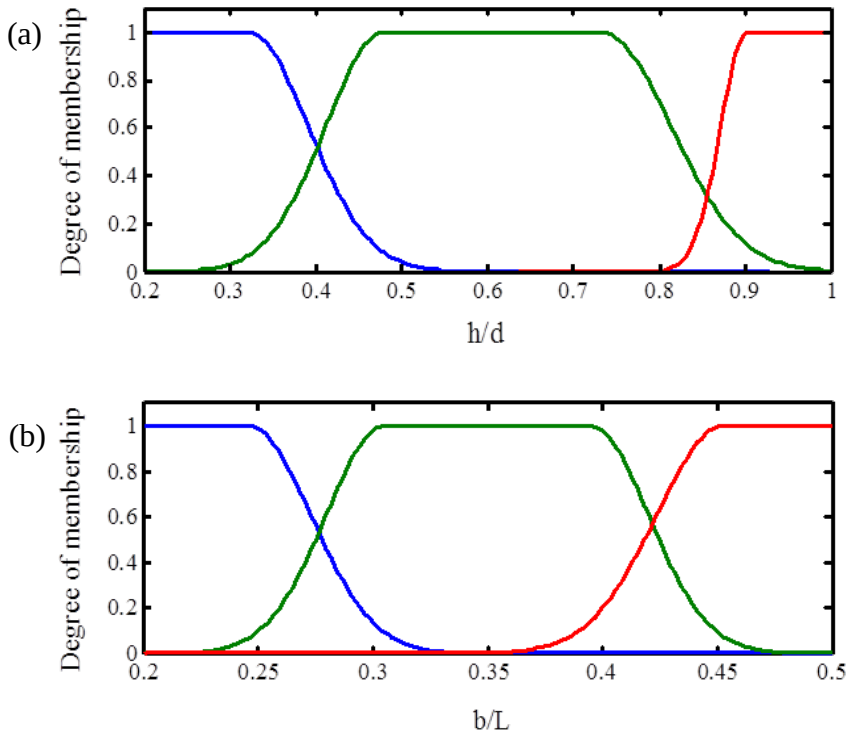

Figure 9.7: Gauss2mf membership function plots for input variables for ANFIS model for San-francisco : (a) *h/d* (b) *b/L*

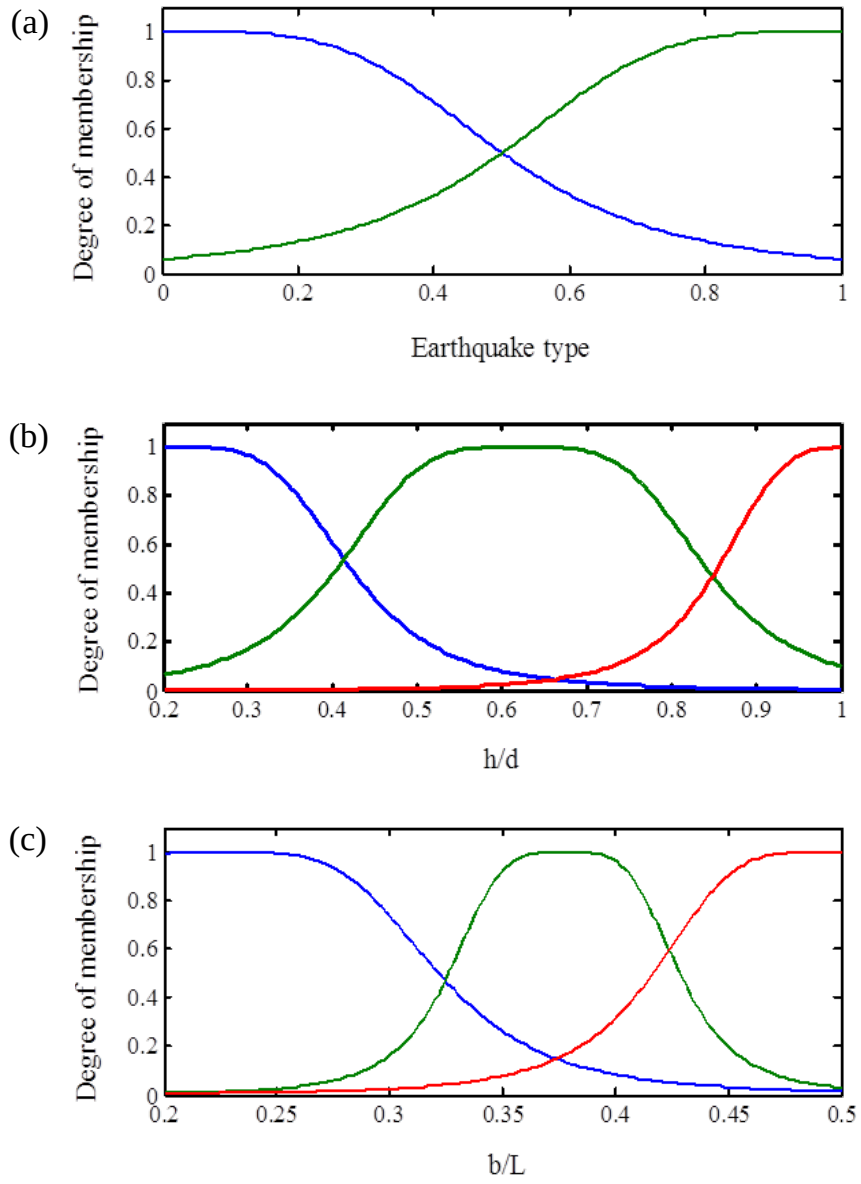

Figure 9.8: Generalized bell shaped membership function (gbellmf) plots for input variables for combined ANFIS model: (a) *h/d* (b) *b/L*

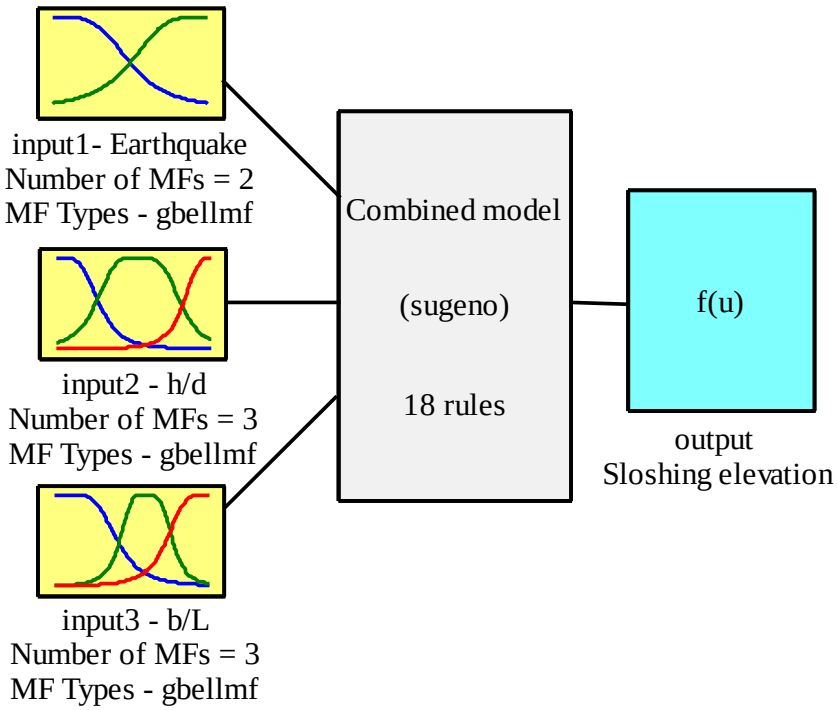

Figure 9.9: A sample set of FIS properties of adaptive neuro-fuzzy inference system for prediction of sloshing response (Combined model)

The sample set rule viewer of sloshing elevation mapping the inputs and output that describes the FIS is presented in Figure 9.10. Each row in the figure represents one rule and consists of the membership functions corresponding to each of the inputs. The numerals in the extreme left against each row represent the corresponding rule numbers. The last column in the figure is the one for the outputs corresponding to each rule. The aggregation of the output from each rule gives the final value of the output parameter over the output column for the given input values as shown in the figure over the input columns. It may be noted that each data set is combined into the FIS model by application of all logical “and”, “or”, and “not” relationships. The rule viewer can indicate only one calculation at a time along the depth. In the present rule viewer, depicted in the figure, the values of the inputs are; h/d = 0.6 and b/L = 0.2 while the corresponding output of sloshing elevation is 13.2 mm. The values at the bottom of the columns for input and output variables indicate the variation range of the respective variables.

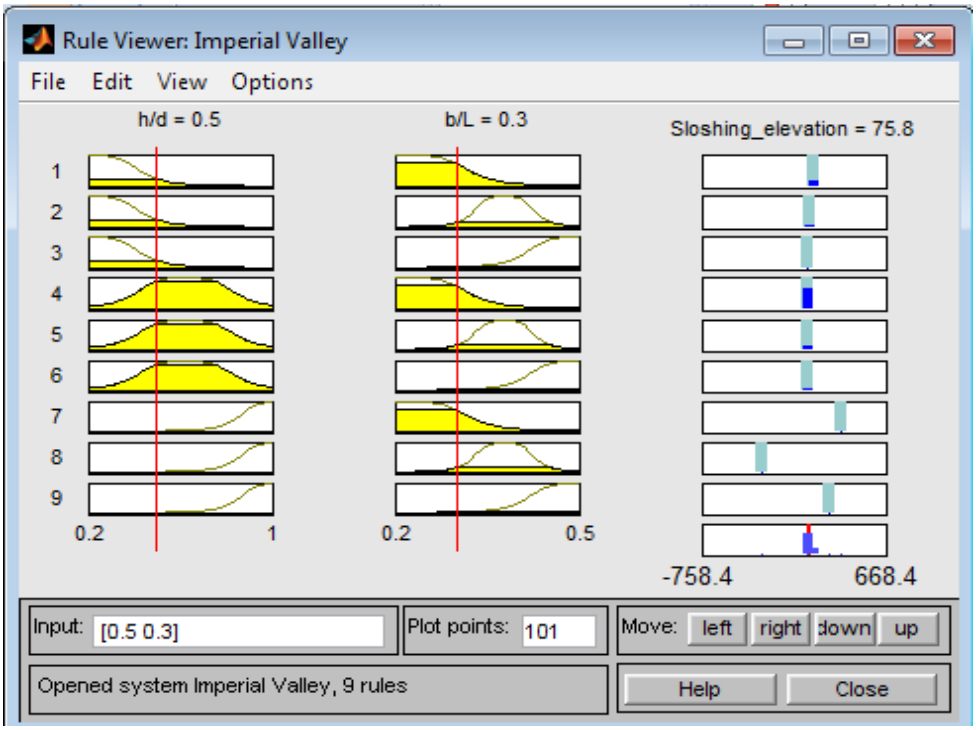

Figure 9.10: A sample set of ANFIS rule viewer for sloshing elevation due to ground motion of San-francisco

The effect of the input variables of baffle height and baffle position on the sloshing elevation is portrayed in the surface plots shown in Figure 9.11. It represents the contour of the output variable, sloshing elevation, over the landscape of decision space defined by the input variables, relative baffle height (*h/d*) and baffle position (*b/L*). It illustrates the trend of variation of sloshing elevation as regard to the variation in the inputs.

In case models based on individual data set for Imperial Valley and San-Francisco earthquakes, there are only two input variables and one output variable. Hence, three dimensional domain of the surface plot suffices to describbe the trend of variation of output vis-à-vis the input variable in all completeness. However, in case of combined model with three input variables, the surface plot can only demonstrate the variation trend of the output variable with respect to any two input variables while requiring to define a fixed value for the third input variable. For the combined model, the surface plots for sloshing variation due to Imperial Valley and San-Francisco are retrieved by defining their respective assigned variable for earthquake type. In this case 0 and 1 are

the assigned variables of earthquake type for Imperial Valley and San-Francisco respectively.

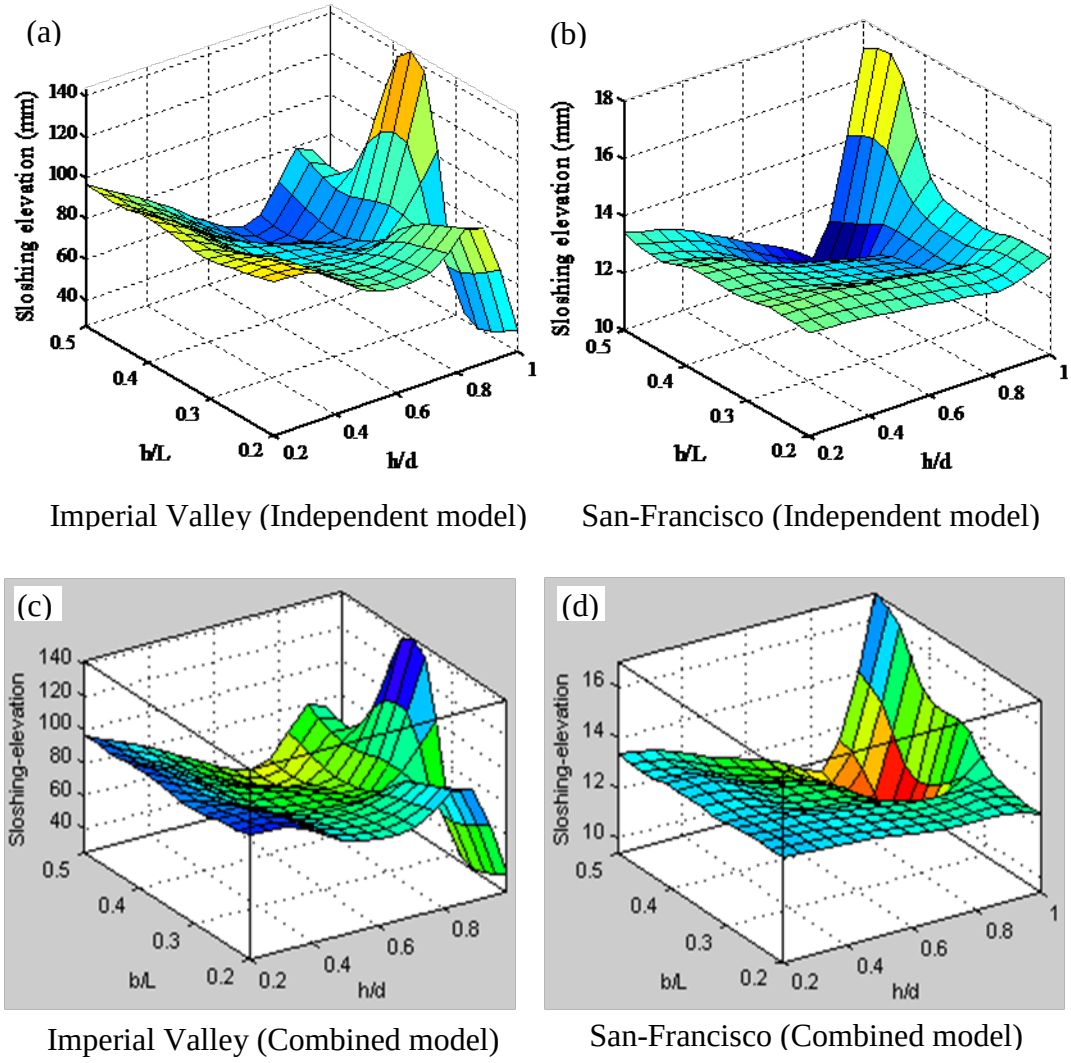

Imperial Valley (Independent model)

San-Francisco (Independent model)

Imperial Valley (Combined model)

San-Francisco (Combined model)

Figure 9.11: Surface plot of sloshing elevation obtained from individual and combined models: (a) Surface plot for Imperial Valley from independent model (b) Surface plot for San-Francisco from independent model (c) Surface plot for Imperial Valley from combined model (d) Surface plot for San-Francisco from combined model

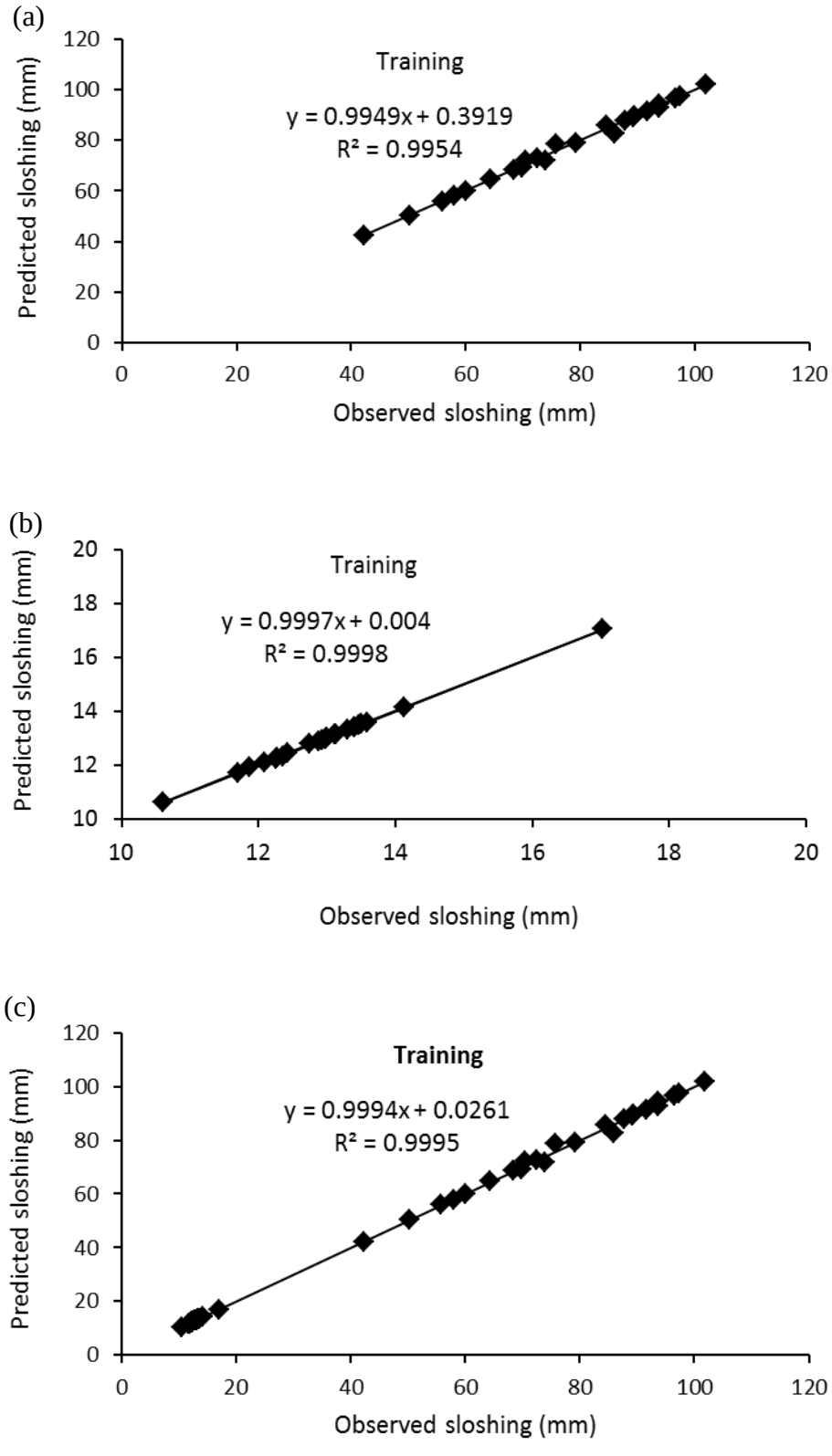

Figure 9.12: Correlation of predicted and actual data (training) for ANFIS models: (a) Imperial Valley (b) San-Franscisco (c) Combined model

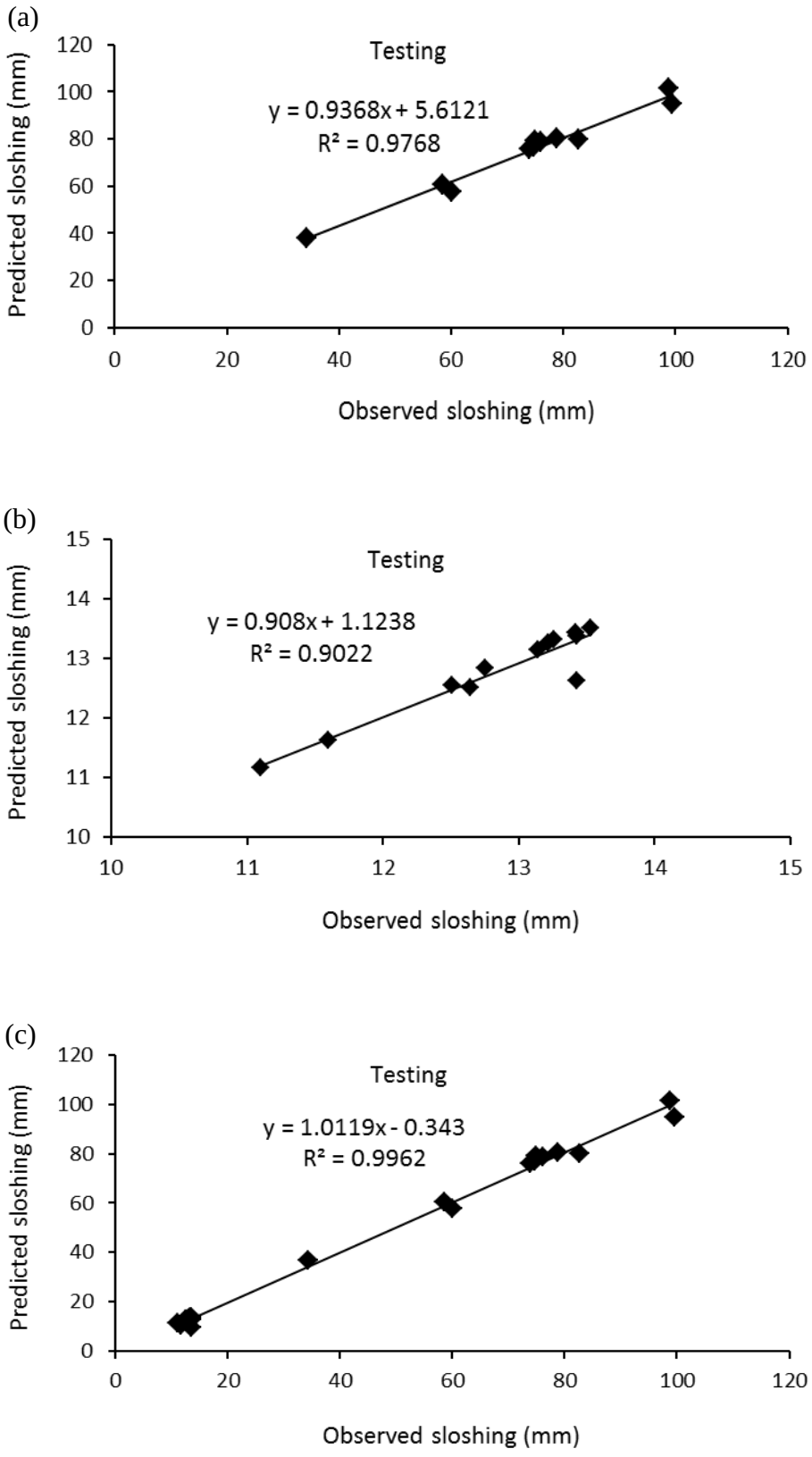

Figure 9.13: Correlation of predicted and actual data (testing) for ANFIS models: (a) Imperial Valley (b) San-Franscisco (c) Combined model

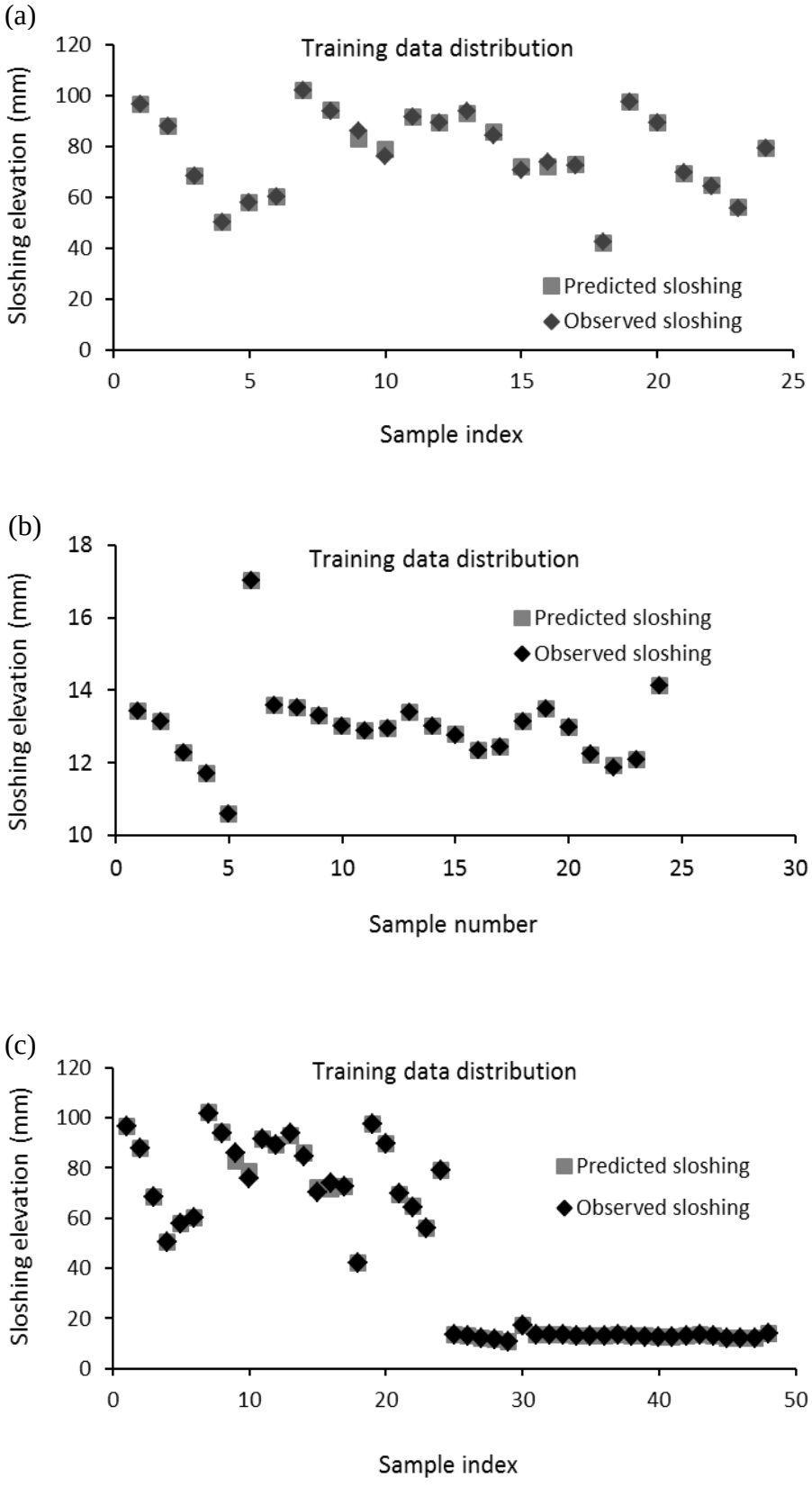

Figure 9.14: Comparison of actual and predicted sloshing (training data) for ANFIS models: (a) Imperial Valley (b) San-Franscisco (c) Combined model

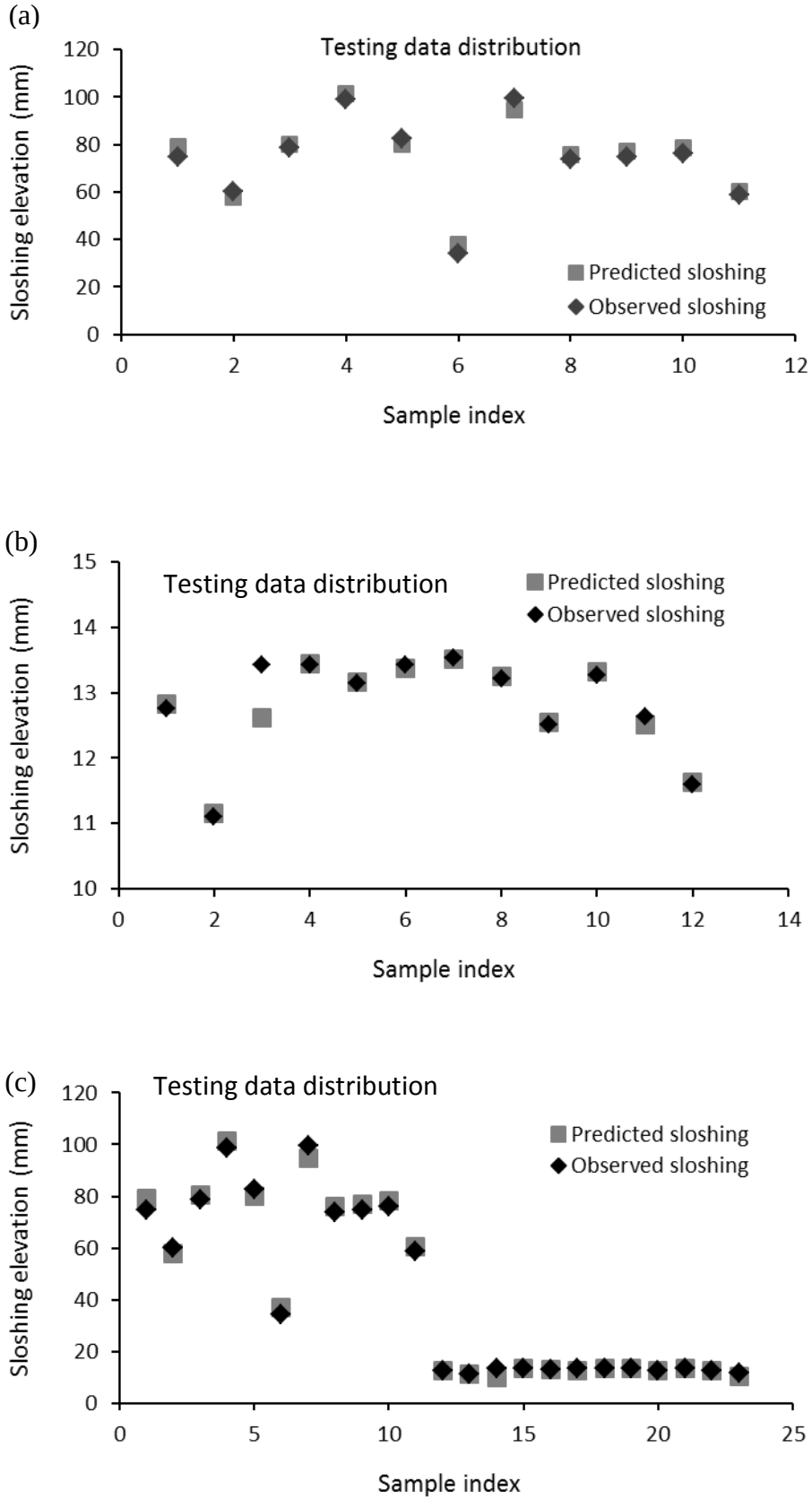

Figure 9.15: Comparison of actual and predicted sloshing (testing data) for ANFIS models: (a) Imperial Valley (b) San-Franscisco (c) Combined model

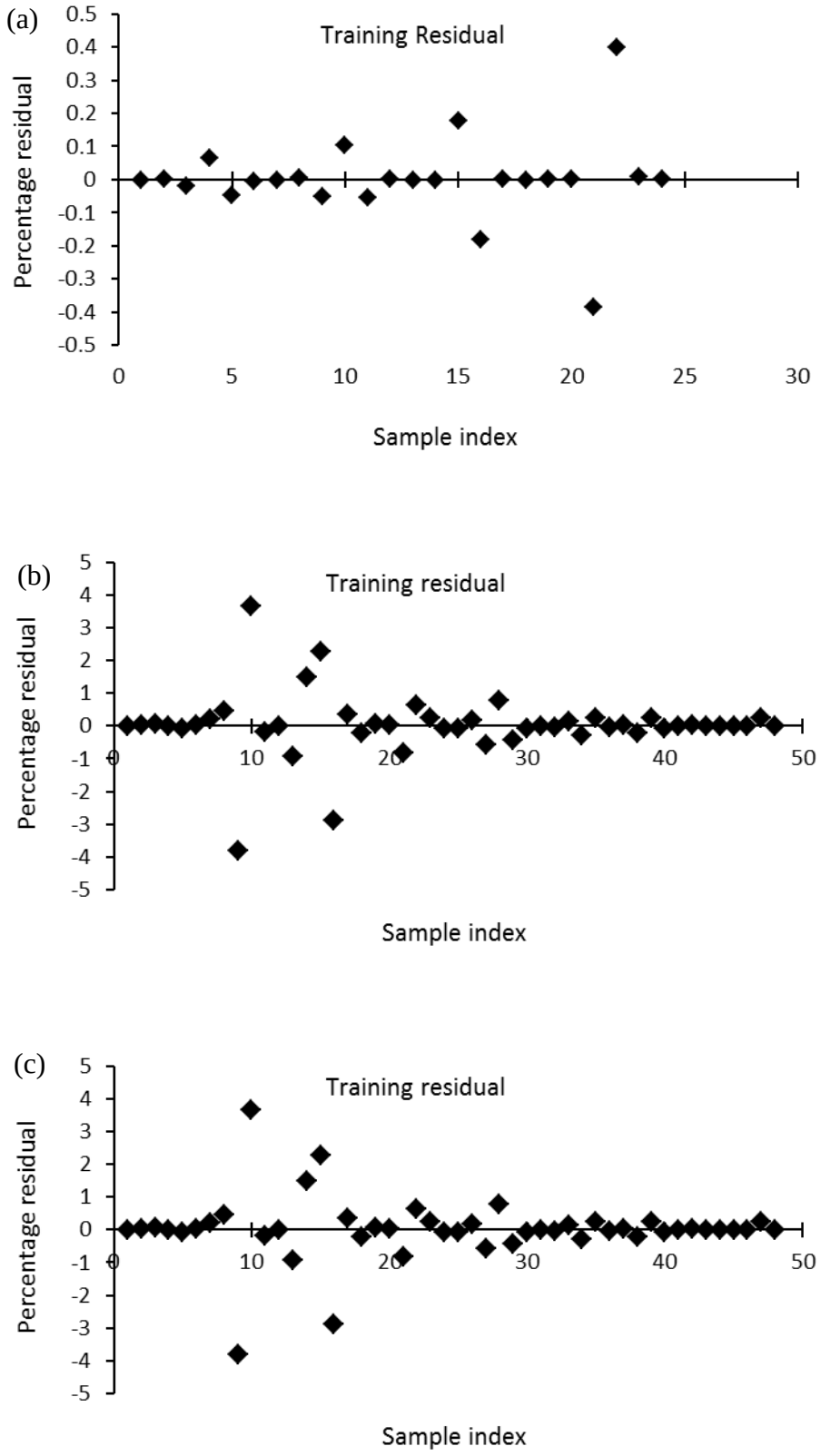

Figure 9.16: Residual distribution of training data: (a) Imperial Valley (b) San-Franscisco (c) Combined model

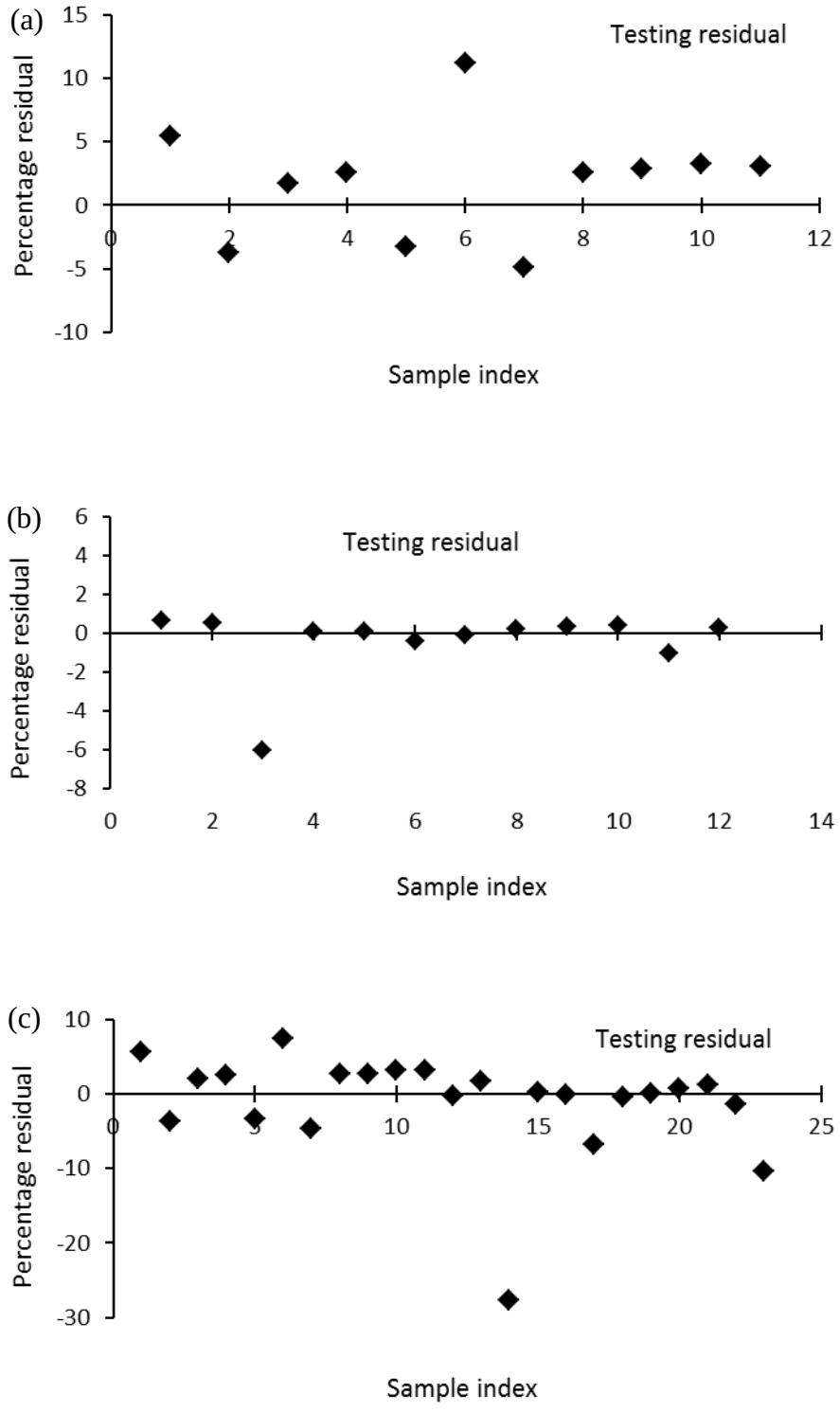

Figure 9.17: Residual distribution of testing data: (a) Imperial Valley (b) San-Franscisco (c) Combined model

The regression curves for all the models are plotted in Figures 9.12 and 9.13 between actual sloshing elevation and predicted sloshing elevation via ANFIS model for training data and testing data respectively. As high values of coefficient of determinations (R^2) are obtained, it can arguably be said that the models possess a greater degree of reliability as far as their predictive abilities are concerned. In Figures 9.14 and 9.15, it can be observed that predicted data pattern follows actual data with little or no exception which thus demonstrates that the models predict the pattern of the data distribution with adequate accuracy. The residual analysis is carried out by calculating the residuals from the actual sloshing data and predicted sloshing data for training data set and testing data set. The residuals are plotted with the sample index as shown in Figures 9.16 and 9.17 for training and testing data sets respectively. It shows that the residuals are distributed evenly along the centerline of the plots. From this illustration, it can be said that the data is well trained and tested, and incorporated the variation pattern and non-linearity that exists between sloshing elevation and baffle parameters.

The performance of the models are also expressed in terms of various statistical parameters such as correlation co-efficient (r), root mean square error (RMSE), coefficient of determination (R^2), mean percentage error (MPE), mean absolute percentage error (MAPE), minimum absolute error (%) and maximum absolute error (%). The values of the above statistical parameters as measures of model performance are presented in Tables 9.4 and 9.5 for training and testing data.

Based on the above statistical parameters, it can arguably be said that the slosh prediction potential of ANFIS is quite promosing and can be used as a supplimentary tool along with the analytical, numerical and experimental analysis of sloshing. The present study suggests that judicious use of ANFIS can thus supplement and complement already existing methodologies in the field of slosh dynamics.

Table 9.4: Statistical performance on training of ANFIS models

	Imperial Valley	San-franscisco	Combined model
Correlation co-efficient, r	0.9949	0.9997	0.9994
Root mean square error (RMSE)	1.0807	0.0194	0.7757
Coefficient of determination (R^2)	0.9954	0.9998	0.9995
Mean percentage error (MPE)	0.0199	0.0002	0.0103
Mean absolute percentage error (MAPE)	0.7570	0.0629	0.4634
Minimum absolute error (%)	0.0035	0.0007	0.0014
Maximum absolute error (%)	3.8164	0.3976	3.8204

Table 9.5: Statistical performance on testing of ANFIS models

	Imperial Valley	San-franscisco	Combined model
Correlation co-efficient, r	0.9368	0.9080	1.0119
Root mean square error (RMSE)	2.9197	0.2395	2.0929
Coefficient of determination (R^2)	0.9768	0.9022	1.0119
Mean percentage error (MPE)	1.9018	-0.4137	1.1149
Mean absolute percentage error (MAPE)	4.0691	0.8475	3.9824
Minimum absolute error (%)	1.7523	0.0913	0.0582
Maximum absolute error (%)	11.1732	6.0082	27.6239

9.7 Conclusion

Adaptive neuro-fuzzy inference system (ANFIS) has been successfully used for the modelling of sloshing behaviour of a rigid rectangular tank with bottom-mounted vertical baffle. Three different ANFIS models; one each for low and high frequency ground motion as external excitation, and the third one, a combined model were developed taking into the input data of both low and high frequency ground motions. Each one of them was based on a different type of the membership function: a gbellmf, a Gauss2mf and a gbellmf membership function. The investigation revealed that ANFIS modelling accuracy is not considerably affected by the type of membership function employed. Several statistical parameters were used to evaluate the model performance of this novel computational tool.

ANFIS modeling is basically a physics independent and data-driven method that correlates input with output values in order to establish a model describing the relationship between them. Simulation results reveal that ANFIS is an efficient and promising tool.

The generated models can predict the sloshing elevation with a reasonable degree of accuracy with coefficient of determinations close to almost 1.0. The residual analysis carried out as well as the statistical parameters computed justify the predictive accuracy of the models. Accuracy in the simulation results demonstrates that ANFIS is an efficient and promising tool for predicting seismic response of partially filled tanks.

CHAPTER 10

10 SUMMARY, CONCLUSIONS AND RECOMMENDATIONS

10.1 Summary

The main objective of the present study was the time-history seismic response analysis of partially filled rectangular liquid tanks with bottom-mounted submerged internal components subjected to lateral earthquake motions of different frequecy content. The primary concern was to study the effect of submerged component on the hydrodynamic responses of the tank vis a vis frequency content of the earthquakes. The problem was kept simple by way of the analysis of rigid tanks because the rigid tank solution helps to identify, by reference to the simplest possible system, the essential features of the problem. Hence, the present analysis consciously followed the rigid tank assumption, leaving tank-liquid interaction or for that matter tank-soil interaction as a part of future scope of study. The effect of nonlinear sloshing on the sloshing elevation as well as the hydrodynamic respone was also one of the objectives of the study.

Keeping in view the objectives, two robust finite element models in two-dimensional space were developed, one model with linear sloshing and the other with nonlinear sloshing. The potential flow formulation was used for the development of the models. Mixed-Eulerian-Lagrangian procedure was adopted for tracking the fluid particles on the free surface in the nonlinear model. The developed models are capable of quantifying both the impulsive and convective response components of hydrodynamic response parameters such as hydrodynamic pressure on the tank as well as block wall,

base shear and overturning base moment including the sloshing elevation. The temporal variations of impulsive and convective response parameters were studied.

Further, an experimentally study on fluid damping was carried out in a model rectangular tank via shake table test. The major objective of the experimental investigation was to examine the relative effectiveness of various configurations of internal objects in slosh damping. Frequency response study of sloshing in rectangular tank fitted with three different configurations of centrally placed internal objects (bottom-mounted baffles, surface-piercing wall-mounted baffles, bottom-mounted submerged block) by means of *sine sweep test.* Free vibration study was carried for identification of important dynamic property of liquid-damping in term of hydrodynamic damping ratio. Also carried out was the dynamic response analysis of tank-liquid system with centrally placed internal objects subjected to sinusoidal horizontal excitation at resonant frequencies for evaluation of sloshing response. The relative effectiveness of various internal objects on sloshing damping was compared.

Finally, adaptive neuro-fuzzy inference system algorithm was used as a soft computing tool to to develop models for prediction of sloshing due different ground motion. The basic idea behind these neuro-adaptive learning techniques is very simple. These techniques provide a method for the fuzzy modelling procedure to acquire information about a data set, in order to compute the membership function parameters that best allow the associated fuzzy inference system track the given input/output data. Two ground motions were used for model development; one low frequency and the other high frequency. Three models were developed: one each for individual ground motion and the third, combining both the ground motion into one model. A number of statstical parameters were checked to asess the prediction efficacies of the models.

10.2 Conclusions

The conclusions are summarized in three different sections based on the methodologies and purpose of investigations.

A. Based on detailed finite element study of linear and nonlinear seismic response of rigid rectangular tank with submerged internal blocks, the following conclusions are drawn:

1. Presence of submerged internal component significantly influences the frequency characteristics of liquid in the container. Fundamental frequency is the most sensitive.
2. The effect of the bottom-mounted submerged blocks has a significant influence on the overall dynamics of the tank-liquid system and such effect differ considerably under seismic motions of different frequency content.
3. The impulsive component of hydrodynamic response parameter is almost independent of the frequency content and is dependent on the PGA which is a measure of intensity of earthquake.. However, frequency content of earthquake has considerable influence on the convective response component and such effect is considerably more in case of low frequency motion and hence on the overal tank dynamics.
4. In time domain analysis local temporal variation of nonlinear convective response and their contribution to total hydrodynamic forces is equally important if not more important than the absolute global peak response of total dynamic response and ought to be considered for the design of tank because of cumulative structural damage sustained by the tank.
5. Contrary to the generally accepted notion of dominancy of impulsive component on the hydrodynamic response, this study finds that although impulsive component dominates the hydrodynamic pressure in high frequency content earthquakes and also has a dominating share in total hydrodynamic response in all other ground motions, the convective components do also play an important role in low frequency earthquakes.
6. Moreover, in case of low frequency ground motion of Imperial Valley, increase in the height of submerged block greatly increases the convective response so much so that the total dynamic response is dominated by the convective component which is an antithesis to the result obtained for tank without any submerged block.
7. In addition, submerged blocks decrease the impulsive responses equally irrespective of the frequency content of the ground motion.

B. Based on experimental investigation of of sloshing in a miniature model rectangular tank, the following conclusions are drawn.

1. Presence of centrally installed internal object decreases the fundamental frequency of liquid and such decrease is monotonic with the increase in height of the internal object regardless of the configurations: bottom-mounted vertical baffle, surface-piercing baffles, and bottom-mounted submerged blocks.
2. Flow over a vertical baffle produces a shear layer and energy is dissipated by viscous effect of the fluid.
3. Hydrodynamic damping due to centrally placed internal objects is a function of relative liquid depth, relative baffle height, and position of baffle (bottom-mounted or surface piercing). The damping coefficient increases with relative baffle height.
4. With the top of the baffle approaching closer to the quiescent free surface, the damping ratio significantly increases. This fact is consistent with the flow dynamics as there is higher concentration of convective mass near the free surface of fluid block. The relative motion between the convective fluid block and the baffle helps in dissipating the sloshing energy and thus the increase in damping ratio.
5. Submerged blocks were found to reduce the fundamental sloshing frequencies more as compared to the bottom-mounted vertical baffles of similar heights. However, such reductions did not translate into increase in damping ratio. The reason may be ascribed to the fact that due to greater width of the submerged block the sharp edge effect gets diminished.
6. Surface-piercing baffles give higher damping than bottom-mounted baffles of similar heights and are effective over a wide range of excitation frequencies.

C. Based on the ANFIS models developed for prediction of sloshing elevation in tank due to ground motions of different frequency content, the following conclusion is drawn.

1. Adaptive neuro-fuzzy inference system is a potential soft computing tool for sloshing prediction.

10.3 Recommendations for Future Studies

1. Dynamic response of tank considering fluid and flexible wall interaction remains an area to be investigated in future study in which the structural nonlinearity due to flexible wall can also be studied.
2. Further studies with various tank geometries can also be carried out including the presence of submerged components.
3. The present analysis can be extended to three dimensional space to find out the effect of three-dimensional sloshing on the hydrodynamic response.
4. Analytical study of fluid damping due to the presence of baffle or submerged internal component is left as a future scope of study. The result enumerated in the present experimenal investigation can be used for validation of the the analytical model.
5. Experimental investigation of fluid damping with various baffle configurations can be carried out in tanks of different geometries such as horizontal cylindrical or elliptical tanks which are more commonly used for liquid transporting vehicles. Sloshing damping potential of vertical baffles with slots of different geometries; square, circular and elliptical can also be tested. Flexible baffles of similar configurations can also be tried out.
6. Other soft computing methodologies such as ANN, Genetic Algorithm, etc. can be tried out and their predictive capability can be compared with the results obtained from ANFIS in the current study.

REFERENCES

Abramson, H. N, (1966), “The dynamic behavior of liquids in moving containers”, NASA SP-106, National Aeronautics and Space Administration, Washington, D.C.

Agarwal, P. and Shrikhande, M., (2009), “Earthquake resistant design of structures”, PHI Learning Pvt Ltd., 18, 314.

Akyildız, H. and Unal, N. E., (2006), “Sloshing in a three-dimensional rectangular tank: Numerical simulation and experimental validation”, Ocean Engineering, 33, 2135–2149.

Akyildiz, H., (2012), “A numerical study of the effects of the vertical baffle on liquid sloshing in two-dimensional rectangular tank”, Journal of Sound and Vibration, 331, 41–52.

Akyildiz, H., Unal, N.E. and Aksoy, H., (2013), “An experimental investigation of the effects of the ring baffles on liquid sloshing in a rigid cylindrical tank”, Ocean Engineering, 59, 190–197.

Alembagheri, M. and Estekanchi, H.E., 2011, “Seismic assessment of unanchored steel storage tanks by endurance time method”, Earthquake Engineering and Engineering Vibration, 10(4), 591-604.

Almazan, J.L., Cerda, F.A., Llera, J.C.D.L. and Lopez-Garcıa, D., 2007, “Linear isolation of stainless steel legged thin-walled tanks”, Engineering Structures, 29, 1596–1611.

American Petroleum Institute, (1995), “Seismic Design of Storage Tanks - Appendix E: Welded Steel Tanks for Oil Storage (API Standard 650)”, Washington, DC.

Anderson, J. C. and Bertero, V. V., (1987), “Uncertainties in establishing design earthquakes”, Journal of Structural Engineering, ASCE, 113(8), 1709–1724.

Armenio, V. and Rocca, M.L., (1996), “On the analysis of sloshing of water in rectangular containers: numerical study and experimental validation”, Ocean Engineering, 23(8), 705-739.

ASCE Committee on Gas and Liquid Fuel Lifelines (Technical Council on Lifeline Earthquake Engineering), (1984), “Guidelines for the Seismic Design of Oil and Gas Pipeline Systems”, New York.

Askari, E. and Daneshmand, F., (2009), “Coupled vibration of a partially fluid-filled cylindrical container with a cylindrical internal body”, Journal of Fluids and Structures, 25, 389–405.

Askari, E. and Daneshmand, F., (2010), “Free vibration of an elastic bottom plate of a partially fluid-filled cylindrical container with an internal body”, European Journal of Mechanics A/Solids, 29, 68–80.

Askari, E., Daneshmand, F. and Amabili, M., (2011), “Coupled vibrations of a partially fluid-filled cylindrical container with an internal body including the effect of free surface waves”, Journal of Fluids and Structures, 27, 1049–1067.

Bakhshi, A. and Hassanikhah, A., (2008), “Comparison between seismic responses of anchored and unanchored cylindrical steel tanks”, 14 th World Conference on Earthquake Engineering, Beijing, China, October 12-17, 2008.

Banerji, P., Murudi, M., Shah, A. H. and Popplewell, N., (2000), “Tuned liquid dampers for controlling earthquake response of structures”, Earthquake Engineering and Structural Dynamics, 29, 587-602.

Bass, R.L., Bowles, E.B. and Cox, P.A., (1980), “Liquid dynamic loads in LNG cargo tanks”, SNAME Trans., 88, 103-126.

Bauer, H. F., (1964), “Fluid oscillations in containers of a space vehicle and their influence on stability”, NASA TR R-197, 1964.

Belakroum, R., Kadja, M., Mai, T.H. and Maalouf, C., (2010), “An efficient passive technique for reducing sloshing in rectangular tanks partially filled with liquid”, Mechanics Research Communications, 37, 341–346.

Berg, G. V. and Stratta, J. L., (1974), “Anchorage and the Alaska earthquake of 1964”, American Iron and Steel Institute, July, 1974.

Bertero, V.V., Anderson, J. C., Krawinkler, H. and Miranda, E., (1991), “The CUREe and Kajima Research Teams. 1991. Design Guidelines for Ductility and Drift Limits: Review of State-of-the-Practice and State-of-the-Art in Ductility and Drift-Based Earthquake-Resistant Design of Tall Buildings”, Berkeley, California: Earthquake Engineering Research Center, University of California at Berkeley. UCB/EERC-91/15.

Bertero, V. V., Herrera, R. A. and Mahin, S. A., (1976), “Establishment of design earthquakes - evaluation of present methods”, International Symposium on Earthquake Structural Engineering, St. Louis, Missouri.

Biggs, J. M., (1964), “Introduction to Structural Dynamics”, McGraw-Hill, New York.

Biswal, K. C., Bhattacharya, S. K. and Sinha, P. K., (2003a), “Dynamic characteristics of liquid filled rectangular tank”, Journal Institution Engineers (India), 84, 145-148.

Biswal, K.C., Bhattacharyya, S.K. and Sinha, P.K., (2003b), “Free-vibration Analysis of liquid-filled tank with baffles”, Journal of Sound and Vibration, 259, 177–192.

Biswal, K. C., Bhattacharya, S. K. and Sinha, P. K., (2004), “Dynamic response analysis of a liquid filled cylindrical tank with annular baffle”, Journal of Sound and Vibration, 68, 317-337.

Biswal, K.C., Bhattacharyya, S.K. and Sinha, P.K., (2006), “Non-linear sloshing in partially liquid filled containers with baffles”. International Journal for Numerical Methods in Engineering, 68 (3), 317–337.

Bouaanani, N., Goulmot, D. and Miquel, B., 2012, “Seismic Response of Asymmetric Rectangular Liquid-Containing Structures”, Journal of Engineering Mechanics, ASCE, 138(10), 1288-1297.

Bradley, B. A., (211), “Correlation of Significant Duration with Amplitude and Cumulative Intensity Measures and Its Use in Ground Motion Selection”, Journal of Earthquake Engineering, 15, 809–832.

Celebi, M. S. , Kim, M. H. and Beck, R. F., (1998), “Fully non-linear 3-D numerical wave tank simulation”, Journal of Ship Research, 42(1), 33-45.

Chatterjee, P. and Basu, B., 2001, “Non-stationary seismic response of tanks with soil interaction by wavelets”, Earthquake Engineering and Structural Dynamics, 30, 1419–1437.

Chatterjee, P. and Basu, B., 2004, “Wavelet-based non-stationary seismic rocking response of flexibly supported tanks”, Earthquake Engineering and Structural Dynamics, 33, 157-181.

Chen, B-F. and Chiang, H-W., (1999), “Complete 2D and fully nonlinear analysis of ideal fluid in tanks”, Journal of Engineering Mechanics, ASCE, 125(1), 70-78.

Chen, B-F. and Nokes, R., (2005), “Time-independent finite difference analysis of fully non-linear and viscous fluid sloshing in a rectangular tank”, Journal of Computational Physics, 209, 47–81.

Chen, W., Haroun, M. A. and Liu, F., (1996), “Large amplitude liquid sloshing in seismically excited tanks”, Earthquake Engineering and Structural Dynamics, 25, 653-669.

Chen, Y.G., Djidjeli, K. and Price, W.G., (2009), “Numerical simulation of liquid sloshing phenomena in partially filled containers”, Computers & Fluids, 38, 830–842.

Chen, J.Z. and Kianoush M.R., (2005), “Seismic response of concrete rectangular tanks for liquid containing structures”, Canadian Journal of Civil Engineering, 32, 739–752.

Chen, J.Z. and Kianoush,M.R., (2009), “Generalized SDOF system for seismic analysis of concrete rectangular liquid storage tanks”, Engineering Structures, 31, 2426-2435.

Chen, Y.H., Hwang, W.S. and Ko, C.H., (2007), “Sloshing behaviours of rectangular and cylindrical liquid tanks subjected to harmonic and seismic excitations”, Earthquake Engineering and Structural Dynamics, 36, 1701–1717.

Cho K. H., Kim, M. K., Lim, Y. M. and Cho, S. Y., (2004), “Seismic response of base-isolated liquid storage tanks considering fluid–structure–soil interaction in time domain”, Soil Dynamics and Earthquake Engineering. 24, 839–852.

Cho, J.R. and Lee, H.W., (2003), “Dynamic analysis of baffled liquid-storage tanks by the structural-acoustic finite element formulation”, Journal of Sound and Vibration, 258, 847–866.

Cho, J. R. and Lee, H. W., (2004), “Non-linear finite element analysis of large amplitude sloshing flow in two-dimensional tank”, International Journal for Numerical Methods in Engineering, 61, 514–531.

Cho, J. R. and Lee, S. Y., (2003), “Dynamic analysis of baffled fuel-storage tanks using the ALE finite element method”, International Journal for Numerical Methods in Fluids 41, 185–208.

Cho, J.R. and Lee, H.W., (2004), “Numerical study on liquid sloshing in baffled tank by nonlinear finite element method”, Comp. Methods Appl. Mech. Engng. 193, 2581–2598.

Cho, J. R., Lee, H. W. and Ha, S. Y., (2005) “Finite element analysis of resonant sloshing response in 2-D baffled tank”, Journal of Sound and Vibration, 288, 829–845.

Choun, Y.S. and C.B. Yun, (1996), “Sloshing characteristics in rectangular tanks with a submerged block”, Computers and Structures, 61(3), 401–413.

Choun, Y.S. and Yun, C.B., (1999), “Sloshing analysis of rectangular tanks with a submerged structure by using small-amplitude wave theory” Earthquake Engineering and Structural Dynamics, 28, 763–783.

Chwang, A. T. and Housner G.W., (1978), “Hydrodynamic pressures on sloping dams during earthquakes. Part 1. Momentum method”, Journal of Fluid Mechanics, 87(2), 335-341, Printed in Great Britain.

Cleary, W. A. Jr., (1982), “Subdivision, stability, liability”, Marine Technology, 19, 228-244.

Eswaran, M., Saha, U. K. and Maity, D., (2009), “Effect of baffles on a partially filled cubic tank: Numerical simulation and experimental validation”, Computers and Structures, 87, 198–205.

Comité Européen de Normalization, (1998), “Eurocode, 8, Part 4: Silos, Tanks and Pipelines (Annex A)”, CEN ENV-1998-4.

Cooper, T. W., (1997), “A study of the performance of petroleum storage tanks during earthquakes 1933-1995”, NIST GCR 97-720, National Institute of Standards and Technology

Curadelli, O., Ambrosini, D. Mirasso, A.and Amani, M., 2010, “Resonant frequencies in an elevated spherical container partially filled with water: FEM and measurement”, Journal of Fluids and Structures 26, 148–159.

Dodge, F. T., Kana, D. D. and Abramson, H. N., (1965), “Liquid surface oscillation in longitudinally excited rigid cylindrical containers”, AIAA Journal, 3, 685-695.

Dogangun, A., Durmus, A. and Ayvaz, Y., (1996), “Static and dynamic analysis of rectangular tanks using the Lagrangian fluid finite element”, Computers and Structures, 59(3), 547-552.

Dommermuth, D. G. and Yue, D. K. P., (1987) “Numerical simulations of nonlinear axisymmetric flows with a free surface”, Journal of Fluid Mechanics, 178, 195-219.

Dommermuth, D. G., Yue, D. K. P., Chan, E. S. and Melville, W. K., (1988) “Deep-water plunging beakers: A comparison between potential theory and experiments”, Journal of Fluid Mechanics, 189, 423-442.

Dutta, S.C., Dutta, S. and Roy, R., 2009, “Dynamic behavior of R/C elevated tanks with soil-structure interaction”, Engineering Structures, 31, 2617-2629.

Dutta, S., Mandal, A. and Dutta, S. C., 2004, “Soil–structure interaction in dynamic behaviour of elevated tanks with alternate frame staging configurations” Journal of Sound and Vibration. 277, 825–853.

Earthquake Engineering Research Institute, (1995a), “Northridge Earthquake Reconnaissance Report, Vol. 1” in Earthquake Spectra: EERI Supplement C to v. 11 (April issue), Oakland, California, pp. 239.

Edwards, N. W., (1969), “A procedure for dynamic analysis of thin walled cylindrical liquid storage tanks subjected to lateral ground motions”, Ph.D. Thesis, University of Michigan, Ann Arbor, Michigan.

EERI, “Loma Prieta Reconnaissance Report,” Earthquake Spectra, Earthquake Engineering Research Institute, Supplement to Vol. 6, May 1990.

El Damatty, A.A., Korol, R.M. and Mirza, F. A., 1997a, “Stability of elevated liquid-filled conical tanks under seismic loading, Part I-theory”, Earthquake Engineering and Structural Dynamics, 26, 1191-1208.

El Damatty, A.A., Korol, R.M. and Mirza, F. A., 1997b, “Stability of elevated liquid-filled conical tanks under seismic loading, Part II-application”, Earthquake Engineering and Structural Dynamics, 26, 1209-1229.

Epstein, H. I., (1976), “Seismic Design of Liquid-Storage Tanks”, Journal of the Structural Division, ASCE, 102(9), 1659-1673.

Evans, D.V. and McIver, P., (1987), “Resonant frequencies in a container with vertical baffle”, Journal of Fluid Mechanics, 175, 295–307.

Faltinsen, Odd M., (1974), “A nonlinear theory of sloshing in rectangular tanks”, Journal of Ship Research, 18(4), 224-241.

Faltinsen, Odd M., (1978), “A numerical nonlinear method of sloshing in tanks with two-dimensional flow”, Journal of Ship Research, 22(3), 193-202.

Faltinsen, Odd M., Rognebakke, O. F., Lukovskey, I. A. and Timokha, A. N., (2000), “Multidimensional modal analysis of nonlinear sloshing in a rectangular tank with finite water depth”, Journal of Fluid Mechanics, 407, 201-234.

Gavrilyuk, I., Lukovsky, I., Trotsenko, Yu. and Timokha, A., (2006), “Sloshing in a vertical circular cylindrical tank with an annular baffle. Part 1. Linear fundamental solutions”, Journal of Engineering Mathematics, 54, 71–88.

Gavrilyuk, I., Lukovsky, I., Trotsenko, Yu. and Timokha, A., (2007), “Sloshing in a vertical circular cylindrical tank with an annular baffle. Part 2. Nonlinear resonant waves”, Journal of Engineering Mathematics, 57(1), 57-78.

Gedikli, A. and Erguven, M.E., (1999), “Seismic analysis of a liquid storage tank with a baffle”, Journal of Sound and Vibration 223, 141–155.

Ghaemmaghami, A. R. and Kianoush, M. R., (2010), “Effect of wall flexibility on dynamic response of concrete rectangular liquid storage tanks under horizontal and vertical ground motions”, Journal of Structural Engineering, ASCE, 136(4), 441-451.

Goudarzi, M.A., Sabbagh-Yazdi, S.R. and Marx, W., (2010), “Investigation of sloshing damping in baffled rectangular tanks subjected to the dynamic excitation”, Bulletin of Earthquake Engineering, 8, 1055–1072.

Graham, E.W. and Rodriguez, A.M., (1952), “The characteristics of fuel motion which affects airplane dynamics”, Journal of Applied Mechanics, 19(3), 381-388.

Hamdan,F.H., (2000), “Seismic behaviour of cylindrical steel liquid storage tanks”, Journal of Constructional Steel Research, 53, 307–333

Hanson, R. D., (1973), Behavior of liquid.storage tanks, the great Alaska earthquake of 1964, National Academy of Sciences, 7, 1973.

Harlow, F. H. and Welch, J. E., (1966), “Numerical study of large-amplitude free surface motions”, The Physics of Fluids, 9 (5), 842-851.

Haruki, N., (2012), “Damage on hazardous materials facilities”, Proceedings of the International Symposium on Engineering Lessons Learned from the 2011 Great East Japan Earthquake, March 1-4, 2012, Tokyo, Japan

Haroun, M.A., (1983), “Vibration Studies and Tests of Liquid Storage Tanks”, Earthquake Engineering and Structural Dynamics, 11, 190-206.

Haroun, M.A., (1984), “Stress analysis of rectangular walls under seismically induced hydrodynamic loads”, Bulletin of the Seismological Society of America, 74(3), 1031-1041.

Haroun, M. A. and Ellaithy M. H., (1984), “Seismically induced fluid forced on elevated tanks”, Journal of Technical Topics in Civil Engineering, 111, 1–15.

Haroun, M. A. and Tayel, M. A., (1985), “Response of tanks to vertical seismic excitations”, Earthquake Engineering Structural Dynamics, 13, 583–95.

Haroun, M. A. and Tayel, M. A., (1985a), “Axisymmetrical vibrations of tanks-Numerical”, Journal of Engineering Mechanics, ASCE, 111(3), March, 1985. Paper No. 19537.

Haroun, M. A., and Tayel, M. A., 1985b. “Axisymmetrical vibrations of tanks-Analytical”, Journal of Engineering Mechanics, ASCE, 111(3), March, 1985. Paper No. 19538.

Haroun, M.A. and Abou-Izzeddine, W., (1992a), “Parametric study of seismic soil–tank interaction. I: horizontal excitation”, Journal of Structural Engineering, ASCE, 118(3), 783–797.

Haroun, M.A. and Abou-Izzeddine, W., (1992b), “Parametric study of seismic soil–tank interaction. II: vertical excitation”, Journal of Structural Engineering, ASCE, 118(3), 798-812.

Haroun, M.A., Mourad, S.A. and Izzeddine, W., (1991), “Performance of liquid storage tanks during the 1989 Loma Prieta earthquake”, Proceedings of Lifeline Earthquake Engineering, Los Angeles, ASCE, 1991, 1152-1160.

Hasheminejad, S.M. and Aghabeigi, M., (2012), “Sloshing characteristics in half-full horizontal elliptical tanks with vertical baffles”, Applied Mathematical Modelling, 36, 57–71.

Heidebrecht, A. C. and Lu, C. Y., (1988), “Evaluation of the seismic response factor introduced in the 1985 edition of the National Building Code of Canada”, Canadian Journal of Civil Engineering, 15, 332-338.

Herna´ndez-Barrios, H., Heredia-Zavoni, E. and Aldama-Rodr´ıguezc, A.A., (2007), “Nonlinear sloshing response of cylindrical tanks subjected to earthquake ground motion”, Engineering Structures, 29, 3364–3376.

http://peer.berkeley.edu/nga (Accessed 14 Feb 2012)

Hoskins, L.M. and Jacobsen, L.S., (1934), “Water pressure in tank caused by a simulated earthquake”, Bulletin of the seismological society of America, 24(1), 21-34

Housner, G. W., (1957), “Dynamic Pressure on Accelerated Fluid Containers”, Bulletin of the Seismological Society of America, 47(1) 15-35.

Housner, G. W., (1963), “The dynamic behaviour of water tanks”, Bulletin of the Seismological Society of America, 53, 381-387.

Hwang, J. H., Kim., I. S., Seol, Y. S., Lee, S. C., and Chon, Y. K., (1992), “Numerical simulation of liquid sloshing in three-dimensional tanks”, Computers and Structures, 44 (1-2), 339-342.

Isaacson, M., and Ryu, Chung-Son, (1998), “Earthquake-induced sloshing in vertical container of arbitrary section”, Journal of Engineering Mechanics, ASCE, 124(2), 158-166.

Jacobsen, L. S., (1949), “Impulsive hydrodynamics of fluid inside a cylindrical tank and of fluid surrounding a cylindrical pier”, Bulletin of the Seismological Society of America, 39, 189-203.

Jacobsen, L. S. and Ayre, R. S., (1949), “Impulsive hydrodynamics of fluids inside a cylindrical tank”, Bulletin of the Seismological Society of America, 39, 189~203.

Jaiswal, O. R. and Jain, S. K. (2005) “Modified proposed provisions for aseismic design of liquid storage tanks: Part II – commentary and examples”, Journal of Structural Engineering, 32(4): 297-310.

Jang, J. S. R., (1993), “ANFIS : Adaptive-network-based fuzzy inference system”, IEEE Transactions On Systems, Man, And Cybernetics, 23(3), 665-685.

Jang, J. S. R. and Sun, C. T., (1997), “Neuro-fuzzy modeling and control”, Proceedings IEEE, 83(3), 378–406.

Kachadoorian, R., (1965), “Effects of the earthquake of March 27, 1964 at Whittier, Alaska”, U.S. Geological Survey Professional Paper 542-B.

Kana, D. D., (1989), “Validated spherical pendulum model for rotary liquid slosh”, Journal of Spacecraft, 188-195

Kianoush, M.R. and Chen, J.Z., (2006), “Effect of vertical acceleration on response of concrete rectangular liquid storage tanks” Engineering Structures, 28(5), 704–715.

Kianoush, M.R., Mirzabozorg, H. and Ghaemian, M., (2006), “Dynamic Analysis of Rectangular Liquid Containers in Three-Dimensional Space”. Canadian Journal of Civil Engineering, 33, 501-507.

Kianoush, M.R. and Ghaemmaghami, A.R., (2011), “The effect of earthquake frequency content on the seismic behavior of concrete rectangular liquid tanks using the finite element method incorporating soil–structure interaction”, Engineering Structures, 33, 2186-2200.

Kim, H-S. and Lee, Y-S., (2008), “Optimization design technique for reduction of sloshing by evolutionary methods”, Journal of Mechanical Science and Technology, 22, 25-33.

Kim, J. K., Koh, H. M. and Kwahk, I. J., 1996, “Dynamic Response of Rectangular Flexible Fluid Containers”, Journal of Engineering Mechanics, ASCE, 122(9), 807-817.

Kim, N.S. and Lee, D.G., 1995, “Pseudodynamic test for evaluation of seismic performance of base isolated liquid storage tanks”, Engineering Structures, 17(3), 198-208.

Kobayashi, N., Mieda, T., Shbat, H., and Shinozaki, Y., (1989), “*A* study of the liquid slosh response in horizontal cylindrical tanks”, Journal of Pressure Vessel Technology, Transaction of the ASME, 111(1), 32-38.

Komatsu, K., (1987), “Nonlinear slosh analysis of liquid in tank with arbitrary geometries”, International Journal of Nonlinear Mechanics, 22(3), 193-207.

Larkin, T., 2008, “Seismic Response of Liquid Storage Tanks Incorporating Soil Structure Interaction”, Journal of Geotechnical and Geoenvironmental Engineering, 134(12), 1808-1814.

Lau, D. T., Marquez, D. and Qu, F., (1996), “Earthquake resistant design of liquid storage tanks”, Eleventh World Conference on earthquake Engineering, Paper no. 1293.

Leon, G. S. and Kausel E.A.M., (1986), “Seismic analysis of fluid storage tanks”, Journal of Structural Engineering, ASCE, 112(1), 1-18.

Lepelletier, T. G., and Raichlen, F., (1988), “Nonlinear oscillations in rectangular tanks”, Journal of Engineering Mechanics, ASCE, 114(1), 1-23.

Li, T. F., Lin, C. C. and Luk, C. H., (1981), “Three-directional fluid pool seismic sloshing analysis”, Journal of Pressure Vessel Technology, ASME, 103, 10-15.

Liu, Z. and Huang Y., (1994), “A new method for large amplitude sloshing problems”, Journal of Sound and Vibration, 175(2), 185-195.

Livaoglu, R. and Dogangun, A., 2006, “Simplified seismic analysis procedures for elevated tanks considering fluid–structure–soil interaction”, Journal of Fluids and Structures, 22, 421–439.

Livaoglu, R., (2008), “Investigation of seismic behavior of fluid-rectangular tank-soil/foundation systems in frequency domain”, Soil Dynamics and Earthquake Engineering, 28(2), 132-146.

Longet-Higgins, M. S., and Cokelet, E. D., (1976), “The deformation of steep surface waves on water: A numerical method of computation”, Proceedings of Royal Society of London, 350, 1-26.

Ma , D.C., Gvyldys, J., Chang, Y.W. and Liu, W.K., (1982), “Seismic behaviour of liquid-filled shells”, Nuclear Engineering and Design, 70, 437-455

Mahin, S. A., Bertero, V. V., Chopra, A. K. and Collins, R. G., (1976), “Response of the olive view hospital main building during the San Fernando earthquake”, Technical Report 1976-10, Earthquake Engineering Research Center, University of California, Berkeley.

Maleki, A. and Ziyaeifar, M., (2008), “Sloshing damping in cylindrical liquid storage tanks with baffles”, Journal of Sound and Vibration, 311, 372–385.

Malhotra, P. K., (1996), “Seismic uplifting of flexibly supported-storage tanks,” 11 th World conference of earthquake engineering, Paper no. 873.

Malhotra, P. K., 1997a, “Method for seismic base isolation of liquid-storage tanks”, Journal of Structural Engineering, ASCE, 123(1), 113-116.

Malhotra, P. K., 1997b, “New method for seismic isolation of liquid-storage tanks”, Earthquake Engineering and Structural Dynamics, 26, 839-847.

Malhotra, P. K. 1997c. Seismic response of soil-supported Unanchored Liquid-Storage Tanks", Journal of Structural Engineering, ASCE, 123(4), 440-450.

Malhotra, P.K., Wenk, T. and Wieland, M., (2000), Simple Procedure for Seismic Analysis of Liquid-Storage Tanks", Structural Engineering International, 3, 197-201.

Manos, G. C., (1991), "Evaluation of the earthquake performance of anchored wine tanks during the San Juan, Argentina, 1977 earthquake", Earthquake Engineering and Structural. Dynamics, 20(12), 1099-1114.

Mclver, P., (1989), "Sloshing frequencies for cylindrical and spherical containers filled to an arbitrary depth", Journal of Fluid Mechanics, 201, 243-257.

Mirzabozorg, H., Hariri-Ardebili M.A. and Nateghi, A.R, 2012, "Seismic behaviour of three dimensional concrete rectangular containers including sloshing effects", Coupled Systems Mechanics, 1(1), 79-98

Mitra, S. and Sihnamapatra, K.P., (2007) "Slosh dynamics of liquid-filled containers with submerged components using pressure-based finite element method", Journal of Sound and Vibration, 304, 361–381.

Moiseyev, N. N., (1998), "On the theory of non-linear vibrations of a liquid of finite volume", Applied Mathematics and Mechanics, 22(5).

Nakayama, T and Washizu, K. (1980), "Nonlinear analysis of liquid motion in a container subjected to forced pitching oscillation", International Journal for Numerical Methods in Engineering, 15, 1207-1220.

Nakayama, T and Washizu, K., (1981), "The boundary element method applied to the analysis of two-dimensional nonlinear sloshing problems", International Journal for Numerical Methods in Engineering, 17, 1631-1646.

Nielsen, R. and Kiremidjian, A.S., (1986), "Damage to oil refineries from major earthquakes", Journal of Structural Engineering, ASCE, 112(6), 1481-1491.

Omidinasab. F. and Shakib, H., 2012, "Seismic Response Evaluation of the RC Elevated Water Tank with Fluid-Structure Interaction and Earthquake Ensemble", KSCE Journal of Civil Engineering, 16(3), 366-376.

Pal, N.C., Bhattacharyya, S.K. and Sinha, P.K., (2003), "Non-linear coupled slosh dynamics of liquid-filled laminated composite containers: a two dimensional finite element approach", Journal of Sound and Vibration, 261, 729-749.

Pal, P., Bhattacharyya S.K., (2010), "Sloshing in partially filled liquid containers-Numerical and experimental study for 2-D problems", Journal of Sound and Vibration, 329, 4466–4485.

Panchal, V.R. and Jangid, R.S., 2008, “Variable friction pendulum system for seismic isolation of liquid storage tanks”, Journal of Nuclear Engineering and Design, 238, 1304–1315.

Panchal, V.R. and Jangid, R.S., 2011, “Performance of variable friction pendulum system for torsionally coupled structures”, Journal of Vibration and Control, 18(3), 323-343.

Panchal, V.R. and Jangid, R.S., 2011, “Seismic response of liquid storage steel tanks with variable frequency pendulum isolator”, KSCE Journal of Civil Engineering, 15(6),1041-1055.

Panigrahy, P.K., Saha, U.K. and Maity, D., (2009), “Experimental studies on sloshing behaviour due to horizontal movement of liquids in baffled tanks”, Ocean Engineering, 36, 213–222.

Park, J. H., Koh, H. M. and Kim, J., (1990), “Liquid-Structure Interaction Analysis by Coupled Boundary Element-Finite Element Method in Time Domain”, Proc. 7th International Conference on Boundary Element Technology, BE-TECH/92, Computational Mechanics Publication, Southampton, England, 89-92.

Park, J. H., Koh, H.M. and Kim, J.K., 2000, “Seismic isolation of pool-type tanks for the storage of nuclear spent fuel assemblies”, Journal of Nuclear Engineering and Design, 199, 143-154.

Peek, R. and El-Bkaily, M., (1997), “Mechancial Analogies for Liquid Storage Tanks and Action of Eccentric Gravity Loads”, Journal of Engineering Mechanics, ASCE, 123(6), 561-567.

Power, M.S., Chang, C.-Y., Idriss, I.M. and Kennedy, R.P., 1986, “Engineering characterization of ground motion, Task II: Summary Report”, United States Nuclear Regulatory Commission, NUREG/CR-3805, Vol. 5

Priestley, M. J. N., Wood, J. H. and Davidson, B. J., (1986), “Seismic design of storage tanks”, Bulletin of the New Zealand National Society for Earthquake Engineering, 19(4), December.

Rai, D. C., (2002), “Seismic retrofitting of R/C shaft support of elevated tanks”, Earthquake spectra, 18(4), 745–760.

Rinnie, J. F., (1967), “Oil storage tanks, The Prince William Sound, Alaska Earthquake of 1964 and Aftershocks”, Vol. IIA, U. S. Coast and Geodetic Survey, Environmental Science Service Administration, 1967.

Romero, V.J. and Ingber, M.S. (1995), “A numerical model for 2-D sloshing of pseudo-viscous liquids in horizontally accelerated rectangular containers”, Boundary element XVIII 1, 567-583.

Ruifu, Z., Dagen, W. and Xiaosong, R., 2011, “Seismic analysis of a LNG storage tank isolated by a multiple friction pendulum system”, Earthquake Engineering and Engineering Vibration. 10(2), 253-262.

Rupakhety, R. and Sigbjörnsson, R., (2011), “Can Simple Pulses Adequately Represent Near-Fault Ground Motions?”, Journal of Earthquake Engineering, 15, 1260–1272.

Seismic fragility formulations for water systems, Part 2 – Appenices, April 2001, www.americanlifelinesalliance.org.

Sezen, H. and Whittaker, A. S., (2006), “Seismic performance of industrial facilities affected by the 1999 Turkey earthquake”, Journal of Performance of Constructed Facilities, 20(1), 28–36.

Sezen, H., Livaoglu.R. and Dogangun, A., (2008), “Dynamic analysis and seismic performance evaluation of above-ground liquid-containing tanks”, Engineering Structures, 30, 794-803.

Shekari, M.R., Khaji, N. and Ahmadi, M.T., 2009, “A coupled BE–FE study for evaluation of seismically isolated cylindrical liquid storage tanks considering fluid–structure interaction”, Journal of Fluids and Structures, 25, 567–585.

Shenton H. W. III. and Hampton, F. P., 1999, “Seismic Response of isolated elevated water tanks”, Journal of Structural Engineering, ASCE, 125(9), 965-976.

Shih, C. F. and Babcock, C. D., (1987), “Buckling of oil storage tanks in SPPL tank farm during the 1979 Imperial Valley earthquake”, Journal of Pressure Vessel Technology, ASME, 109(2), 249-255.

Shivakumar, P. and Veletsos, A. S., (1995), “ Dynamic response of rigid tanks with inhomogeneous liquids”, Earthquake Engineering and Structural Dynamics, 24, 991-1015.

Shrimali, M.K. and Jangid, R.S., 2002a, “Non-linear seismic response of base-isolated liquid storage tanks to bi-directional excitation”, Journal of Nuclear Engineering and Design, 217, 1-20.

Shrimali, M.K. and Jangid R.S., 2002b, “Seismic response of liquid storage tanks isolated by sliding bearings”, Engineering Structures, 24, 909-921.

Shrimali, M.K., and Jangid, R.S., 2003, “Earthquake response of isolated elevated liquid storage steel tanks”, Journal of Constructional Steel Research, 59, 1267–1288.

Strandberg, L., (1978), “Lateral Stability of Road Tankers”, VTI Report No. 138A, vol. 1,

Steinbrugge, K. V. and Clough, R. W., “Chilean earthquake of May, 1960: A brief trip report”, Unpublished work.

Sweedan, A. M. I. and El Damatty, A. A., 2003, “Experimental identification of the vibration modes of liquid-filled conical tanks and validation of a numerical model”, Earthquake Engineering and Structural Dynamics, 30, 1407–1430.

Sweedan A. M. I. and El Damatty, A. A., 2005, “Equivalent Models of Pure Conical Tanks under Vertical Ground Excitation”, Journal of Structural Engineering, ASCE, 131(5), 725-733.

Takagi, T., and Sugeno, M., (1985), “Fuzzy identification of systems and its applications to modeling and control”, IEEE Transactions on Systems, Man and Cybernetics, 15, 116–132.

Taniguchi, T., (2004), “Rocking behavior of unanchored flat-bottom cylindrical shell tanks under action of horizontal base excitation”, Engineering Structures, 26, 415–426.

Tang, Y., 1993, “Dynamic response of tank containing two liquids”, Journal of Engineering Mechanics, ASCE, 19(3), 531-548.

Tang, Y., (1994a), “Free vibration analysis of tank containing two liquids”, Journal of Engineering Mechanics, ASCE, 120(3), 618-636.

Tang, Y., (1994b), “Rocking response of tanks containing two liquids”, Journal of Nuclear Engineering and Design, 152, 103-115.

Tanugula, R., (2001), “Effects of Baffles on Damping Lateral Fluid Sloshing Oscillations in Tanker Trucks”, M.Sc. Thesis, West Virginia University.

Tokuda, N., Sakurani, T. and Teraoku, T., (1995), “Sloshing analysis method using existing FEM structural analysis code”, Journal of Pressure Vessel Technology, ASME, 117, 268-272.

Tung, A. T. Y. and Kiremidjian, A. S., 1991, “Seismic Relibality analysis of elevated liquid-storage vessels”, Journal of Structural Engineering, ASCE, 117(5), 1372-1392.

Uang, C-M. and Bertero, V. V., 1988. "Implications of Recorded Earthquake Ground Motion on Seismic Design of Building Structures." Berkeley, Calif.: Earthquake Engineering, Research Center, University of California, Berkeley. UCB/EERC-88/13.

Uras, R. A., (1995) “Sloshing analysis of viscous liquid storage tanks. In: Fluid sloshing fluid structure interaction”, ASME, PVP Conference, 314, 63-72.

Veletsos, A. S., (1974), “Seismic effects in flexible liquid storage tanks”, Proceedings of the 5th World Conference on Earthquake Engineering, Rome, Italy, 1, 630-639.

Veletsos, A.S. and Yang, J.Y., (1977), “Earthquake response of liquid storage tanks-advances in civil engineering through mechanics”, ASCE Proceedings of the second engineering mechanics specially conference, Raleigh, NC: 1-24.

Veletsos, A. S., (1984), “Seismic response and design of liquid storage tanks”, Guidelines for the Seismic Design of Oil and Gas Pipeline Systems, ASCE, New York, 255–370.

Veletsos, A.S., and Tang, Y., (1986), “Dynamics of vertically excited liquid storage tanks”, Journal of Structural Engineering, ASCE, 112(6), 1228–1246.

Veletsos, A. S. and Tang, Y., 1987, “Rocking response of liquid storage tanks”, Journal of Engineering Mechanics, ASCE, 113(11), 1774-1792.

Veletsos, A. S. et al. (1990), “Seismic response of anchored steel tanks” Proceedings of the Third Symposium on Current Issues Related to Nuclear Power Plant Structures, Equipment and Piping (Gupta, A. K. Ed.), North Carolina State University, 1990, pp. 2–15.

Veletsos, A. S. and Tang, Yu., 1990, “Soil-Structure Interaction Effects for Laterally Excited Liquid Storage Tanks”, Earthquake Engineering and Structural Dynamics, 19, 473-496.

Veletsos, A. S., Tang, Y. and Tang, H. T., 1992, “Dynamic response of flexibly supported liquid-storage tanks”, Journal of Structural Engineering, ASCE, 118(1), 264-283.

Veletsos, A.S., and Shivakumar, P., (1993), “Sloshing response of layered liquids in rigid tanks”, Earthquake Engineering and Structural Dynamics, 22(9), 801-821.

Veletsos, A. S. and Younan, A. H., (1998), “Dynamics of solid-containing tanks. II flexible tanks”, Journal of Structural Engineering, ASCE, 124(1): 62-70.

Virella, J.C., Godoy, L.A. and Suarez L.E., (2003), “Influence of the roof on the natural periods of empty steel tanks”, Engineering Structures, 25, 877–887.

Virella, J.C., Godoy, L.A. and Suarez L.E., 2006, “Fundamental modes of tank-liquid systems under horizontal motions”, Engineering Structures, 28, 1450–1461.

Virella, J. C., Prato, C. A. and Godoy, L. A., (2008), “Linear and nonlinear 2D finite element analysis of sloshing modes and pressures in rectangular tanks subject to horizontal harmonic motions”, Journal of Sound and Vibration, 312, 442–460.

Wang, C.Z. and Khoo, B.C., (2005), “Finite element analysis of two-dimensional nonlinear sloshing problems in random excitations”, Ocean Engineering, 32, 107–133.

Wang, J.D., Lo S.H. and Zhou, D., (2012), “Liquid sloshing in rigid cylindrical container with multiple rigid annular baffles: Free vibration”, Journal of Fluids and Structures, 34, 138–156.

Wang, Y.P., Teng, M.C. and Chung, K.W., 2001, “Seismic isolation of rigid cylindrical tanks using friction pendulum bearings”, Earthquake Engineering and Structural Dynamics, 30, 1083–1099.

Warnitchai, P., (1998), “Modelling of liquid sloshing in rectangular tank with flow dampening devices”, Engineering Structures, 20(7), 593-600.

Waterhouse, D. D.,(1994), “Resonant sloshing near a critical depth”, Journal of Fluid Mechanics, 281, 313-318.

Watson, E.B.B. and Evans, D.V., (1991), “Resonant frequencies of a fluid container with internal bodies”, Journal of Engineering Mathematics, 25, 115–135.

Westergaard, H. M., (1933), “Earthquake-shock transmission in tall buildings”, Engineering News Record, 112(22), 654–656.

Westergaard, M., (1933), “Water pressure on dams during earthquakes”, Trans. American Society of Civil Engineering, 98, 1933.

Williams, A. N., and Moubayed W. I., (1990), “Earthquake-induced hydrodynamic pressures on submerged cylindrical storage tanks”, Ocean Engineering, 17(3), 181-199.

Wozniak, R. S. and Mitchell, W. W., (1978), “Basis of Seismic Design Provisions for Welded Steel Oil Storage Tanks”, Proceedings American Petroleum Institute, Refining Department.

Wu, G. X and Taylor, R. Eatock (1994), “Finite element analysis of two-dimensional non-linear transient water waves”, Applied Ocean Research, 16, 363-372.

Wu, G. X and Taylor, R. Eatock (1995), “Time stepping solutions of the two-dimensional nonlinear wave radiation problem”, Ocean Engineering, 8, 785-798.

Wu, G. X, Ma, Q. W. and Taylor, R. Eatock (1998), “Numerical simulation of sloshing waves in a 3D tank based on a finite element method”, Applied Ocean Research, 20, 337-355.

Yanev., P. I., Medina, F. and Yanev A. P., (2010), “The magnitude 8.8 offshore Maule region Chile earthquake of February 27, 2010”, Preliminary summary of damage and engineering recommendations, A Report to the World Bank.

Yang, J.Y., (1976), “Dynamic behavior of fluid–tank systems”, Ph.D. thesis, Department of Civil Engineering, Rice University, Houston, Tex.

Yazici, G. and Cili, F., (2008), “Evaluation of the liquid storage tank failures in the 1999 Kocaeli earthquake”, The 14th World Conference on Earthquake Engineering October 12-17, 2008, Beijing, China

Younan, A. H. and Veletsos, A. S., (1998), “Dynamics of solid-containing tanks. I Rigid tanks”, ASCE, Journal of Structural Engineering, 124(1), 52-61.

Younes, M. F., Younes, El-Madah, Y. K. M., Ibrahim, I. M. and El-Dannanh, E. H., (2011), “An experimental investigation of hydrodynamic damping due to vertical baffle arrangements in a rectangular tank”, Proceedings IMechE Vol. 221 Part M: Journal of Engineering for the Maritime Environment, 115-123.

Yuanjuna, H., Xingrui, Ma., Pingping, W. and Benli, W., (2007), “Low-gravity liquid nonlinear sloshing analysis in a tank under pitching excitation”, Journal of Sound and Vibration, 299, 164–177.

Zhang, X.T., Khoo, B.C. and Lou, J., (2006), “Wave propagation in a fully nonlinear numerical wave tank: A desingularized method”, Ocean Engineering, 33, 2310–2331.

Zadeh, L. A., (1975), “The concept of a linguistic variable and its application to approximate reasoning-I”, Information Sciences, 8, 199-249.

Zadeh, L. A., (1965), “Fuzzy sets”, Information And Control, 8, 338-353.

PUBLISHED AND ACCEPTED PAPERS

International Journals

1. **Nayak, S.K**. and Biswal, K.C., "Quantification of seismic response of partially filled rectangular liquid tank with submerged block", *Journal of Earthquake Engineering, DOI:10.1080/13632469.2013.789457.*

2. **Nayak, S.K.** and Biswal, K.C., "Quantification of nonlinear seismic response of rectangular liquid tank", *Journal of Structural Mechanics and Engineering,* DOI:http://dx.doi.org/10.12989/sem.2013.47.5.000.

3. **Nayak, S.K.** and Biswal, K.C., "Nonlinear seismic response of partially-filled rectangular liquid tank with submerged block due to earthquakes of varying frequency content", *Journal of Sound and Vibration,* (revised version sent).

4. **Nayak, S.K.** and Biswal, K.C., "Fluid damping in rectangular tank fitted with various internal objects - An experimental investigation", *Ocean Engineering,* (to be Communicated).

5. **Nayak, S.K.,** Biswal, K.C., and Mohapatra, S. S., "Prediction of seismic induced sloshing response in partially filled baffled rectangular liquid tank using adaptive neuro-fuzzy inference system", *Expert Systems with Applications,* (to be communicated)

International Conferences

1. **Nayak, S. K.** and Biswal, K. C., 2012, "Dynamic characteristics of rectangular liquid tank with internal component", *Fourth International Congress on Computational Mechanics and Simulation"*, 9-12 Dec 2012, Hyderabad, India.

2. Biswal, K. C. and **Nayak, S. K**., 2012, "Nonlinear analysis of sloshing in rigid rectangular tank under harmonic excitation", *Fourth International Congress*

on Computational Mechanics and Simulation", 9-12 Dec 2012, Hyderabad, India.

3. **Nayak, S. K.** and Biswal, K. C., 2012, "Seismic response of partially filled rectangular liquid tank", *Fourth International Congress on Computational Mechanics and Simulation"*, 9-12 Dec 2012, Hyderabad, India.